

A detailed close-up photograph of a hydraulic system, showing various metal components, pipes, and fittings. The image is slightly blurred, emphasizing the mechanical nature of the subject.

# HYDRAULICA

HYDRAULICS-PNEUMATICS-TRIBOLOGY-ECOLOGY-SENSORICS-MECHATRONICS

**2025**

**September**

**No. 3**



ISSN 1453 - 7303  
ISSN-L 1453 - 7303

<https://hidraulica.fluidas.ro>

## CONTENTS

<b>EDITORIAL: Rolul digitalizării și al energiilor regenerabile în reinventarea domeniului hidropneumatic / The Role of Digitalization and Renewable Energy in Reinventing the Fluid Power Field</b> Ph.D. Eng. <b>Gabriela MATACHE</b>	5 - 6
• <b>Experimental Study and Visualizations of Flow with Taylor Vortices</b> Assoc. Prof. PhD eng. <b>Sanda BUDEA</b> , Lecturer PhD eng. <b>Ștefan-Mugur SIMIONESCU</b> , Eng. <b>Ion JITESCU</b>	7 - 14
• <b>Small-Scale Hydraulic Excavation System for Educational Purposes</b> Assoc. Prof. PhD. Eng. <b>Ionel Laurențiu ALBOTEANU</b>	15 - 20
• <b>Hydraulic Systems Security: Addressing Cyber Threats with DNA-Based Cryptography in Cloud-Integrated Control</b> Assoc. Prof. PhD. Eng. <b>Ștefan ȚĂLU</b>	21 - 32
• <b>Solar Drying in Controlled Environments: Sustainable Solution for Preserving Vegetable Products</b> Dipl. Eng. <b>Alina - Iolanda POPESCU</b> , PhD. Eng. <b>Gheorghe ȘOVĂIALĂ</b> , PhD. Eng. <b>Gabriela MATACHE</b>	33 - 41
• <b>The Volumetric Efficiency of Water Ram</b> MSc. <b>Oswaldo Antonio PACHECO BUSQUET</b> , DrC. <b>Celestino Santos ORO ORTIZ</b> , Ing. <b>Ángel Arsenio PACHECO MONTEAGUT</b>	42 - 52
• <b>Artificial Intelligence Use for Forecasting Precipitation and Assessing Groundwater Depletion: A Study Case in Chihuahua City, Mexico</b> M. Eng. <b>Margarita PRECIADO</b> , Dr. <b>Maritza ARGANIS</b> , M.Eng. <b>Jorge CASADOS</b> , Dr. <b>Rodrigo ROBLERO-HIDALGO</b>	53 - 65
• <b>Aspects Regarding Methods for Hydraulic Cylinders Synchronization</b> PhD. Stud. Eng. <b>Ionela Mihaela POPESCU</b> , Ph.D. Eng. <b>Victor CONSTANTIN</b> , MSc. Eng. <b>Daniel NANCA</b>	66 - 72
• <b>Mapping Convective Precipitation Susceptibility in the Peñitas Watershed: A Novel Convectivity Index and Geostatistical Interpolation Framework</b> Dr. <b>Maritza ARGANIS</b> , M. Eng. <b>Margarita PRECIADO</b> , Dr. <b>Faustino DE LUNA</b> , Eng. Student <b>Cristian LÓPEZ</b> , Eng. Student <b>Edgar DE DIOS SEVILLA</b> , M. Eng. <b>Omar CABRERA</b> , Dr. <b>Rodrigo ROBLERO-HIDALGO</b>	73 - 82
• <b>Design of a Positioning System for Cylindrical Parts</b> MSc. Eng. <b>Daniel NANCA</b> , Ph.D. Eng. <b>Viorel GHEORGHE</b> , Ph.D. Eng. <b>Victor CONSTANTIN</b> , PhD. Stud. Eng. <b>Ionela Mihaela POPESCU</b>	83 - 88
• <b>The Evolution of Energy Consumption in Electric Mobility in Bucharest in 2024: Between Efficiency and the Potential of Renewable Sources</b> PhD. Stud. Eng. <b>Anca-Florentina POPESCU</b> , PhD. Stud. Eng. <b>Alexandra BĂDICEANU</b> , Prof. Dr. Habil. Chem. <b>Ecaterina MATEI</b> , PhD. Stud. Eng. <b>Georgiana-Miana ANDRICIUC</b> , Prof. Dr. Habil. Eng. <b>Andra-Mihaela PREDESCU</b>	89 - 100
• <b>Pedagogical Valences of Computer-Assisted Instruction in the Professional Training of Soil Remediation Specialists</b> MA stud. <b>Ioana-Elisabeta CIORUȚA</b> , PhD Eng. IT exp. <b>Bogdan V. CIORUȚA</b> , Assoc. Prof. PhD Eng. habil. <b>Mirela-Ana COMAN</b> , Eng. IT exp. <b>Alexandru L. POP</b>	101 - 112
• <b>Numerical Investigation of Energy Dissipation Efficiency in Stepped Spillway Designs under Flow Conditions</b> Associate professor <b>Fănel Dorel ȘCHEAUA</b>	113 - 118
• <b>Pneumatically Driven Generator for Use with Small-Scale Compressed Air Energy Storage System</b> PhD Eng. <b>Radu-Julian RĂDOI</b> , MSc. Eng. <b>Bogdan-Alexandru TUDOR-ROTILĂ</b> , PhD Student Eng. <b>Robert BLEJAN</b> , MSc. Eng. <b>Ștefan-Mihai ȘEFU</b>	119- 124
• <b>Pedagogical Implications of Computer-Assisted Instruction in Reconfiguring Contents for General and Applied Ecology</b> PhD Eng. IT exp. <b>Bogdan V. CIORUȚA</b> , MA stud. <b>Ioana-Elisabeta CIORUȚA</b> , Assoc. Prof. PhD Eng. habil. <b>Mirela-Ana COMAN</b> , Eng. IT exp. <b>Alexandru L. POP</b>	125 - 134

**BOARD****MANAGING EDITOR**

- PhD. Eng. Petrin DRUMEA - Hydraulics and Pneumatics Research Institute in Bucharest, Romania

**EDITOR-IN-CHIEF**

- PhD.Eng. Gabriela MATAACHE - Hydraulics and Pneumatics Research Institute in Bucharest, Romania

**EXECUTIVE EDITOR, GRAPHIC DESIGN & DTP**

- Ana-Maria POPESCU - Hydraulics and Pneumatics Research Institute in Bucharest, Romania

**EDITORIAL BOARD**

PhD.Eng. Gabriela MATAACHE - Hydraulics and Pneumatics Research Institute in Bucharest, Romania

Assoc. Prof. Adolfo SENATORE, PhD. – University of Salerno, Italy

PhD.Eng. Cătălin DUMITRESCU - Hydraulics and Pneumatics Research Institute in Bucharest, Romania

Prof. Dariusz PROSTAŃSKI, PhD. – KOMAG Institute of Mining Technology in Gliwice, Poland

Assoc. Prof. Andrei DRUMEA, PhD. – National University of Science and Technology Politehnica Bucharest, Romania

Assoc. Prof. Houari AOUED, PhD. – Hassiba Benbouali University of Chlef, Algeria

PhD.Eng. Radu Iulian RĂDOI - Hydraulics and Pneumatics Research Institute in Bucharest, Romania

Prof. Aurelian FĂTU, PhD. – Institute Pprime – University of Poitiers, France

PhD.Eng. Daniela-Doina CIOBOATĂ – National Institute of Research and Development in Mechatronics and Measurement Technique, Romania

Prof. Mihai AVRAM, PhD. – National University of Science and Technology Politehnica Bucharest, Romania

Lect. Iulian Sorin MUNTEANU, PhD. – National University of Science and Technology Politehnica Bucharest, Romania

Lect. Ioan-Lucian MARCU, PhD. – Technical University of Cluj-Napoca, Romania

**COMMITTEE OF REVIEWERS**

PhD.Eng. Corneliu CRISTESCU – Hydraulics and Pneumatics Research Institute in Bucharest, Romania

Assoc. Prof. Pavel MACH, PhD. – Czech Technical University in Prague, Czech Republic

Prof. Ilare BORDEAȘU, PhD. – Politehnica University of Timisoara, Romania

Prof. Valeriu DULGHERU, PhD. – Technical University of Moldova, Chisinau, Republic of Moldova

Assist. Prof. Krzysztof KĘDZIA, PhD. – Wrocław University of Technology, Poland

Prof. Dan OPRUȚA, PhD. – Technical University of Cluj-Napoca, Romania

PhD.Eng. Teodor Costinel POPESCU - Hydraulics and Pneumatics Research Institute in Bucharest, Romania

Assoc. Prof. Ph.D. Basavaraj HUBBALLI - Visvesvaraya Technological University, India

Ph.D. Amir ROSTAMI – Georgia Institute of Technology, USA

Prof. Adrian CIOCĂNEA, PhD. – National University of Science and Technology Politehnica Bucharest, Romania

Prof. Carmen-Anca SAFTA, PhD. - National University of Science and Technology Politehnica Bucharest, Romania

Ph.D.Eng. Dorin BORDEAȘU – Politehnica University of Timisoara, Romania

Assoc. Prof. Mirela Ana COMAN, PhD. – Technical University of Cluj-Napoca, North University Center of Baia Mare, Romania

Prof. Carmen Nicoleta DEBELEAC, PhD. – "Dunarea de Jos" University of Galati, Romania

Assist. Prof. Fănel Dorel ȘCHEAUA, PhD. – "Dunarea de Jos" University of Galati, Romania

PhD.Eng. Marian BLEJAN - Hydraulics and Pneumatics Research Institute in Bucharest, Romania

**Published by:**

**Hydraulics and Pneumatics Research Institute, Bucharest-Romania**

Address: 14 Cuțitul de Argint, district 4, Bucharest, 040558, Romania

Phone: +40 21 336 39 91; Fax: +40 21 337 30 40; e-Mail: [ihp@fluidas.ro](mailto:ihp@fluidas.ro); Web: [www.ihp.ro](http://www.ihp.ro)

**with support from:**

**National Professional Association of Hydraulics and Pneumatics in Romania - FLUIDAS**

e-Mail: [fluidas@fluidas.ro](mailto:fluidas@fluidas.ro); Web: [www.fluidas.ro](http://www.fluidas.ro)

**HIDRAULICA Magazine** is indexed by international databases



**EDITORIAL****Rolul digitalizării și al energiilor regenerabile în reinventarea domeniului hidropneumatic**

Hidraulica și pneumatica, odinioară percepute ca domenii „clasice”, trec astăzi printr-o transformare profundă. Digitalizarea și tranziția către energie verde nu mai sunt simple tendințe, ci realități care dau sens unei noi etape de dezvoltare.



Dr. Ing. Gabriela Matache  
REDACTOR ȘEF

Integrarea senzorilor inteligenți, a IoT și a Inteligenței Artificiale permite monitorizarea în timp real și mentenanța predictivă, crescând fiabilitatea și reducând costurile. În același timp, soluții precum bateriile pneumatice pentru stocarea energiei sau utilizarea hidraulicii în sisteme hibride arată cum tradiția se întâlnește cu inovația.

La nivel global, mari actori precum SUA, China, Japonia și India dezvoltă echipamente de ultimă generație, integrate cu algoritmi de AI și tehnologii verzi. Acest ritm accelerat impune și României să țină pasul, nu doar pentru a rămâne competitivă, ci și pentru a valorifica oportunitățile de colaborare internațională și de transfer tehnologic.

Viitorul nu înseamnă doar modernizarea tehnologiilor, ci și formarea unei noi generații de specialiști. Hidraulica și pneumatica nu mai sunt doar despre presiune și debit, ci despre date, inteligență și responsabilitate față de mediu. Pentru a atrage tinerii către acest domeniu, este important să le arătăm impactul real pe care îl pot avea: de la dezvoltarea de echipamente inteligente și conectate la IoT, până la soluții care reduc consumul de energie și sprijină tranziția către sustenabilitate.

Tinerii își doresc profesii cu sens, iar hidraulica și pneumatica le oferă ocazia să fie parte din marile teme ale prezentului: digitalizare, energie verde și inovație industrială. Prin laboratoare moderne, proiecte interdisciplinare și stagii aplicative, putem transforma acest domeniu într-un spațiu atractiv pentru generația crescută în era digitală. Iar prin atragerea lor, asigurăm nu doar continuitatea, ci și capacitatea României de a răspunde provocărilor globale.

În acest context, rolul **INOE 2000-IHP** devine unul important: un centru capabil să transforme cercetarea în soluții sustenabile pentru industrie, de la echipamente eficiente energetic până la aplicații pentru integrarea energiilor regenerabile.

**Este momentul să folosim aceste schimbări ca o șansă de reinventare și să demonstrăm că domeniul nostru poate contribui direct la economia viitorului.**



**EDITORIAL****The Role of Digitalization and Renewable Energy in Reinventing the Fluid Power Field**

Ph.D.Eng. Gabriela Matache  
EDITOR-IN-CHIEF

Hydraulics and pneumatics, once perceived as “classical” fields, are today undergoing a profound transformation. Digitalization and the transition to green energy are no longer mere trends, but realities that give meaning to a new stage of development.

The integration of smart sensors, IoT, and Artificial Intelligence enables real-time monitoring and predictive maintenance, increasing reliability while reducing costs. At the same time, solutions such as pneumatic batteries for energy storage or the use of hydraulics in hybrid systems demonstrate how tradition meets innovation.

Globally, major players such as the USA, China, Japan, and India are developing next-generation equipment, integrated with AI algorithms and green technologies. This accelerated pace requires Romania to keep up—not only to remain competitive but also to seize opportunities for international collaboration and technology transfer.

The future is not only about modernizing technologies, but also about training a new generation of specialists. Hydraulics and pneumatics are no longer just about pressure and flow; they are about data, intelligence, and environmental responsibility. To attract young people to this field, it is important to show them the real impact they can have: from developing intelligent, IoT-connected equipment to creating solutions that reduce energy consumption and support the transition to sustainability.

Young professionals are seeking meaningful careers, and hydraulics and pneumatics offer them the chance to be part of the defining issues of our time: digitalization, green energy, and industrial innovation. Through modern laboratories, interdisciplinary projects, and applied internships, we can make this domain attractive to a generation raised in the digital era. By engaging them, we ensure not only continuity but also Romania’s capacity to respond to global challenges.

In this context, the role of **INOE 2000–IHP** becomes a crucial one: a center capable of transforming research into sustainable solutions for industry, from energy-efficient equipment to applications for the integration of renewable energy.

**Now is the moment to embrace these changes as an opportunity for reinvention and to demonstrate that our field can directly contribute to the economy of the future.**

## Experimental Study and Visualizations of Flow with Taylor Vortices

Assoc. Prof. PhD eng. **Sanda BUDEA**<sup>1,\*</sup>, Lecturer PhD eng. **Ștefan-Mugur SIMIONESCU**<sup>1</sup>,  
Eng. **Ion JITESCU**<sup>1</sup>

<sup>1</sup> National University of Science and Technologies Politehnica of Bucharest, Romania, Energy Engineering Faculty; Department of Hydraulics, Hydraulic Machinery and Environmental Engineering

\* sanda.budea@upb.ro

**Abstract:** Taylor vortex flow has multiple applications, primarily in the field of turbomachinery, in flows through labyrinths or sealing elements, but also in the protection of sliding bearings, ensuring their proper lubrication. Other applications of vortex flow can also be found in the pharmaceutical industry, in mixing different fluids, but also in cooling systems, in avoiding fluid crystallization, in nano fluidics, etc. The present paper presents theoretical aspects, visualizations and experiments related to the appearance of Taylor vortices, carried out on a laboratory installation with rotating cylinders. The Reynolds and Taylor numbers are essential indicators in identifying the behavior of fluids in vortex flow. The visualizations confirm the theory, namely that the appearance of vortices is dependent on the fluid viscosity, the speed, the Re, Ta numbers and the variation in time of these quantities.

**Keywords:** Taylor vortices, visualizations, experimental study, technical applications

### 1. Introduction - Theoretical aspects

The present paper presents theoretical aspects, visualizations and experiments related to the emergence of Taylor vortices, carried out on a laboratory installation with rotating cylinders. Hydrodynamic phenomena accompanied by instability in the flow of a fluid between two rotating concentric cylinders were observed by Sir G.I. Taylor and first published in 1923 in the paper [1]. Later the topic was studied more extensively by Buhler et al. [2], Larson [3], Koschmieder [4] and Muller [5] and R. Kadar, 2010 [6].

"Most of the time, the movements of real fluids are accompanied by rotational movements caused by the appearance of vortex threads, which then, due to small frictional forces, break up into numerous other vortices that propagate throughout the mass of the fluid. The origin of vortices is generally in discontinuities of contour, velocity or pressure. Thus, we see vortices appearing at the edges of a body in a moving fluid, at the edges of an orifice, when the fluid is displaced by the movement of a solid body and even when a fluid moves around continuously curved profiles. These potential vortical movements create a special type of resistance" [7].

As a result of these considerations, it was possible to define notions of thread, line, vortex surface, vortex tube, characterized by the angular velocity vector  $\omega$  which characterizes the rotational movement of the fluid particle around the instantaneous axis of rotation, defined by the three-dimensional components [7]:

$$\omega_x = \frac{1}{2} \left( \frac{\partial w}{\partial y} - \frac{\partial v}{\partial z} \right); \quad \omega_y = \frac{1}{2} \left( \frac{\partial u}{\partial z} - \frac{\partial w}{\partial x} \right); \quad \omega_z = \frac{1}{2} \left( \frac{\partial v}{\partial x} - \frac{\partial u}{\partial y} \right) \quad (1)$$

The vortex line is tangent to the vectors describing the angular velocity  $\omega$  at a given time, described by the equations of a vortex line:

$$\frac{dx}{\omega_x} = \frac{dy}{\omega_y} = \frac{dz}{\omega_z} \quad (2)$$

The intensity of the vortices and their time duration are important. Thus, we can also define two quantities that characterize the vortices and the circulation along a closed curve - the circulation  $\Gamma$  and the potential  $U$ , thus from the Thomson - Lagrange theorem we have the mathematical expression between the two quantities with respect to time in differential form, equation (3) from [7]:

$$\frac{d\Gamma}{dt} = - \int_A^B \left[ dU + \frac{dp}{\rho} - d\left(\frac{V^2}{2}\right) \right] \quad (3)$$

where the potential  $U$  is uniform,  $p$  is the pressure and  $V$  is the velocity are uniform functions, the derivative of the circulation on a closed curve is canceled and it follows that the circulation  $\Gamma$  is constant. From Stokes' theorem on a closed contour, the velocity circulation is equal to the rotor flux of the velocity that crosses the support surface of the contour, given by the expression for a vortex tube of finite section by integration results [7]:

$$\Gamma = \int_S \text{rot} \vec{V} dS_n = \int_S \Omega dS_n \quad (4)$$

The circulation on the contour that encloses the cross-sectional area  $S_n$  is equal to the vortex rotor flux. By definition, this expression is called the vortex intensity [7].

Parallel vortex threads have parallel movements at different speeds due to their interaction.

a) The parallel vortices in a system are reduced to two parallel threads with the circulations  $\Gamma_1$  and  $\Gamma_2$  of the same direction, or opposite directions, as in Figure 1, with the velocities induced thus:

$$V_1 = \frac{\Gamma_1}{2\pi l}, \quad V_2 = \frac{\Gamma_2}{2\pi l} \quad (5)$$

The complex potential of the motion resulting from parallel vortex strands is given by equations (6):

$$f(z) = \frac{\Gamma}{2\pi l} \ln(z - z_1) - \frac{\Gamma}{2\pi l} \ln(z - z_2);$$

$$f(z) = \frac{\Gamma}{2\pi l} \ln \frac{(z - z_1)}{(z - z_2)} = \frac{\Gamma}{2\pi l} \ln \left( \frac{r_1}{r_2} e^{i(\theta_1 - \theta_2)} \right) \quad (6)$$

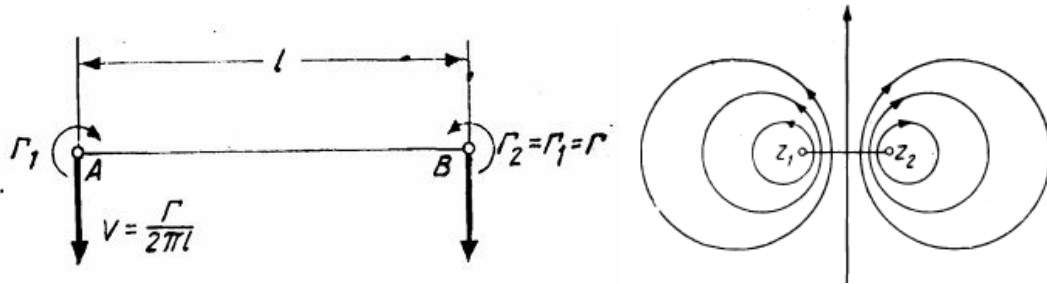


Fig. 1. Parallel, equal and oppositely directed vortices – velocities and streamlines [7]

#### b) Strings of vortices

The flow between two coaxial cylinders, known as Taylor-Couette flow, is a field of research of particular importance in fluid mechanics. It was initiated by the works of G.I. Taylor and has continuously evolved, being studied both from a fundamental and applied point of view (in chemical engineering, rheometry, tribology, etc.). The phenomenon of Taylor-Couette flow has become essential for understanding hydrodynamic instabilities, especially in the context of vortex flows.

#### c) Prandtl's Mixing Length Theory and Taylor's Vortex Transport Theory.

In one-dimensional turbulent motion where the mean velocity is parallel to the dominant flow axis  $Ox$ , vectors ( $u = u(y)$ ,  $v=0$ ,  $w=0$ ), the only apparent non-zero tangential unit stress is according to the paper [8]:

$$\tau_{yx} = -\rho \overline{u'v'} \quad (7)$$

Prandtl establishes the expression for this tension. His theory is based on the idea of conservation of momentum in the direction of the main flow. It is assumed that in turbulent motion there are macroscopic fluid particles that have a proper motion. These macroscopic particles move over a certain length in both the longitudinal and transverse directions, keeping the value of their momentum component on the Ox axis constant. Unlike Prandtl who examined the exchange of momentum (quantity of motion), Taylor examined the exchange of momentum moments (kinetic moments). Taylor's theory of vortex transport or diffusion gives results similar to Prandtl's regarding velocity distributions in a plane jet, but provides better results in other cases [8].

## 2. Experimental Installation

The experimental installation, as can be seen in Figure 2, consists of the following components:

- rotating inner cylinder with diameter  $D_1 = 216.9$  mm, and length  $L = 290$  mm.
- transparent outer cylinder with diameter  $D_2 = 238$  mm,
- 250 W electric drive motor, 1360 rpm, which can be driven with a frequency converter
- drive shaft,
- coupling,
- support and end caps,
- two sealing O-rings.

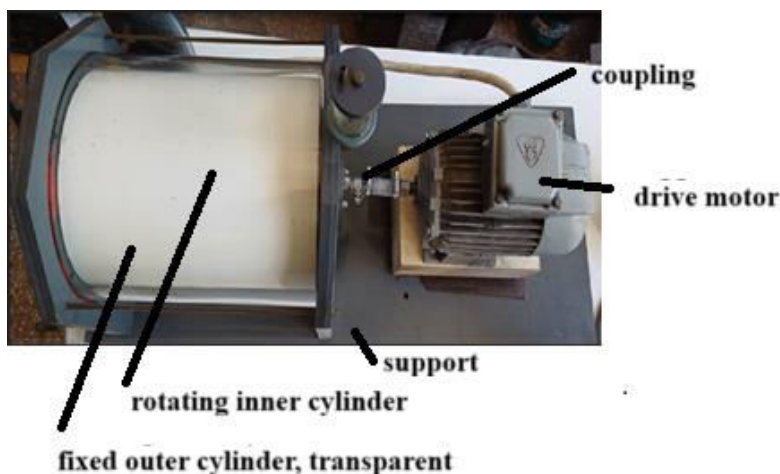


Fig. 2. Experimental setup for studying Taylor vortices

We used two types of oil in the experiments – 80W90 engine oil with kinematic viscosity  $158 \cdot 10^{-6}$  m<sup>2</sup>/s and TR25 transformer oil, with  $8.862 \cdot 10^{-6}$  m<sup>2</sup>/s, and with a density of 860 kg/m<sup>3</sup>.

As measuring devices, we used a tachometer with accuracy  $\pm 0.05\%$ , and visualization / filming techniques, some of them with laser light. In the TR25 oil we also used blue dye for better visualization, the oil being light in color. To change the speed, we drove the electric motor through a frequency converter.

### 2.1 Visualisations

In our own laboratory setup, with the two types of oils, we obtained the visualizations like in Figures 3-7. The characteristic Reynolds and Taylor numbers were calculated according to the relations (8-9). For the TR25 oil, with low viscosity and light color, we also used a blue dye for better visualization. The large difference in viscosity of the two oils led to different results depending on the speed of the inner cylinder.





**Fig. 3.** Visualizations with the formation of Taylor vortex layers for TR25 and 80W90 oil respectively



**Fig. 4.** Strings of vortices at speed  $n = 136$  rot/min,  $Re = 37681$ ,  $Ta = 340438$ , oil TR25.



**Fig. 5.** Strings of vortices at speed  $n = 470$  rot/min,  $Re = 130697$ ,  $Ta = 4095718$ , oil TR25



**Fig. 6.** The formation of Taylor vortices at speed  $n = 57$  rot/min,  $Re = 892$ ,  $Ta = 191$ , oil 80W90



**Fig. 7.** The formation of Taylor vortices at speed  $n = 61$  rot/ min,  $Re = 964$ ,  $Ta = 223$ , oil 80W90.

## 2.2 Experimental results

To characterize the fluid flow in the gap created by the two cylinders, the Reynolds and Taylor numbers are used. We used computation relations (8) and (9) to determine the Reynolds and Taylor numbers, according to the paper [9].

$$Re = \frac{uD_1}{\nu} = \frac{\Omega D_1^2}{2\nu} \quad (8)$$

$$Ta = \frac{4 \cdot R_1^2 \cdot (R_2 - R_1)^2 \cdot \Omega^2}{\nu^2 \cdot (R_2 + R_1)^2} \quad (9)$$

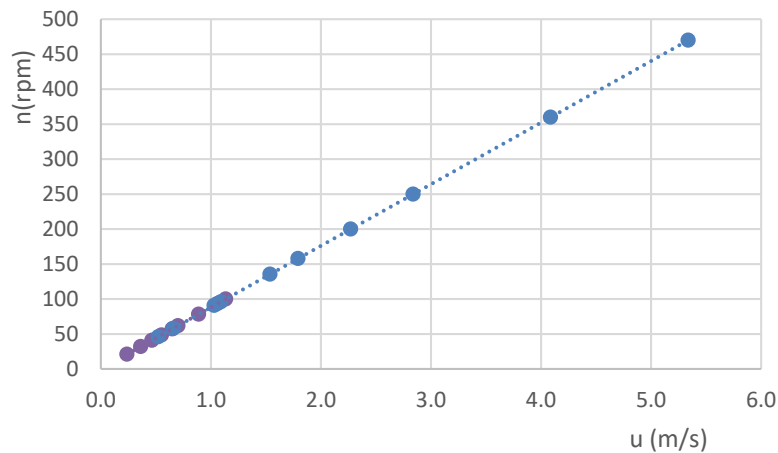
The notations refer to  $\Omega$  - angular velocity of rotation,  $\nu$  - kinematic viscosity of the fluid, diameters or radii of the inner and outer cylinders.

In Table 1 we have centralized the results of speed measurements, converter frequencies  $f$  (Hz), calculations of tangential velocity  $u$  (m/s) and angular velocity  $\Omega$  (s<sup>-1</sup>), respectively we have determined the Reynolds and Taylor numbers. The results are very different, influenced by the viscosity of the fluids and implicitly by the speed.

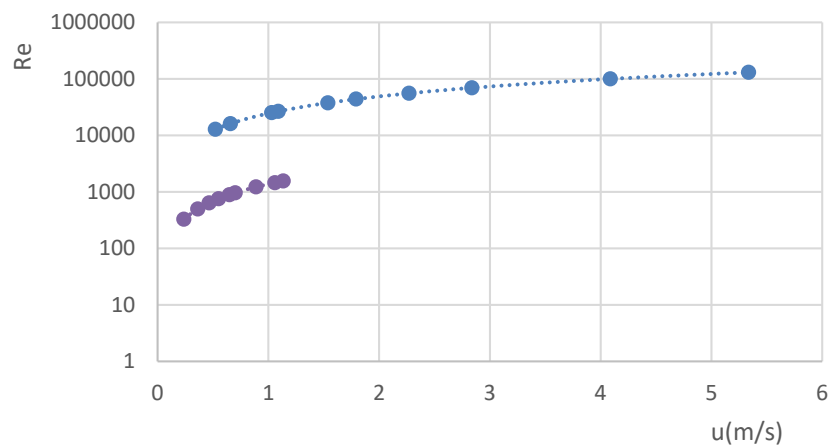
**Table 1:** Experimental results

n(rpm)	u(m/s)	f (Hz)	Re	$\Omega$ (s <sup>-1</sup> )	Ta	80W90
21	0.238	3	328	2.2	26	
32	0.363	4	499	3.3	60	
41	0.466	5	639	4.3	98	
48.6	0.552	6	758	5.1	138	
57.2	0.650	7	892	6.0	191	
61.8	0.702	8	964	6.5	223	
78.4	0.890	10	1223	8.2	359	
93.4	1.061	12	1457	9.8	509	
100	1.136	14	1560	10.5	583	
n(rpm)	u(m/s)	f (Hz)	Re	$\Omega$ (s <sup>-1</sup> )	Ta	TR25
46	0.523	1	12806	4.8	39322	
58	0.659	2	16129	6.1	62372	
91	1.031	3	25243	9.5	152790	
96	1.090	4	26695	10.0	170874	
136	1.539	5	37681	14.2	340438	
158	1.793	6	43899	16.5	462080	
200	2.271	8	55616	20.9	741642	
250	2.839	10	69519	26.2	1158816	
360	4.088	15	100108	37.7	2402920	
470	5.337	20	130697	49.2	4095718	

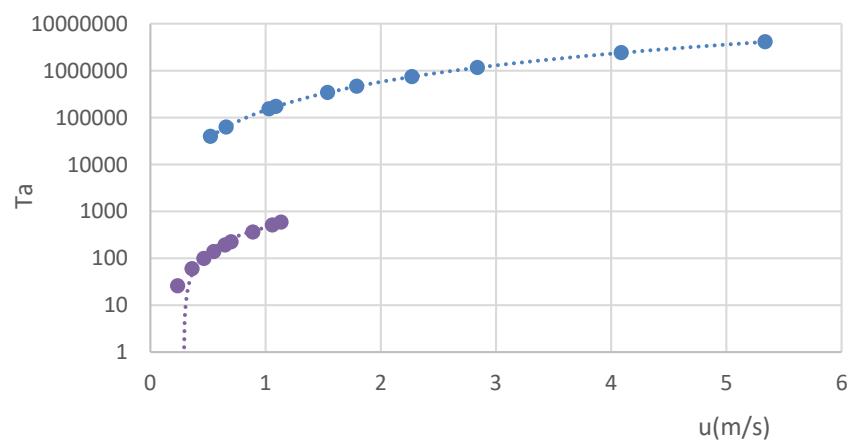
In Figures 8, 9 and 10 we have graphically represented the variation of the speed with the tangential velocity, the Reynolds and Taylor numbers as a function of the tangential velocity for the 80W90 oil in light blue, and for TR25 in dark blue. We used the logarithmic scale, the difference in the values being large. A stabilization of the circular or toroidal vortices was found, depending on the Taylor number.



**Fig. 8.** Speed function of tangential velocities



**Fig. 9.** Reynolds number as a function of tangential velocities



**Fig. 10.** Taylor number as a function of tangential velocities

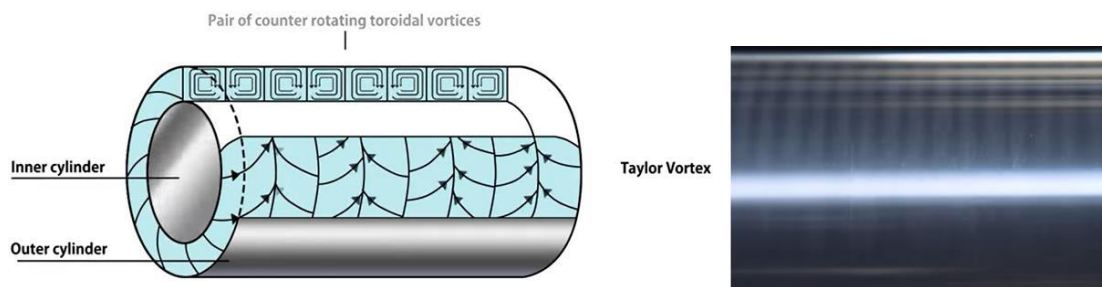
### 3. Applications for Taylor Vortices Flow

Taylor vortices flow has multiple applications, primarily in the field of turbomachinery, in flows through labyrinths or sealing elements, but also in the protection of sliding bearings, ensuring their proper lubrication.

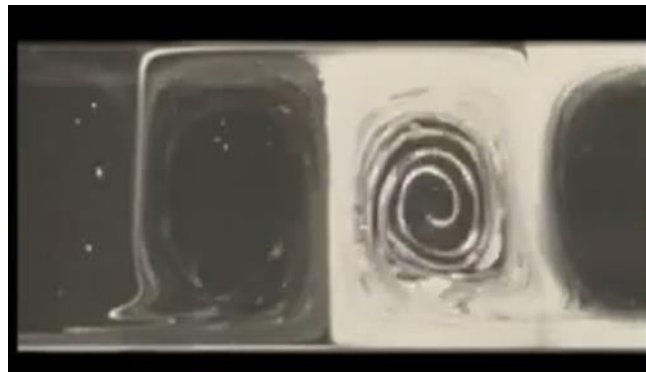
Applications for vortices flow can also be found in the pharmaceutical industry, in mixing different fluids, but also in cooling systems, in avoiding fluid crystallization, in nano fluidics, in chemical engineering, rheometry, tribology, etc.

In specialized literature [10], we can observe the formation of paired Taylor vortices in the study of flow in nano-reactors, as in Figure 11, or the formation of paired vortices of opposite direction in the interstices between rotating cylinders, Figure 12, as in the case of labyrinth rings [11].

**Taylor Vortex Flow - Prevention of axial diffusion + uniform crystallization/reaction time**



**Fig. 11.** Taylor Vortex Flow Nano Reactor [10]



**Fig. 12.** Taylor vortices between rotating cylinders [11]

### 3. Conclusions

- Reynolds and Taylor numbers are essential indicators in identifying the behavior of fluids in Taylor–Couette flow.
- Viscosity plays a key role: the higher it is, the greater the stability of the flow.
- Vortex stability is influenced by the drive speed, respectively by the motor frequency.
- The visualizations confirm the theory – the appearance of vortices is dependent on  $Re$ ,  $Ta$  and the time variation of these quantities.
- The results are comparable with the literature, validating both the methods and the interpretations.
- Further developments will analyze more diameters of the moving cylinder, the interior, thus varying the space between the cylinders, and more fluids conveyed. The multiple applications of Taylor vortex flow justify the in-depth analysis of the field.



**References**

- [1] Taylor, G.I. “Stability of a Viscous Liquid Contained between Two Rotating Cylinders.” *Philosophical Transactions of the Royal Society of London. Series A, Containing Papers of a Mathematical or Physical Character* 223 (1923): 289-343.
- [2] Buhler, K., J. Coney, M. Wimmer, and J. Zierep. “Advances in Taylor vortex flow: A report on the fourth Taylor vortex flow working party meeting.” *Acta Mechanica* 62 (November 1986): 47–61.
- [3] Koschmieder, E. *Bénard Cells and Taylor Vortices*. Cambridge, Cambridge University Press, 1993.
- [4] Larson, R. “Instabilities in viscoelastic flows.” *Rheologica Acta* 31, no. 3 (May 1992): 213–263.
- [5] Muller, S. “Elastically influenced instabilities in Taylor-Couette and other flows with curved streamlines: a review.” *Korea-Australia Rheology Journal* 20, no. 3 (June 2008): 117–125.
- [6] Kadar, Roland. *Flow of Pure Viscous and Viscoelastic Fluids Between Concentric Cylinders with Applications to Rotational Mixers*. PhD thesis. Politehnica University of Bucharest, Faculty of Power Engineering, Bucharest, 2010.
- [7] Mateescu, Cristea. *Hydraulics / Hidraulica*. Bucharest, Didactic and Pedagogical Publishing House, 1963, 242-266.
- [8] Florea, Julieta, and Valeriu Panaitescu. *Fluid Mechanics / Mecanica fluidelor*. Bucharest, Didactic and Pedagogical Publishing House, 1979, 291-294.
- [9] McElligott, Patrick, Nathan Grund, and Luc Livio. “ME3340 Course Project: Taylor-Couette Flow”, December 6, 2021. Accessed in June 2025. <https://www.youtube.com/watch?v=qb9QjdSTzIQ>.
- [10] Tripton Corp. “Taylor vortex flow Nano Reactor "TVF" Series”, September 27, 2024. Accessed in June 2025. <https://www.youtube.com/watch?v=CI24uxXEwP8>.
- [11] American Physical Society. “Tussle of the Vortices”, November 19, 2021. Accessed in June 2025. [https://www.youtube.com/watch?v=A\\_18yQli8J8](https://www.youtube.com/watch?v=A_18yQli8J8).

## Small-Scale Hydraulic Excavation System for Educational Purposes

Assoc. Prof. PhD. Eng. Ionel Laurențiu ALBOTEANU<sup>1,\*</sup>

<sup>1</sup> 1 University of Craiova, Faculty of Electrical Engineering

\* ialboteanu@em.ucv.ro

**Abstract:** *The paper presents the development of a scaled-down excavation installation model, designed to highlight the operation of the hydraulic system and the electromechanical actuation system. The project aims to replicate the fundamental principles of force transmission through miniaturized hydraulic cylinders, as well as their interaction with the mechanical structure to ensure the characteristic movements of the excavation process. Furthermore, the electromechanical subsystem integrates motors, sensors, and control elements, providing both the actual actuation of the system and the sequential control of operations. This combination enables a small-scale simulation of real working conditions and offers a clear perspective on the interdependence between the mechanical, hydraulic, and electrical subsystems. The model thus serves as a valuable demonstrative and educational tool, contributing to a deeper understanding of the fundamental principles of hydraulic and electromechanical actuations employed in modern excavation installations.*

**Keywords:** Hydraulic drive, excavation system, didactic model

### 1. Introduction

Hydraulic systems employed in excavation equipment represent a key component in the field of mechanical engineering and modern construction, ensuring the efficient conversion of mechanical energy into controlled, high-force motion. These systems operate on the principle of transmitting energy through an incompressible fluid—typically hydraulic oil—for the actuation of the machine's working elements. Owing to their ability to generate substantial forces at controllable speeds, hydraulic installations constitute the preferred solution in lifting, digging, loading, and handling mechanisms for heavy materials [1, 2].

In excavators, the hydraulic system is responsible for operating the boom, stick, and bucket, as well as the rotation mechanisms of the superstructure and the movement of tracks or wheels. The optimal configuration of circuits, accurate component sizing, and the selection of the appropriate pump, valve, and cylinders determine both the performance and reliability of the equipment. The integration of modern technologies, such as proportional electro-hydraulic control and digital monitoring systems, has significantly enhanced energy efficiency while reducing component wear [3, 4].

Therefore, the study of hydraulic excavation systems extends beyond constructive aspects, encompassing a thorough understanding of fluid mechanics phenomena, subsystem interactions, and preventive maintenance strategies. Such analysis is essential for optimizing on-site productivity and ensuring an extended service life of the machinery [5, 6, 7]. In this paper, a small-scale excavation installation model is presented, designed for educational use by students in electrical and mechanical engineering programs.

### 2. Structure of the Hydraulic System of the Excavation Installation

The main components and the corresponding workflow of an excavation installation are outlined below and schematically represented in Figure 1:

- Hydraulic oil reservoir – stores the working fluid, ensuring continuous supply and partial heat dissipation.
- Hydraulic pump – driven by the excavator's internal combustion engine (typically diesel), it converts mechanical energy into hydraulic energy by increasing the fluid pressure.
- Suction and return filters – retain impurities to prevent wear and potential component failure.

- Hydraulic distributors (control valves) – direct the oil flow to the different circuits (boom, stick, bucket, rotation, tracks).
- Hydraulic cylinders – transform hydraulic energy into linear motion for actuating the working elements.
- Hydraulic motors – in certain applications (superstructure rotation, travel), convert hydraulic energy into rotary motion.
- Pipes and high-pressure hoses – ensure fluid transfer between components.
- Safety and control valves – protect the system against overpressure and regulate flow rate and direction.
- Hydraulic oil cooler – maintains the fluid at an optimal temperature for performance and durability.

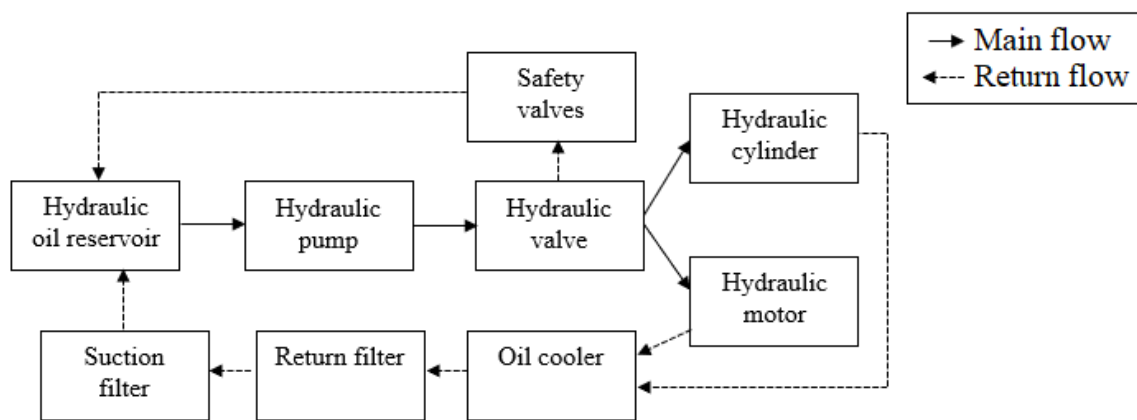


Fig. 1. Block diagram of hydraulic system

For the didactic model, a modular structure of the hydraulic system for the excavation installation was proposed [8]. The scaled-down model comprises the mechanical, hydraulic, electrical, and control subsystems, without including the propulsion system. The proposed structure is illustrated in Figure 2.

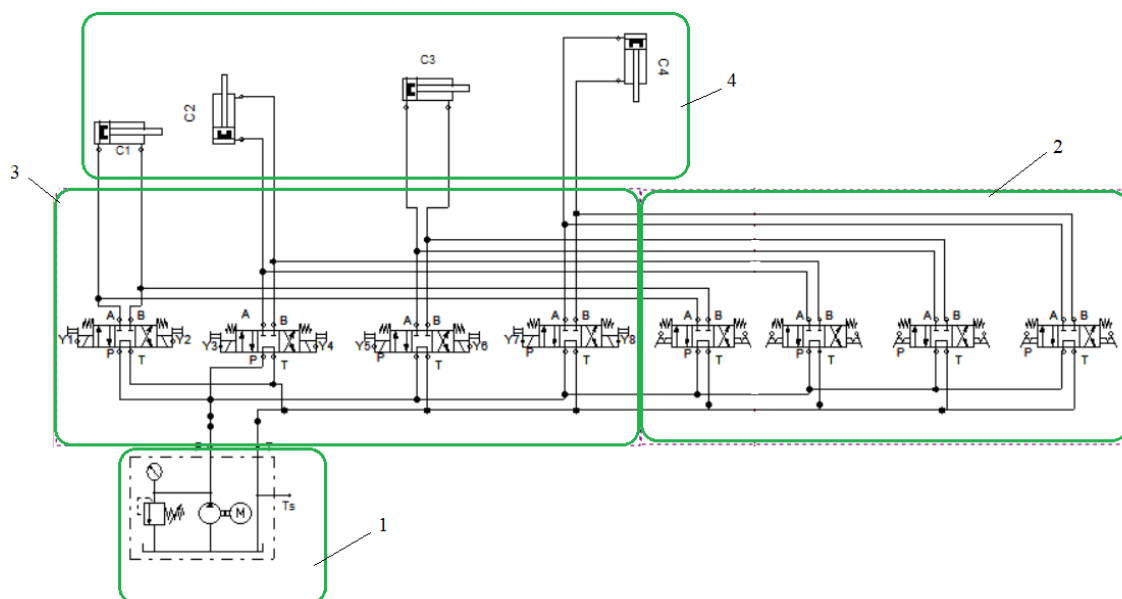


Fig. 2. Structure of the proposed hydraulic system for the excavation installation

The hydraulic system is organized into four modules, as represented in Figure 2:

- 1- Pumping system module
- 2- Mechanically actuated distributor module
- 3- Electrically actuated distributor module
- 4- Hydraulic cylinder module

The hydraulic cylinders shown in the figure have the following designations:

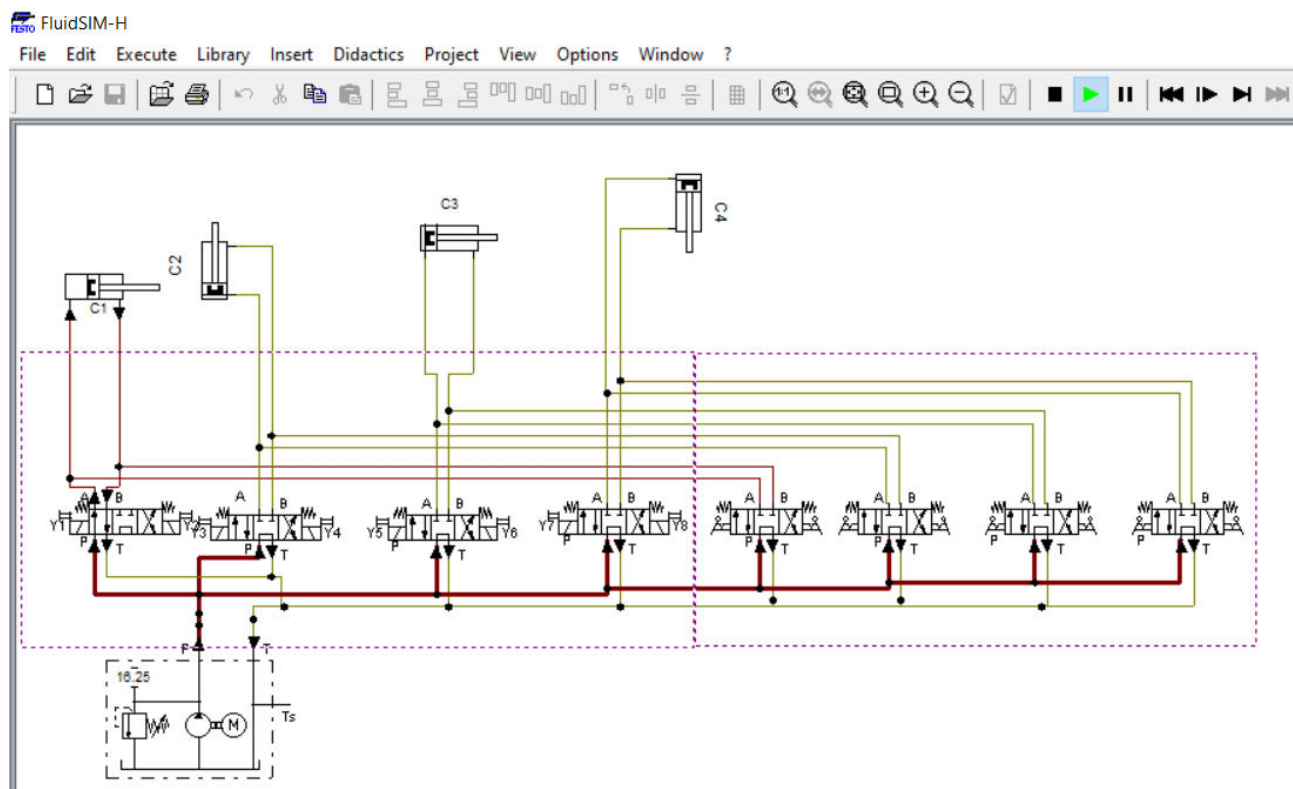
- C1 – hydraulic cylinder for boom rotation
- C2 – hydraulic cylinder for actuating joint 1 of the boom
- C3 – hydraulic cylinder for actuating joint 2 of the boom
- C4 – hydraulic cylinder for actuating the excavator bucket

Since the model was designed for educational purposes, two different types of distributor modules were used in parallel.

### 3. Excavation System Simulation

For simulating the proposed hydraulic installation, the dedicated FluidSIM software was employed. Simulation with FluidSIM enables a clear and interactive visualization of hydraulic actuation processes, thus facilitating the learning of component operating principles (cylinders, valves, pumps, etc.) and their interactions [9, 10, 11, 12].

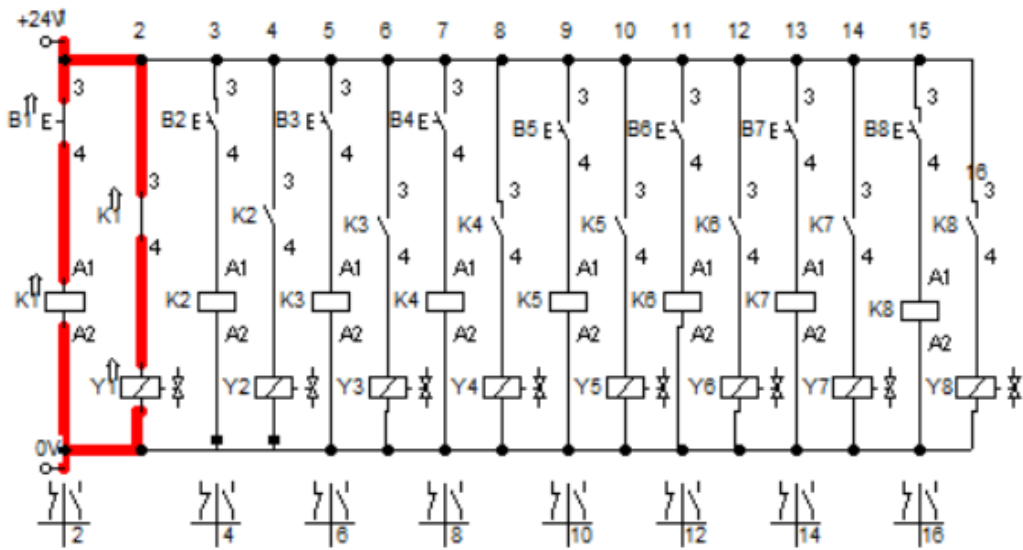
Through simulation, complex hydraulic circuits can be tested and validated without physical risks or material costs, while also eliminating design errors prior to practical implementation. Figure 3 illustrates the program window during the simulation of the C1 cylinder movement.



**Fig. 3.** FluidSim simulation of hydraulic system

For the control of the electrically actuated valves, a command circuit based on contacts and relays was designed (Fig. 4). Figure 4 illustrates the activation of the control sequence for executing the forward stroke of cylinder C1.





**Fig. 4.** Control circuit with contacts and relays for operating the electrically actuated valves

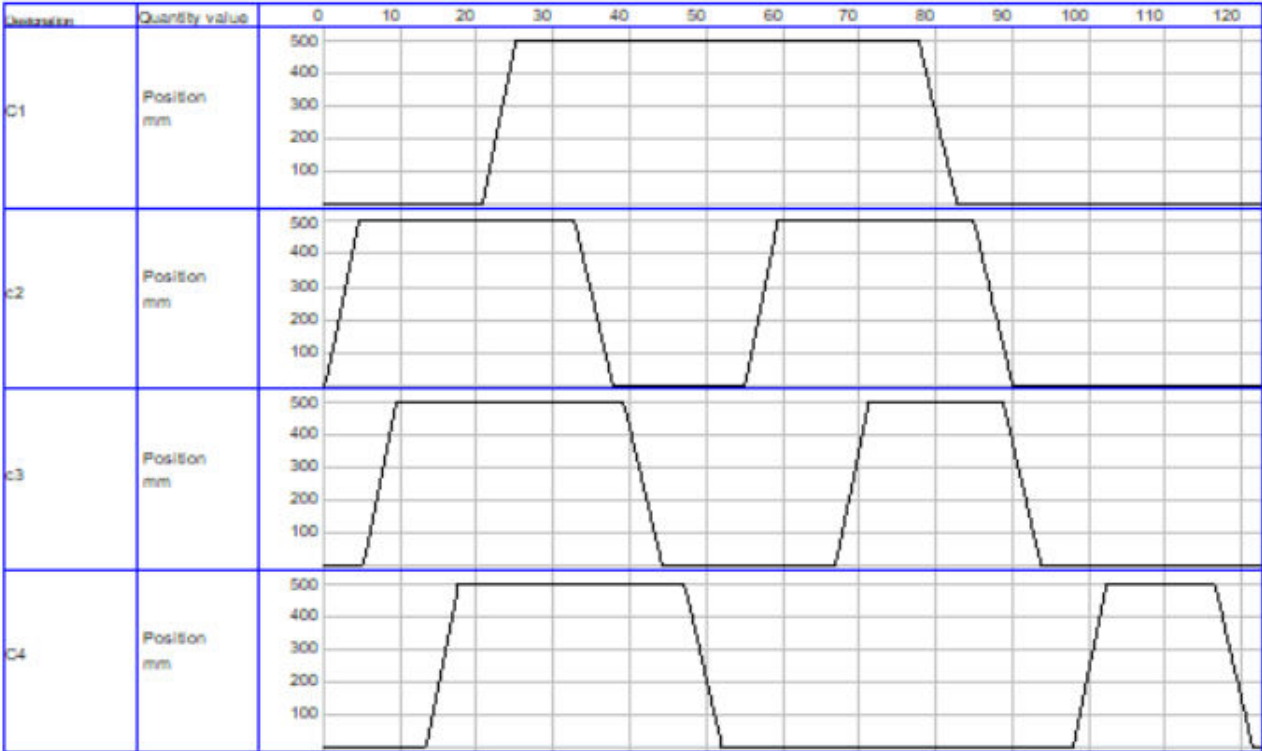
The notations used in the diagram have the following meanings:

B1...B8- control push button;

K1...K8- intermediate relay;

Y1...Y8- valves coils.

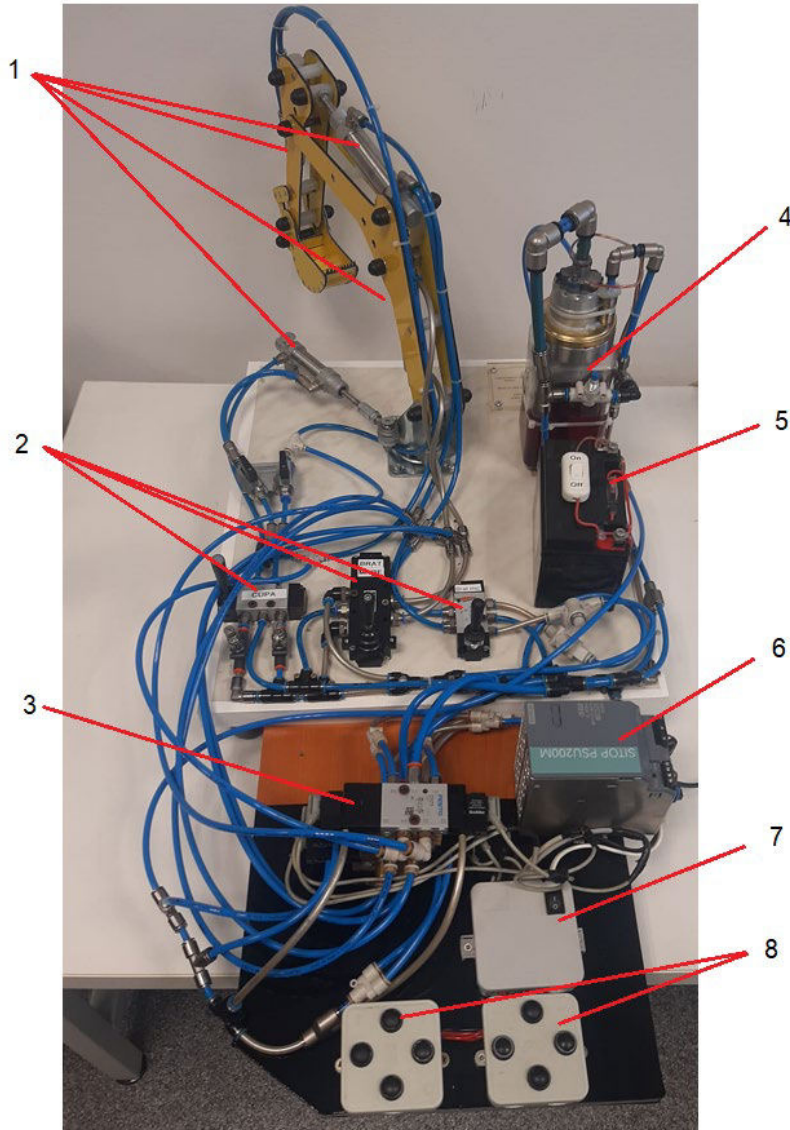
The FluidSIM software enables the display of a state diagram for the elements within the hydraulic actuation system. Figure 5 presents the state diagram of the hydraulic cylinders of the excavation installation during the execution of a work cycle.



**Fig. 5.** State diagram of the cylinders during a work cycle

#### 4. Description of the Educational Model

After completing the simulation using the FluidSIM software, the scaled-down excavation installation model was built (Fig. 6).



**Fig. 6.** Constructed model of the excavation installation

The components of the educational model are as follows:

- 1- Hydraulic cylinders
- 2- Mechanically actuated valves group
- 3- Electrically actuated valves group
- 4- Pumping system
- 5- 12 V DC battery for pump power supply
- 6- 24 V DC power supply for valves coil activation
- 7- Switch for activating the electric control of the valves
- 8- Push buttons for the electrical control of the valves

The inclusion of two types of valves in the model was implemented for educational purposes. Mechanical control is suitable for simple, robust applications where automation is not required. Electrical control is preferred in modern, automated applications that require precision, remote control, and integration into complex systems.

The choice of control method should consider the desired level of automation, system complexity, cost, and operating conditions. In the future, it is planned to complete the model with an automation subsystem (sensors, PLC, display, etc.).

## 5. Conclusions

The hydraulic system realized in the form of a model is capable of performing all the intended functions, with operating parameters consistent with the objectives pursued during its development process.

The model successfully reproduces the fundamental principles of an excavation installation, illustrating the operational workflow and the sequence of technological stages. At a reduced scale, the main mechanisms can be more easily observed and analysed.

The model serves as a valuable tool for presenting the technological process, facilitating the understanding of its operating principles. It is suitable for educational activities, exhibitions, or demonstrations of basic excavation mechanization concepts.

The excavation installation can be further enhanced by integrating automated control systems or simulating real working conditions. It can serve as a foundation for designing more complex experimental models.

## References

- [1] Lee, D., I. Jang, J. Byun, H. Seo, and H.J. Kim. “Real-Time Motion Planning of a Hydraulic Excavator using Trajectory Optimization and Model Predictive Control.” *ArXiv preprint* (2021): arXiv:2107.02366.
- [2] Nisar, Z., and H. Munawar. “System Identification and Controller Design for Hydraulic Actuator.” *ArXiv preprint* (2021): arXiv:2108.11756.
- [3] Ullah, S., Y. Zhou, M. Lai, X. Dong, T. Li, X. Xu, Y. Li, and T. Peng. “Design and Testing for Steel Support Axial Force Servo System.” *ArXiv preprint* (2024): arXiv:2407.19867.
- [4] Liu, J., F. Cheng, X. Guo, Z. Lu, and Z. Li. “Hydraulic System Design of Temporary Support for Fast Excavation of Top Coal.” Paper presented at The 2020 International Symposium on Geographic Information, Energy and Environmental Sustainable Development GIEES 2020, Tianjin, China, December 26-27, 2020. *IOP Conf. Series: Earth and Environmental Science* 772 (2021): 012053.
- [5] Duffy, D. P. “Hydraulic Systems for Excavators.” *GX Contractor*, August 14, 2015. Accessed August 6, 2025. <https://www.gxcontractor.com/equipment/article/13019077/hydraulic-systems-for-excavators>.
- [6] Chen, J. “How Excavator Hydraulics Function.” *YNF Machinery*, November 26, 2024. Accessed August 6, 2025. <https://www.ynfmachinery.com/how-excavator-hydraulics-function/#:~:text=Hydraulic%20systems%20in%20excavators%20provide,lifting%2C%20digging%2C%20and%20moving>.
- [7] Drighiciu, M.A., and I.L. Alboteanu. *Hydraulic and Pneumatic Drives/Acționări hidraulice și pneumatice*. Craiova, Publishing House of University of Craiova, 2017, ISBN 978-606-14-1176-4.
- [8] Alboteanu, I.L. “Pneumatic Tracking System for Photovoltaic Panel.” *Hidraulica Magazine*, no. 1 (March 2015): 32-39.
- [9] Axinte, T., E. Maican, M. Cazacu, E. G. Curcă, L. Calancea, and M. Diaconu. “Simulation and Improvement of Hydraulic Systems with FluidSim.” *Hidraulica Magazine*, no. 2 (June 2025): 48-54.
- [10] Alboteanu, I.L. “Modeling an Automatic Processing Station Using Fluidsim Software.” *Hidraulica Magazine*, no. 3 (September 2017): 27-30.
- [11] Diaconu, M., E. G. Curcă, L. Calancea, T. Axinte, C. Pascu, and I. Tomozei. “Modelling and Simulation of Hydraulic Circuits Using 4/2-Way Hand-Lever Valves.” *Hidraulica Magazine*, no. 2 (June 2024): 41-47.
- [12] FESTO. FluidSIM Hydraulics 4.2, Software, User manual.

## Hydraulic Systems Security: Addressing Cyber Threats with DNA-Based Cryptography in Cloud-Integrated Control

Assoc. Prof. PhD. Eng. Ștefan ȚĂLU<sup>1,\*</sup>

<sup>1</sup> Technical University of Cluj-Napoca, The Directorate of Research, Development and Innovation Management (DMCDI), Constantin Daicoviciu Street, no. 15, Cluj-Napoca, 400020, Cluj county, Romania

\* stefan\_ta@yahoo.com; stefan.talu@auto.utcluj.ro

**Abstract:** Hydraulic control systems, widely used in industrial automation, aerospace, and energy sectors, are increasingly integrated with cloud platforms and Internet of Things (IoT) technologies to enhance monitoring, predictive maintenance, and operational efficiency. However, this digital integration exposes hydraulic infrastructures to a wide range of cyberattacks, including denial-of-service (DoS), ransomware, and advanced persistent threats (APT). Existing cybersecurity solutions for industrial control systems (ICS) rely on conventional cryptographic algorithms such as Advanced Encryption Standard (AES) and Rivest–Shamir–Adleman, which may be resource-intensive and vulnerable in constrained environments. This article explores cybersecurity challenges in hydraulic systems, analyzes real-world attack scenarios, and introduces Deoxyribonucleic Acid (DNA)-based cryptography as a novel, lightweight, and biologically inspired approach for securing cloud-integrated hydraulic infrastructures. Comparative evaluations are shown between DNA-based schemes and lightweight cryptography standards, highlighting performance, scalability, and resistance to classical attacks. Experimental insights, supported by graphical models and tabulated data, demonstrate the feasibility of DNA-based approaches for future-proofing hydraulic cybersecurity.

**Keywords:** Cloud security, cybersecurity, DNA cryptography, industrial control systems, hydraulic systems, IoT security

### 1. Introduction

Hydraulic systems are critical components in powering industrial and infrastructure applications [1–3], including manufacturing plants, heavy machinery, aircraft control surfaces, automotive braking systems, construction equipment, and renewable energy platforms, where their efficiency, reliability, and adaptability are indispensable [4–7].

Recent research has highlighted the growing need to protect hydraulic systems from potential cyber-attacks, particularly as they evolve toward cloud-integrated industrial architectures. The adoption of cloud-based control and monitoring introduces new vulnerabilities, rendering hydraulic systems increasingly susceptible to cyber threats [8–10].

This heightened risk is driven by the proliferation of sensors and IoT-enabled actuators, which enable real-time monitoring, remote operation, and predictive maintenance via cloud platforms [11–14]. While these capabilities enhance operational efficiency and allow advanced analytics for fault detection and remaining useful life estimation, they simultaneously enlarge the attack surface [15], creating opportunities for malicious actors to compromise critical hydraulic operations. Consequently, safeguarding cloud-integrated hydraulic systems has become a strategic priority, motivating research into advanced cybersecurity solutions, including encryption, Deoxyribonucleic Acid (DNA)-based cryptography, and machine learning approaches [16,17].

Industrial Control Systems (ICS), including SCADA and Distributed Control Systems (DCS), form the backbone of modern manufacturing, transportation, and energy infrastructures [18–22]. Traditionally, hydraulic systems operated in isolated environments, but the growing adoption of Industry 4.0 [23] and Industrial Internet of Things (IIoT) [24] paradigms has shifted many operations toward cloud-integrated architectures [25, 26].

Conventional cryptographic techniques, including the Advanced Encryption Standard (AES), Rivest–Shamir–Adleman (RSA) public-key cryptosystem, and Elliptic Curve Cryptography (ECC), are widely employed to ensure the confidentiality, integrity, and authenticity of communications within Industrial Control Systems (ICS) [19]. While these algorithms offer strong security guarantees, their computational complexity and memory requirements render them less suitable



for resource-constrained embedded devices, such as microcontrollers that govern sensors and actuators in hydraulic systems [1, 2]. Furthermore, many legacy ICS communication protocols - such as Modbus Transmission Control Protocol (Modbus/TCP), Distributed Network Protocol version 3 (DNP3), and the International Electrotechnical Commission standard 61850 (IEC 61850)- were originally designed without integrated mechanisms for encryption or authentication [27,28]. Consequently, when these protocols are interfaced with modern cloud-based platforms, they become vulnerable to a range of cyber threats, including man-in-the-middle (MITM) attacks, denial-of-service (DoS) attacks, and unauthorized data injection, thereby compromising both operational reliability and system safety [9, 10, 29].

Several real-world incidents underscore the critical vulnerabilities in ICS. In 2020, the energy sector in Europe experienced a significant uptick in cyberattacks, with 48 successful incidents reported in that year alone. These attacks disrupted various infrastructures, including hydraulic and pneumatic systems integrated with (SCADA) systems, underscoring the vulnerabilities of legacy ICS protocols when extended to cloud-based environments [30].

Traditional security mechanisms rely heavily on symmetric and asymmetric cryptography. However, industrial hydraulic systems often operate with resource-constrained embedded controllers that cannot sustain heavy cryptographic loads. To address this challenge, DNA-based cryptography emerges as a promising solution. By encoding digital information into biologically inspired DNA sequences, this method offers large keyspaces, inherent parallelism, and potential resistance against quantum computing threats [16].

This article aims to (i) review the cybersecurity landscape of hydraulic systems, (ii) analyze vulnerabilities and attack vectors, and (iii) propose DNA-based cryptography as a complementary approach to safeguard cloud-enabled hydraulic infrastructures.

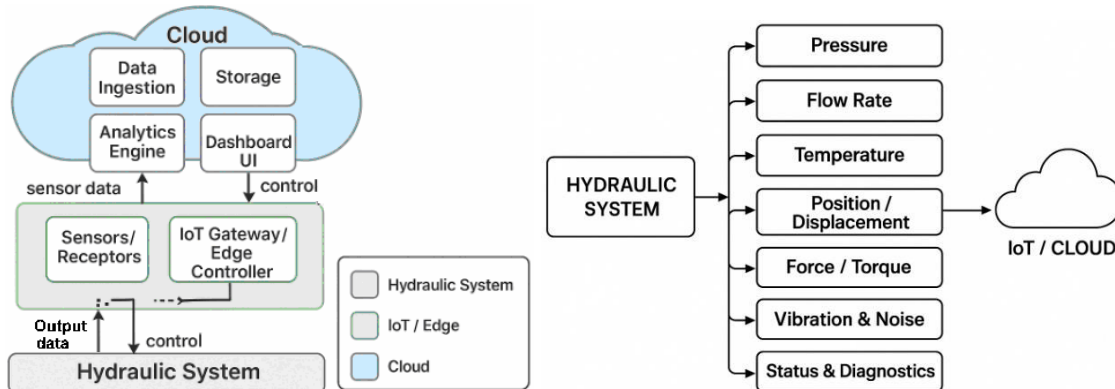
## 2. Hydraulic systems and cloud integration

The integration of cloud technologies into hydraulic control systems has transformed traditional fluid power architectures into intelligent, data-driven infrastructures. Modern hydraulic systems are no longer limited to mechanical and electro-hydraulic components; instead, they embed a network of sensors, actuators, and supervisory controllers capable of continuous data acquisition. Parameters such as pressure, temperature, flow rate, vibration, and fluid quality are monitored in real time and transmitted through industrial communication protocols to higher-level platforms [31]. A critical advancement in this domain is the adoption of edge–cloud frameworks. Edge devices perform preliminary signal processing and anomaly detection close to the machine, thereby reducing latency and communication overhead. Processed or aggregated data is subsequently transmitted to cloud platforms, where advanced analytics, machine learning models, and digital twin simulations are applied. This dual-layer approach allows operators not only to track system health in real time but also to anticipate potential failures before they occur.

In this context, the main output data streams from a hydraulic system arise from embedded sensor networks and represent essential operational variables.

- Pressure data, obtained from pressure transducers, provides information on system load conditions and early indicators of leaks or blockages.
- Flow rate measurements\*, acquired through flow meters, determine actuator speed and detect abnormal consumption patterns.
- Temperature data is monitored to ensure that the hydraulic fluid remains within optimal viscosity ranges, preventing overheating and cavitation.
- Position or displacement feedback, supplied by linear sensors or encoders, enables precise control of actuator movements.
- Force and torque values, either calculated from pressure-area relationships or directly measured by load/torque sensors, provide insight into output performance.
- Vibration and acoustic emissions, captured by accelerometers and microphones, are vital for predictive maintenance and early fault diagnosis.
- Status and diagnostic signals, such as valve positions, oil level, and contamination indicators, complement the data stream by enabling comprehensive system supervision.

Figure 1 illustrates the typical architecture of a cloud-enabled hydraulic system, where field devices connect to edge controllers and cloud servers, as well as the main categories of output data generated from the hydraulic subsystem.



**Fig. 1.** a) Typical architecture of a cloud-integrated hydraulic system (schematic representation); b) Main output data from a hydraulic system.

By enabling predictive maintenance strategies, cloud-integrated hydraulic systems minimize unplanned downtime, extend the operational lifetime of components, and optimize energy consumption. Additionally, the cloud provides scalability and centralized data storage, supporting multi-site monitoring and integration with enterprise-level decision-making tools. In industrial practice, this convergence of hydraulics and cloud computing represents a key enabler for Industry 4.0, where cyber-physical systems enhance efficiency, safety, and resilience in critical infrastructures [32].

## 2.1 Cybersecurity considerations in cloud-enabled hydraulics

While cloud connectivity enhances operational efficiency and enables advanced monitoring capabilities, it simultaneously increases exposure to a broad spectrum of cyber threats. The bidirectional communication between field devices, edge controllers, and cloud servers introduces vulnerabilities that attackers can exploit through weak authentication schemes, unsecured communication protocols, or outdated firmware in programmable logic controllers (PLCs) and edge gateways. Such attack vectors can compromise data integrity, disrupt machine operation, or lead to unauthorized remote manipulation of hydraulic actuators [29-31].

The integration of hydraulic infrastructures into the Industrial Internet of Things (IIoT) also expands the attack surface by interconnecting multiple devices across networks. Cyber adversaries may leverage man-in-the-middle (MitM) attacks, ransomware injection, or cloud API exploitation to interfere with system availability and reliability. In critical applications such as aerospace, energy, or manufacturing, the consequences of such breaches extend beyond financial losses, potentially endangering human safety and environmental sustainability [14,15].

Despite these risks, cloud integration provides significant benefits when combined with robust security architectures. Predictive maintenance algorithms can reduce unplanned downtime, while remote monitoring facilitates real-time oversight of geographically dispersed assets. Additionally, cloud-hosted machine learning models and digital twins optimize resource allocation and operational efficiency. Therefore, the challenge lies in balancing these benefits against the potential cybersecurity threats by embedding encryption protocols, intrusion detection systems, and regular firmware updates into the system design [29,32]. Table 1 summarizes the main benefits and risks associated with cloud integration in hydraulic systems.

**Table 1:** Benefits and risks of cloud integration in hydraulic systems.

Cloud integration benefits	Cybersecurity risks
Predictive maintenance	Increased attack surface
Remote monitoring	Man-in-the-Middle attacks
Data analytics for efficiency	Ransomware injection
Resource optimization	Cloud API exploitation

Building upon these general considerations, the following section outlines the specific categories of cyber threats most relevant to hydraulic infrastructures.

### 3. Cybersecurity threat landscape in hydraulic systems

Hydraulic systems within industrial control networks face diverse cyber threats, many of which parallel those in broader ICS/SCADA systems [8,20]. Common threats include:

1. Denial-of-Service (DoS) attacks – In such scenarios, adversaries deliberately saturate the communication channels that connect programmable logic controllers (PLCs), sensors, and supervisory units. This saturation prevents legitimate control signals from reaching hydraulic actuators, ultimately resulting in system downtime, disrupted fluid regulation, and, in critical infrastructures, potentially catastrophic failures of mission-critical operations.
2. Ransomware infiltrations – Ransomware constitutes one of the most disruptive threats to hydraulic control networks. Malicious code infiltrates the controllers or Human-Machine Interfaces (HMIs), encrypting operational databases, configuration files, or firmware images of hydraulic controllers. System operators are then coerced into paying a ransom to regain access. The consequence is not only economic loss but also operational paralysis, as encrypted systems disable the fine-grained actuation needed for hydraulic safety and stability.
3. Spoofing and data tampering attacks – A particularly insidious threat involves the manipulation of sensor data streams or the injection of falsified telemetry values into the control loop. For hydraulic systems, false readings of pressure, flow rate, or temperature can mislead control algorithms, prompting unsafe actuator commands such as over-pressurization, cavitation-inducing flow changes, or unintended valve closures. Such manipulations jeopardize both physical safety and process integrity.
4. Advanced Persistent Threats (APTs) – Unlike opportunistic attacks, APTs are characterized by their sophistication, longevity, and strategic intent, often attributed to state-sponsored or highly resourced actors. These infiltrations exploit zero-day vulnerabilities and maintain covert access over extended periods, enabling attackers to exfiltrate sensitive operational data, manipulate hydraulic system parameters, or prepare for coordinated sabotage of critical infrastructures such as energy, aerospace, or water distribution systems.

Taken together, these cyber threats highlight the urgent need for holistic security frameworks that integrate cryptographic protections, anomaly detection mechanisms, and resilient control protocols tailored to the unique real-time and safety-critical constraints of hydraulic infrastructures.

### 4. Conventional security mechanisms and their limitations

In response to the cyber threats outlined in the previous section, industrial control environments traditionally rely on well-established security protocols such as Advanced Encryption Standard in Galois/Counter Mode (AES-GCM) for authenticated encryption, RSA-based Public Key Infrastructure (PKI), Transport Layer Security/Secure Sockets Layer (TLS/SSL) protocols for secure communication, and industrial-grade firewalls to enforce network segmentation and access control [31,32]. These mechanisms form the backbone of security architectures in enterprise IT networks and, to a large extent, have been adapted into SCADA and broader ICS. However, when applied to the domain of hydraulic systems integrated into cloud-enabled IIoT infrastructures, several structural limitations emerge that undermine their effectiveness.

- Computational overhead – Most conventional cryptographic primitives, particularly asymmetric algorithms such as RSA or ECC, impose significant processing requirements. Low-power edge controllers and programmable logic controllers (PLCs) commonly used in hydraulic systems are often resource-constrained, with limited CPU cycles, memory, and energy budgets. Implementing heavyweight encryption and authentication routines on these devices can degrade system performance or prove infeasible in real-time operations. Recent advances in WebAssembly (Wasm) offer a potential mitigation, as lightweight Wasm modules enable portable execution of optimized cryptographic routines across heterogeneous devices without requiring full native stacks. This allows critical security functions to be offloaded or modularized while maintaining deterministic performance [33-35].

- Latency sensitivity – Hydraulic systems are inherently time-critical, as fluid pressure regulation, actuator positioning, and valve control must occur within strict temporal boundaries to avoid instability or unsafe operation. Conventional protocols such as TLS, while secure, introduce handshake delays and computational latency. In scenarios involving frequent sensor-actuator feedback loops, even millisecond-scale delays can accumulate, disrupting precise hydraulic actuation or delaying anomaly response. WebAssembly’s near-native execution speeds and sandboxed modules can be deployed at the edge to minimize cryptographic overhead while maintaining security guarantees.

- Key management challenges – Effective deployment of PKI or TLS infrastructures requires secure key generation, distribution, storage, and rotation across a distributed network of field devices. In hydraulic environments, where devices may be geographically dispersed, intermittently connected, or deployed in harsh conditions, maintaining key lifecycles becomes a major operational challenge. Weaknesses in key management create exploitable vulnerabilities, potentially nullifying the intended cryptographic protections.

In addition to cryptographic challenges, cloud-integrated hydraulic systems must also address network-level threats such as distributed denial-of-service (DDoS) attacks, which can disrupt real-time telemetry and actuator control. Recent studies demonstrate that Extended Berkeley Packet Filtering (eBPF) and eXpress Data Path (XDP) technologies in Kubernetes-based deployments can effectively mitigate high-volume traffic attacks, ensuring reliable operation of cloud-enabled IIoT infrastructures [36]. Such network-level defenses complement application-layer encryption, enhancing both security and availability of hydraulic control networks.

- Domain-specific limitations. Standard IT-oriented security mechanisms are not designed for safety-critical, real-time hydraulic infrastructures. Hydraulic controllers must maintain deterministic timing while withstanding environmental stressors such as vibration, electromagnetic interference, and harsh temperature conditions. Conventional cryptographic stacks, optimized for enterprise applications, often fail under these constraints.

These limitations illustrate that while conventional security mechanisms provide a baseline of protection in enterprise settings, they are not inherently optimized for resource-constrained, latency-sensitive, and safety-critical hydraulic infrastructures. As such, there is a growing demand for lightweight cryptographic primitives and domain-specific security frameworks that can deliver strong confidentiality, integrity, and authentication guarantees without overwhelming the computational or temporal constraints of hydraulic controllers. Such innovations represent a crucial step toward securing hydraulic systems against the evolving cyber threat landscape in Industry 4.0 environments.

## 5. DNA-Based Cryptography: a novel paradigm

DNA-based cryptography represents an emergent frontier in secure information processing, leveraging the inherent biochemical properties of nucleic acids to encode, transmit, and manipulate data in a manner fundamentally distinct from conventional digital cryptosystems [16]. By mapping binary information onto the four nucleotide bases—adenine (A), thymine (T), cytosine (C), and guanine (G)—these schemes exploit the combinatorial complexity of DNA sequences, offering an exponentially large keyspace and biologically inspired mechanisms for encryption and obfuscation. The versatility of DNA as an information carrier allows for innovative encoding strategies such as substitution, mutation, crossover, and logical operations, which mimic natural genomic processes, thereby introducing an additional layer of cryptographic unpredictability [16, 37-39].

A growing body of research has begun to formalize specific algorithmic implementations within this paradigm. One such approach is the Bi-directional DNA Encryption Algorithm (BDEA), initially proposed for securing cloud environments. BDEA achieves two-tier protection by converting Unicode plaintext into binary, mapping the binary digits to DNA bases (e.g., 00→A, 01→T, 10→G, 11→C), and applying polymerase chain reaction (PCR) amplification before transmission. Secure key exchange in this context is achieved through traditional mechanisms such as the Diffie–Hellman protocol, underscoring the potential of hybrid DNA–classical cryptosystems for practical deployment [40].

Other innovations include DNA steganography methods, such as least significant base (LSBase) substitution, where cryptographic keys are embedded within codons without altering the amino acid



they encode. This subtle manipulation enables hidden key distribution while maintaining biological plausibility. Additionally, schemes combining One-Time Pad (OTP) encryption with DNA encoding exploit the near-unbreakable nature of OTP while leveraging the vast storage capacity of DNA sequences to manage long random keys. Multi-layer constructions further enhance resilience by embedding encrypted DNA messages within cover sequences, thereby integrating secrecy with authenticity [40]. Beyond these methods, more biologically inspired models draw upon transcription and translation analogies, where plaintext is encoded into DNA, then virtually “expressed” into RNA and protein forms according to genetic codon mappings. This multi-step transformation increases resistance to classical cryptanalytic techniques by complicating the relationship between ciphertext and original message. Similarly, “three-dimensional DNA-level permutations”—which reorganize elements within a 3D DNA matrix—introduce additional confusion and diffusion properties. By randomizing positional assignments, such schemes enhance robustness against known-plaintext and structural attacks [40].

Key advantages of DNA-based cryptography include [16, 37-40]:

- **Exponentially large keyspace:** The combinatorial permutations of nucleotide sequences permit key sizes that surpass those of classical symmetric and asymmetric algorithms, effectively mitigating brute-force attacks and enhancing resistance to exhaustive key search.
- **Massive parallelism:** Analogous to biological replication and hybridization, DNA computing paradigms enable the simultaneous processing of multiple encryption/decryption operations, significantly improving throughput for complex cryptographic tasks.
- **Potential quantum resistance:** Unlike traditional algebraic-based ciphers, DNA cryptographic schemes rely on biochemical operations and sequence manipulations that are currently resistant to known quantum algorithms, such as Shor’s or Grover’s algorithm, suggesting a viable pathway toward post-quantum security.
- **Adaptability for constrained environments:** Although still in experimental stages, DNA-inspired encoding strategies can be optimized for low-resource environments, offering a promising complement to lightweight cryptography for IoT devices and ICS.

**Table 2:** Comparative features of cryptographic methods

Feature	AES-128	RSA-2048	ASCON-128	DNA-Crypto (Hybrid)
Keyspace size	$2^{128}$	$2^{2048}$	$2^{128}$	$>2^{4096}$
Computational overhead	High	Very High	Low	Moderate
Quantum resistance	Weak	Weak	Moderate	Strong (potential)
Suitability for IoT/ICS	Limited	Very Limited	High	Promising

*Note: DNA-Crypto (Hybrid) refers to a DNA-based cryptographic scheme that combines multiple encoding or processing techniques rather than relying on a single DNA-inspired operation.*

In essence, DNA-based cryptography leverages natural information-processing mechanisms to expand secure communication paradigms and, as computational biology advances, promises to complement lightweight and post-quantum schemes in constrained environments—including IoT-enabled hydraulic systems—offering energy-efficient, low-latency, and memory-conscious alternatives while enabling hybrid and error-tolerant implementations. Such approaches can enhance the security of real-time hydraulic control networks by protecting sensor-actuator communications against interception and tampering, ensuring operational reliability and data integrity in industrial and cloud-integrated systems.

## 6. Integration and performance evaluation of DNA-Based cryptography in IoT-Enabled Hydraulic Systems

### 6.1 System model and simulation setup

To evaluate the feasibility of DNA-based cryptography for IoT-enabled hydraulic control networks, we designed a hybrid experimental–simulation framework reflecting real industrial conditions. The setup combined a hydraulic subsystem, embedded controllers, IoT sensor nodes, and cloud-based analytics infrastructure.

The hydraulic plant was modeled as an axial piston pump operating in a closed-loop turbine control configuration. The working fluid circuit was parameterized with the following realistic specifications:

Maximum operating pressure: 10 MPa ( $\approx 100$  bar); Nominal flow rate: 120 l/min; Operating fluid temperature: 60 °C under steady-state conditions; Control loop: pump–valve–actuator circuit with vibration monitoring to capture transient anomalies. Although the system focuses on axial piston pumps, previous studies on centrifugal pumps have provided valuable insights into cavitation, lubrication, and wear phenomena, which are generally relevant for understanding hydraulic pump behavior in industrial environments [41, 42]. Additionally, micro- and nanoscale surface characterization methods offer critical insights into wear patterns and frictional behavior of hydraulic components, supporting predictive maintenance and system degradation assessment [43]. The supervisory logic and cryptographic operations were executed on a PLC-class microcontroller representative of resource-constrained industrial controllers: Device: STM32F0 Cortex-M0, 48 MHz clock; Memory footprint: 32 KB SRAM, 128 KB Flash; RTOS: deterministic scheduler with microsecond-level task granularity; Time synchronization: Precision Time Protocol (PTP, IEEE 1588) for jitter minimization.

The field layer consisted of distributed IoT nodes integrated into the hydraulic loop: 20 pressure and flow sensors (payloads: 128–4096 bytes per message); 5 actuator nodes controlling proportional valves and servo-driven actuators; Sampling rate: 1 Hz (low-load mode) and 50 Hz (stress-test mode); Network jitter:  $\pm 2$  ms added to emulate non-deterministic industrial networks.

Telemetry was securely transmitted to the cloud for storage, analytics, and anomaly detection: Cloud platform: AWS IoT Core, with 1 Gbps virtualized backbone for data streaming; Real-time analytics: machine learning models for anomaly detection and predictive maintenance (e.g., cavitation, leakage, seal wear); Communication protocol: MQTT over TLS 1.3 (persistent connections maintained, since session resumption is not currently supported by AWS IoT Core).

1. The following cryptographic algorithms were evaluated:

- No-Enc (Baseline) – no encryption applied.
- AES-128 – conventional symmetric encryption.
- ASCON-128 – NIST-approved lightweight authenticated cipher.
- PRESENT-80 – lightweight block cipher.
- SPECK-64 – lightweight block cipher optimized for constrained devices.
- DNA-Crypto (Hybrid) – biologically inspired hybrid encoding combining mutation, substitution, and logical operations for encryption and integrity protection.

2. Simulation assumptions: • Deterministic RTOS scheduling; • TLS 1.3 for secure cloud communication; • Message streams at 1 msg/s and 50 msgs/s; • Edge clocks synchronized using Precision Time Protocol (PTP); • Jitter added to emulate realistic industrial networks.

## 6.2 Performance metrics

The evaluation focused on the following metrics:

1. Latency per packet (ms). Latency per packet measures the time it takes for a single data packet to travel from a source (sensor/actuator) to the destination (controller or cloud) and optionally back. It reflects the responsiveness of the system.
2. Throughput (kbps). Throughput represents the rate at which data is successfully transmitted over a communication channel.
3. ROM/RAM footprint (KB). Memory footprint quantifies the storage and operational memory required by firmware, software modules, and buffers on the microcontroller.
4. CPU load (%). CPU load indicates the fraction of processor cycles consumed during operation relative to total available cycles.
5. Mitigation success (%) against replay, injection, and DoS attacks. Measures the effectiveness of implemented security mechanisms in preventing or mitigating specific cyberattacks.
6. End-to-end cloud latency (ms). Total time taken for data to traverse the entire system, from sensor/actuator through the network, processing nodes, cloud server, and back. Includes transmission, queuing, processing, and response delays.

## 6.3 Results and discussions

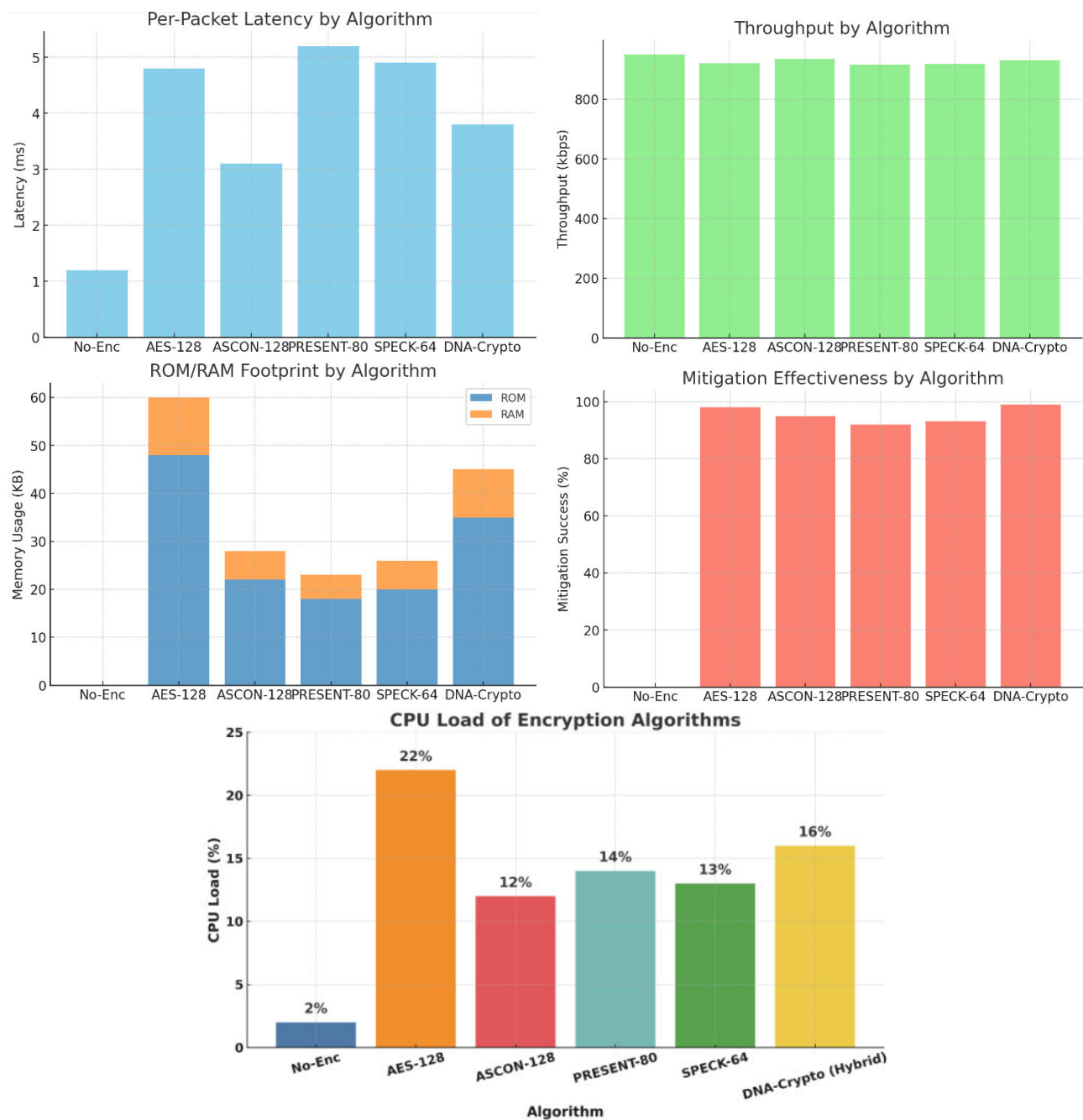
The performance and security metrics of six lightweight cryptographic algorithms—No-Enc, AES-128, ASCON-128, PRESENT-80, SPECK-64, and DNA-Crypto (Hybrid)—were evaluated in the context of resource-constrained IoT systems. The results, presented in Table 3 and figure 2,



highlight key aspects such as latency, throughput, memory usage, CPU load, and mitigation success against potential attacks.

**Table 3:** Simulation results summary

Algorithm	Latency (ms)	Throughput (kbps)	Memory Usage (ROM / RAM KB)	CPU load (%)	Mitigation success (%)
No-Enc	1.2	950	0 / 0	2	0
AES-128	4.8	920	48 / 12	22	98
ASCON-128	3.1	935	22 / 6	12	95
PRESENT-80	5.2	915	18 / 5	14	92
SPECK-64	4.9	918	20 / 6	13	93
DNA-Crypto (Hybrid)	3.8	930	35 / 10	16	99



**Fig. 2.** a) Per-Packet Latency by Algorithm. b) Throughput by Algorithm; c) ROM/RAM Footprint by Algorithm; d) Mitigation Effectiveness by Algorithm; e) CPU load by Algorithm.

Latency and throughput are critical parameters for evaluating the efficiency of cryptographic algorithms in real-time applications. In our experiments, No-Enc exhibited the lowest latency (1.2 ms) and highest throughput (950 kbps), as expected due to the absence of encryption. However, this comes at the cost of security, with a mitigation success rate of 0%. Among the encryption algorithms, ASCON-128 demonstrated a balanced performance with a latency of 3.1 ms and throughput of 935 kbps. This is consistent with findings from a study that reported ASCON's efficient performance on Arduino devices, achieving a throughput of approximately 550 cycles/byte (NIST Computer Security Resource Center). AES-128, while widely recognized for its security, exhibited higher latency (4.8 ms) and lower throughput (920 kbps) compared to ASCON-128. This aligns with literature indicating that AES-128 requires significantly more processing cycles per byte than lightweight ciphers, resulting in higher latency and reduced throughput on resource-constrained microcontrollers such as STM32F0-class devices. PRESENT-80 and SPECK-64 offered competitive performance with latencies of 5.2 ms and 4.9 ms, and throughputs of 915 kbps and 918 kbps, respectively. These results corroborate with existing research highlighting the suitability of PRESENT and SPECK for low-latency applications due to their lightweight design. The DNA-Crypto (Hybrid) algorithm achieved a latency of 3.8 ms and throughput of 930 kbps, demonstrating its potential for secure communication in IoT systems. This is supported by studies exploring DNA-based cryptographic systems, which have shown promising results in terms of speed and memory efficiency.

Memory usage is a pivotal factor in the deployment of cryptographic algorithms on microcontrollers with limited resources. No-Enc required no additional memory for encryption processes, thus consuming 0 KB of ROM and RAM. AES-128 necessitates 48 KB of ROM and 12 KB of RAM, reflecting its complex key scheduling and encryption rounds. This substantial memory requirement can be a limiting factor in memory-constrained devices. ASCON-128 is designed to be memory-efficient, utilizing 22 KB of ROM and 6 KB of RAM. This efficiency makes it suitable for IoT devices with stringent memory constraints. PRESENT-80 and SPECK-64 also demonstrate low memory usage, with PRESENT-80 requiring 18 KB of ROM and 5 KB of RAM, and SPECK-64 requiring 20 KB of ROM and 6 KB of RAM. These characteristics are advantageous for deployment in embedded systems. The DNA-Crypto (Hybrid) algorithm consumed 35 KB of ROM and 10 KB of RAM, as shown in Table 3, confirming its moderate but feasible footprint.

CPU load is an important indicator of how much processing power is consumed by the cryptographic algorithm. No-Enc has a minimal CPU load of 2%, as it performs no encryption. AES-128 exhibits a higher CPU load of 22%, reflecting its computational complexity. This increased load can impact the performance of other tasks on the device. ASCON-128 maintains a moderate CPU load of 12%, balancing security and efficiency. PRESENT-80 and SPECK-64 have CPU loads of 14% and 13%, respectively, indicating their lightweight nature and suitability for resource-constrained environments. The DNA-Crypto (Hybrid) algorithm's CPU load is 16%, being typically designed to minimize CPU usage, ensuring efficient operation in IoT devices.

In terms of mitigation success against potential attacks, AES-128 achieved a high success rate of 98%, demonstrating its robustness. ASCON-128 and SPECK-64 also showed strong mitigation success rates of 95% and 93%, respectively. PRESENT-80 had a mitigation success rate of 92%, while DNA-Crypto (Hybrid) achieved the highest rate at 99%, indicating its strong security posture.

## 7. Conclusions

As hydraulic systems evolve into cloud-integrated cyber-physical infrastructures, they face increasingly complex cybersecurity threats arising from connectivity, remote monitoring, and IoT-enabled sensors. Conventional cryptographic approaches, such as AES and lightweight ciphers (PRESENT, SPECK, ASCON), provide robust protection; however, their computational and memory demands, as well as latency constraints, can limit their applicability on microcontroller-constrained industrial controllers. This study demonstrates that DNA-based cryptography represents a promising alternative, leveraging the vast combinatorial potential of biological DNA sequences. Experimental results indicate that hybrid DNA-based schemes, while incurring slightly higher computational costs than classical lightweight ciphers, achieve superior mitigation success against replay, injection, and DoS attacks without significantly compromising throughput or latency.

The DNA-Crypto (Hybrid) algorithm, in particular, exhibited a balanced performance profile with moderate CPU load (16%), memory usage of 35 KB ROM / 10 KB RAM, and mitigation success of 99%, making it suitable for real-time, secure hydraulic control applications. Comparative analysis with conventional lightweight algorithms confirms that AES-128 offers strong security but is less practical for resource-limited controllers due to its elevated CPU load and memory footprint. ASCON-128 and SPECK-64 remain viable for latency-sensitive operations but provide slightly lower resilience against sophisticated attacks. A hybrid cryptographic framework, employing DNA-based encryption for cloud-level communication and lightweight ciphers for local real-time loops, emerges as a practical, forward-looking strategy. Such an approach balances security, performance, and energy efficiency while remaining compatible with emerging technologies, including Digital Twins, AI-driven anomaly detection, and blockchain-based logging for auditability and operational integrity. Overall, DNA-based cryptography presents a compelling paradigm for future hydraulic cyber-physical systems, offering enhanced protection against evolving cyber threats, operational robustness, and scalability for IoT-enabled industrial infrastructures. Future research should focus on hardware-software co-design, cross-layer security integration, and real-world deployment studies to fully exploit the potential of this biologically inspired cryptographic approach.

**Conflicts of Interest:** The author declares no conflict of interest.

**ORCID:** Ștefan Țălu, <https://orcid.org/0000-0003-1311-7657>.

## References

- [1] Zhang, Qin. *Basics of Hydraulic Systems*, 2<sup>nd</sup> Edition. CRC Press, Boca Raton, 2019. <https://doi.org/10.1201/9780429197260>.
- [2] Manning, Noah D., and Roger C. Fales. *Hydraulic Control Systems*. John Wiley & Sons, Inc., 2019. <https://doi.org/10.1002/9781119418528>.
- [3] Țălu, Mihai, Ștefan Țălu, and Mircea Rădulescu. *Fluid Mechanics. Volumetric and hydrodynamic machines. Theory and simulation*, Craiova, Universitaria Publishing House, 2011. ISBN 978-606-14-0035-5.
- [4] Darshan, Katgeri, and Basavaraj Hubballi. "A review & progress on digital hydraulic pumps and valves." *Hidraulica Magazine*, no. 1 (2019): 116-123.
- [5] Țălu, Ștefan. "Assessing the remaining useful life of hydraulic pumps: a review." *Hidraulica Magazine*, no. 3 (2024): 7-18.
- [6] Țălu, Ștefan. "New developments in intelligent diagnostic methods for hydraulic piston pumps faults." *Hidraulica Magazine*, no. 4 (2024): 7-16.
- [7] Țălu, Ștefan. "Insights on hydroponic systems: understanding consumer attitudes in the cultivation of hydroponically grown fruits and vegetables." *Hidraulica Magazine*, no. 1 (2024): 56-67.
- [8] Bhamare, Deval, Maede Zolanvari, Aiman Erbad, Raj Jain, Khaled Khan, and Nader Meskin. "Cybersecurity for industrial control systems: A survey." *Computers & Security* 89 (2020): 101677. <https://doi.org/10.1016/j.cose.2019.101677>.
- [9] Md Enam, Mahfuzur Rahman, Md Mofakhkharul Islam Joarder, MD Toukir Yeasir Taimun, and S. M. Mobasshir Islam Sharan. "Framework for Smart SCADA Systems: Integrating Cloud Computing, IIoT, and Cybersecurity for Enhanced Industrial Automation." *Saudi Journal of Engineering and Technology* 10, no. 4 (2025): 152-158.
- [10] Țălu, Mircea. "Exploring machine learning algorithms to enhance cloud computing security." *Digital Technologies Research and Applications* 4, no. 2 (2025): 33–47. <https://doi.org/10.54963/dtra.v4i2.1272>.
- [11] Dallaev, Rashid, Tatiana Pisarenko, Ștefan Țălu, Dinara Sobola, Jiří Majzner, and Nikola Papež. "Current applications and challenges of the Internet of Things." *New Trends In Computer Sciences* 1, no. 1 (2023): 51–61. <https://doi.org/10.3846/ntcs.2023.17891>.
- [12] Nazarov, Anton D., Dmitriy M. Nazarov, and Ștefan Țălu. "Information security of the Internet of Things." Paper presented at the International Scientific and Practical Conference on Computer and Information Security (INFSEC 2021), Yekaterinburg, Russia, April 5-6, 2021. <https://doi.org/10.5220/0010619900003170>.
- [13] Țălu, Ștefan. "Strategic measures in improving cybersecurity management in micro and small enterprises." Paper presented at the 2nd International Scientific and Practical Conference on Digital Economy (ISCDE 2020), Yekaterinburg, Russia, November 5-6, 2020. Appolloni, A., F. Caracciolo, Z. Ding, P. Gogas, G. Huang, G. Nartea, T. Ngo, W. Strielkowski, and S. Joshi (eds.). *Advances in Economics, Business and Management Research (AEBMR)* 156 (2020): 522-528. <https://doi.org/10.2991/aebmr.k.201205.087>.

- 
- [14] Țălu, Mircea. "Security and privacy in the IIoT: threats, possible security countermeasures, and future challenges." *Computing & AI Connect* 2 (2025): 0011. <https://doi.org/10.69709/CAIC.2025.139199>.
- [15] Țălu, Mircea. "Cyberattacks and cybersecurity: concepts, current challenges, and future research directions." *Digital Technologies Research and Applications* 4, no. 1 (2025): 44–60. <https://doi.org/10.54963/dtra.v4i1.919>.
- [16] Țălu, Mircea. "DNA-based cryptography for internet of things security: concepts, methods, applications, and emerging trends". *Buletin Ilmiah Sarjana Teknik Elektro* 7, no. 2 (2025): 68–94. <https://doi.org/10.12928/biste.v7i2.12942>.
- [17] Yong, Bang Xiang, and Alexandra Brintrup. "Multi Agent System for Machine Learning Under Uncertainty in Cyber Physical Manufacturing System." Paper presented at the International Workshop on Service Orientation in Holonic and Multi-Agent Manufacturing SOHOMA 2019, Valencia, Spain, 3-4 October 2019. In: Borangiu, T., D. Trentesaux, P. Leitão, A. Giret Boggino, and V. Botti (eds.) *Service Oriented, Holonic and Multi-agent Manufacturing Systems for Industry of the Future. Studies in Computational Intelligence* 853 (2020). Springer, Cham. [https://doi.org/10.1007/978-3-030-27477-1\\_19](https://doi.org/10.1007/978-3-030-27477-1_19).
- [18] Drias, Zakarya, Ahmed Serhrouchni, and Olivier Vogel. "Analysis of cyber security for industrial control systems." Paper presented at the 2015 International Conference on Cyber Security of Smart Cities, Industrial Control System and Communications (SSIC), Shanghai, China, August 5-7, 2015. <https://doi.org/10.1109/SSIC.2015.7245330>.
- [19] Arora, Pallavi, Baljeet Kaur, and Marcio Andrey Teixeira. "Security in Industrial Control Systems Using Machine Learning Algorithms: An Overview." In: Fong, S., N. Dey, and A. Joshi (eds.) *ICT Analysis and Applications. Lecture Notes in Networks and Systems* 314 (2022). Springer, Singapore. [https://doi.org/10.1007/978-981-16-5655-2\\_34](https://doi.org/10.1007/978-981-16-5655-2_34).
- [20] Hoday, Aydin, Christos Chrysoulas, Brahim El Boudani, Mario de Sousa, and Martin Wollschlaeger. "A security and authentication layer for SCADA/DCS applications." *Microprocessors and Microsystems* 87 (2021): 103479. <https://doi.org/10.1016/j.micpro.2020.103479>.
- [21] Ara, Anees. "Security in Supervisory Control and Data Acquisition (SCADA) based Industrial Control Systems: Challenges and Solutions." Paper presented at the International Conference on Sustainability: Developments and Innovations (ICSIDI-2022), Riyadh, Saudi Arabia, February 19-22, 2022. *IOP Conference Series: Earth and Environmental Science* 1026 (2022): 012030. <https://doi.org/10.1088/1755-1315/1026/1/012030>.
- [22] Robles-Durazno, Andres, Naghmeh Moradpoor, James McWhinnie, Gordon Russell, and Jorge Porcel-Bustamante. "Implementation and Evaluation of Physical, Hybrid, and Virtual Testbeds for Cybersecurity Analysis of Industrial Control Systems." *Symmetry* 13, no. 3 (2021): 519. <https://doi.org/10.3390/sym13030519>.
- [23] Brandstetter, Reinhard, Till Deubel, Rudolf Scheidl, Bernd Winkler, and Klaus Zeman. "Digital hydraulics and "Industrie 4.0"." *Proceedings of the Institution of Mechanical Engineers, Part I: Journal of Systems and Control Engineering* 231, no. 2 (2016): 82-93. <https://doi.org/10.1177/0959651816636734>.
- [24] Jing, Yongfeng, Haiyan Yang, Jian Jiao, Chen Lu, and Hongyan Dui. "IoT-Enhanced Fault Diagnosis and Two-Stage RUL Prediction Method for Aircraft Hydraulic Systems Based on Sensor Data." *IEEE Sensors Journal* 25, no. 16 (2025): 31391-31402. <https://doi.org/10.1109/JSEN.2025.3585130>.
- [25] Kumares, P. S., E. Sivanantham, L. K. Shoba, W. D. Priya, N. Mohankumar, and B. Elango. "Real-Time Hydraulic Fluid Leak Detection in Heavy Machinery Using Cloud-Integrated Wireless Sensor Networks for Proactive Maintenance." Paper presented at the 2024 10th International Conference on Communication and Signal Processing (ICCSP), Melmaruvathur, India, April 12-14, 2024. <https://doi.org/10.1109/ICCSP60870.2024.10543226>.
- [26] Chen, Gang, Wanshun Zhang, Xin Liu, Hong Peng, Feng Zhou, Hao Wang, Qian Ke, and Boyang Xiao. "Development and application of a multi-centre cloud platform architecture for water environment management." *Journal of Environmental Management* 344 (2023): 118670. <https://doi.org/10.1016/j.jenvman.2023.118670>.
- [27] Grzesik, Piotr, and Dariusz Mrozek. "Combining Machine Learning and Edge Computing: Opportunities, Challenges, Platforms, Frameworks, and Use Cases." *Electronics* 13, no. 3 (2024): 640. <https://doi.org/10.3390/electronics13030640>.
- [28] Belchandan, Rakesh Kumar, and Aamir Akhtar. "Comparative Analysis of DNP3 and IEC 61850 from Architectural, Data Mapping, Data Modeling and Data Reporting View." Paper presented at the 2023 North American Power Symposium (NAPS), Asheville, NC, USA, October 15-17, 2023. <https://doi.org/10.1109/NAPS58826.2023.10318666>.
- [29] Ahmad, Waqas, Aamir Rasool, Abdul Rehman Javed, Thar Baker, and Zunera Jalil. "Cyber Security in IoT-Based Cloud Computing: A Comprehensive Survey." *Electronics* 11, no. 1 (2022): 16. <https://doi.org/10.3390/electronics11010016>.
- [30] Alomari, Mohammad Ahmed, Mohammed Nasser Al-Andoli, Mukhtar Ghaleb, Reema Thabit, Gamal Alkaws, Jamil Abedalrahman Jamil Alsayaydeh, and AbdulGuddoos S. A. Gaid. "Security of Smart Grid:



- Cybersecurity Issues, Potential Cyberattacks, Major Incidents, and Future Directions." *Energies* 18, no. 1 (2025): 141. <https://doi.org/10.3390/en18010141>.
- [31] Jurayev Aburaykhon, Kholikulovich, and Suhrobkhon Jafar Ugli Tojiboyev. "Possibilities of using digital technologies in control and management of hydraulic facilities." *Academic Research in Educational Sciences* 4, no. 2 (2023): 89-92.
- [32] Kumar, Krishna, and R.P. Saini. "Data-driven internet of things and cloud computing enabled hydropower plant monitoring system." *Sustainable Computing: Informatics and Systems* 36 (2022): 100823. <https://doi.org/10.1016/j.suscom.2022.100823>.
- [33] Țălu, Mircea. "A review of vulnerability discovery in WebAssembly binaries: insights from static, dynamic, and hybrid analysis." *ACTA TECHNICA CORVINIENSIS – Bulletin of Engineering* 17, no. 4 (2024): 13-22.
- [34] Țălu, Mircea. "A review of advanced techniques for data protection in WebAssembly." *ANNALS of Faculty of Engineering Hunedoara, International Journal of Engineering* 22, no. 4 (2024): 131-136.
- [35] Țălu, Mircea. "A comparative study of Webassembly runtimes: performance metrics, integration challenges, application domains, and security features." *Archives of Advanced Engineering Science* (2025): 1–13. <https://doi.org/10.47852/bonviewAAES52024965>.
- [36] Țălu, Mircea. "DDoS Mitigation in Kubernetes: A Review of Extended Berkeley Packet Filtering and eXpress Data Path Technologies." *JUTI: Jurnal Ilmiah Teknologi Informasi (Scientific Journal of Information Technology)* 23, no. 2 (2025): 60-73. <https://doi.org/10.12962/j24068535.v23i2.a1268>.
- [37] Namasudra, Suyel, and Ganesh Chandra Deka. *Advances of DNA Computing in Cryptography*, 1st ed. New York, Chapman and Hall/CRC. 2018. <https://doi.org/10.1201/9781351011419>.
- [38] Niu, Ying, Kai Zhao, Xuncai Zhang, and Guangzhao Cui. "Review on DNA Cryptography." Paper presented at the 14th International Conference, BIC-TA 2019, Zhengzhou, China, November 22–25, 2019. Pan, L., J. Liang, and B. Qu. (eds.). *Bio-inspired Computing: Theories and Applications*, BIC-TA 2019 (2020): 1160. [https://doi.org/10.1007/978-981-15-3415-7\\_11](https://doi.org/10.1007/978-981-15-3415-7_11).
- [39] Chu, Ling, Yanqing Su, Xiangyu Yao, Peng Xu, and Wenbin Liu. "A Review of DNA Cryptography." *Intelligent Computing* 4 (2025): 0106. <https://doi.org/10.34133/icomputing.0106>.
- [40] Gao, Jiechao, and Tiange Xie. "Chapter three - DNA computing in cryptography." Namasudra, S. (ed.). *Advances in Computers* 129 (2023): 83-128. <https://doi.org/10.1016/bs.adcom.2022.08.002>.
- [41] Țălu, Ștefan. "Signal Processing Techniques and Mathematical Modeling for Analyzing and Diagnosing Cavitation in Centrifugal Pumps." *Hidraulica Magazine*, no. 1 (2025): 13-26.
- [42] Țălu, Ștefan. "Tribological Mechanisms in Water Hydraulic Axial Piston Pumps: Insights into Lubrication, Cavitation, and Wear Control." *Hidraulica Magazine*, no. 2 (2025): 7-18.
- [43] Țălu, Ștefan. *Micro and nanoscale characterization of three dimensional surfaces. Basics and applications*. Cluj-Napoca, Napoca Star Publishing House, 2015.

## Solar Drying in Controlled Environments: Sustainable Solution for Preserving Vegetable Products

Dipl. Eng. **Alina - Iolanda POPESCU**<sup>1,\*</sup>, PhD. Eng. **Gheorghe ȘOVĂIALĂ**<sup>1</sup>,  
PhD. Eng. **Gabriela MATACHE**<sup>1</sup>

<sup>1</sup> National Institute of Research & Development for Optoelectronics/INOE 2000, Subsidiary Hydraulics and Pneumatics Research Institute/IHP, Romania

\* alina.ihp@fluidas.ro

**Abstract:** *The paper analyzes the drying process of vegetable products using solar systems, as an efficient and sustainable solution for reducing food losses. The fundamental differences between natural drying and dehydration are presented, as well as the technological classification of solar dryers (direct, indirect, mixed), depending on the operating mode (passive vs. active). The heat transfer principles involved (convection, radiation) are highlighted and the contribution of the constructive elements to optimizing energy efficiency is detailed. The application part includes a calculation breviary for sizing a convective dryer with a solar air collector, highlighting the correlation between the useful thermal power, the collector surface area, the operating mode and the water evaporation requirements. The results emphasize the potential of these systems in small and medium-scale agri-food and industrial applications.*

**Keywords:** Solar dryers, calculation breviary, dryer types

### 1. Introduction

Food waste is one of the most pressing challenges of our time. According to the Food and Agriculture Organization of the United Nations (FAO), approximately one third of global food production is lost along the chain from harvest to consumption, which is equivalent to approximately 930 million tons annually. Among the major causes are inadequate infrastructure for storing and preserving food, especially fruits and vegetables, which leads to product degradation, reduced supply and, implicitly, increased prices.

To counteract these effects, food preservation becomes essential, aiming to extend shelf life and maintain nutritional and organoleptic qualities. Among the traditional preservation methods, drying stands out as one of the oldest and most widely used techniques. It usually involves exposing food products to direct sunlight, thus reducing their humidity and, implicitly, their weight. By removing water – a key factor in the initiation of biological and chemical reactions that lead to food spoilage – drying allows for long-term storage and easy transport of products [1,3].

In recent decades, solar energy has become an increasingly viable option in the context of fossil fuel depletion and environmental pollution concerns. Being a renewable, free and abundant source, solar energy is frequently used in thermal processes, including food drying [2]. However, conventional solar drying has a number of disadvantages: significant heat loss, risk of contamination with impurities, exposure to weather and pest attacks.

To overcome these limitations, solar drying systems have been developed in controlled environments, which allow for the maintenance of optimal and constant temperatures. These modern solar dryers use dedicated equipment to capture and convert solar radiation into heat, thus improving the efficiency of the process compared to direct solar drying [4]. The essential difference between conventional solar drying and solar dryers lies in the control of the drying environment and the use of solar energy harvesting technology. The applicability of solar dryers has expanded beyond the agricultural field, finding applications in industries such as food (seafood), pharmaceuticals, paper, ceramics, and biomass processing [5].



## 2. Considerations regarding the drying process of vegetable products

Drying of vegetables and fruits is the technological process by which the natural water content is reduced to a level that prevents the activity of microorganisms, without destroying the tissues or depreciating the food value of the products.

The set of phenomena that occur during drying leads to the concentration of dry matter, the reduction of the volume of raw materials used, the increase in food value per unit weight and more or less profound physicochemical changes in the state of membranes and cellular components, which are externalized by the limits of the rehydration capacity.

Dehydration is the process by which fruits and vegetables lose a certain amount of water, as a result of which a conducive physicochemical state to maintaining their nutritional value and qualitative attributes is achieved: taste, smell, aroma.

Drying differs from dehydration by the lack of regulation of temperature, relative humidity and air movement, for which purpose the expression natural drying is also used, unlike dehydration, which is artificial drying.

In the first case, by simple exposure to air and ambient temperature, the moisture is removed from the products through the evaporation process. In the second case, to continue the dehydration process, an additional heat input is used, the water removal being done through the vaporization process.

Evaporation occurs by the passage of water in a vapor state in an environment in which, in addition to water vapor, there is also air and other gases, and vaporization by the passage of water in a vapor state, in an environment in which there is only water vapor.

The fruit and vegetable drying installation in which the air movement is done by itself, based on the thermal difference between the atmosphere in the drying chamber and the external atmosphere is known in the specialized literature as an *evaporator*.

The rate of dehydration depends on the relative humidity of the air in the installation; the lower it is, the shorter the drying time. If the temperature of the air in the drying installation increases, the relative humidity of the air decreases, so it will be able to take on new amounts of water vapor. On the contrary, if the air temperature decreases, it will become saturated with water vapor, and if it decreases even more, the water vapor in the air will condense. This is the *dew point* or dew temperature.

Therefore, during the drying process, the air in the installation must be in continuous circulation and be heated, in order to increase its capacity to take on new amounts of water vapor.

In drying installations, water evaporation occurs both based on the temperature difference between that of the product being dried and that of the heated air, and especially through the difference between the vapor pressure inside the tissues and that of the vapor contained in the air in the installation. Evaporation is also influenced by the surface tension (force) of the water vapor in the product. Evaporation occurs until an equilibrium is reached between the vapor pressures of the two media, in other words until the warm air in the installation has been saturated with water vapor.

## 3. Theoretical foundations of solar drying

Regardless of the constructive configuration, all types of solar dryers operate on the same fundamental principle: the removal of water from food by evaporation, a process determined by the transfer of heat to the product. This transfer can be achieved by convection, radiation or a combination of the two, depending on the technical solution adopted [6].

Over time, numerous researchers have developed and tested various configurations of solar dryers, evaluating them from the point of view of energy efficiency and the quality of the products obtained. Their classification can be done according to several factors: the direction and mechanism of hot air circulation, the type of heat transfer or the way in which solar radiation is captured and used [7].

### 3.1 Types of solar dryers

There are 3 types of solar dryers:

### • Direct-type dryers (Fig. 1)

In this variant, the products are directly exposed to solar radiation inside a chamber covered with a transparent cover, which allows the radiation to pass through, but provides protection against external factors (precipitation, dust, pests) [8].



Fig. 1. Direct-type dryers

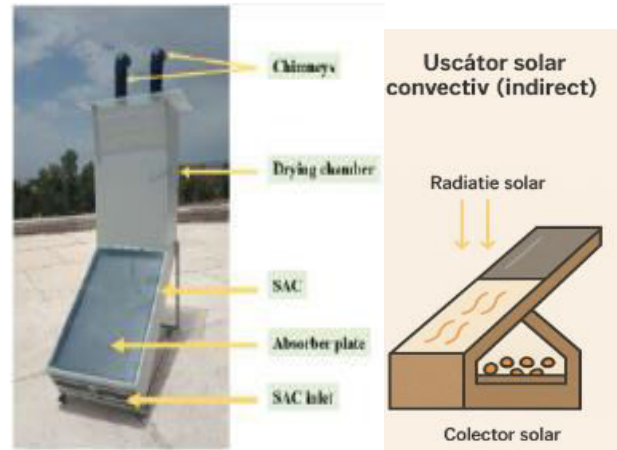
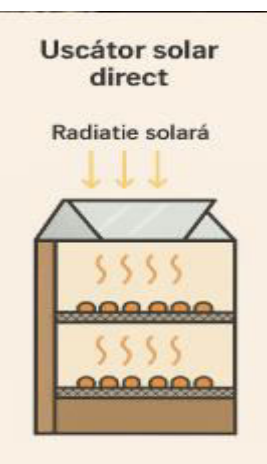


Fig. 2. Indirect-type dryers

### • Indirect-type dryers (Fig. 2)

In this case, the air is heated in a solar collector and then directed to the drying chamber, where the heat is transferred to the product by convection. This method offers better control over the process and higher thermal efficiency [8].

### • Mixed dryers (Fig. 3)

These systems combine the advantages of the direct and indirect types: the products are simultaneously exposed to direct solar radiation and preheated air. Heat transfer occurs both by convection and radiation, which accelerates the drying process and improves the uniformity of the results [9,10].

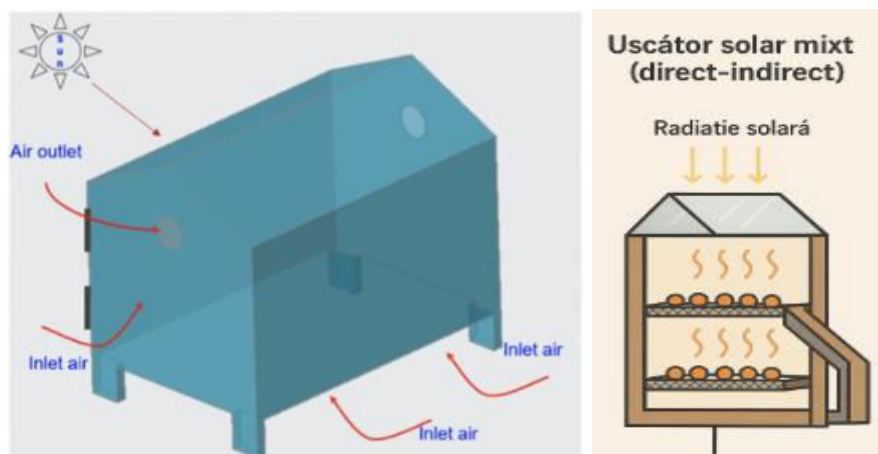


Fig. 3. Mixed dryers

## 3.2 Operating mode: passive vs. active

### • Passive systems

These are direct-type dryers. In these dryers, air circulates naturally through the thermal effect of buoyancy or pressure differences. They usually consist of a drying chamber with transparent covers and openings for ventilation. Solar radiation penetrates the chamber, heating the opaque walls and generating a greenhouse effect that facilitates product drying. Passive dryers are simple,

economical and suitable for small volumes of fruit, vegetables or cereals. However, their efficiency varies between 20–40%, depending on climatic conditions and system geometry [11].

The limitations related to the low air circulation speed can lead to product overheating and quality loss. For this reason, passive dryers are rarely used for intensive loads or sensitive products [12].

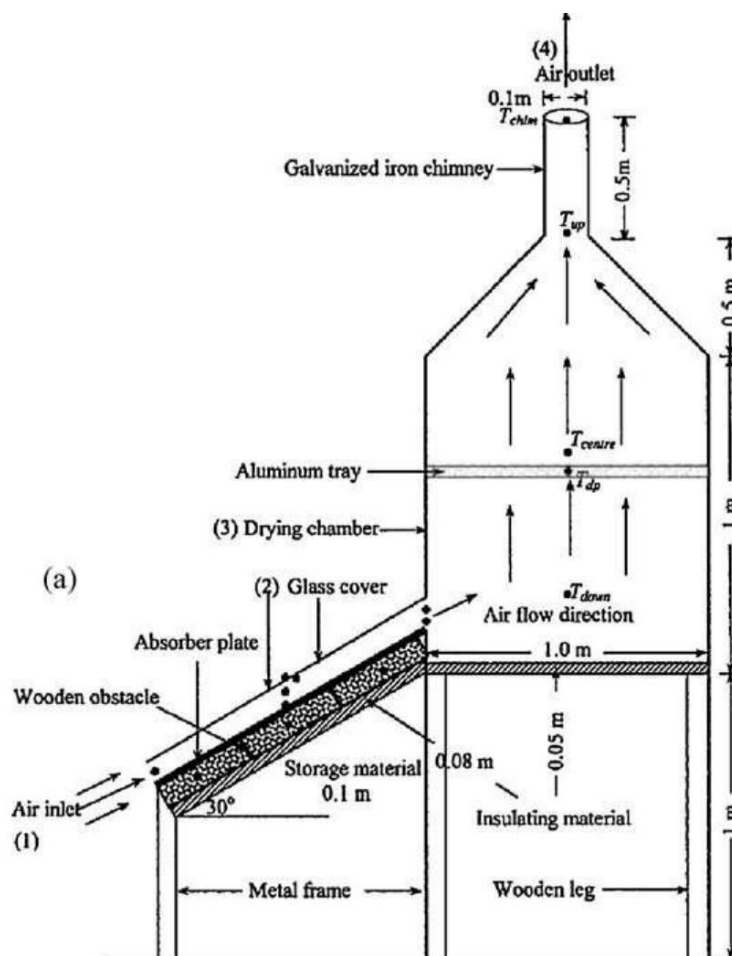
- **Active systems**

These can be indirect or mixed-type dryers. In these installations, air circulation is achieved by force, using fans or blowers, allowing for more precise control over the process. They are recommended for products with high humidity (e.g. tomatoes, kiwi, papaya), offering reduced drying times and minimal quality losses. The integration of external heat sources or preheating systems contributes to uniform and efficient drying, even in adverse weather conditions [12].

Studies show that the use of active systems, in combination with thermal energy storage components, can increase the efficiency of the process by up to 28%. For example, in arid conditions, drying meat with direct and indirect active systems has demonstrated efficiencies of 7–10% and 15–18%, respectively.

### 3.3 Hybrid solar drying systems

Hybrid systems integrate solar drying with *other energy sources or auxiliary technologies* to increase efficiency and process continuity. They may include *thermal energy storage systems* (TES), *solar electrical components* (SES), or *phase change materials* (PCM), which allow drying to be extended outside of direct sunlight hours [13].



**Fig. 4.** The operating principle of a dryer using solar energy [14]

A relevant example is the hybrid solar-LPG dryer, built in Mexico, which achieved a 75% moisture reduction of nopal and achieved a solar fraction of 80%. The system combines direct and indirect heating sources, along with a backup system, and has demonstrated an economic payback period between 28 and 68 months [14] - fig.4.

### 3.4 Optimizing dryer performance

To improve the efficiency of the drying process, *numerous technical innovations can be applied*:

- the use of collectors with an extended surface and high roughness for increased turbulence and more efficient heat transfer;
- fans driven by photovoltaic panels, to reduce operating costs;
- air collectors with multiple passes (double/triple), to intensify the air flow;
- thermal energy storage systems, for continuous drying outside the sun's intervals.

All these improvements contribute to increasing yield, reducing process time and maintaining the quality of food products, especially in rural or medium- and large-scale agricultural applications.

## 4. Calculation breviary (sizing) for a solar-heated convective dryer with air collector

### 4.1. Theoretical framework and basic equation

For a solar-heated convective dryer with air collector, *the instantaneous useful thermal power* is classically expressed by the relationship:

$$P_u = G[W/m^2] \times A[m^2] \times \eta_c$$

where the parameters of instantaneous useful thermal power (Table 1) are:

**Table1:** The parameters of instantaneous useful thermal power

Symbol	Significance	Typical values from literature
G	solar irradiation on the collector surface	600 – 800 W m <sup>-2</sup> as a daily average; can reach ≈ 1000 W m <sup>-2</sup> at noon on clear days [15,16]
A	useful collector area	established at design
η <sub>c</sub>	instantaneous collector efficiency	0.30 – 0.75 (30 – 75 %) as a function of geometry and air flow [15,17]

### 4.2. Available thermal power range

Combining the limits in the tables, the instantaneous useful thermal power can be evaluated:

- **Minimally realistic:**  $G=600 \text{ W m}^{-2}$ ;  $\eta_c=0,30 \Rightarrow P_u \approx 180 \text{ W m}^{-2}$
- **Reported maximum:**  $G=1000 \text{ W m}^{-2}$ ;  $\eta_c=0,75 \Rightarrow P_u \approx 750 \text{ W m}^{-2}$

This results in a practical range of 0.18 – 0.75 kW for each m<sup>2</sup> of collector.

### 4.3 Numerical example (instantly)

Common assumptions in fruit/vegetable dryer design work:

- sunny day,  $G=800 \text{ W m}^{-2}$
- glazed flat collector,  $\eta_c=0.60$  (typical forced yield)
- collector surface  $A=2.0 \text{ m}^2$

$P_u = G \cdot A \cdot \eta_c = 800 \cdot 2.0 \cdot 0.60 \approx 960 \text{ W}$  (0.96 kW), so, almost 1 kW of useful heat is instantly available for heating the drying air.

### 4.4. Daily useful energy and water evaporation capacity

$$E_{\text{useful}} = P_u[\text{kW}] \cdot t[\text{operating hours/day}] = 0.96 \cdot 8 = 7.68 \text{ kWh} (\approx 27.648 \text{ MJ})$$

$$1 \text{ kWh} = 3.6 \text{ MJ}; 1 \text{ MJ} = 0.277778 \text{ kWh}$$

In relation to the drying requirements of vegetable products, the specialized literature mentions the *thermal energy required to evaporate one kg of water in solar/hybrid convective dryers*, depending on the product and configuration [18] at 12.6 – 38 MJ.

Therefore, with 27.648 MJ available, the following amounts of water can be removed from the product daily:

- to superior efficiency ( $12.6 \text{ MJ kg}^{-1}$ )  $\rightarrow \approx 2.194 \text{ kg}$
- to medium efficiency ( $25 \text{ MJ kg}^{-1}$ )  $\rightarrow \approx 1.105 \text{ kg}$ .

This calculation confirms that **the sizing of the collector surface** (Table 2) must be correlated with:

1. the amount of water to be removed per batch,
2. the desired drying time,
3. the overall efficiency (collector + chamber + air flow).

**Table 2:** The sizing of the collector surface

Steps	Algorithm	Observations
1.	The following are determined: product mass and humidity that must be eliminated	Determine the amount of water to be removed [kg]
2.	The $E_{\text{specific}}$ value ( $\text{MJ kg}^{-1}$ ) is chosen from the bibliography for a similar product/construction.	Lower values for forced mix-mode dryers, higher for passive ones
3.	Calculate the total energy required $E_{\text{tot}}$ .	$E_{\text{tot}} = m_{\text{water}} \times E_{\text{specific}}$
4.	The daily operating duration (h) is chosen and the average power required $P_{\text{med}}$ is determined.	$P_{\text{med}} = E_{\text{tot}}/t$
5.	The equation $P_u = GA\eta_c$ is used, with the average value of $G$ from the respective location.	The area $A$ is dimensioned.

The process parameters and equations used to estimate the performance of the solar dryer are given below.

$m_i$  = mass of the sample before drying;

$m_f$  = mass of the sample after drying.

Humidity content of the sample:

$$m_w = m_i - m_f \text{ (kg)} \quad (1)$$

Amount of heat required to evaporate the humidity:

$$Q = m_w \times h_{fg} \text{ (kJ)} \quad (2)$$

where  $h_{fg}$  = is the latent heat of water vaporization (kJ/kg).

$$\text{Average drying rate} = \frac{m_w}{m_i \times t_{\text{total of drying}}} \text{ (kg / kgh)} \quad (3)$$

The energy efficiency of the greenhouse solar dryer is estimated by:

$$\eta_{\text{energ}} = \frac{Q_d}{Q_c} \quad (4)$$

where the heat used for drying (dissipated heat),  $Q_d$  is:

$$Q_d = \frac{Q}{t_{\text{total of drying}}} = \frac{Q}{8 \times 3600} \quad (5)$$

and the heat received by the collector,  $Q_c$  is:



$$Q_c = (\alpha \times I \times A_c) - h \times A_c \times (T_1 - T_5) \quad (6)$$

To determine the convection heat transfer coefficient,  $h$  (W/m<sup>2</sup>K),

$$T_e = T_1 - 0.25 (T_1 - T_5) \quad (7)$$

For the air drying agent, the *parameters leading to the calculation of the convection heat transfer coefficient  $h$*  are the thermal conductivity of the acrylic collector  $k$  (W/mK), the Nusselt number  $Nu$  and the vertically length  $L$ .

$$h = \frac{Nu \cdot k}{L} \quad (8)$$

$$Nu = 0.56 (Gr \times Pr \times \cos\theta)^{0.25} \quad (9)$$

where  $Gr$  is Grashof number,  $Pr$  is Prandtl number,  $\theta = 23^\circ$ .

$$Gr = \frac{g \beta L^3}{\gamma^2} \Delta T, \text{ where } \beta = \frac{1}{T_5 + 273} \quad (10)$$

$\gamma$  (m<sup>2</sup> / s) is the kinematic viscosity and  $g$  (m/s<sup>2</sup>) is the gravitational acceleration.

Average drying rate,  $V_{m\ us}$ :

$$V_{m\ us} = \frac{m_w}{m_i \cdot t_{us}} \quad (11)$$

where  $t_{us}$  is total drying time.

The nomenclature of quantities in the equations above:

$T_1$  = Temperature of the glass exterior (°C)

$T_2$  = Temperature of the glass interior (°C)

$T_3$  = Temperature of the drying enclosure (°C)

$T_4$  = Temperature of the output air (°C)

$T_5$  = Ambient (atmospheric) temperature (°C)

$T_e$  = Exterior (outlet from the drying chamber) temperature (°C)

$H_1$  = Relative humidity of the exterior surface (%)

$H_2$  = Relative humidity of the interior surface (%)

$H_3$  = Relative humidity of air in the drying enclosure (%)

$H_4$  = Relative humidity of air at the output (%)

$\alpha$  = Acrylic collector absorption = 0.26

$I$  = Average intensity of solar radiation per day (W/m<sup>2</sup>)

$A_c$  = Surface of the collecting plate = 0,1375 m<sup>2</sup>

$g$  = Gravitational acceleration (m/s<sup>2</sup>)

$h$  = Thermic transfer coefficient by convection (W/m<sup>2</sup>K)

$Nu$  = Nusselt number

$Gr$  = Grashof number

$Pr$  = Prandtl number

$k$  = Thermal conductivity of acrylic collector (W/mK)

$\gamma$  = Cinematic viscosity (m<sup>2</sup> /s)

$L$  = Vertically length on which the heat transfer occurs by free convection (m)

## 5. Useful conclusions from the specialized literature

Based on what is presented in the article, it can be observed that food waste is a major problem globally, and one of its main causes is the lack of effective preservation solutions, especially for perishable products such as fruits and vegetables.

Food drying is a traditional, efficient and accessible method of preservation, which contributes to extending the shelf life of products, reducing their volume and facilitating transport.

The use of **solar energy** in the drying process offers a sustainable alternative, with reduced impact on the environment, in the context of the depletion of conventional resources and increasing energy costs.



**Solar dryers in controlled environments** – whether direct, indirect, mixed, passive or active – allow the optimization of the dehydration process by maintaining stable thermal conditions and reducing the risks of contamination.

Also, from the specialized literature it is observed that:

- Glazed flat-plate collectors with fins can exceed  $\eta_c \approx 0.70$ , especially at high forced air flows [15].
- In tropical/semi-arid climates, a design heat flux of  $400\text{--}500\text{ W m}^{-2}$  is usually used, offering a reasonable compromise between surface area and cost.
- Reduction of specific energy ( $\text{MJ kg}^{-1}$ ) is achieved by partial air recirculation and latent heat storage (PCM). Recent examples have dropped to  $\approx 12\text{ MJ kg}^{-1}$  [18].

The literature places the instantaneous solar thermal power between  $0.18$  and  $0.75\text{ kW per m}^2$  of collector; choosing average values ( $\approx 0.4\text{--}0.5\text{ kW m}^{-2}$ ) realistic estimates can be made for most small convective dryers. The final sizing must always be linked to the specific drying energy of the product and the overall efficiency of the system.

**Active and hybrid** systems, which use auxiliary components such as fans, multiple air collectors or thermal energy storage, significantly improve the drying efficiency and allow the technology to be used even in adverse weather conditions.

Modeling the drying process and **correctly sizing the installations** based on physical and energy parameters ensures operating efficiency and constant results, being essential in the design of high-performance solar dryers.

Expanding the use of these technologies in rural areas or in industries with limited access to conventional energy can significantly contribute to reducing post-harvest losses and increasing food security.

### Acknowledgments

This work was supported by a grant of the Ministry of Research, Innovation and Digitization, CCCDI - UEFISCDI, project number PN-IV-P7-7.1-PTE-2024-0039, within PNCDI IV.

### References

- [1] Ahmad, M., J.C. Hauser, C. Heijnen, and M.A. Chaudry. “Solar drying of fruits and vegetables.” *Pakistan Journal of Agricultural Research* 17, no. 3 (2002): 237–244.
- [2] Scheer, Hermann. *The Solar Economy: Renewable Energy for a Sustainable Global Future*, vol. 3. Earthscan Publications Ltd., 2002.
- [3] Fortunatus, R., R. Marealle, N. Nenguwo, and T. Stoilova. *Solar Dryers. Principles and basics*. World Vegetable Center, 2017.
- [4] Rajkumar, P., S. Kulanthaisami, G.S.V. Raghavan, Y. Gariépy, and V. Orsat. “Drying Kinetics of Tomato Slices in Vacuum Assisted Solar and Open Sun Drying Methods.” *Drying Technology* 25, no. 7-8 (2007): 1349-1357.
- [5] Wafa, B.C., M. Ahmed, M.E.A. Slimani, L. Akil, A. Hamid, and A. Khellaf. “Experimental investigation of an active direct and indirect solar dryer with sensible heat storage for camel meat drying in Saharan environment.” *Solar Energy* 174 (April 2018): 328-341.
- [6] Chavan, A., V. Vitankar, A. Mujumdar, and B. Thorat. “Natural convection and direct type (NCDT) solar dryers: a review.” *Drying Technology* 39, no. 13 (2021): 1969-1990.
- [7] Mohana, Y., R. Mohanapriya, T. Anukiruthika, K.S. Yoha, J.A. Moses, and C. Anandharamakrishnan. “Solar dryers for food applications: Concepts, designs, and recent advances.” *Solar Energy* 208 (September 2020): 321-344.
- [8] Ameri, B., S. Hanini, A. Benhamou, and D. Chibane. “Comparative approach to the performance of direct and indirect solar drying of sludge from sewage plants, experimental and theoretical evaluation.” *Solar Energy* 159 (January 2018): 722-732.
- [9] Shalaby, S.M., M.A. Bek, and A.A. El-Sebaili. “Solar dryers with PCM as energy storage medium: a review.” *Renewable and Sustainable Energy Reviews* 33 (May 2014): 110-116.
- [10] Dhalsamant, K., P.P. Tripathy, and S.L. Shrivastava. “Heat transfer analysis during mixed-mode solar drying of potato cylinders incorporating shrinkage: Numerical simulation and experimental validation.” *Food and Bioprocess Processing* 109 (May 2018): 107-121.
- [11] Udomkun, P., S. Romuli, S. Schock, B. Mahayothee, M. Sartas, T. Wossen, E. Njukwe, B. Vanlauwe, and J. Müller. “Review of solar dryers for agricultural products in Asia and Africa: An innovation landscape approach.” *Journal of Environmental Management* 268 (August 2020): 110730.

- [12] Chauhan, P.S., A. Kumar, C. Nuntadusit, and J. Banout. “Thermal modeling and drying kinetics of bitter gourd flakes drying in modified greenhouse dryer.” *Renewable Energy* 118 (April 2018): 799-813.
- [13] Mishra, L., A. Sinha, and R. Gupta. “Recent Developments in Latent Heat Energy Storage Systems Using Phase Change Materials (PCMs)—A Review.” Paper presented at The 1st International Conference on Green Buildings and Sustainable Engineering GBSE 2018, Kochi, India, January 24-25, 2018.
- [14] Fudholi, A., K. Sopian, M.H. Ruslan, M.A. Alghoul, and M.Y. Sulaiman. “Review of solar dryers for agricultural and marine products.” *Renewable & Sustainable Energy Reviews* 14, no. 1 (January 2010): 1-30.
- [15] Gulcimen, F., H. Karakaya, and A. Durmus. “Drying of sweet basil with solar air collectors.” *Renewable Energy* 93 (August 2016): 77-86.
- [16] Lingayat, A.B., V.P. Chandramohan, V.R.K. Raju, and V. Meda. “A review on indirect type solar dryers for agricultural crops – Dryer setup, its performance, energy storage and important highlights.” *Applied Energy* 258 (January 2020): 114005.
- [17] Prakash, O., V. Laguri, A. Pandey, A. Kumar, and A. Kumar. “Review on various modelling techniques for the solar dryers.” *Renewable and Sustainable Energy Reviews* 62 (September 2016): 396-417.
- [18] Alinia, A.M., and M. Sheikholeslami. “Development of a new solar system integrating photovoltaic and thermoelectric modules with paraffin-based nanomaterials.” *Scientific Reports* 15 (2025): 1336.

## The Volumetric Efficiency of Water Ram

MSc. Osvaldo Antonio PACHECO BUSQUET<sup>1,\*</sup>, DrC. Celestino Santos ORO ORTIZ<sup>2</sup>,  
Ing. Ángel Arsenio PACHECO MONTEAGUT<sup>3</sup>

<sup>1</sup> Solar Energy Research Center, Santiago de Cuba, Cuba

<sup>2</sup> West University, Santiago de Cuba, Cuba

<sup>3</sup> Worker particular, Santiago de Cuba, Cuba

\* opachecob61@gmail.com

**Abstract:** *In the present work the research problem related to the low and limited efficiency of hydraulic rams is addressed, for whose solution the behavior physical process of the volumetric efficiency of the multipulsor hydraulic ram was taken as an object of investigation, and as a field of action: The mathematical process to determine the relation of the volume of the air chamber with the volumetric efficiency of the multipulsor hydraulic ram. The modeling of the field of action is carried out with the nonlinear regression tool and the least square method, closely related to the steps to develop an investigation, finding the solution with the help of Microsoft Excel software. The objective of the investigation: To model the volumetric efficiency of the hydraulic ram in direct and inversely proportional relation with the volume of the air chamber, and of the pumping pipe respectively.*

**Keywords:** *Hydraulic ram, air chamber, hammers water, volumetric efficiency, pumping pipe, hydraulic friction*

### 1. Introduction

The hydraulic ram pump is a device that uses the energy of a waterfall to generate power and continuously raise a percentage of the incoming water to a height greater than the drop height [1]. Its operation is based on the cyclical phenomenon known as "water hammer," which is repeated indefinitely if there is no dissipating force. Previous work has already defined the influence of the relationship between the dimensions of the supply pipes and the impulse valves on the efficiency of the ram [1]; the research problem is objectively related to the low and limited efficiency of ram pumps, and the solution to improve it. The efficiency of the hydraulic ram is relatively lower than that of other pumps [2]. The documentary analysis carried out revealed that in one hundred and fifty portable document formats, only three of them carried out experiments related to the air chamber, and in a fourth we found a basis for considering the following scientific research assumption: the volume of the air chamber should be approximately equal to the volume of the pumping pipe in the practice. Mathematical modeling is carried out by following the steps of an investigation [3], where the physical process of the volumetric efficiency of the multi-drive hydraulic ram is considered as the object of research, and the mathematical process to determine the relationship between volumetric efficiency and the volume of the air chamber is considered as the field of action. The object of research is corroborated by the experimental method, and the field of action is corroborated by the mathematical method of least squares. It is one of the best methods for obtaining such formulas [4].

The objective is to model the relationship between volumetric hydraulic efficiency and the ram's air chamber volume, keeping the other parameters constant. Volumetric hydraulic efficiency is calculated from the results of the experimental work. By maintaining the same length of the pumping or discharge pipe, with the variation of the volume of the air chamber, the fraction between the volumes of the air chamber and the discharge or pumping pipe  $V_c/V_b$  also varies. This led to the scientifically groundbreaking conclusion that the volume of the air chamber is 38 percent larger than the volume of the pumping pipe. The research focuses on three key elements: the tabulation of experimental results, the mathematical analysis, and their characteristics. The Microsoft Excel 2010 software spreadsheet is used as a solution and for modeling the procedure [5].

## 2. Experimental study for the evaluation of the volumetric efficiency of the Multi-Drive Hydraulic Ram

The study was conducted using the experimental method in the Rio Carpintero community, Santiago de Cuba. The continuous source of water from the river feeds a reservoir [6]. The dam of more than  $10 \text{ m}^3$  requires the use of a ram feed pipe of 0.101 and 8 m in diameter and length respectively, and the distance to the distribution reservoir is 0.050 and 145 m in diameter and length. As a more economical alternative to feed the hydraulic ram, the siphon mechanism was used (Figures 1 and 2).

The reservoir without water is shown in Figure 1.



Fig. 1. Reservoir for feeding the ram

Reservoir filled with water is shown in Figure 2.



Fig. 2. Reservoir for feeding the ram

The Water ram designed and manufactured CITA-4 supports a maximum feed flow of  $0.004 \text{ m}^3/\text{s}$  permissible in a pipe with a diameter of 0.101 m. The efficiency, calculated by the relationship between the height of the discharge and impulse pipe [7], turned out to be 5, which is equivalent to 67%. In Water ram hydraulic pumps, losses or loads in the feed and pumping pipes are another important condition to take into account for the design [8].

Calculated from the Darcy equation, [9] in particular turned out to be 0.025 and 0.8 m, respectively. The experimental work consisted of evaluating the characteristics of volumetric hydraulic efficiency. Five chambers with different volumes were tested. By maintaining the same pumping or discharge pipe, the ratio between the volumes of the air chamber and the discharge or pumping pipe,  $V_c/V_b$ , also varies with the variation in the volume of the air chamber.



### 2.1. Procedures for carrying out the experiments

- a) Mount the 0.016 m<sup>3</sup> air chamber on the multi-drive ram (Figure 3).
  - b) Keep the impulse valves closed.
  - c) Operate the shut-off valve and frequently press the impulse valves until the ram pumps.
  - d) Measure the spill and discharge or pumping flow rates using the volumetric method. Tabulate the values.
  - e) Repeat steps **a** through **d** for the remaining chambers (Figures 4 and 5).
- First air chamber inserted into the experiment - Figure 3.



Fig. 3. 0.016 m<sup>3</sup> air chamber

Third air chamber inserted in the experiment - Figure 4.



Fig. 4. 0.064 m<sup>3</sup> air chamber

Fifth air chamber inserted in the experiment - Figure 5.



Fig. 5. 0.130 m<sup>3</sup> air chamber

The results of the experiments, carried out under real conditions on a test bench for hydraulic rams in the Rio Carpintero community of the Santiago de Cuba municipality, are shown in Table 1.



**Table1:** Behavior of the air chamber volume and volumetric efficiency

$V_c$ ( m <sup>3</sup> )	$V_b$ ( m <sup>3</sup> )	$q$ (10 <sup>-3</sup> m <sup>3</sup> /s)	$Q+q$ (10 <sup>-3</sup> m <sup>3</sup> /s)	$V_c/V_b$	$\eta_v$ %
0.016	0.058	0.04	3.34	0.27	1.1
0.032	0.058	0.05	3.35	0.55	1.4
0.060	0.058	0.065	3.365	1.03	1.9
0.105	0.058	0.06	3.36	1.8	1.7
0.130	0.058	0.05	3.35	2.24	1.4

Source: Author

**Nomenclature**

$V_c$  - Volume of the air chamber (m<sup>3</sup>)  
 $V_b$  –Volume of the pumping line (m<sup>3</sup>)  
 $q$  - Pumping flow rate (m<sup>3</sup>/s)  
 $Q+q$  - Feed flow rate (m<sup>3</sup>/s)  
 $V_c/V_b$  - Dimensionless volume ratio  
 $\eta_v$  - Volumetric efficiency (%)

Economic and site conditions allowed for the installation of the ram and the measurement of parameters - The pumping line volume includes two sections of pipe with restricted diameters, which increases losses (Table 2).

**Table 2:** Parameters of the feed and pumping pipe

$H$ (m)	$h$ (m)	$L$ (m)	$H_r$ (m)	$L_b$ 1” (m)	$h_r$ 1” (m)	$L_b$ 3/4” (m)	$h_r$ 3/4” (m)	$L_b$ (m)	$h_r$ (m)	$V_b$ (m <sup>3</sup> )
3	15	10.30	1.027	80.7	0.48	66	1.2	146.7	1.68	0.058

Source: Author

**Nomenclature**

$H$  - Feed height m  
 $h$  - Pumping height m  
 $L$  - Feed pipe length m  
 $H_r$  - Feed pipe losses m  
 $L_b$  - Pumping pipe length m  
 $h_r$  - Pumping pipe losses m  
 $V_b$  - Pumping pipe volume m<sup>3</sup>

**3. Analysis of research using the traditional method**

Mathematical Modeling is carried out by following the steps [3] (The research in particular conforms to the steps):

- The research problem. Hydraulic rams have a relatively low and limited volumetric efficiency compared to other hydraulic pumps. The objective is to model the volumetric efficiency of the hydraulic ram in relation to the volume of the air chamber and the volume of the pumping pipe. The results are: the theoretical contribution is a mathematical model; the practical contribution is a technological procedure for optimizing resources in the development of technological charts; and the scientific innovation is an integrative formula for the physical quantities involved in the relationship between volumetric efficiency and the volume of the air chamber.
- Knowledge that contributes to research. Fluid mechanics, with Bernoulli's and Torricelli's laws, Poisson's equation, N. Zhukovski's principle, the concepts of efficiency, water hammer, turbulent flow, losses, load and flow.

- c) Formulation of the problem situation in mathematical terms. The performance of renewable energy technologies behaves as a convex parabola. The parabolic or quadratic model is given by  $Y = a + bx + cX^2$  where  $a$  remains the intersection with the Y-axis, and  $b$  and  $c$  are related to the slope and the rate of change of the curve respectively.
- d) The solution is carried out using the nonlinear regression model and the least square method.

The quadratic model is represented by the general second degree equation (1).

Scope of action: Mathematical process that relates volumetric efficiency to the volume of the air chamber.

$$Y = ax^2 + bx + c \quad (1)$$

Where  $c$  is still the intercept with the Y-axis, and ( $b$  and  $a$ ) are related to the slope and the rate of change.

The prediction equation of the parabola that fits a set of  $n$  points of the form  $(x_i, y_i)$ ,  $i = 1, 2, \dots, n$ , has the equation:

$$\hat{Y} = \hat{a}x^2 + \hat{b}x + \hat{c} \quad (2)$$

Prediction model - where  $\hat{a}$ ,  $\hat{b}$ ,  $\hat{c}$  are the least square estimators of  $a$ ,  $b$  and  $c$ , determined by solving the normal system of the least square method [4].

$$nc + b \sum_{i=1}^n x_i + a \sum_{i=1}^n x_i^2 = \sum_{i=1}^n y_i \quad (3)$$

$$\sum_{i=1}^n x_i + b \sum_{i=1}^n x_i^2 + a \sum_{i=1}^n x_i^3 = \sum_{i=1}^n x_i y_i \quad (4)$$

$$c \sum_{i=1}^n x_i^2 + b \sum_{i=1}^n x_i^3 + a \sum_{i=1}^n x_i^4 = \sum_{i=1}^n x_i^2 y_i \quad (5)$$

**Table 3:** Volumetric efficiency calculated from the mathematical model

	$\eta_v$	$(V_c/V_b)$	$(V_c/V_b)^2$	$(V_c/V_b)^3$	$(V_c/V_b)^4$	$\eta_v * (V_c/V_b)$	$\eta_v * (V_c/V_b)^2$
	1.1	0.27	0.07	0.019	0.005	0.29	0.08
	1.4	0.55	0.30	0.16	0.09	0.77	0.42
	1.9	1.03	1.06	1.09	1.12	1.9	2.01
	1.7	1.8	3.24	5.8	10.4	3.06	5.5
	1.4	2.24	5.01	11.23	25.17	3.13	7.01
addition	7.5	5.89	9.68	18.2	36.7	9.15	15.02
Average	1.5	1.17	1.9	3.6	7.3	1.83	3

Source: Author

Covariance is a statistical measure that can indicate the linear relationship or association between variables.  $X$  and  $Y$ . ( $X = (V_c/V_b)$ , and ( $Y = \eta_v$ )

Substituting the values in equation (6)

$$C_{ov} = \frac{\sum_{i=1}^n (X_i - \bar{X})(Y_i - \bar{Y})}{n} = \overline{XY} - \bar{X} * \bar{Y} \quad (6)$$

Cov= 0.075 means that there is no possible direct linear association between  $X$  and  $Y$ .

Substituting the values calculated in table 3 in equations (3, 4 and 5) gives the following system of equations:

$$5c + 5.89b + 9.68a = 7.5 \quad (7)$$

$$5.89c + 9.68b + 18.2a = 9.15 \quad (8)$$

$$9.68c + 18.2b + 36.7a = 15.02 \quad (9)$$

To calculate the coefficient matrix  $\Delta$ , the Sarrus method is used.

$$\Delta = \begin{vmatrix} 5 & 5.89 & 9.68 \\ 5.89 & 9.68 & 18.2 \\ 9.68 & 18.2 & 36.7 \end{vmatrix} = 15.19 \quad (10)$$

$$\Delta_c = \begin{vmatrix} 7.5 & 5.89 & 9.68 \\ 9.15 & 9.68 & 18.2 \\ 15.02 & 18.2 & 36.7 \end{vmatrix} = 16.94 \quad (11)$$

$$\Delta_b = \begin{vmatrix} 5 & 7.5 & 9.68 \\ 5.89 & 9.15 & 18.2 \\ 9.68 & 15.02 & 36.7 \end{vmatrix} = 11.29 \quad (12)$$

$$\Delta_a = \begin{vmatrix} 5 & 5.89 & 7.5 \\ 5.89 & 9.68 & 9.15 \\ 9.68 & 18.2 & 15.02 \end{vmatrix} = -3.85 \quad (13)$$

$$\hat{a} = \frac{\Delta_c}{\Delta} = 1.11 \quad (14)$$

$$\hat{b} = \frac{\Delta_b}{\Delta} = 0.74 \quad (15)$$

$$\hat{c} = \frac{\Delta_a}{\Delta} = -0.25 \quad (16)$$

#### Nomenclature

$\Delta$ : coefficient matrix.

$\Delta_a$ : coefficient matrix in which the column of coefficients of  $a$  is replaced by the column of the second members of the equations

$\Delta_b$ : coefficient matrix in which the column of coefficients of  $b$  is replaced by the column of the second members of the equations.

$\Delta_c$ : coefficient matrix in which the column of coefficients of  $c$  is replaced by the column of the second members of the equations.

The prediction model by the traditional method is given by (17) replacing the values of (14), (15) and (16).

$$\hat{Y} = -0.25x^2 + 0.74x + 1.11 \quad (17)$$

$$\hat{y}_i = -0.25(0.27)^2 + 0.74(0.27) + 1.11 = 1.29$$

$$\hat{y}_i = -0.25(0.55)^2 + 0.74(0.55) + 1.11 = 1.44$$

$$\hat{y}_i = -0.25(1.03)^2 + 0.74(1.03) + 1.11 = 1.60$$

$$\hat{y}_i = -0.25(1.8)^2 + 0.74(1.8) + 1.11 = 1.63$$

$$\hat{y}_i = -0.25(2.24)^2 + 0.74(2.24) + 1.11 = 1.51$$

**Table 4:** Prediction of values

$\hat{y}_i$	$y_i$	$\bar{y}$	$(\hat{y}_i - \bar{y})^2$	$(y_i - \bar{y})^2$
1.29	1.1	1.5	0.04	0.16
1.44	1.4	1.5	0.003	0.01
1.60	1.9	1.5	0.01	0.16
1.63	1.7	1.5	0.016	0.04
1.51	1.4	1.5	0.0001	0.01

Source: Author

$$R^2 = \frac{\sum_{i=1}^n (\hat{y}_i - \bar{y})^2}{\sum_{i=1}^n (y_i - \bar{y})^2} 100 \% = \frac{0.073}{0.38} 100\% = 19 \% \quad (18)$$

**Table 5:** Volumetric efficiency from the mathematical model

	$\eta_v$	$(V_c/V_b)$	$(V_c/V_b)^2$	$(V_c/V_b)^3$	$(V_c/V_b)^4$	$\eta_v^*$ $(V_c/V_b)$	$\eta_v^*$ $*(V_c/V_b)^2$	$\eta_{vest}$	$e_{est}$	$(\eta_{vest}-\bar{\eta}_v)^2$	$e_{es}^2$
	1.1	0.27	0.07	0.019	0.005	0.29	0.08	1.29	-0.19	0.04	0.03
	1.4	0.55	0.30	0.16	0.09	0.77	0.42	1.44	-0.04	0.003	0.0016
	1.9	1.03	1.06	1.09	1.12	1.9	2.01	1.60	0.3	0.01	0.09
	1.7	1.8	3.24	5.8	10.4	3.06	5.5	1.63	0.07	0.016	0.0049
	1.4	2.24	5.01	11.23	25.17	3.13	7.01	1.51	-0.11	0.0001	0.012
addition	7.5	5.89	9.68	18.2	36.7	9.15	15.02	7.47	0.03	0.069	0.137
Average	$\bar{\eta} = 1.5$				Average $\eta_{est}$			1.49	$R^2= 0.19$		
addition $(\eta-\bar{\eta})^2$	36				addition $(\eta_{est}-\bar{\eta})^2$			0.069			
Parameters	a=-0.25	b=0.74	c=1.11	n=5							

Source: Author

**Nomenclature** $\eta_{est}$  – Estimated volumetric efficiency $e_{est}$  – Estimated error $\bar{\eta}$  – Average volumetric efficiency $\eta_v$  – Volumetric efficiency

By replacing the values from Table 5 in the coefficient of determination (18), it is shown that 19% of the volumetric efficiency behavior is explained by the volume ratio of the air chamber and pumping pipe, using the parabolic method. The above differs from the solution using Excel software, which is 96%.

General equation of a polynomial of the second degree (19)

$$\eta_v = -a \left( \frac{V_c}{V_b} \right)^2 + b \left( \frac{V_c}{V_b} \right) + c \% \quad (19)$$

Equation solution from calculations using the least square method

$$\eta_v = -0.25 \left( \frac{V_c}{V_b} \right)^2 + 0.74 \left( \frac{V_c}{V_b} \right) + 1.11 \% \quad (20)$$

Finding the roots of equation (19) and linking it with the energy efficiency equation (21) and the volumetric performance [10] (22), equation (23) is determined.

$$\eta_E = \frac{q h}{Q H} 100\% \quad (21)$$

$$\eta_v = \frac{q}{Q} 100\% \quad (22)$$

$$\frac{V_c}{V_b} = \left( \frac{-b \mp \sqrt{b^2 - 4a \left( \frac{hc - \eta_E H}{h} \right)}}{2a} \right) \quad (23)$$

The volumetric efficiency has its maximum value defined in equation (24)

$$\frac{V_c}{V_b} = \frac{-b}{2a} = 1.5 \quad (24)$$

Substituting the values in (23) and clearing, the values of the chamber volumes for which the volumetric efficiency is minimum are obtained.

$$V_{c1} = 0.3 V_b \quad (25)$$

$$V_{c2} = 2.8 V_b \quad (26)$$

#### 4. Results

By replacing the values of the magnitudes in (20) the following percentage efficiency results are obtained:

$$\eta_V = -0.25 \left( \frac{V_c}{V_b} \right)^2 + 0.74 \left( \frac{V_c}{V_b} \right) + 1.11 \%$$

$$V_c = V_b = 0.058 \text{ m}^3 \quad \eta_V = 1.59\%$$

$$V_c = 0.3 V_b = 0.017 \text{ m}^3 \quad \eta_V = 1.3 \%$$

$$V_c = 2.8 V_b = 0.162 \text{ m}^3 \quad \eta_V = 1.2\%$$

$$V_c = 1.5 V_b = 0.087 \text{ m}^3 \quad \eta_V = 1.65\%$$

$$V_c = 2 V_b = 0.116 \text{ m}^3 \quad \eta_V = 1.59\%$$

$$V_c = 0.5 V_b = 0.029 \text{ m}^3 \quad \eta_V = 1.41\%$$

$$V_c = 1.2 V_b = 0.069 \text{ m}^3 \quad \eta_V = 1.63\%$$

This shows that the highest volumetric efficiency is achieved for a volume 1.5 times the volume of the pumping or discharge pipe. Using Microsoft Excel grids, this is shown in Figure 6.

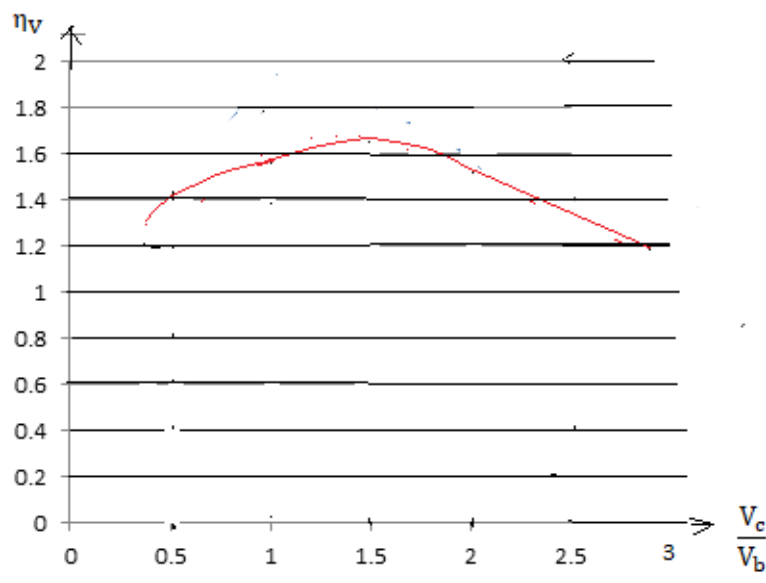


Fig. 6. Volumetric efficiency and volume ratio



With the methodology of the Microsoft Word Excel tool, the equation (27) is achieved.

The prediction solution equation by Excel software is

$$\hat{Y} = -0.68x^2 + 1.85x + 0.63 \quad \text{Excel} \quad (27)$$

The coefficient of determination for this last equation is  $R^2 = 0.96$ .

$V_c = V_b = 0.058 \text{ m}^3$	$\eta_V = 1.8\%$
$V_c = 0.3V_b = 0.017 \text{ m}^3$	$\eta_V = 0.98 \%$
$V_c = 2.8V_b = 0.162 \text{ m}^3$	$\eta_V = 1.10\%$
$V_c = 1.36V_b = 0.075 \text{ m}^3$	$\eta_V = 1.89\%$
$V_c = 1.5V_b = 0.087 \text{ m}^3$	$\eta_V = 1.87\%$
$V_c = 2 V_b = 0.116 \text{ m}^3$	$\eta_V = 1.61\%$
$V_c = 0.5V_b = 0.029 \text{ m}^3$	$\eta_V = 1.38\%$
$V_c = 1.2 V_b = 0.069 \text{ m}^3$	$\eta_V = 1.87\%$

Its characterization is determined in Figure 7.

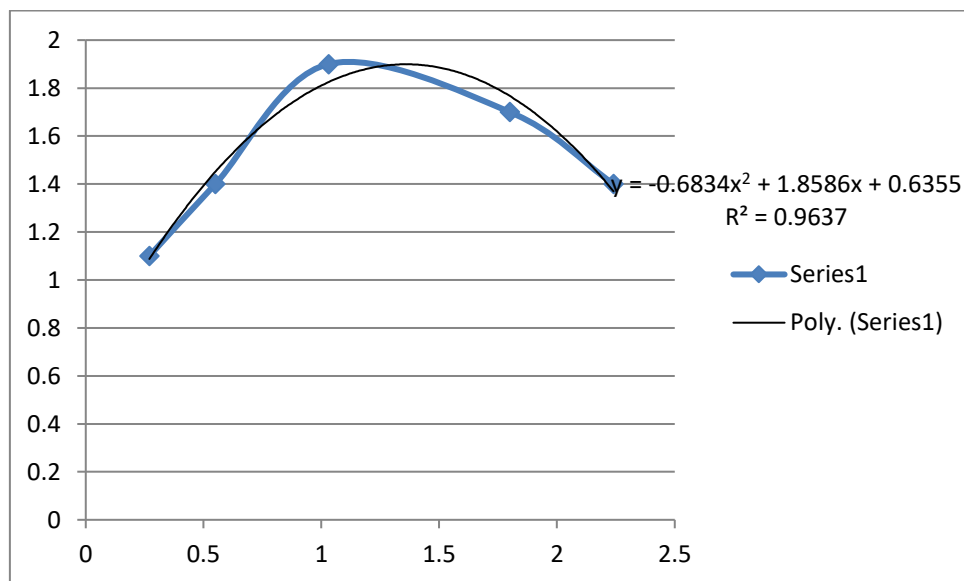


Fig. 7. Volumetric efficiency and volume ratio

e) Comparison of the model with the real situation.

The theoretical polynomial equation describing the experimental results obtained using the traditional procedure (20). The maximum efficiency with equation (24) when solving for the volume of the air chamber shows that it is fifty percent greater than the volume of the pumping pipe.

$$V_c = V_b + 50\% V_b$$

$$V_c = 1.5V_b$$

Table 6 defines that the law of conservation of energy is fulfilled, where it is shown that the energy efficiency of 6.7% is never exceeded by the volumetric efficiency.

**Table 6:** Volumetric efficiency of the hydraulic ram

Volume (m <sup>3</sup> ) Air chamber	Volumetric Efficiency (%)
0.016	1.1
0.032	1.4
0.058	1.9
0.105	1.7
0.130	1.4

Source: Author

The theoretical polynomial equation that describes the experimental results is obtained using Excel software (27). The maximum performance with equation (24) when clearing the volume of the air chamber shows that it is greater by thirty-eight percent more than the volume of the pumping pipe.

## 5. Discussion

f) Analysis of the restrictions to the model.

Restricted for pumping systems for renewable energy sources, with pumping pipe volumes exceeding hundreds of meters, as otherwise, it requires a disproportionate volume of the air chamber.

g) Application scenario of the model, as well as its interpretation

In multi-drive hydraulic ram pumps that have alternative air chambers, where it is interpreted that their volume is directly proportional to the volume of the pumping pipe.

The results show that the volume is equivalent to the volume of the pumping line plus fifty percent of that same volume, an analysis performed using the traditional method. Using Excel software, it shows that the volume is equivalent to the volume of the pumping line plus thirty-eight percent of that same volume. The entire study corroborates compliance with the law of conservation of energy, and the formula found is a specific example of the general formula for energy efficiency.

## 6. Conclusions

The volume of the air chamber is directly proportional to the volume of the pumping pipe, and to the square root of fourfold times the energy efficiency.

The mathematical modeling of volumetric efficiency is characterized with the help of Microsoft Excel software, and by the traditional method.

The highest volumetric efficiency is achieved when the volume of the air chamber is equal to the volume of the pumping pipe plus thirty-eight percent of the latter, a solution found by the Microsoft Excel software.

The traditional method shows that the highest volumetric efficiency is achieved when the volume of the air chamber is equal to the volume of the pumping pipe plus fifty percent of the latter.

## Acknowledgments

To our families for their unconditional support of our work

## References

- [1] Arapa Quispe, J.B. "Performance evaluation of the BAH-1.1/2 hydraulic ram by varying the length of the feed pipe and operating conditions of the impulse valve." / "Evaluación del rendimiento del Ariete Hidráulico BAH-1.1/2 variando la longitud de la tubería de alimentación y condiciones de operación de la válvula de impulso." *Anales Científicos* 77, no. 2 (2016): 155-165. <https://doi.org/10.21704/ac.v77i2.485>.

- [2] Ayala Chauvin, M.I. *Design and construction of a multi-drive ram / Diseño y construcción de un ariete multipulsor*. Bachelor's thesis. National University of Loja, Ecuador, 2006.
- [3] Plaza Gálvez, L.F. “Mathematical modeling in engineering.” / “Modelación matemática en ingeniería.” *IE Revista de Investigación Educativa de la REDIECH* 7, no. 13 (2016): 47-57.
- [4] Kudriávsev, V., and B. Demidóvich. *Short course in higher mathematics / Breve curso de matemáticas superiores*. Moscow, Mir Publishing House, 1989.
- [5] Torrelavega. “Least squares adjustment.” / “Ajuste por mínimos cuadrados.” August 10, 2020. Accessed September 18, 2023. OpenCourseWare (OCW) - Universidad de Cantabria (UNICAN). <https://ocw.unican.es/pluginfile.php/2101/course/section/1887/Ajuste%20por%20minimos%20cuadrados.pdf>.
- [6] Peralta Surco, H. *Application of hydraulic water hammer to harness spring water in Quequerana Moho / Aplicación del golpe de ariete hidráulico para el aprovechamiento del agua de manantial en Quequerana Moho*. Thesis. National University of the Altiplano, Peru, 2015.
- [7] Crisóstomo Armas, E. *Efficiency in the water supply by ram pump to the Utcucucho - Uchusquillo property, San Luis District - Ancash / Eficiencia en el abastecimiento de agua por bomba de ariete al predio de Utcucucho - Uchusquillo, distrito de San Luis - Ancash*. Undergraduate thesis. Cesar Vallejo University, Peru, 2020.
- [8] Aguirre Morales, F. *Supply of drinking water for rural communities / Abastecimiento de agua potable para comunidades rurales*. 1st edition. Machala (Ecuador), Technical University of Machala, 2015.
- [9] Galarza, F. *Study of hydraulic factors in a ram pump and its effect on efficiency / Estudio de factores hidráulicos en una bomba de ariete y su efecto sobre la eficiencia*. Research work. Technical University of Ambato, Ecuador, 2013.
- [10] Rengifo Hincapié, S., and J.D. Gallego Cadena. *Design and construction of a hydraulic ram system for the use of rainwater / Diseño y construcción de un sistema de ariete hidráulico para el aprovechamiento de aguas lluvias*. Bachelor thesis. Technological University of Pereira, Colombia, 2016.

## Artificial Intelligence Use for Forecasting Precipitation and Assessing Groundwater Depletion: A Study Case in Chihuahua City, Mexico

M. Eng. Margarita PRECIADO<sup>\*,1</sup>, Dr. Maritza ARGANIS<sup>\*,2,3</sup>, M.Eng. Jorge CASADOS<sup>1</sup>,  
Dr. Rodrigo ROBLERO-HIDALGO<sup>1</sup>

<sup>1</sup> Instituto Mexicano de Tecnología del Agua, Paseo Cuauhnáhuac 8532, c.p. 62550 Jiutepec, Mor., México

<sup>2</sup> Universidad Nacional Autónoma de México. Instituto de Ingeniería. Av. Universidad 3000 Ciudad Universitaria Edif 17 c.p. 04510 Coyoacán CDMX, México

<sup>3</sup> Universidad Nacional Autónoma de México. Facultad de Ingeniería. Av. Universidad 3000 Ciudad Universitaria c.p. 04510 Coyoacán CDMX, México

\* MArganisJ@iingen.unam.mx, preciado@tlaloc.imta.mx

**Abstract:** *This study presents an integrated methodology for assessing water resource vulnerability in Chihuahua City, Mexico, by combining satellite-based hydrological data and advanced time-series modeling. Using Long Short-Term Memory (LSTM) neural networks, the research forecasts monthly precipitation trends and identifies critical drought periods, notably between 2029 and 2032. Concurrently, GRACE satellite data reveal persistent groundwater depletion in the El Sauz–Encinillas aquifer, corroborated by historical piezometric measurements. The Río Conchos 3 basin exhibits surface water deficits, with future availability projections varying significantly across hydrological models. The approach enables early detection of water stress, supports operational optimization, and informs adaptive governance strategies. These findings underscore the importance of integrating predictive analytics with physical observations to enhance resilience in semi-arid urban regions.*

**Keywords:** *Artificial Intelligence, Groundwater Depletion, Precipitation Forecasting, LSTM, GRACE, Chihuahua, Water Governance, Hydrological Modeling*

### 1. Introduction

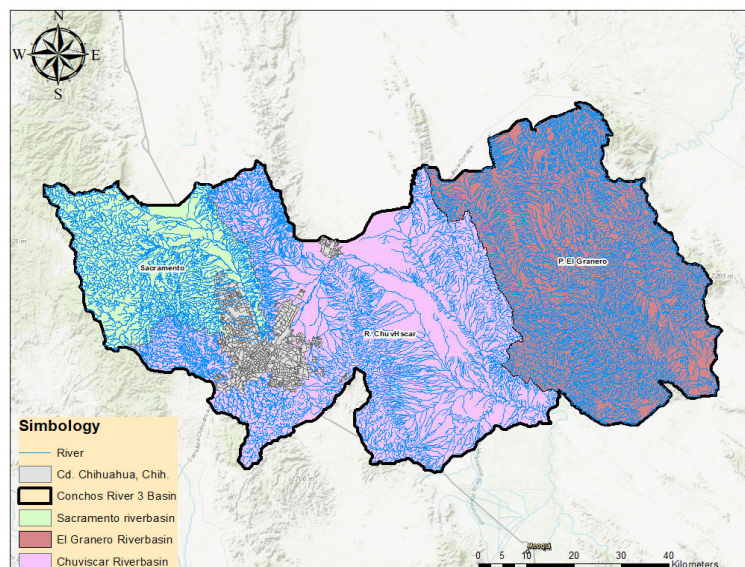
Water scarcity is a growing concern in semi-arid regions around the world, where factors such as climate variability, population growth, and agricultural demands place increasing pressure on limited water resources. In northern Mexico, the state of Chihuahua faces significant challenges, including declining precipitation, aquifer overexploitation, and infrastructure that could be strengthened for greater resilience. The aquifers overexploitation is a well-documented issue in many parts of Mexico, leading to a long-term decline in groundwater levels [1].

Recent advances in artificial intelligence (AI) and remote sensing offer innovative tools for addressing these challenges. Machine learning models—particularly those designed for sequential data, such as Long Short-Term Memory (LSTM) neural networks—enable more accurate forecasting of climatic variables, including precipitation. Research by Hamed and, Rao, 1998, Ni et al., 2020 [2,3] have demonstrated the effectiveness of LSTM models for hydrological forecasting. Simultaneously, satellite missions like NASA’s Gravity Recovery and Climate Experiment (GRACE) provide valuable insights into terrestrial water storage dynamics, revealing trends in groundwater depletion that are often not visible through surface monitoring alone [4,5].

This paper presents an integrated approach to water resource assessment in Chihuahua City, Mexico. It combines AI-based precipitation forecasting with satellite-derived groundwater anomaly detection. By applying LSTM models to historical rainfall data and correlating the results with GRACE observations and well measurements, this research seeks to improve drought prevention, quantify aquifer stress, and propose adaptive management strategies. The findings demonstrate the value of merging predictive analytics with physical hydrological data to support sustainable water governance in climate-sensitive regions.

Chihuahua City faces challenges related to water management due to limited precipitation, aquifer overexploitation, and the need for more resilient hydraulic infrastructure. These issues are further complicated by the lack of timely and integrated data systems to support proactive water

management. An effective strategy could involve segmenting hydrometric districts based on water availability versus user demand. This would allow for better control and integration of service provision, helping to ensure the quality, quantity, and pressure of water delivery. Strengthening the system's resilience, a concept explored by Lukat et al., 2022 [6], can help mitigate the impacts of stress caused by growing populations and climate variability in semi-arid regions like Chihuahua. Chihuahua City is located within the Río Conchos 3 basin, which is composed of three sub-basins: the Sacramento, El Granero, and Chuviscar. The Río Conchos is a critical river in Chihuahua, draining almost half of the state's territory and serving as the primary Mexican tributary to the Río Bravo (Rio Grande). The strategic importance of this basin for both Mexico and the United States has been a subject of diplomatic and scientific discourse for decades, highlighting the need for careful binational water management [7].



**Fig. 1.** Río Conchos 3 River basin at Chihuahua City and their subbasins. Source: Own design

Although this region possesses notable surface water sources, their reliability has been significantly compromised by prolonged drought conditions. Consequently, Chihuahua city relies predominantly on local groundwater aquifers to meet its direct water supply needs (Figure 2). The primary aquifers serving the city include:

- **Chihuahua-Sacramento Aquifer (CHS):** This aquifer underlies most of Chihuahua City's urban area and is part of the larger Bravo-Conchos hydrological basin. It covers an area of 1,889 km<sup>2</sup>.
- **El Sauz–Encinillas Aquifer:** Located approximately 92 km north of Chihuahua City, this aquifer is crucial for the city's water supply. It resides within a closed (endorheic) basin surrounded by mountain ranges.

Chihuahua City is located at a semi-arid region where groundwater is the primary permanent water source. However, the available data from Conagua indicates significant challenges:

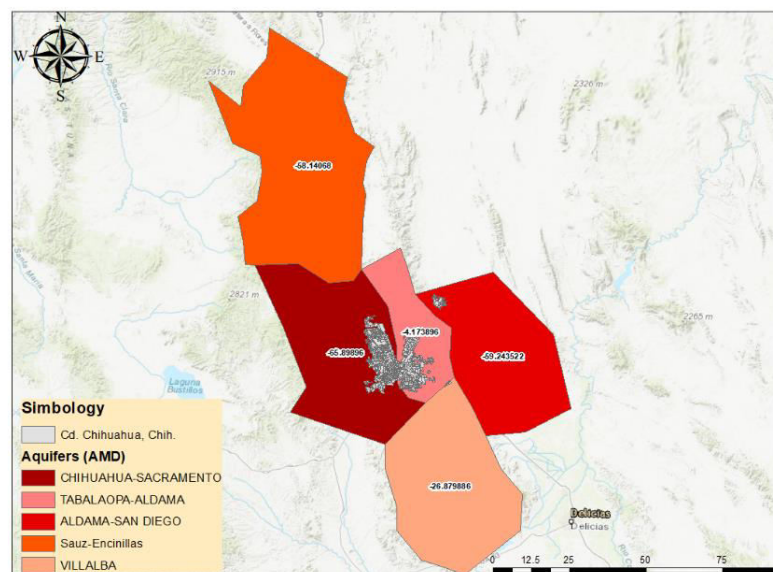
**Overexploitation:** Many aquifers in Chihuahua, including El Sauz-Encinillas, are overexploited, meaning water extraction significantly exceeds natural recharge rates. Out of 61 aquifers supplying drinking water in the state, 42 are overexploited, and 9 have no reported availability.

**Declining Water Levels:** This overexploitation leads to a consistent drop in water table levels, a trend observed through satellite data (GRACE) and validated by historical well measurements.

**Increasing Demand:** Despite the deficit, water demand from Chihuahua City's growing population and the agricultural sector continues to rise, exacerbating the water scarcity issues.

**Slow Recharge:** Deep aquifers, which often contain "fossil" water, recharge very slowly, and prolonged extraction can lead to increased salinity, making the water unsuitable for various uses.





**Fig. 2.** Aquifers surrounding Chihuahua City and their AAD annual average availability. Source: [8]

Figure 2 shows a geospatial groundwater configuration availability in the Chihuahua region according to Conagua 2023, based on the annual average availability (AAA) as defined by the *NOM-011-CONAGUA-2015*. This standard specifies the methodology for calculating groundwater availability through a balance of recharge (R), committed natural discharge (CND), and extraction volumes (EV).

In the Figure 2, it showed a groundwater availability situation according to the color, for example:

- Chihuahua – Sacramento (dark red): Indicates a high deficit, a negative availability approximately  $-65.89 \text{ hm}^3/\text{year}$ .
- Tabalaopa – Aldama (red): Shows a negative availability around  $-59.24 \text{ hm}^3/\text{year}$ .
- El Sauz - Encinillas (orange): Also shows a negative availability around to  $-58.14068 \text{ hm}^3/\text{year}$ .
- Aldama – San Diego (light orange): Moderate deficit with availability near to  $-26.87 \text{ hm}^3/\text{year}$ .
- Villalba (pink): Slightly less stressed with availability near to  $-4.17 \text{ hm}^3/\text{year}$ .

## 2. Methodology

Advanced Artificial Intelligence (AI) integration models, including recurrent neural networks (RNNs) like Long Short-Term Memory (LSTM) and machine learning algorithms such as XGBoost, have significantly improved in preventing water scarcity events in Chihuahua City. These models are proven on historical data sets taking into account temperature, precipitation, streamflow, and piezometric levels, generating projections that adapt to emerging climatic and anthropogenic patterns [9,10]. One of the key strengths of these approaches lies in their ability to identify early signals of aquifer stress and surface water deficits. By detecting subtle shifts in recharge dynamics and consumption patterns, they support the timely implementation of mitigation strategies. For instance, ensemble models combining LSTM with convolutional layers or attention mechanisms have achieved high accuracy in drought prediction, outperforming conventional models in both spatial and temporal resolution [11,12].

Beyond forecasting, these tools contribute to operational optimization. Algorithms can define efficient water redistribution routes, adjust pressure zones, and prioritize service areas based on consumption history and infrastructure vulnerability. Pilot implementations have reported reductions in water losses ranging from 14% to 22%, particularly in urban districts with aging networks.

Moreover, decision support systems enhanced by machine learning are increasingly used to visualize hydrological scenarios in real time. These platforms integrate geospatial data, alerts, and

predictive simulations, facilitating coordinated responses among agencies. Studies have shown that such systems improve institutional readiness and foster collaborative governance, especially when combined with explainable AI frameworks that clarify model outputs for non-technical stakeholders [13,14].

In the context of climate change, models are being calibrated to reflect projected increases in temperature and reductions in recharge rates. For example, simulations for semi-arid basins suggest a potential rise of +2.4 °C and a 38% decrease in aquifer replenishment, underscoring the urgency of adaptive planning. In summary, the integration of advanced machine learning techniques into hydrological modeling not only enhances predictive capacity but also strengthens institutional decision-making and public policy formulation. Future research should explore hybrid approaches that combine physical models with data-driven algorithms, ensuring both accuracy and interpretability in water resource planning.

### 3. Results and Discussion

#### 3.1 Surface water: Río Conchos 3 Basin Analysis

The Río Conchos 3 basin, spanning an area of 6,508 km<sup>2</sup>, revealed a negative surface water availability of –6.37 hm<sup>3</sup>/year in the base 2020 Study scenario, classifying it as a basin "without availability." This condition reflects a significant imbalance between the committed downstream volume (251.17 hm<sup>3</sup>) and the available runoff (244.8 hm<sup>3</sup>). This deficit is further exacerbated by registered extractions (53.6 hm<sup>3</sup>) and limited returns (57.7 hm<sup>3</sup>).

**Table 1:** surface Availability water at Rio Conchos 3 Basin According to DOF 2020

Parameter	Value	Unit
Area	6,508.00	km <sup>2</sup>
Available Runoff (Ab)	244.8	hm <sup>3</sup> /year
Committed Volume Downstream (Rxy)	251.17	hm <sup>3</sup> /year

Different hydrological models present varying projections for the basin's future water availability according to Bravo-Jácome et al., 2025 [15]:

TURC Model: Application of the TURC model projects a significantly improved availability of 2,007.59 hm<sup>3</sup>/year by 2034, suggesting a more favorable outlook under certain climatic conditions.

Runoff Coefficient (RC) Method: In contrast, RC method estimates a more severe decline, with an availability of –13.34 hm<sup>3</sup>/year, reinforcing the risk of water stress under conservative scenarios.

**Table 2:** Different hydrological models present varying projections for the basin's future water availability

Basin	Deficit (D) 2020 Study (hm <sup>3</sup> /year)	Deficit (D) 2034 TURC Model (hm <sup>3</sup> /year)	Deficit (D) 2034 Runoff Coefficient (RC) Method (hm <sup>3</sup> /year)
Río Conchos 3	-6.37	2007.59	-13.34

These discrepancies between modeling methods highlight the basin's sensitivity to climatic variations and land-use changes. They underscore the critical need for implementing adaptive management policies and continuous monitoring to ensure sustainable water resources in the face of uncertainty.

#### 3.2 Forecasting Monthly Precipitation Using LSTM

LSTM neural networks are deep learning architectures designed to learn from sequential data. In this study, monthly precipitation records from Río Conchos 3 Basin were preprocessed using:

- Imputation of missing values
- Rolling statistics and lag features
- Robust scaling to mitigate outlier influence

Monthly precipitation records (1982–2018) were preprocessed using imputation of missing values, rolling statistics, lag features, and robust scaling. An LSTM neural network was trained using five-fold time series cross-validation. The model achieved:

- Mean Absolute Error (MAE): 73.59 mm
- Coefficient of Determination ( $R^2$ ): 0.29

Despite moderate  $R^2$ , the model effectively captured transitions from normal rainfall to prolonged dry periods. Forecasts for 2019–2033 suggest stable precipitation through 2028, followed by a severe drought from 2029 to 2032. These projections support strategic water rationing, infrastructure reinforcement, and drought contingency planning.

### 3.3 Time Series Decomposition

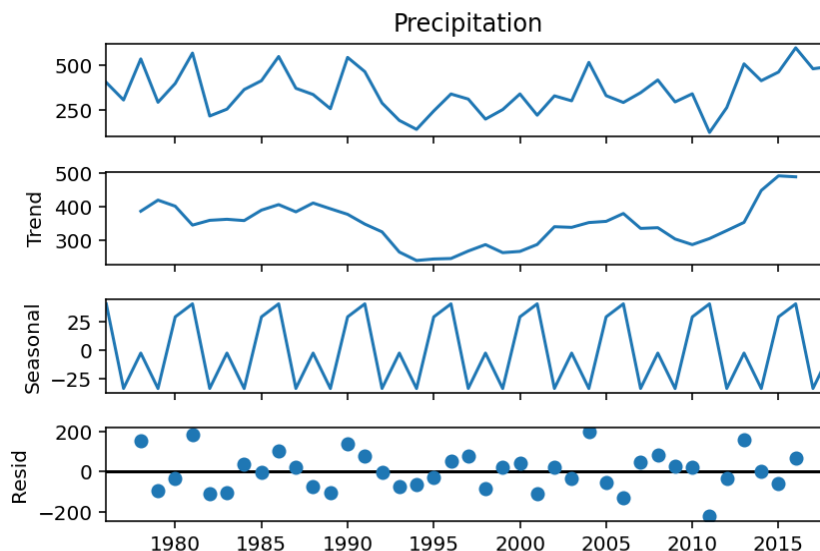
The precipitation series was decomposed into:

- Observed Component: High interannual variability with peaks (2004–2006) and dips (early 1980s, mid-1990s)
- Trend Component: Declining trend until mid-1990s, followed by gradual recovery
- Seasonal Component: Stable oscillations around zero, indicating consistent seasonal cycles

This decomposition supports the use of periodic models like RNNs and enhances interpretability for water resource planning.

The model was evaluated using five-fold time series cross-validation. Performance metrics yielded a Mean Absolute Error (MAE) of 73.59 mm and a coefficient of determination ( $R^2$ ) of 0.29. Despite moderate  $R^2$ , the LSTM model successfully captured interannual variability and key shifts from normal precipitation to prolonged dry periods.

The forecast (2019–2033) indicated stable rainfall through 2028, followed by severe drought from 2029 to 2032. These predictions were translated into actionable recommendations—such as water rationing policies and infrastructure readiness—to enhance drought resilience.



**Fig. 3.** Precipitation time series AI model results for Rio Conchos 3 Basin

Figure 3 breaks down the precipitation time series into three key components:

a). Observed Precipitation

- Displays the raw annual precipitation values.
- Shows high interannual variability, with peaks around 2004–2006 and dips in the early 1980s and mid-1990s.

- The fluctuations suggest alternating wet and dry years, typical of semi-arid basins influenced by regional climate patterns.

## b). Trend Component

- Reveals the long-term direction of the data.
- Initially, there's a declining trend from 1980 to the mid-1990s, followed by a gradual recovery toward 2015.
- This may reflect broader climatic shifts or land-use changes affecting rainfall patterns over time.

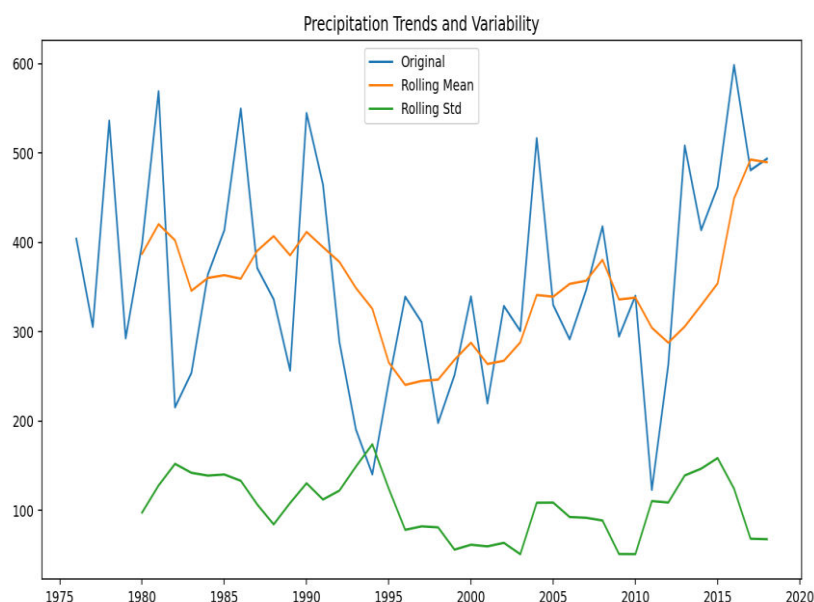
## c). Seasonal Component

- Captures recurring patterns or cycles in the data.
- The seasonal variation is relatively stable and symmetric, oscillating around zero.
- This suggests that while the magnitude of precipitation changes year to year, the seasonal rhythm remains consistent, likely tied to predictable wet and dry seasons.
- Any remaining variability not explained by the trend or seasonality.
- These are important for identifying anomalous years or extreme events that deviate from expected patterns.
- The decomposition confirms that precipitation at Río Conchos 3 Basin is highly variable, but with a recovering trend post-1995.
- The stable seasonal component supports the use of models that assume periodicity, like RNNs.
- Understanding these components helps improve forecasting accuracy and supports adaptive water management policies.

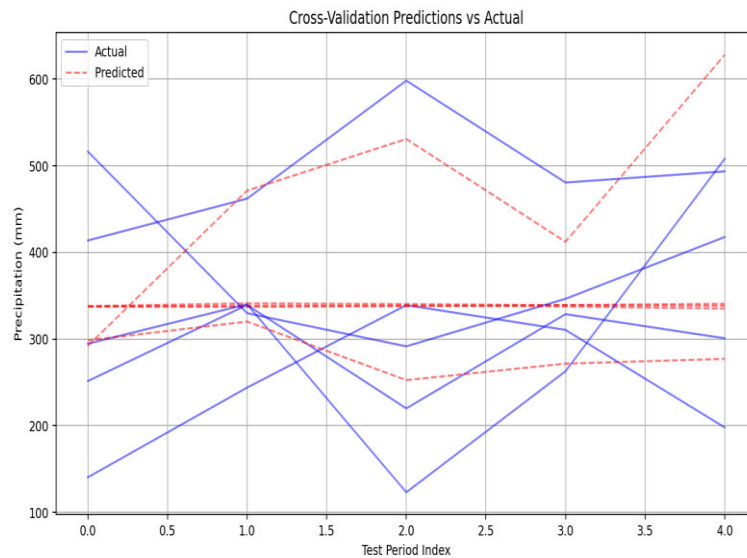
We can observe at Figure 4; precipitation series was decomposed into:

- Observed Component: High interannual variability with peaks (2004–2006) and dips (early 1980s, mid-1990s)
- Trend Component: Declining trend until mid-1990s, followed by gradual recovery
- Seasonal Component: Stable oscillations around zero, indicating consistent seasonal cycles

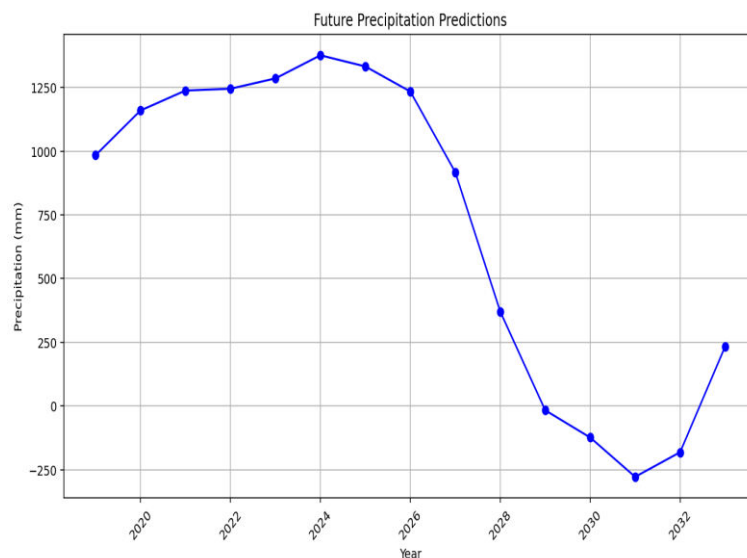
This decomposition supports the use of periodic models like RNNs and enhances interpretability for water resource planning.



**Fig. 4.** Precipitation trends and variability at Río Conchos 3 Basin



**Fig. 5.** Precipitation cross-validation prediction vs actual at Rio Conchos 3 Basin



**Fig. 6.** Precipitation future prediction at Rio Conchos 3 Basin

- In several points, the predicted values closely follow the real ones, indicating the model captures the general trend.

At Figure 7 we can observe there are some sample indices where the prediction deviates noticeably from the actual temperature—this could be due to:

- Sudden climate anomalies
- Limited training data for extreme years
- Lag effects not captured by the model

Also, it visually confirms that the model performs reasonably well but may benefit from:

- Including additional predictors (e.g., NDVI, humidity, wind)
- Using lagged features or temporal smoothing
- Trying a sequential model like RNN or LSTM for better temporal learning



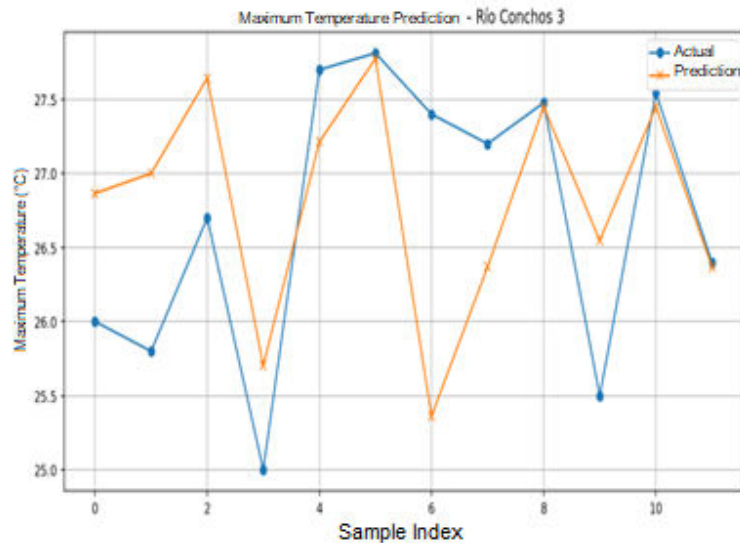


Fig. 7. Temperature Maximum prediction at Rio Conchos 3 Basin

### 3.4 Groundwater: El Sauz-Encinillas Aquifer

The Sauz-Encinillas aquifer (0807), is situated in the Chihuahua state central portion, in Mexico. It spans latitudes 28°53'31" N to 29°39'41" N and longitudes 106°09'35" W to 106°43'27" W, covering an area of 2,743 km<sup>2</sup>. It shares its northern boundary with the Laguna de Tarabillas and Flores Magón-Villa Ahumada aquifers; its eastern boundary with Laguna de Hormigas and Laguna El Diablo; its southern boundary with Chihuahua Sacramento and Alto Río San Pedro; and its western boundary with Santa Clara and Cuauhtémoc, all within Chihuahua state. The aquifer system is characterized by heterogeneity and anisotropy. It is predominantly unconfined, though local semi-confined conditions exist due to the interdigitation of low-permeability strata. Geologically, it is situated within a tectonic graben filled with sediments of varying grain sizes. These alluvial sediments reach a maximum thickness of 800 m, thinning towards the slopes of the surrounding mountain ranges where alluvial fans are present. At greater depths, fractured volcanic rocks and limestones exhibit secondary permeability, forming an unexploited unit with evidence of its presence derived from mining operations, primarily in adjacent aquifers.

#### Hydraulic Parameters

As part of a 2009 study, eight pumping tests were conducted, encompassing both drawdown and recovery phases, with durations ranging from 4 to 12 hours. Interpretation of these tests, utilizing various methods, yielded transmissivity values varying from 24 to 455 m<sup>2</sup>/day ( $0.3$  to  $5.3 \times 10^{-3}$  m<sup>2</sup>/s), with an average of 191 m<sup>2</sup>/day ( $2.2 \times 10^{-3}$  m<sup>2</sup>/s). Considering an average saturated thickness of 170 m, this translates to an average hydraulic conductivity of 1.1 m/day ( $1.3 \times 10^{-5}$  m/s). For the storage coefficient (S) in the central valley area, the average value was determined to be  $7.1 \times 10^{-4}$ . Specific yield (Sy) values ranged from 0.06 to 0.21 [8].

#### Static Water Level Elevation

In the context of Mexico's National Water Commission (CONAGUA), piezometric levels represent measurements of groundwater pressure within an aquifer, typically obtained through monitoring wells or piezometers. These readings are essential for analyzing subsurface water dynamics and ensuring sustainable groundwater management. You can explore official data through CONAGUA's Piezometric Measurements Portal <https://sigagis.conagua.gob.mx/rp20/> [8]. Groundwater level analysis in the region is based on data collected between 2001 and 2009. In 2009, static water level depths varied significantly across the aquifer:

#### Range of Depths: 5 to 120 meters

Shallowest Levels: Found near Encinillas and Ejido Nuevo Delicias, located in the central and northern zones of the aquifer

Southern Sector: Depths ranged from 20 to 120 meters, with topography playing a key role in the deeper measurements

El Sauz–Chihuahua Aqueduct Zone: Near the well fields supplying this aqueduct, depths ranged from 10 to 80 meters

These variations reflect both natural geological influences and anthropogenic pressures, underscoring the importance of continuous monitoring for effective water resource planning. The static water level elevations in 2009 (Table 3) ranged from 1515 to 1570 meters above sea level (masl), showing no significant spatial or value change from previous configurations. Elevations generally increased topographically from the valley towards the mountain foothills. A more pronounced cone of depression was observed in the southern portion of the aquifer, indicative of concentrated water extraction.

#### Static Water Level evolution

Based on piezometric data from 2001 and 2009, the evolution of the static water level revealed average annual drawdowns varying from 0 to 3 m. As expected, the most significant drawdowns were recorded in the southernmost part of the aquifer. This area exhibits a distinct cone of depression, directly attributed to the concentration of wells extracting potable water for Chihuahua City.

Table 3 details the annual storage change calculation for the El Sauz-Encinillas aquifer from 2001 to 2009.

**Table 3:** Annual storage change calculation for the El Sauz-Encinillas aquifer from 2001-2009 year

Drawdown (m)	Area (km <sup>2</sup> )	Sy	$\Delta V(S)$ (hm <sup>3</sup> /year)
-24.0	28.3	0.2	-135.7
-16.0	70.0	0.2	-224.1
-8.0	33.4	0.2	-53.4
-5.6	12.9	0.2	-14.5
-4.0	90.5	0.2	-72.4
-4.0	35.1	0.2	-28.0
TOTAL	270.2	TOTAL	-528.1
Annual Average			-66.0

According to table 3 storage net change is  $\Delta VS = -66.0 \text{ hm}^3/\text{year}$ .

Table 3 shows various segments of the aquifer experiencing different drawdown levels and their corresponding storage changes. The overall picture indicates a significant negative change in groundwater storage over this nine-year period:

The cumulative net storage change for the entire analyzed area (270.2 km<sup>2</sup>) is -528.1 hm<sup>3</sup>/year.

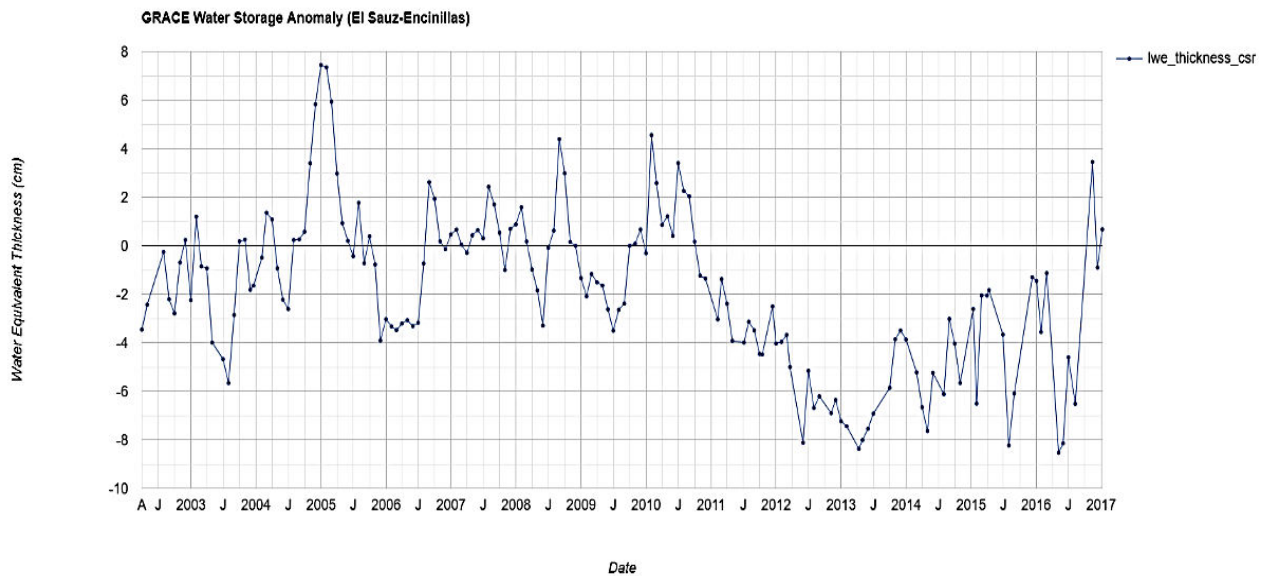
The average annual net change in storage for the aquifer is a concerning -66.0 hm<sup>3</sup>/year. This negative value directly indicates that the aquifer is experiencing depletion, meaning more water is being extracted or lost than is being recharged annually.

### 3.5 Groundwater Depletion Detected by GRACE

The integrated methodology, combining Ai-based forecasting with satellite and field-based hydrological monitoring, has been specifically applied to the El Sauz-Encinillas aquifer to address its complex water management challenges. Long Short-Term Memory (LSTM) neural networks are used to predict long-term rainfall trends, offering insights into future precipitation patterns relevant to the aquifer's recharge. Simultaneously, GRACE satellite data provides crucial information on terrestrial water storage variations over the El Sauz-Encinillas aquifer, revealing a marked declining trend in water storage with persistent negative anomalies. These GRACE-derived negative trends

coincide with the predicted reduction in precipitation by the LSTM model, validating concerns over future water scarcity in the aquifer. This combined approach quantifies aquifer stress and enhances drought anticipation, thereby supporting adaptive management strategies for the sustainable water governance of El Sauz-Encinillas.

Figure 8 illustrates the terrestrial water storage anomaly in the El Sauz–Encinillas aquifer between 2003 and 2017, based on GRACE satellite data. The y-axis represents liquid water equivalent thickness anomalies in centimeters (cm), ranging from approximately –10 cm to +8 cm, while the x-axis displays the time series with monthly markers. The data line, `lwe_thickness_csr`, reflects fluctuations in subsurface water storage.



**Fig. 8.** GRACE satellite-derived terrestrial water storage anomaly in the El Sauz–Encinillas aquifer (2003–2017)

A pronounced downward trend is evident, particularly from 2012 onward, indicating sustained groundwater depletion. These negative anomalies are consistent with intensified extraction and reduced natural recharge, especially during dry years. Seasonal oscillations are visible, with short-term recoveries followed by deeper deficits—suggesting that wet-season recharge is insufficient to offset withdrawals and evaporation losses.

The most severe anomalies occurred between 2013 and 2015, likely linked to compounded drought conditions and increased water demand. This period underscores the aquifer’s vulnerability to both climatic variability and anthropogenic pressures.

The persistent negative anomalies have significant implications for aquifer sustainability, agricultural planning, and ecological resilience. These data are critical for hydrological modeling and can be used to:

- Adjust recharge estimates
- Validate groundwater simulations
- Support early warning systems for water stress

The GRACE-derived trends align with LSTM model predictions of reduced precipitation, reinforcing concerns over future water availability in the region.

Groundwater Table Measurements from Wells Monitoring

Complementing the satellite data, historical well measurements from 1996 to 2012 across the El Sauz–Encinillas aquifer were analyzed using piezometric well records (Figure 9) obtained from CONAGUA’s official repository [8]. These measurements consistently show increasing water table depths, confirming the depletion observed in GRACE data.

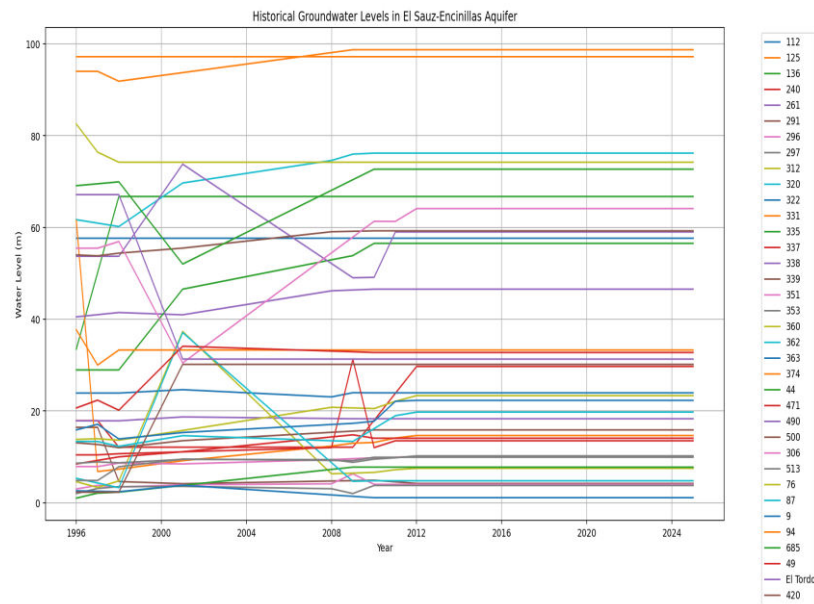


Fig. 9. Piezometric level well Behavior

Table 4 summarizes selected observations from monitoring wells, highlighting spatial variability in depletion rates due to differences in geology, recharge conditions, and extraction intensity.

Table 4: Well, piezometric levels from Sauz-Encinillas aquifer (1996-2012 year)

Well	Curb Elevation	1996	1997	1998	1999	2000	2001	2002	2003	2004	2005	2006	2007	2008	2009	2010	2011	2012
112	1585.65			57.73														
125	1656.73		94	91.85											98.71			
136	1593.85	33.48		66.73														
240	1549.95		17.89	12.1											12.1			29.7
261	1552.45			17.85			18.7								18.3			
291	1528.25		16.43	4.62			4.15									4.9		4.2
296	1525.20	3	3.78	3.42			3.9							4.13	6.3	4.01		
297	1530.95	2	3.12	3.5			3.56							3.05	2	3.76		
312	1544.70	4.59	3.34	4.75			37.33							6.3		6.61	7.2	7.5
320	1610.10	61.68		60.18			69.67							74.58	75.96	76.18		
322	1561.30			23.9			24.64							23.06	23.98	23.95		
331	1541.20	61.5	6.8	7.32			9.16							12.35	12.97	13.14	14.1	14.65
335	1538.05	1	2.1	2.3											7.76			
337	1545.98	8.45		10			11.11								14.8	14.06		
338	1585.40	40.5		41.45			40.95							46.18		46.54		
339	1542.30	13.06	12.7	12			13.52									15.87		
351	1529.15	7.89	7.88	8.64			8.46							9.4		9.8	9.9	10.1
353	1529.30	8.6	8.89	8.7			9.45							9.4	8.8	9.5	9.8	10.21
360	1562.20	13.8	13.95	13.63			15.75							20.8		20.52	22.1	23.34
362	1534.80	5.32		3.28			37.08								4.67	4.79		
363	1535.70	2.6		2.4			3.81									1.1		
374	1659.05			97.22														
44	1568.15			28.94			46.54								53.85	56.52		
471	1528.68		10.43	10.68			11.09							12.02	31.25	12.01	13.5	

Well	Curb Elevation	1996	1997	1998	1999	2000	2001	2002	2003	2004	2005	2006	2007	2008	2009	2010	2011	2012
490	1605.40			53.7			73.77								49.02	49.11	59	59
500	1596.95	54	53.8	54.38			55.48							59.05		59.25		
306	1601.29		55.46	56.92			30.46									61.32	61.3	64.1
513	1543.36		4.85	7.84			9.51								9.18	9.91		
76	1601.30	82.53	76.4	74.2														
87	1562.98		13.35	12.29			14.62								13.35		18.96	19.75
9	1555.78	15.86	17.1	13.9			15.3								17.3	17.76	22.1	22.3
94	1577.60	37.7	30	33.28														
685	1609.80	69.08		69.92			52.01									72.68		
49	1543.30	20.65	22.35	20.16			34.1									32.74		
El Tordo	1618.02			67.13			31.3											
420	1528.05			2.3			30.15											

Together, the GRACE satellite anomalies and field-based piezometric measurements present a consistent and compelling narrative of long-term groundwater depletion in the El Sauz–Encinillas aquifer. This convergence of evidence highlights the urgent need for adaptive management strategies and continuous hydrological monitoring.

Figure 9, which displays GRACE-derived terrestrial water storage anomalies from 2003 to 2017, offers independent, satellite-based validation of the depletion trend. This figure reveals a pronounced decline in liquid water equivalent thickness, with persistent negative anomalies—particularly from 2012 onward—some exceeding  $-8$  cm. These anomalies are indicative of intensified groundwater extraction and insufficient natural recharge. Satellite observations align closely with field data presented in Table 4, which documents negative annual storage changes between 2001 and 2009. This cross-validation between remote sensing and in-situ measurements reinforces the severity of aquifer stress and underscores the reliability of the findings across different methodologies and temporal scales.

Moreover, the GRACE anomaly trends coincide with precipitation reductions forecasted by the LSTM model, further substantiating concerns over future water scarcity. The integration of satellite data, machine learning forecasts, and field measurements provides a robust framework for understanding aquifer dynamics and guiding sustainable water resource planning in the region.

#### 4. Conclusions

This paper demonstrates the valuable potential of integrating advanced artificial intelligence (AI) with both satellite and field-based hydrological data to enhance water resource management in semi-arid regions. The detailed analysis of the El Sauz-Encinillas aquifer and the Río Conchos 3 basin offers key insights into current and future water availability challenges.

This finding shows that Long Short-Term Memory (LSTM) models are effective in anticipating drought conditions and forecasting rainfall variability. This predictive capability is a useful tool for a more proactive approach to water management.

Data from the GRACE satellite provides strong evidence of long-term groundwater depletion. For the El Sauz-Encinillas aquifer, GRACE data from 2003–2017 revealed a clear declining trend in water storage. This aligns with and is reinforced by field data, which showed an average annual storage loss of  $-66.0$   $\text{hm}^3/\text{year}$  for the 2001–2009 period. The confirmation of GRACE observations with historical well measurements further validates this evidence. Within the Río Conchos 3 basin, hydrological modeling confirmed the methodologies used. The basin faces a surface water deficit, and future projections show significant variability depending on the model used. These discrepancies highlight the basin's sensitivity to climate and land-use changes. AI models proved essential for predicting periods of low water availability in advance, identifying vulnerable urban areas, and optimizing operational responses.



The synergy between predictive analytics and physical hydrological data provides a robust toolkit for building resilience to climate impacts. We recommend that future research explore integrating additional factors such as evapotranspiration, land cover, and socio-economic indicators for more holistic and effective planning.

Scaling these successful models to other cities in northern Mexico and investing in the necessary digital infrastructure and personnel training are suggested next steps. The widespread adoption of AI-powered tools holds the potential to significantly improve water security across arid and semi-arid landscapes. This integrated approach is essential for building resilient water infrastructure, guiding effective policy, and ensuring sustainable water availability in regions facing climate uncertainty.

## References

- [1] Scanlon, Bridget R., Sarah Fakhreddine, Ashraf Rateb, Inge de Graaf, Jay Famiglietti, Tom Gleeson, Quentin Grafton, et al. “Global Water Resources and the Role of Groundwater in a Resilient Water Future.” *Nature Reviews Earth & Environment* 4 (2023): 87–101. <https://doi.org/10.1038/s43017-022-00378-6>.
- [2] Hamed, Khaled H., and A. Ramachandra Rao. “A Modified Mann-Kendall Trend Test for Autocorrelated Data.” *Journal of Hydrology* 204, no. 1-4 (January 1998): 182–196. [https://doi.org/10.1016/S0022-1694\(97\)00125-X](https://doi.org/10.1016/S0022-1694(97)00125-X).
- [3] Ni, Lingling, Dong Wang, and Jianfeng Wu. “Streamflow Forecasting Using Long Short-Term Memory Network.” In: Huang, Chongfu, and Zoe Nivolianitou (eds.). *Risk Analysis Based on Data and Crisis Response Beyond Knowledge*, 264–269. London, CRC Press, 2019. <https://doi.org/10.1201/9780429286346-39>.
- [4] Rodell, Matthew, Isabella Velicogna, and James S. Famiglietti. “Satellite-Based Estimates of Groundwater Depletion in India.” *Nature* 460, no. 7258 (2009): 999–1002. <https://doi.org/10.1038/nature08238>.
- [5] Famiglietti, James S. “The Global Groundwater Crisis.” *Nature Climate Change* 4 (2014): 945–948. <https://doi.org/10.1038/nclimate2425>.
- [6] Lukat, Evelyn, Andrea Lenschow, Ines Dombrowsky, Franziska Meergans, Nora Schütze, Ulf Stein, and Claudia Pahl-Wostl. “Governance towards Coordination for Water Resources Management: The Effect of Governance Modes.” *Environmental Science and Policy* 141 (March 2023): 50–60. <https://doi.org/10.1016/j.envsci.2022.12.016>.
- [7] González-Velázquez, Rodrigo Israel, and José Luis Castro-Ruiz. “Water Management in the Rio Conchos Basin: Impacts on Water Deliveries Under the 1944 Treaty.” *Texas Water Journal* 13, no. 1 (2022): 47–63. <https://doi.org/10.21423/twj.v13i1.7139>.
- [8] National Water Commission / Comisión Nacional del Agua (CONAGUA). “Update on Water Availability in the El Sauz-Encinillas Aquifer, Chihuahua State”/ “Actualización de la Disponibilidad de Agua en el Acuífero El Sauz Encinillas, estado de Chihuahua”, Ciudad De México, 2024. Available in: [https://sigagis.conagua.gob.mx/gas1/Edos\\_Acuiferos\\_18/chihuahua/DR\\_0807.pdf](https://sigagis.conagua.gob.mx/gas1/Edos_Acuiferos_18/chihuahua/DR_0807.pdf).
- [9] Hyndman, Rob J., and George Athanasopoulos. *Forecasting: Principles and Practice*. 3rd ed. Melbourne, OTexts, 2021. <https://otexts.com/fpp3/>.
- [10] Hochreiter, Sepp, and Jürgen Schmidhuber. “Long Short-Term Memory.” *Neural Computation* 9, no. 8 (1997): 1735–1780. <https://doi.org/10.1162/neco.1997.9.8.1735>.
- [11] Tanriverdi, İrem, and İnci Batmaz. “AI-Driven U.S. Drought Prediction Using Machine Learning and Deep Learning.” *Climate Dynamics* 63 (2025): 249. <https://doi.org/10.1007/s00382-025-07720-w>.
- [12] Zhang, Huihui, Hugo A. Loaiciga, and Tobias Sauter. “A Novel Fusion-Based Methodology for Drought Forecasting.” *Remote Sensing* 16, no. 5 (2024): 828. <https://doi.org/10.3390/rs16050828>.
- [13] Chang, Fi-John, Li-Chiu Chang, and Jui-Fa Chen. “Artificial Intelligence Techniques in Hydrology and Water Resources Management.” *Water* 15, no. 10 (2023): 1846. <https://doi.org/10.3390/w15101846>.
- [14] Gacu, Jerome G., Cris Edward F. Monjardin, Ronald Gabriel T. Mangulabnan, Gerald Christian E. Pugat, and Jerosse G. Solmerin. “Artificial Intelligence in Surface Water Management: A Comprehensive Review of Methods, Applications, and Challenges.” *Water* 17, no. 11 (2025): 1707. <https://doi.org/10.3390/w17111707>.
- [15] Bravo-Jácome, José Avidán, Margarita Elizabeth Preciado-Jiménez, José Alberto Báez-Durán, Eduardo Alexis Cervantes-Carretero, Roel Simuta-Champo, Rodrigo Roblero-Hidalgo, Héctor Giovanni Rodríguez-Vázquez, Ana Palacios-Fonseca, Yolanda Solís-Alvarado, Maritza Arganis-Juárez, and Héctor Alonso Ballinas-González. “Surface Water Assessment Availability and Potential Impacts on Mexico’s 757 Hydrographic Basins for Future Hydroelectric Development.” *Atmósfera* 39 (2025): 489–524. <https://doi.org/10.20937/ATM.53384>.

## Aspects Regarding Methods for Hydraulic Cylinders Synchronization

PhD. Stud. Eng. **Ionela Mihaela POPESCU**<sup>1</sup>, Ph.D. Eng. **Victor CONSTANTIN**<sup>1</sup>,  
MSc. Eng. **Daniel NANCA**<sup>1,\*</sup>

<sup>1</sup> National University of Science and Technology POLITEHNICA Bucharest

\* daniel.nanca@stud.mec.upb.ro

**Abstract:** *To address the issue of synchronization of the hydraulic cylinders, that can lead to safety hazards for the operators, this study develops a hydraulic circuit intended for vehicles service lifting. The study covered two variants that were compared through Fluid SIM design and simulation while monitoring important parameters, demonstrating the main differences between electrical and proportional controlled transmissions. Testing highlighted a better precision regarding the proportional transmission, but at a higher cost while it also requires specialized personnel to handle due to its complex design.*

**Keywords:** *Hydraulic cylinder, proportional control, flow divider, hydraulic system*

### 1. Introduction

Hydraulic systems are indispensable in many industrial fields [1] due to their ability to develop large forces and moments. These forces, which they develop, allow the lifting, supporting, blocking and transportation of very large installations, equipment, etc., which cannot be moved or handled otherwise than with high-power systems.

One solution for the synchronization of hydraulic cylinders can be the use of an external controller to synchronize the movement of the cylinders and a non-linear internal control system for the cylinders [2]. Nowadays hydraulic press plays a role in the heavy industry to which synchronized hydraulic cylinder is the key component, therefore a thorough investigation is needed through simulation and testing [3].

In industrial manufacturing systems, it is often needed to synchronize two, three or more hydraulic cylinders to assure a better control of an automatic and synchronized system [4]. Advanced research on multi-cylinder synchronization confirms this requirement, especially in forging hydraulic presses [5]. Thus, to assure it, the cylinders are going to be accompanied by position sensors. Several methods of cylinder synchronization can be identified in the specialized literature [6]:

- flow divider;
- rigid cylinder coupling mechanism;
- pumps with equal flow rates for individual supply of each cylinder;
- proportional directional control valves.

The flow divider is the most frequently used method of synchronization of hydraulic cylinders, due to its constructive simplicity and the results obtained. It prevents kinematic discrepancy and improves vehicle mobility; the most important types of flow dividers are spool type and gear type. Each type has its own characteristics as accuracy, pressure drop and application parameters [7].

Coupling the cylinders by a rigid mechanism is another method used for their simultaneous movement. This solution assumes that one of the cylinders is forced to move at the same speed as the other, even if there is a difference in flow rate between the branches. Although in the short term it ensures good positioning accuracy, over time, due to repeated forcing, premature mechanical wear occurs, which affects the operation of the entire system.

Using two pumps with equal flow rates can ensure an identical fluid flow rate for both cylinders and, implicitly, synchronized operation. However, this solution cannot be applied in any type of system, but only where the configuration allows the integration of two hydraulic pumps. Doubling the equipment in the system leads to an increase in size, maintenance costs and circuit complexity.

The use of proportional directional control valves for position control allows for high precision, thanks to position sensors that provide a quick response to the movement of the directional control valve spool. Although the precision is very good, the cost of acquiring the equipment can be

disproportionate to the workload of the system. In this case, a rigorous assessment of the possibility of recovering the initial investment is necessary.

For the proposed model, the use of a flow divider was chosen as the method of synchronization of the movement. This equipment consists of two throttles, which allow the adjustment of the fluid flow entering the cylinder feed holes. Depending on the application, the two throttles can have identical or different flow sections.

## **2. Modelling and simulation of the hydraulic circuit intended for servicing vehicle lifting installations**

The proposed transmission model, which will serve a vehicle lifting platform with energy, was designed so that the hydraulic energy produced no longer has a carbon footprint, due to the way it is generated. Thus, using the wind engine as an energy source, hydraulic energy has a minimal impact on the environment.

To model a circuit that allows a vehicle to be lifted with a platform, the literature [6] was consulted, which indicates that the use of a flow divider allows the synchronization of the hydraulic cylinders. Their synchronized movement is a common problem in hydraulic drive systems that use linear motors.

Two variants of the transmission model serving the vehicle lifting platform are analysed:

- Electrically controlled;
- Proportional controlled.

The first variant is based on the use of electrically controlled equipment. This is a more affordable technical solution in terms of costs. A main disadvantage, observed during the simulation, was the delay that occurred when switching between one state and another of the circuit. Considering the scope of application, such delays can be acceptable. The lowering or raising of the vehicle is performed relatively slowly, to avoid instability that may occur due to the mass that the platform must lift.

The second proposed variant uses proportional hydraulic equipment, with closed-loop control. Proportional control equipment makes precise adjustments, positioning the cylinders exactly at the desired height. This solution requires solid knowledge in the use of proportional equipment and its control, knowledge that those who use the platform may lack. Compared to classic technology, with manual or electric control, proportional technology is much more sensitive to environmental conditions. External factors can influence the proper functioning of the circuit. This type of equipment has high acquisition costs and requires dedicated electronics, as well as specialized personnel for installation and commissioning. Maintenance costs could reduce the profitability of the solution.

### **2.1 Electrically controlled lifting platform**

Vehicle lifting systems are manually operated by the people who carry out technical checks on cars. As a rule, there are two hydraulic cylinders mounted on either side of the platform on which the vehicle is placed. After placing it on the platform, depending on the technical problems it has or the necessary checks, it is raised to a certain height, which allows easy access for the mechanic under the vehicle, to make an assessment of the actual situation of the vehicle.

The manual operation of this platform allows employees who do not have technical training to operate the system easily. Both manual and electric operation can be used for such simple systems, but essential for carrying out technical checks on vehicles. One advantage of these is the low cost of the hydraulic components used. Having a simple to use operating principle and a not very advanced technological level, the cost of acquisition, maintenance and replacement of equipment is low.

Considering that this system works against quite large forces, generated by the weight distribution on the platform, an emergency stop system is necessary. This prevents the sudden lowering of the platform if, for various reasons, the hydraulic circuit fails and one of the directional control valves does not maintain its position. An emergency system is proposed that is triggered to protect the personnel performing the checks, by blocking the cylinders in the extended position.

This is achieved using a series of accumulators, which release the fluid stored on the circuit that allows the cylinders to be extended. Simultaneously, two auxiliary directional control valves, which under normal operating conditions are in the preferential "open" position, close, blocking the fluid in the first chamber of the cylinder.

Testing of the proposed hydraulic circuit does not include the safety system, since the purpose of the simulation is to observe the behaviour of the system and its degree of controllability, as well as to identify technical obstacles, but also those related to costs, in relation to the degree of innovation brought by each proposed model.

Thus, an electric drive system for the advance and retraction of the cylinders was designed and built, corresponding to the lifting and lowering movement of the platform. The user has two buttons that activate the electromagnets of the 4/3 directional control valves, responsible for switching the spool to the position through which the chambers that allow the cylinders to advance are supplied, but also for their retraction. Each button activates an electromagnet of each directional control valve, corresponding to the advance and retraction command of the cylinder. Speed adjustment is achieved using track throttles, mounted on both the advance and return circuits.

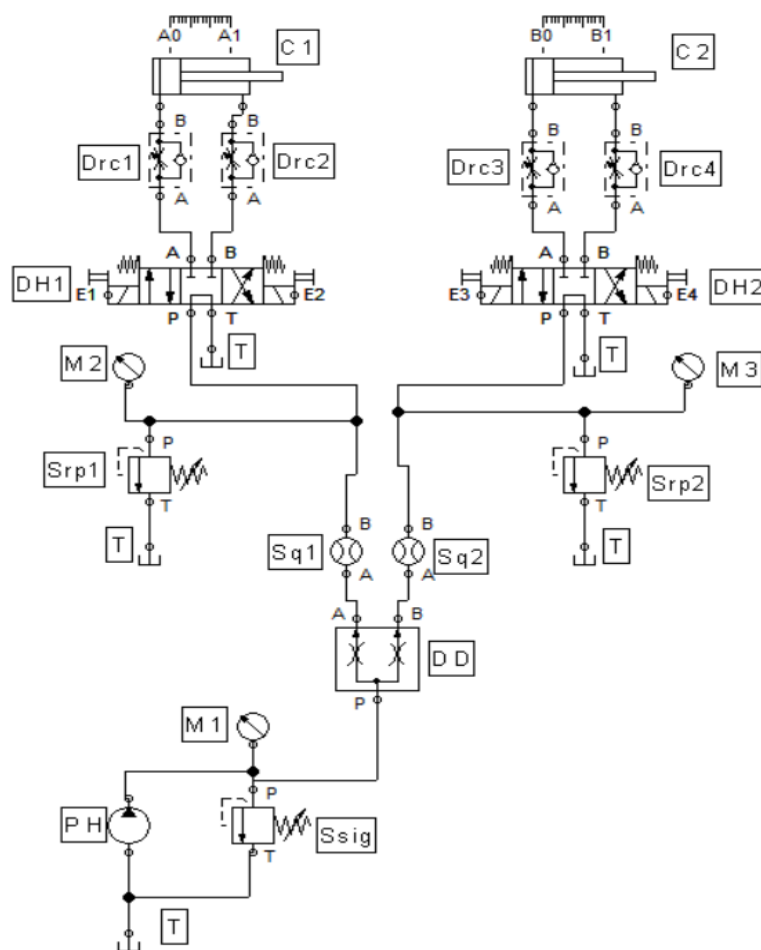


Fig. 1. Hydraulic circuit for supplying and operating a platform for lifting vehicles

Fig.1 shows the hydraulic power supply and drive circuit of a vehicle lifting system. The hydraulic power supply system consists of: PH – hydraulic pump, which ensures a constant fluid flow; M1 – pressure gauge, for checking and monitoring the pressure on the pump discharge; Ssig – safety valve, ensures circuit protection and allows the flow to be diverted to the tank when the set working pressure is exceeded; T – hydraulic fluid tank.

The hydraulic circuit is completed by the cylinder drive system, which consists of the following equipment: DD – flow divider, which ensures equal distribution of the flow on the two branches of the drive circuit; Sq1 and Sq2 – flow sensors, through which the flow values obtained after the

divider are monitored; Spr1 and Spr2 – pressure valves, which have the role of reducing the pressure that is created on the supply branch due to the configuration of the circuit, but also of the directional control valve, which does not allow, in the central position, the sending of the fluid flow to the tank. Thus, as a safety measure, the two pressure valves were installed, which send the fluid flow to the tank. The pressure at the connection points is measured with two pressure gauges, M2 and M3. Two 4/3 bistable directional control valves are also installed in the circuit, with electrical control, but also manual, with spring return. In the preferential position, these have the P, T, A, B ports blocked. When the electromagnet E1, respectively E3, are powered, the directional control valves switch the spool to the position that connects P-A and B-T. When the electromagnet E2, respectively E4, are powered, the directional control valves switch the spool to the position that allows communication between the P-B and A-T ports. The hydraulic circuit for driving the hydraulic cylinders, which are part of the vehicle lifting system, has been completed and improved by integrating track throttles, Drc1, Drc2, Drc3, Drc4, on the circuit branches that advance and retract them, respectively. Double-acting hydraulic cylinders, C1 and C2, were chosen for this application.

Fig. 2 shows the electrical diagram of the circuit for driving the vehicle lifting platform. This electrical circuit activates the electromagnets that control the advance of the cylinders, as well as the electromagnets that control their retraction. The electrical circuit has been designed to operate manually, by pressing two buttons. The user sets the required height at which the vehicle should be positioned, depending on its height and the required technical intervention.

To verify the functionality of this drive system, a series of important parameters were monitored, such as: flow and pressure variation, pump speed, cylinder advance.

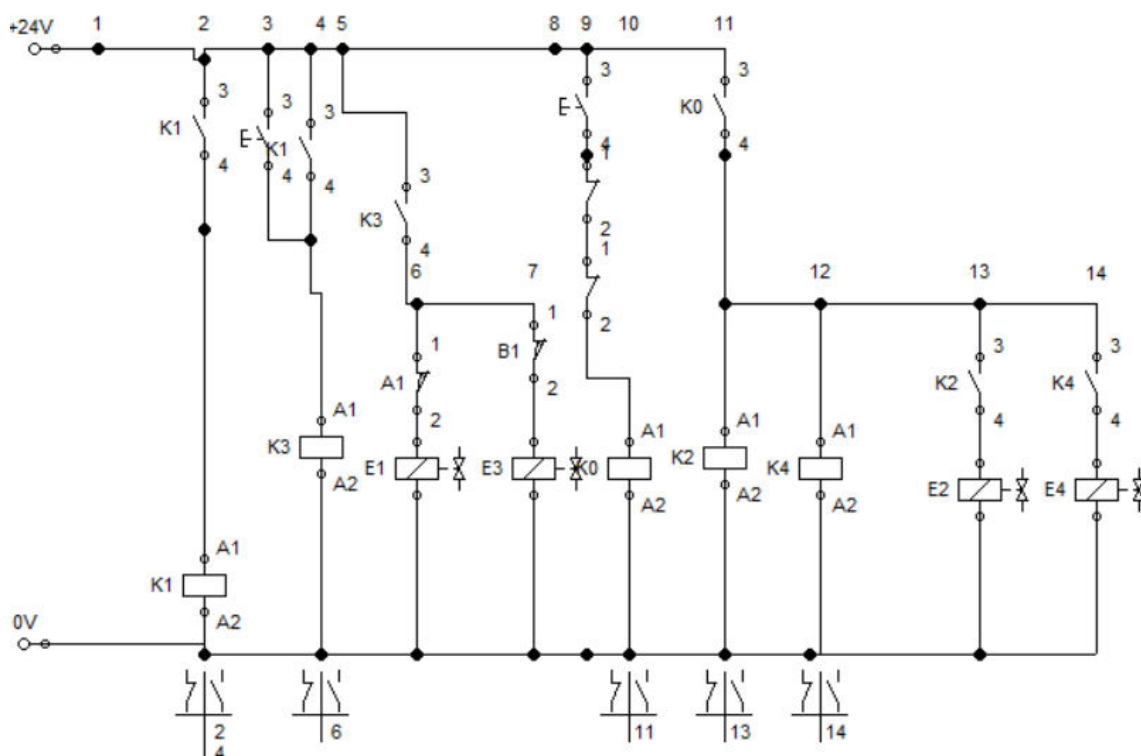


Fig. 2. Electrical diagram of the vehicle lift platform drive circuit

## 2.2. Proportional controlled lifting platform

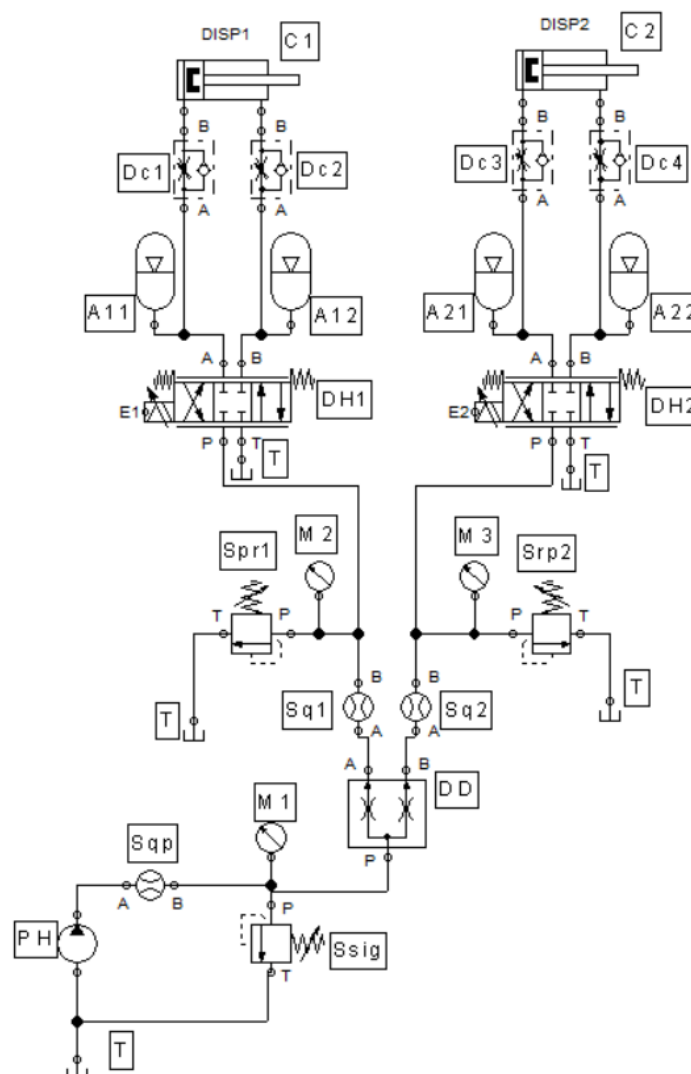
During the testing of the functionality of the simulation scheme, an oscillatory movement of the hydraulic cylinders that raise the platform was observed. This oscillatory movement is determined by the variation of the flow section of the directional control valve, which occurs during positioning. Although the flow section is also implicitly regulated by the proportional directional control valve, the flow speed varies uncontrollably, so the cylinders move either too fast or too slow. To regulate the speed at which the two cylinders raise the platform, it was necessary to improve the drive



circuit scheme by adding on each branch of the circuit a track throttle and an accumulator. Considering the simulation carried out for variant 1, it was possible to deduce that the use of accumulators with a larger capacity could have prevented the flow and pressure drops during the switching of the two buttons.

For this simulation, hydraulic accumulators were chosen, with a pre-charge pressure of 10 bar and a volume of 3 l. To simplify the electrical control scheme and reduce the electronic components, it was decided to use two monostable proportional directional control valves, 4/3. The position adjustment of the hydraulic cylinders is performed in a closed loop, by using a position transducer on each cylinder.

Fig. 3 shows the hydraulic diagram of the circuit for lifting vehicles, variant 2, which includes proportional control of the movement of the two cylinders by means of two directional control valves. The simulation of the circuit operation was performed without considering human presence. Sensor systems for user protection will be considered if, following the analysis of the results obtained, it is decided to implement this technical solution.



**Fig. 3.** Hydraulic circuit diagram for vehicle lifting with proportional control

The hydraulic diagram of the tested circuit includes the following equipment:

- PH – fixed-flow hydraulic pump, similar to variant 1;
- Sqp – flow sensor, introduced because of the results obtained from the simulation of the first variant, to avoid possible phenomena that may go unnoticed in the hydraulic energy supply system;
- Ssig – safety valve, adjusted to the system's working pressure;

- T – hydraulic fluid tank;
- DD – flow divider;
- Sq1, Sq2 – flow sensors, which monitor both the flow and the proper functioning of the divider. At small flow sections, the flow divider may suffer blockages, which would lead to the supply of only one circuit branch with a much too large volume of fluid, generating a malfunction;
- Spr1, Spr2 – pressure valves, which protect the system from backpressure;
- M2, M3 – pressure gauges, allow for quick verification of the pressure values on the the two branches of the hydraulic circuit;
- DH1, DH2 – monostable hydraulic directional control valve, 4/3, with proportional control;
- A11, A12, A21, A22 – hydraulic accumulators, which store and release energy when needed;
- Dc1, Dc2, Dc3, Dc4 – track throttle, allows precise adjustment of the piston speed, both on advance and on retraction;
- DISP1, DISP2 – position transducers;
- C1, C2 – hydraulic cylinders.

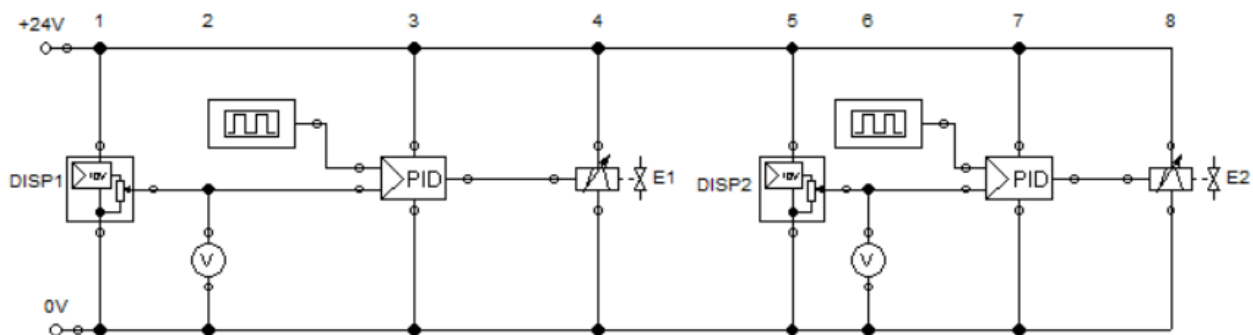


Fig. 4. Electrical and control diagram of the hydraulic circuit

Fig. 4 shows the electrical control diagram of the drive circuit. The following notations can be seen: DISP1 and DISP2 – are the position transducers, which operate on a principle similar to that of a potentiometer; the reading of the voltage drop corresponding to the position of the cylinder rod is carried out by a voltmeter, symbolized by V, positioned between the central pin of the sensor and GND.

A P-type (proportional) controller was used for each controlled electromagnet. The sensor signal pin and an output signal from a function generator are connected to the controller inputs.

A rectangular signal was chosen for the electromagnet control, with a variation range of 0–10 V, at a frequency of 0.1 Hz. Regarding the adjustment range of the P-controller, a range between -10 and 10 V was chosen, specific to hydraulic equipment with proportional control. This range covers the three states that the proportional valve can have: -10 V – the valve is switched to the P-B, A-T position; 0 V – central position, locked; 10 V – the valve connects P-A, B-T.

### 3. Conclusions

Both transmission model variants have their advantages and disadvantages; an electrically controlled transmission is easier to command and cheaper to maintain, but it presents a delay between the raising and the lowering of the platform. As for the proportional controlled transmission, it has a better precision, it can be commanded to lift or lower to a certain height, but it needs specialized personnel and represents a higher cost. Therefore, for a vehicle lifting platform used by mechanics to service cars, the electrically controlled transmission might be advantageous, but overall the proportional controlled transmission represents a better and more reliable option, especially for advanced projects or automatic lifting use.

**References**

- [1] Li, Ruichuan, Wentao Yuan, Xinkai Ding, Jikang Xu, Qiyu Sun, and Yisheng Zhang. “Review of Research and Development of Hydraulic Synchronous Control System.” *Processes* 11, no. 4 (2023): 981. <https://doi.org/10.3390/pr11040981>.
- [2] Woś, Piotr, and Ryszard Dindorf. “Synchronization of the Movement for Multi-Cylinder Electrohydraulic Servo Driver.” Paper presented at the 14th International Conference “Experimental Fluid Mechanics 2019” - EFM19, Františkovy Lázně, Czech Republic, November 19-22, 2019. *EPJ Web of Conferences* 269 (2022): 01069. <https://doi.org/10.1051/epjconf/202226901069>.
- [3] Yu, Jin, Ming Zhen Fan, Guo Qin Huang, and Min Yu. “Simulation and Analysis on Main Synchronized Hydraulic Cylinder of Huge Hydraulic Press.” *Applied Mechanics and Materials* 233 (2012): 150-153. <https://doi.org/10.4028/www.scientific.net/amm.233.150>.
- [4] Adenuga, Olukorede Tijani, and Khumbulani Mpofu. “Control System for Electro-hydraulic Synchronization on RBPT.” *Procedia CIRP* 17 (2014): 835–840. <https://doi.org/10.1016/j.procir.2014.01.135>.
- [5] Xu, Cong, Xiao Xu, Zhao Liu, and Xin Wang. “Research on multi-cylinder synchronous control system of multi-directional forging hydraulic press.” Paper presented at the 8th International Conference on Applied Materials and Manufacturing Technology (ICAMMT 2022), Hangzhou, China, April 15-17, 2022. *Journal of Physics: Conference Series* 2338, no. 1 (2022): 012081. <https://doi.org/10.1088/1742-6596/2338/1/012081>.
- [6] Avram, Mihai. *Fluid Power / Actionari Hidraulice și Pneumatice*. Bucharest, University Publishing House, 2005.
- [7] Przybysz, Mirosław, Marian Janusz Łopatka, Marcin Małek, and Arkadiusz Rubiec. “Influence of Flow Divider on Overall Efficiency of a Hydrostatic Drivetrain of a Skid-Steer All-Wheel Drive Multiple-Axle Vehicle.” *Energies* 14, no. 12 (2021): 3560. <https://doi.org/10.3390/en14123560>.

## Mapping Convective Precipitation Susceptibility in the Peñitas Watershed: A Novel Convectivity Index and Geostatistical Interpolation Framework

Dr. Maritza ARGANIS<sup>\*,1,2</sup>, M. Eng. Margarita PRECIADO<sup>\*,3</sup>, Dr. Faustino DE LUNA<sup>1</sup>,  
Eng. Student Cristian LÓPEZ<sup>1</sup>, Eng. Student Edgar DE DIOS SEVILLA<sup>1</sup>,  
M. Eng. Omar CABRERA<sup>1</sup>, Dr. Rodrigo ROBLERO-HIDALGO<sup>3</sup>

<sup>1</sup> Universidad Nacional Autónoma de México. Instituto de Ingeniería. Av. Universidad 3000 Ciudad Universitaria Edif 17 c.p. 04510 Coyoacán CDMX, México

<sup>2</sup> Universidad Nacional Autónoma de México. Facultad de Ingeniería. Av. Universidad 3000 Ciudad Universitaria c.p. 04510 Coyoacán CDMX, México

<sup>3</sup> Instituto Mexicano de Tecnología del Agua, Paseo Cuauhnáhuac 8532, c.p. 62550 Jiutepec, Mor., México

\* MArganisJ@iingen.unam.mx; preciado@tlaloc.imta.mx

**Abstract:** Convective precipitation poses significant hydrometeorological risks in the Peñitas River Basin, where short-duration, high-intensity rainfall events often trigger flash floods and landslides. This study introduces a novel empirical index—the Convectivity Factor (CF)—to spatially characterize convective susceptibility using high-frequency precipitation data from CFE’s automated weather stations and topographic inputs from INEGI’s Digital Elevation Model. The CF, defined as the ratio of maximum 1-hour to 24-hour precipitation, was calculated using annual historical maxima and mapped via three interpolation techniques: Inverse Distance Weighting (IDW), Kriging, and CoKriging. CoKriging, which incorporates elevation as a secondary variable, produced the most topographically coherent results. The resulting CF maps identify zones of elevated convective risk, supporting rainfall-runoff modeling and infrastructure planning in data-scarce regions. Though empirical, the CF provides a scalable tool for adaptive water management. Future research should integrate radar-derived instability indices and validate CF maps against observed extreme events.

**Keywords:** Convective precipitation, Convectivity factor, Spatial interpolation, Hydrometeorological risk, Rainfall-runoff modeling, CoKriging, Peñitas Watershed

### 1. Introduction

Convective precipitation is a primary driver of hydrological extremes, particularly in vulnerable regions such as the Peñitas Watershed in southern Mexico. Localized and intense rainfall events frequently trigger flash floods, landslides, and severe soil erosion. These phenomena are becoming increasingly frequent and intense due to climate change, highlighting the urgent need for diagnostic tools that can spatially characterize convective susceptibility using high-resolution, accessible data sources [1-2].

A dramatic illustration of these risks occurred on the night of November 4, 2007, when a massive landslide released approximately 48 million cubic meters of rock and mud over an 80-hectare area. This event created a natural dam across the Grijalva River—one of Mexico’s largest—between the Peñitas (downstream) and Malpaso (upstream) dams. The resulting barricade measured 80 meters in height, 800 meters in length, and 300 meters in width. The rural town of San Juan de Grijalva, situated along the riverbank, was devastated by the moving mass and the wave-induced flooding that followed. Tragically, 25 lives were lost. Using remote sensing and geographic information systems (GIS), this study contextualizes the landslide within the broader Grijalva River Watershed and links it to abnormal precipitation patterns observed in late October and early November 2007.

To address the need for spatial diagnostics of convective risk, this paper introduces the Convectivity Factor (CF)—a novel empirical index designed to map the annual frequency of convective events across the Peñitas Watershed. The CF integrates daily precipitation thresholds derived from the Comisión Federal de Electricidad (CFE)’s automated weather station reanalysis dataset. This approach offers a computationally efficient and scalable method for identifying

regions prone to convective activity.

Although empirical, the CF provides a robust foundation for future enhancements in convective hazard diagnostics. Its reliance on open-access reanalysis data ensures broad applicability, especially in regions with sparse observational networks. By bridging the gap between large-scale climate datasets and localized hazard mapping, the CF contributes to adaptive strategies for managing convective risks in a changing climate.

Beyond climatological analysis, the CF has practical implications for hydrological modeling. CF maps support the estimation of design hyetographs—critical tools for rainfall-runoff simulations and hydraulic infrastructure planning. These maps are particularly valuable in data-scarce regions, enabling accurate modeling of short-duration rainfall events using daily records [3-4-5].

In areas with dense rainfall monitoring networks, CF maps enhance the regionalization of precipitation events and improve the reliability of hydrological models. In Mexico, Baeza (2007) [5] developed a Convectivity map that has been instrumental in estimating intensity-duration-frequency (IDF) relationships. Similarly, various authors [6-7] have advanced in hydrological modeling and water resources management through convection-based methodologies.

These efforts underscore the value of developing Convectivity maps in countries with extensive measurement networks, optimizing both planning and response to extreme hydrometeorological events.

In this paper, a Convectivity map for the Peñitas Watershed was developed by correlating maximum 1-hour precipitation with 24-hour totals. Nine automatic weather stations distributed across the basin provided precipitation records at 1-hour intervals. For each station, historical averages of maximum 1-hour and 24-hour precipitation were calculated, and the CF was derived accordingly. The Peñitas Watershed Digital Elevation Model (DEM), obtained from INEGI [8], was used as a reference for topographic adjustments.

Three interpolation methods were applied to generate this map:

Inverse Distance Weighting (IDW), Kriging and CoKriging, implemented in ArcGIS®, which also incorporated topographic data.

## 2. Methodology

This paper presents a robust framework for defining and mapping a novel Convectivity Factor (CF) across Peñitas Watershed, integrating reanalysis data, high-frequency precipitation records, and advanced spatial interpolation techniques.

### 2.1 Study Area

The Peñitas Watershed, located in southern Mexico, holds significant hydrological, ecological, and socio-economic importance. The Peñitas Dam, officially known as the Central Hidroeléctrica Ángel Albino Corzo, is a major hydroelectric facility on the lower Grijalva River. It has an installed capacity of 420 megawatts, contributing substantially to Mexico's renewable energy supply. This Riverbasin is situated in one of the rainiest regions of Mexico, making it highly susceptible to extreme precipitation and runoff. This dam plays a vital role in regulating water flow and mitigating flood risks, especially in downstream areas like Tabasco, which have experienced severe inundations during extreme weather events. Due to its high rainfall and complex terrain, the Peñitas Watershed is a hotspot for convective precipitation, making it a valuable case study for climate impact assessments and hydrological modeling. Events like the 2007 landslide and subsequent flooding underscore the basin's vulnerability to climate-driven hydrometeorological hazards. Flooding and landslides in the region have historically caused loss of life, displacement, and economic disruption, emphasizing the need for resilient infrastructure and early warning system [9].





Fig. 1. Study site: Peñitas Watershed Location and their climatic Network. Source: Own design.

## 2.2 Data Sources

CFE's automated weather stations reanalysis Data: Daily maximum precipitation data from 2005 to 2025 year distributed across Peñitas Watershed provided 1-hour interval precipitation records, sufficient for calculating maximum 1-hour and 24-hour rainfall values.

Table 1: CFE's automated weather station's location and elevations. Source [10-11]

Automated weather stations name	Latitude	Longitude	Elevation Masl	Date
Aza-Pac	17.26	- 93.42	229.00	2005-09-06 to 2025-08-04
Emiliano Zapata	17.22	- 93.34	382.00	2005-09-06 to 2025-08-04
Presa Malpaso	17.18	- 93.60	200.00	2005-09-06 to 2025-08-04
Ocotepéc	17.23	- 93.15	200.00	2005-09-06 to 2025-08-04
Peñitas Dam	17.44	- 93.46	53.00	2005-09-06 to 2025-08-04
Romulo Calzada	17.35	- 93.55	119.00	2005-09-06 to 2025-08-04
Sayula	17.40	- 93.33	51.00	2005-09-06 to 2025-08-04
Tuneles de Juan de Grijalva	17.36	- 93.42	123.00	2005-09-06 to 2025-08-04
Tzimbac	17.23	- 93.41	200.00	2005-09-06 to 2025-08-04

Digital Elevation Model (DEM): A 15x15 meters, download from INEGI [8] supporting topographic corrections and spatial interpolation.

### 2.3 Convectivity Factor Definition

A convective day was empirically defined a criterion:

- Daily precipitation > 0.1 mm

The Convectivity Factor (CF), also referred to as Factor R, is calculated as shown in equation 1 [5]:

$$R = \frac{P_{1h}}{P_{24h}} \quad (1)$$

Where:

- $P_{1h}$ : Maximum 1-hour precipitation
- $P_{24h}$ : Total 24-hour precipitation

This factor is valuable for estimating the intensity of short-duration rainfall from daily records, facilitating the development of design hyetographs for rainfall-runoff modeling and crucial for hydraulic infrastructure planning in data-scarce regions.

### 2.4 Procedure for Convectivity Factor Calculation

Procedure 1 was employed to obtain the Convectivity factor:

Procedure 1: Annual Historical Maxima from nine automated weather stations elected automatic stations set across Peñitas Watershed was utilized. For each station, the annual historical maximum 1-hour and 24-hour precipitation values were calculated and then averaged. The Convectivity factor for each station was subsequently determined using Equation (1).

### 2.5 Spatial Aggregation and Mapping

Daily convective flags were aggregated over 365 days to compute annual Convectivity frequency for each grid point. Resulting Convectivity map visually represents convective number days per year, generated using ArcGIS and Python-based visualization tools.

Spatial interpolations were performed using open-source software tools. Inverse Distance Weighting (IDW) and Kriging interpolations were applied in QGIS, while CoKriging was employed in ArcGIS®. Spatial interpolation generates raster cell values from known points, applicable to geographical variables like elevation or precipitation.

Inverse Distance Weighting (IDW): This deterministic technique assigns values to unsampled locations by averaging known values in their vicinity, with closer points exerting greater influence. It is widely used for its simplicity when spatial correlation structure is unknown. The IDW method general expression appears in equation 2.

$$z(x_0) = \frac{\sum_{i=1}^n \frac{Z(x_i)}{d(x_0, x_i)^p}}{\sum_{i=1}^n \frac{1}{d(x_0, x_i)^p}} \quad (2)$$

Where:

$z(x_0)$ : Estimated value

$Z(x_i)$  Known values

$d(x_0, x_i)$ : Distance between points

$p$ : Power parameter controlling influence

This method is widely used for its simplicity and effectiveness in contexts where information on the spatial structure of the phenomenon is not available [12-14].

Kriging: A geostatistical technique that considers not only distance but also the spatial correlation structure modeled by a variogram. It provides an optimal and unbiased estimation under certain stationarity conditions, allowing for uncertainty prediction quantification. The simple Kriging basic form appears in equation 3.

$$Z^*(x) = m + \sum_{i=1}^n \lambda_i [Z(x_i) - m] \quad (3)$$

Where:

$Z^*(x)$  Estimated value

$m$  Mean of the random field

$\lambda_i$ . Weights from variogram equations

CoKriging: A Kriging extension of Esri [15] that incorporates auxiliary variables spatially correlated with the principal variable (in this case we applied elevation with precipitation) to enhance estimation accuracy, particularly with limited primary variable sampling. While more complex to implement, CoKriging can yield improved results when relevant auxiliary variables are available.

This method is ideal when sufficient information is available to model spatial dependence, and it allows for quantifying the uncertainty of predictions [16-17].

The ArcGIS program offers the option of adding complementary tools. In this case, Cokriging interpolation was considered, as this procedure allows for interpolation of functions of two or more variables. Specifically, in this analysis, it was important to consider the topography of the selected stations, so the interpolation was based not only on precipitation but also on station elevation. CoKriging interpolation is performed using equation 4.

$$Z^*(x) = \sum_{i=1}^n \lambda_i Z_1(x_i) + \sum_{j=1}^m \mu_j Z_2(x_j) \quad (4)$$

Where:

$Z_1$  Primary variable (precipitation)

$Z_2$  Secondary variable (elevation)

$\lambda_i, \mu_j$ . Weights from autocorrelation and cross-correlation

Although more complex to implement, CoKriging can offer better results when relevant auxiliary variables are available, such as altitude in precipitation studies [18]. CoKriging was implemented in ArcGIS©, enhancing spatial coherence by integrating topographic data.

### 3. Results and Discussion

This section presents the results derived from mapping the Convectivity factor (CF) across Peñitas Watershed using two distinct methodologies, followed by a comprehensive spatial patterns discussion, hydrometeorological implications, and the performance of various interpolation techniques. In Table 2 it can be observed calculated values for each station.

**Table 2:** CFE's automated weather station's results for Convectivity Factor

Automated weather stations name	R Convectivity Factor
Aza-Pac	0.53
Emiliano Zapata	0.51
Presa Malpaso	0.40
Ocotepec	0.57
Peñitas Dam	0.51
Romulo Calzada	0.57
Sayula	0.51
Tuneles de Juan de Grijalva	0.54
Tzimbac	0.54

It is worth noting that when spatial interpolation is performed at the national scale, the Convectivity map developed by Baeza (2007) indicates an approximate average value of 0.45 for the region encompassing the Peñitas Watershed. This value highlights the basin's pronounced susceptibility to convective precipitation, consistent with its location in one of the rainiest regions of Mexico.



### 3.1 Convectivity Factor Mapping: Procedure 1

Initial mapping of the Convectivity factor (CF), using the Inverse Distance Weighting (IDW) interpolation method and data from a sample of nine selected automated weather stations. The interpolation was performed using the Inverse Distance Weighting (IDW) method to capture regional variations in convective susceptibility. CF values were classified into three distinct ranges: low (green: 0.402–0.474), moderate (yellow: 0.475–0.529), and high (red: 0.530–0.571). These classifications delineate zones with varying degrees of convective activity, with red areas indicating elevated risk of convective precipitation events. This mapping provides a valuable tool for identifying regions potentially vulnerable to intense rainfall, flash flooding, and related hydrometeorological hazards.

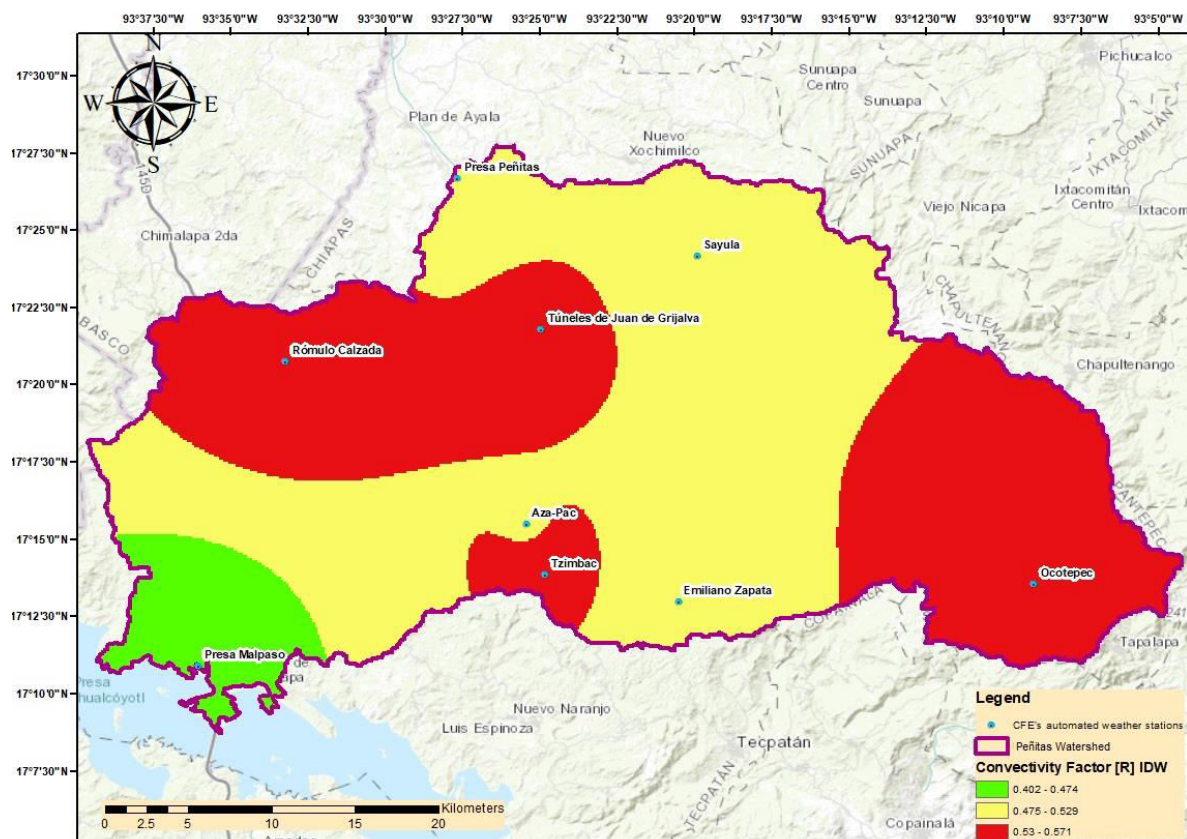
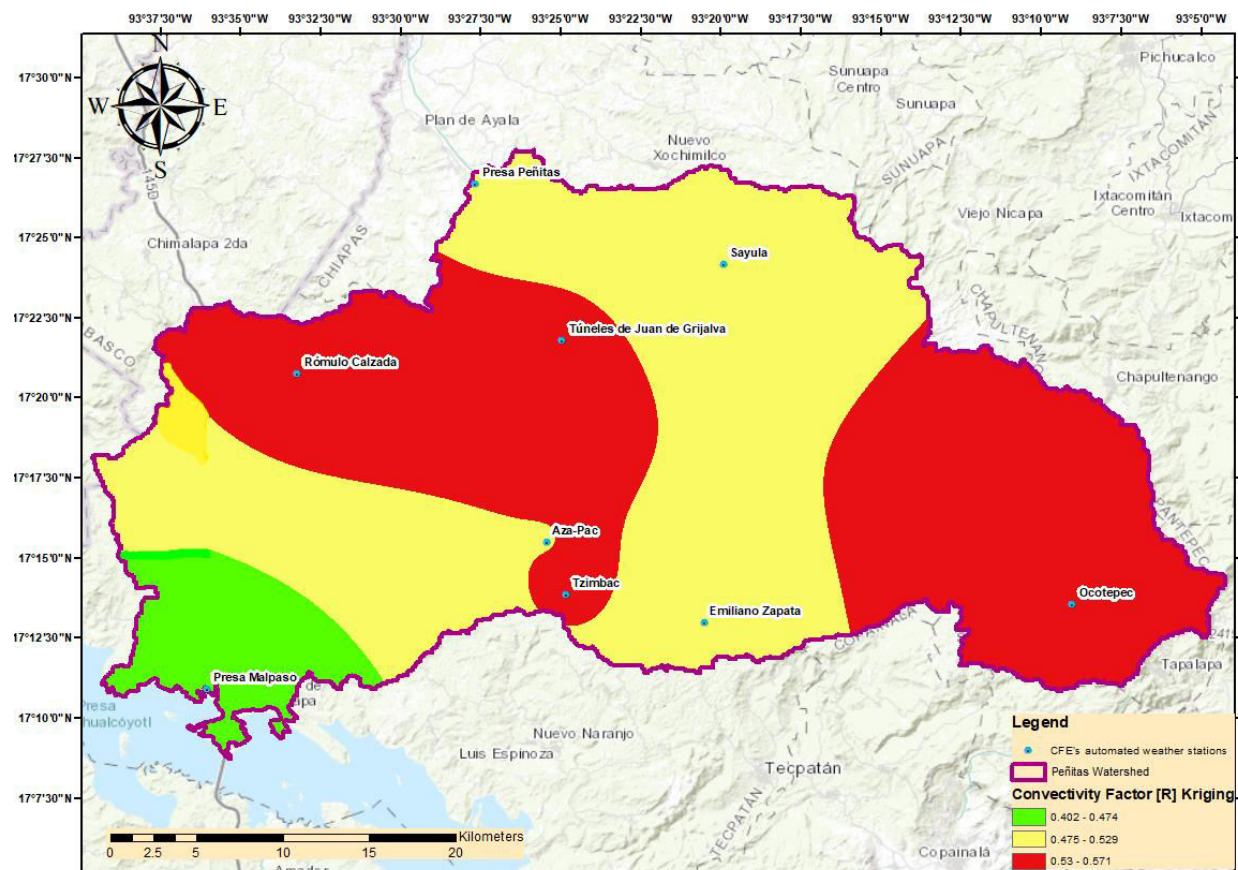


Fig. 2. Peñitas Watershed Convective factor map using IDW interpolation. Source: Own design

Figure 3 illustrates the spatial distribution of the Convectivity Factor (CF) across the Peñitas Watershed using the Kriging interpolation method. This geostatistical approach provides a more nuanced representation of spatial autocorrelation compared to deterministic methods like IDW. The CF values are categorized into three ranges: low (green: 0.402–0.474), moderate (yellow: 0.475–0.529), and high (red: 0.530–0.571), allowing for the identification of zones with varying convective potential. The map includes the boundaries of the Peñitas Watershed and the locations of CFE's automated weather stations, with key geographic references such as Presa Malpaso, Emiliano Zapata, and Tzimbac clearly labeled. The inclusion of a compass rose and coordinate grid ensures spatial orientation and georeferencing. Compared to the IDW-based map (Figure 2), the Kriging interpolation reveals smoother transitions and potentially more reliable estimates in areas with sparse data, enhancing the understanding of convective dynamics in the region.



**Fig. 3.** Peñitas Watershed Convective factor map using Kriging interpolation. Source: Own design

Figure 4 displays the spatial distribution of the Convectivity Factor (CF) across the Peñitas Watershed using the Cokriging interpolation method, which integrates elevation as a secondary variable to enhance spatial prediction accuracy. By leveraging the covariance between CF and elevation, this geostatistical technique improves the interpolation in areas with limited primary data. The CF values are classified into three ranges—low (green: 0.402–0.474), moderate (yellow: 0.475–0.529), and high (red: 0.530–0.571)—highlighting zones with varying convective potential. The map includes the boundaries of the Peñitas Watershed (outlined in purple), the locations of CFE’s automated weather stations (blue dots), and key geographic references such as Presa Peñitas, Sayula, and Ocoatepec. Compared to IDW and Kriging methods, Cokriging offers a more refined spatial representation by accounting for topographic influence, which is particularly relevant in mountainous or elevation-sensitive region



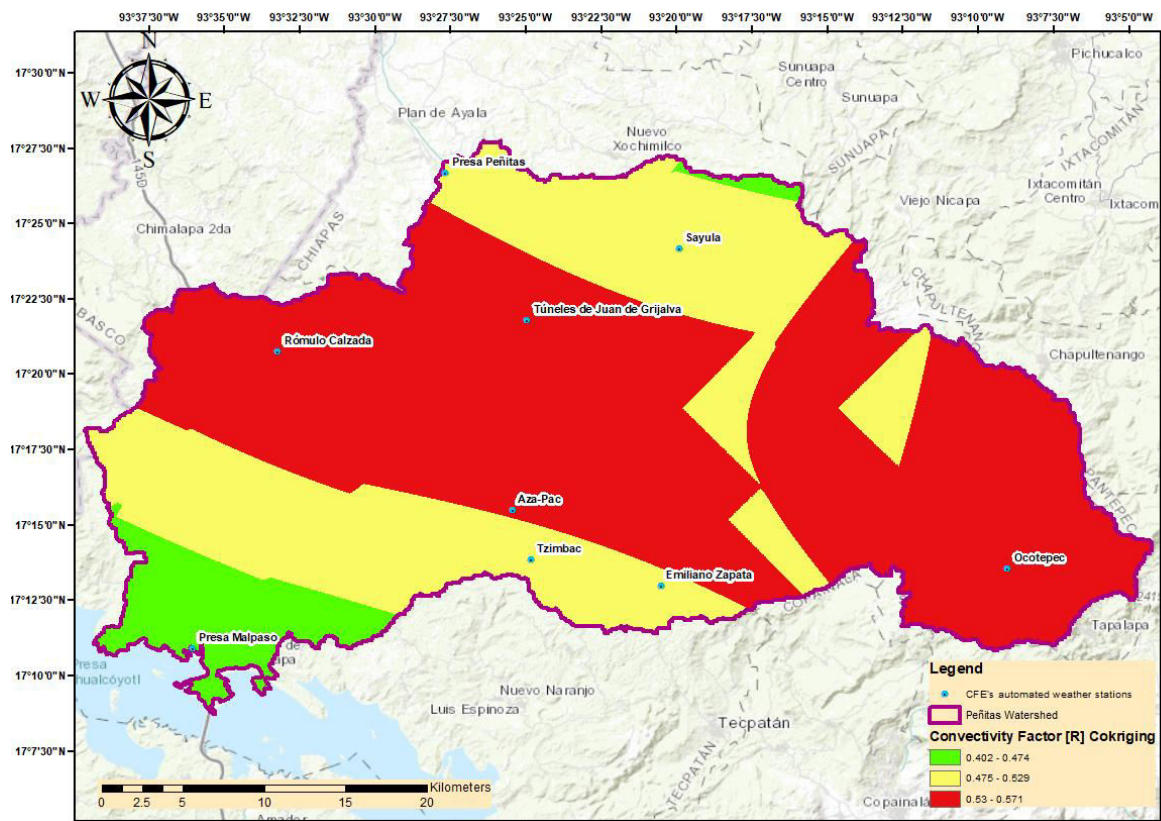


Fig. 4. Peñitas Watershed Convective factor map Cokriging interpolation. Source: Own design

### 3.2 Convectivity Spatial Patterns

The spatial distribution of the Convectivity Factor (CF) across the Peñitas Watershed reveals distinct regional patterns influenced by both meteorological inputs and topographic variability. Using three interpolation methods—IDW, Kriging, and Cokriging—the CF maps consistently identified zones of elevated convective activity concentrated in the central and southeastern portions of the basin. These areas, marked in red ( $CF > 0.530$ ), suggest a higher likelihood of intense convective precipitation events. While IDW provided a straightforward visualization of CF gradients, Kriging offered smoother transitions and better spatial continuity, especially in regions with sparse data. The Cokriging method, incorporating elevation as a covariate, further refined the interpolation by capturing terrain-driven influences on convective dynamics. This approach revealed subtle shifts in CF hotspots, particularly in elevated zones where orographic effects may enhance convective processes. Overall, the spatial patterns suggest that Convectivity is not uniformly distributed across the basin, but rather modulated by a combination of atmospheric and geomorphological factors. These insights are critical for identifying vulnerable zones and guiding localized hydrometeorological assessments.

### 3.3 Convectivity and Hydrometeorological Risk

High Convectivity values are closely associated with increased hydrometeorological risk, particularly in regions prone to intense rainfall, flash flooding, and slope instability. The CF maps generated through spatial interpolation highlight several high-risk zones within the Peñitas Watershed, where convective activity exceeds critical thresholds.

Areas with CF values above 0.530—especially those identified through Cokriging—correspond to regions with steep terrain, limited drainage infrastructure, and historical records of extreme weather events. These zones are likely to experience rapid runoff, soil erosion, and potential landslides during convective storms. Moreover, the proximity of critical infrastructure, such as Presa Peñitas and Presa Malpaso, to high CF regions underscores the importance of integrating Convectivity analysis into reservoir management and emergency planning.

By linking Convectivity patterns with hydrometeorological hazards, this study provides a framework

for proactive risk mitigation. The results support the development of early warning systems, targeted monitoring strategies, and adaptive land-use planning to reduce vulnerability and enhance resilience in the basin.

### 3.4 Limitations and Future Research

Despite the methodological robustness of the proposed Convectivity framework, several limitations warrant attention are explained below.

Regarding the data coverage constraints, the spatial interpolation relied on a limited number of automated weather stations, which may affect CF accuracy in underrepresented zones.

Temporal Aggregation Bias takes place because using annual historical maxima may obscure intra-annual variability and miss short-term convective anomalies.

While elevation was integrated via CoKriging, the 15×15 m DEM may not fully capture microtopographic influences on convective dynamics and that leads to a DEM Resolution Sensitivity.

The CF, while practical, lacks direct linkage to atmospheric instability indices such as CAPE or lifted index, limiting its physical interpretability.

Future Research Directions worth mentioning are described next.

Integration with Atmospheric Indices with the combination of CF with radar-derived convective parameters (e.g., CAPE, reflectivity) to enhance physical realism.

Multi-source Data Fusion with the Incorporation of satellite-based rainfall products (e.g., GPM, CHIRPS) to improve spatial resolution and temporal granularity.

Validation Against Extreme Events helped with Cross-reference CF hotspots with historical flood and landslide records to assess predictive reliability.

Machine Learning Enhancements with the exploration of hybrid models that fuse geostatistics with supervised learning for dynamic Convectivity mapping.

## 4. Conclusions

This paper presents a novel Convectivity index (CF) tailored to the Peñitas Watershed, offering a computationally efficient method for identifying regions prone to convective precipitation. By leveraging high-frequency rainfall data and integrating elevation through CoKriging, the resulting CF maps reveal spatial patterns aligned with known hydrometeorological risks.

The comparative analysis of IDW, Kriging, and CoKriging underscores the value of geostatistical methods in enhancing spatial coherence, particularly when auxiliary variables are available. The CF values—ranging from 0.40 to 0.57—suggest that a significant portion of daily rainfall is concentrated in short-duration events, reinforcing the need for refined hyetograph design and flood modeling.

While empirical, the CF framework provides a foundation for scalable hazard diagnostics and supports climate adaptation strategies in data-scarce regions. Future enhancements should focus on integrating atmospheric instability metrics, validating against observed events, and expanding the framework to other convective-prone basins.

The spatial patterns observed for 2021 year demonstrate strong contrasts that align with known climatological and hydrological risks in Peñitas Watershed. While empirical in nature, the Convectivity factor serves as a robust baseline for the continued development of advanced convective hazard diagnostics, particularly through the utilization of open reanalysis datasets. For future research, it is recommended to validate these maps against observed extreme events and to refine the treatment of stations with missing data to further enhance the estimations accuracy.

## Acknowledgments

We would like to thank the Research and Development Secretariat of the Coordination of Scientific Research, UNAM, and the TUBs-UNAM project Validation of precipitation reanalysis products for rainfall-runoff modeling in Mexico (VIP MEXICO) for their support in carrying out this research.

## References

- [1] Purr, C., E. Brisson, and B. Ahrens. “Convective Rain Cell Characteristics and Scaling in Climate Projections for Peñitas Riverbasin.” *Geo-LEO*, 2021.
- [2] Perschke, M., B. Schmalz, and E. Ruiz Rodriguez. “Regional Analysis of Convective Heavy Rain Events in Hesse.” *EGUsphere*, 2023.
- [3] Bell, F. C. “Generalized Rainfall-Duration-Frequency Relationships.” *Journal of Hydraulic Division*, ASCE 95 (1969): 311–327.
- [4] Chen, C. L. “Rainfall Intensity-Duration-Frequency Formulas.” *Journal of Hydraulic Engineering* 109, no. 11 (1983): 1603–1621. [https://doi.org/10.1061/\(ASCE\)0733-9429\(1983\)109:12\(1603\)](https://doi.org/10.1061/(ASCE)0733-9429(1983)109:12(1603)).
- [5] Baeza Ramírez, Carlos. *Regional estimation of convective factors for calculating intensity-duration-frequency relationships / Estimación regional de factores de convectividad para el cálculo de las relaciones intensidad-duración-frecuencia*. Master's Thesis. National Autonomous University of Mexico, 2007.
- [6] Campos Aranda, D. F., and R. Gómez De Luna. “Procedure for obtaining intensity-duration-frequency curves from rainfall records.” / “Procedimiento para la obtención de curvas intensidad-duración-frecuencia a partir de registros pluviométricos.” *Tecnología y Ciencias del Agua* (May–Aug 1990): 39–52. <https://revistatyca.org.mx/index.php/tyca/article/view/636/529>.
- [7] Domínguez Mora, R., E. Carrizosa-Elizondo, G. E. Fuentes-Mariles, M. L. Arganis-Juárez, J. Osnaya-Romero, and A. Galván-Torres. “Regional analysis for estimating design rainfall in the Mexican Republic” / “Análisis regional para la estimación de precipitaciones de diseño en la República Mexicana.” *Tecnología y Ciencias del Agua* 9, no. 1 (2018): 5–29. <https://www.revistatyca.org.mx/index.php/tyca/article/view/1515>.
- [8] National Institute of Statistics and Geography / Instituto Nacional de Estadística y Geografía (INEGI). 2025. Available in: <https://www.inegi.org.mx/>.
- [9] Federal Electricity Commission / Comisión Federal de Electricidad (CFE). “Extraction at Peñitas Dam Increases to Prioritize Population Safety; CFE Prepares for Rainy Season” / “Extracción en Presa Peñitas Aumenta para Privilegiar Seguridad de la Población; CFE se Prepara para Temporada de Lluvias.” *Official Gazette / Boletín oficial*, May 3, 2022. [https://app.cfe.mx/Aplicaciones/OTROS/Boletines/boletin?i=2512\[1\]\(https://app.cfe.mx/Aplicaciones/OTROS/Boletines/boletin?i=2512\)](https://app.cfe.mx/Aplicaciones/OTROS/Boletines/boletin?i=2512[1](https://app.cfe.mx/Aplicaciones/OTROS/Boletines/boletin?i=2512)).
- [10] Becerril Olivares, Mauricio. *Distributed parameter rainfall-runoff model for the Peñitas basin / Modelo de lluvia-escurrimiento de parámetros distribuidos para la cuenca Peñitas*. Master's Thesis. Postgraduate in Civil Engineering, UNAM, Mexico, 2016.
- [11] National Water Commission / Comisión Nacional del Agua (CONAGUA). Southern Border Regional Management. CFE information requested from CONAGUA / Gerencia Regional Frontera Sur. Información de CFE solicitada a la CONAGUA. 2025.
- [12] Shepard, D. “A Two-Dimensional Interpolation Function for Irregularly-Spaced Data.” Paper presented at the 23rd ACM National Conference, Las Vegas, USA, August 27 - 29, 1968; 517–524. <https://doi.org/10.1145/800186.810616>.
- [13] Panigrahi, N. “Inverse Distance Weight.” In *Encyclopedia of Earth Sciences Series*, Springer, 2014. [https://link.springer.com/content/pdf/10.1007/978-3-030-26050-7\\_166-1.pdf](https://link.springer.com/content/pdf/10.1007/978-3-030-26050-7_166-1.pdf).
- [14] Esri. “Interpolation methods using ArcGIS” / “Métodos de interpolación usando ArcGIS.” *ArcGIS Pro Documentation*, 2025. <https://pro.arcgis.com/es/pro-app/latest/tool-reference/spatial-analyst/comparing-interpolation-methods.htm>.
- [15] Esri. “ArcGIS Geostatistical Analyst: Inverse Distance Weighting.” *ArcGIS Pro Documentation*, 2007. <https://pro.arcgis.com/en/pro-app/latest/tool-reference/geostatistical-analyst/idw.htm>.
- [16] Ma, L., P. Wang, B. Song, X. Wang, and H. Dong. “An Efficient Kriging Modeling Method for High-Dimensional Design Problems Based on Maximal Information Coefficient.” *Structural and Multidisciplinary Optimization* 61, no. 1 (2019): 39–57. <https://doi.org/10.1007/s00158-019-02342-3>.
- [17] Krause, E., and K. Krivoruchko. “Kriging: An Introduction to Concepts and Applications.” *Esri User Conference Proceedings*, 2018. [https://proceedings.esri.com/library/userconf/proc18/tech-workshops/tw\\_1533-272.pdf](https://proceedings.esri.com/library/userconf/proc18/tech-workshops/tw_1533-272.pdf).
- [18] Dowd, P. A., and E. Pardo-Igúzquiza. “The Many Forms of Co-Kriging: A Diversity of Multivariate Spatial Estimators.” *Mathematical Geosciences* 56 (2024): 387–413. <https://doi.org/10.1007/s11004-023-10104-7>.

## Design of a Positioning System for Cylindrical Parts

MSc. Eng. **Daniel NANCA**<sup>1,\*</sup>, Ph.D. Eng. **Viorel GHEORGHE**<sup>1</sup>,  
Ph.D. Eng. **Victor CONSTANTIN**<sup>1</sup>, PhD. Stud. Eng. **Ionela Mihaela POPESCU**<sup>1</sup>

<sup>1</sup> National University of Science and Technology POLITEHNICA

\* daniel.nanca@stud.mec.upb.ro

**Abstract:** *This paper presents the design, development and testing of a semi-automatic inspection machine for cylindrical parts dedicated to the automotive industry. The system integrates an optical micrometre and multiple smart cameras along a linear rail positioning mechanism. The paper attacks the industrial challenges and motivations, the evolutions of quality control machines, from conveyor and rotary based solutions to robotic arms and linear rail systems. The machine contains a Keyence TM-3000 optical micrometre with four Keyence IV-2 cameras, supported by a poka-yoke like positioning base. The technical principles of measurement and visual inspection are analysed in detail to provide a wider understanding. Experimental testing was realised through PneuAlpha, validating the accuracy and repeatability of the proposed system. The economic evaluation demonstrates a payback period of approximately two years, making the system viable for mass quality control in the automotive sector.*

**Keywords:** *Quality control, positioning system, machine learning, mechatronics*

### 1. Introduction

In industrial manufacturing, the role of quality control has become increasingly critical over the last decades. As markets become more competitive and product lifecycles shorter, companies are under pressure to increase productivity and also guarantee that every product is up to standards before leaving the factory. This is particularly evident in the automotive industry, where safety is of up-most importance to avoid recalls, warranty claims and lost customer trust that can reach millions of euros in losses [1].

Traditionally, quality inspection was performed manually by trained operators. While manual inspection is flexible and low in initial investment, it is subject to human variability, fatigue, and limited repeatability [2]. These limitations have become dealbreakers in industries that require micrometric-level tolerance and continuous production flow. Consequently, automation has become the dominant trend in inspection, supported by technological advances in mechatronics, sensors, and machine vision [3].

The beginning of Industry 4.0 has further accelerated this transition. Modern inspection systems are no longer isolated islands, but are integrated into digital manufacturing ecosystems, providing real time data for process optimization, predictive maintenance, and closed-loop control [3]. Automated inspection is not only a tool for detecting defects, but it can also improve overall equipment effectiveness to try and achieve zero-defect manufacturing [4].

This led to evolution of hybrid inspection systems that combine dimensional metrology with visual defect detection. Dimensional deviations represented by out-of-tolerance diameters or lengths, can be captured with the high precision optical micrometre, while visual anomalies such as scratches, iron filings or incomplete machining can be identified through the smart cameras from Keyence that are supported by machine learning algorithms [5]. When these subsystems are integrated into precise positioning mechanisms, the result is a powerful inspection machine that meets the dual requirements of speed and accuracy.

This paper presents the design and validation of such a system, dedicated to cylindrical parts used in automotive applications. The installation combines a Keyence TM-3000 optical micrometre with four Keyence IV-2 smart cameras mounted in circle on a linear rail positioning system. The purpose is to demonstrate that merging advanced measurement equipment with a good positioning solution, it is possible to achieve reliable, repeatable, and economically viable inspections.



## **2. State of the art on quality control machines**

The evolution of quality control machines has followed the trajectory of industrial manufacturing itself, progressing from purely manual checks performed by trained operators to complex automated installations. As the need for accuracy and repeatability has increased, industries have moved away from human-centred verification to machine-centred inspection, where sensors, actuators and a software replace the eyes, the hands and the brain of the humans [6].

Modern quality control machines can be classified according to the type of transport and positioning system used to bring the part into the inspection area. While the inspection principle may vary, depending on the product, the effectiveness of the inspection depends heavily on how consistently and precisely the part can be positioned relative to the sensors. In this field, four main categories of positioning systems stand out: conveyor-based systems, rotary table machines, robotic arm solutions, and linear rail systems. Each category has its own domain of application, advantages, and limitations.

### **2.1. Conveyor-based machines**

Conveyor-based machines are among the most widely used solutions in the large-scale manufacturing, particularly in industries where parts must be inspected at high speed in continuous flow. The basic principle relies on a belt or a chain conveyor that transports parts through one or several inspections stations. At each station, measurements or visual checks are performed by sensors or cameras synchronized with the conveyor motion.

These systems are common in the electronics, packaging, and food industries, where large volumes of products pass through identical inspection routines. The advantage of conveyors includes easy integration into automated production lines, and relatively low mechanical complexity. However, positioning accuracy is often limited by vibrations, belt slippage and difficulty to stop the parts for high-precision checks. This makes conveyor systems better suited for simple surface and dimensional checks rather than micrometric-level inspections [2].

### **2.2. Rotary table systems**

Rotary table inspection machines use a circular platform divided into multiple stations, with parts placed in fixtures mounted around the table perimeter. As the table rotates step by step, each part sequentially passes through various inspection points, such as dimensional measurement, surface analysis, or functional testing.

These machines are particularly efficient when multiple inspection operations must be performed in sequence within a compact footprint. Their cyclical operation ensures consistent cycle times and repeatability. Rotary tables are frequently encountered in small component manufacturing, such as connectors, small auto parts and precision moulded parts. It's a compact machine that can realise multiple inspections at the same time in a small space, that facilitates using this type of machines in a small size factory that has a higher production.

The main advantage of rotary table systems are their compact design, high productivity, and ability to integrate several tests within one rotation. However, limitations include wear of the rotating mechanism, the need for precise synchronization of sensors, and reduced flexibility for handling parts of significantly different geometries [7].

### **2.3. Robotic arm systems**

Robotic arm systems represent the most flexible approach to automated inspection. Equipped with multi-axis manipulators, grippers, and advanced vision systems, robotic arms can handle parts of varying geometries and place them precisely in front of different sensors. They are often combined with coordinate measuring machines or high-resolution cameras to perform complex inspections.

The key advantage of robotic arm systems lies in their adaptability: a single installation can inspect multiple product types simply by changing the inspection program. This makes them well suited for high-mix, low-volume production environments. In addition, robotic systems integrate easily into Industry 4.0 ecosystems, with connectivity to manufacturing and real time data analytics platforms. Despite their flexibility, robotic arm inspection machines come with drawbacks. Their acquisition cost is significantly higher than that of a conveyor or rotary system, and their operation requires



specialized programming and maintenance expertise. In addition, cycle times are generally longer due to the need of precise movements, making them less efficient in high-throughput scenarios [8].

#### 2.4. Linear rail systems

Linear rail systems have emerged as highly precise alternative for applications where accuracy and repeatability are important. These machines rely on a guided linear motion, typically supported by ball bearing rails, to transport parts to the inspection zone. The motion can be driven by stepper motors, servo motors or pneumatic actuators, with belt or screw mechanism providing power transmission.

The main advantage of linear rail machines is their ability to provide stable, repeatable positioning of parts, even at high speeds. For cylindrical or prismatic parts that must be measured under strict tolerances, linear motion eliminates many of the uncertainties associated with conveyors or rotary systems. Furthermore, linear rails are mechanically simpler than robotic arms, while still offering flexibility in integrating different types of sensors or cameras along the inspection path.

Applications of linear rail inspection machines include the automotive, aerospace, and medical device industries, where product reliability depends on micrometric precision. The installation presented in this paper belongs to this category, as it combines optical and vision sensors within a linear rail positioning framework [9].

### 3. Description of the proposed installation

The developed inspection machine integrates dimensional and visual inspection subsystems into a single installation. The dimensional verification is achieved using the Keyence TM-3000 optical micrometre, which uses telecentric optics and high-speed scanning to capture profiles with a micrometric accuracy. Visual inspection is performed by four Keyence IV-2 smart cameras, with 3 of them mounted at 120° relative to each other, to eliminate blind spots, and a fourth camera above the part to check its upper profile. These cameras utilize machine learning algorithms trained with datasets of conform and defective parts, enhancing accuracy against variable surface finishes.

The cameras are mounted inside a lightproof chamber to eliminate interference from external illumination. This ensures repeatable conditions across inspection cycles. The micrometre and cameras are synchronized through a central control system, which coordinates measurement acquisition with the movement of the positioning system.



Fig. 1. General view of the semi-automatic inspection installation

#### 4. Positioning system analysis

The positioning system represents the backbone of the inspection machine, as the reliability of the measurement process depends directly on how accurately and consistently the part can be placed under the sensors. Any deviation in positioning introduces uncertainty in both dimensional and visual inspection, which is unacceptable in applications requiring micrometric-level tolerances [10]. To minimize these risks, the installation was equipped with a support for the parts based on the poka-yoke principle. This represents the first layer of inspection as an undersized cylindrical part will not be able to fit on the support, also it won't be able to fit, if the part is flipped as the base is wider than the top of the cylinder, thereby eliminating operator error. Through this constrains of geometry, the cylindrical components are going to arrive in front of the sensors under identical conditions, which guarantees consistency across repeated inspections.

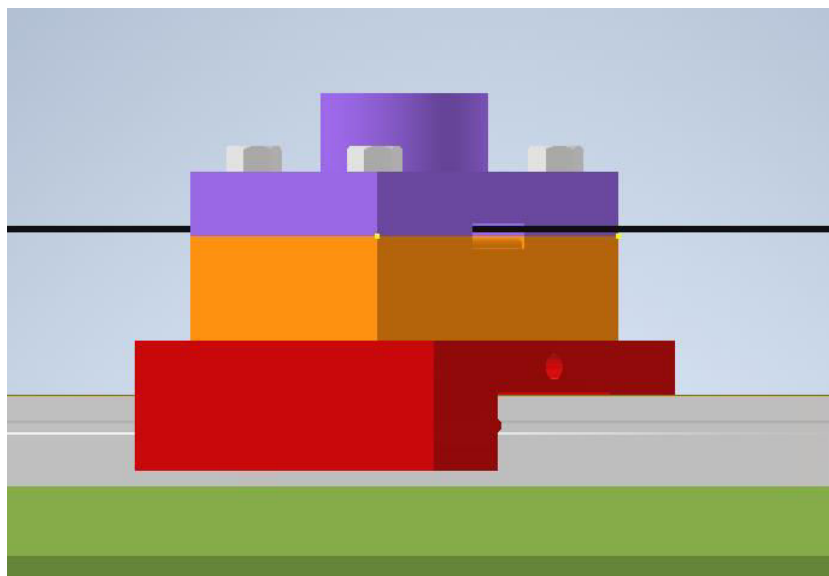
The translational movement of the support is achieved using a linear rail with recirculating ball bearings. This solution provides low friction and high stiffness, which are essential characteristics for precision positioning. The rail guides the part smoothly along a single axis, aligning it with the optical micrometre and camera system.

Motion is generated by a NEMA 17 stepper motor, chosen for its balance of torque, compact dimensions, and ease of integration with digital drivers. The motor is controlled through a micro-stepping driver, which allows smooth movement and high-resolution positioning. Power is transmitted by a GT2 timing belt, tensioned with a spring-loaded mechanism to prevent slack and eliminate backlash effect. This arrangement ensures that the system maintains table and repeatable displacement, even at higher speeds.

Alternative solutions were considered during the design stage. Ball screw mechanism, while capable of providing higher rigidity and precision, involve greater mechanical complexity and increased costs. Pneumatic actuators were also analysed as a low-cost alternative, but their limited control and lower repeatability made them unsuitable for micrometric inspection tasks. The final choice of a belt-driven linear rail represented probably the best compromise between precision, reliability, and economic feasibility.

Comparable approaches, where numerical optimization and CFD simulations support the validation of high-precision mechatronic systems, are reported in a research on centrifugal pumps for spacecraft cooling systems [11].

Experimental validation confirmed the performance of the chosen design. The system demonstrated the ability to achieve speeds of up to 180 mm/s without loss of steps, maintaining accurate synchronization with the acquisition cycle of the micrometre and cameras. The repeatability of the positioning system ensured that the inspections process could be performed under controlled and stable conditions, which is a critical requirement for industrial adaptation.



**Fig. 2.** Positioning system mounted on the linear rail

## 5. Experimental testing with the PneuAlpha

Validation simulations were carried out on the PneuAlpha app, which replicates production-like conditions. The objective was to better understand and simulate the steps of the system when checking one cylindrical component. The Keyence IV-2 cameras were trained with datasets of both conform and non-conform parts, and the algorithm parameters were adjusted to minimize false positives and negatives. The system consistently detected defects such as scratches and pores with high reliability, while dimensional results from TM-3000 confirmed deviations within tolerance limits.

Similar validation procedures combining numerical modelling with experimental tests have been successfully applied in optimization of aerospace pumping systems [11].

Future experiments will involve an extended data sheet with more defect types and deliberately introducing environmental variations, such as lighting changes and vibration, to further test adaptability.

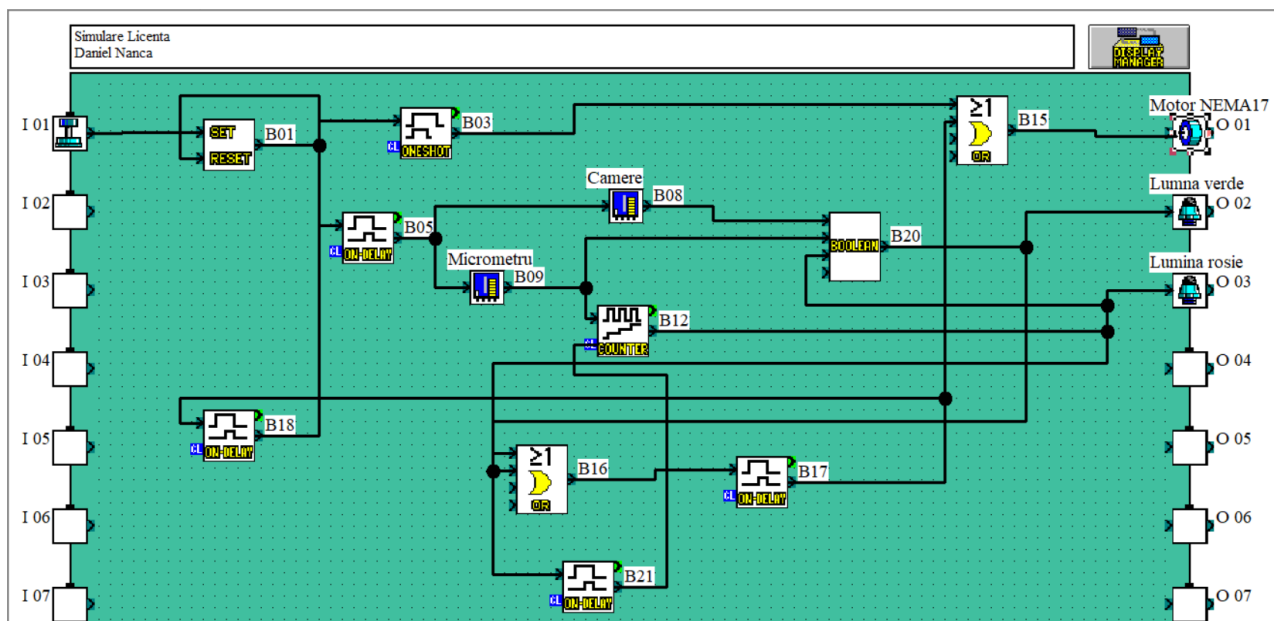


Fig. 3. Experimental setup with the Pneu Alpha stand

## 6. Economic efficiency evaluation

From an economic perspective, the main costs of the installation derive from acquiring the optical micrometre, smart cameras, and the positioning system components. However, these are offset by reductions in operator involvement, inspection cycle time, and defect-related losses. The estimated payback period is approximately two years, which aligns with industry benchmarks for automation investments; in addition, indirect benefits such as improved customer satisfaction and reduced warranty claims further enhance the economic case.

## 7. Conclusions

This project presents the design, analysis, and validation of a semi-automatic inspection machine for cylindrical parts. By integrating a Keyence TM-3000 optical micrometre with IV-2 smart cameras in a linear rail positioning system, the solution demonstrated micrometric accuracy and reliable defect detection. Testing the model on the PneuAlpha app, confirmed repeatability, experimenting with the visual cameras confirmed accuracy, while economic analysis indicated a favourable return on investment. Future developments will focus on extending automation towards a fully autonomous inspection line and broadening the detection capabilities with additional sensor integration.

**References**

- [1] Li, R., W. Yuan, X. Ding, J. Xu, Q. Sun, and Y. Zhang. "Review of Research and Development of Hydraulic Synchronous Control System." *Processes* 11, no. 4 (2023): 981. <https://doi.org/10.3390/pr11040981>.
- [2] Ahmed, B.E. (ed.) *Modern Approaches to Quality Control*. IntechOpen, 2011.
- [3] ISO 9001:2015 – Quality Management Systems – Requirements.
- [4] Oluyisola, O.E., K. Mpofu, and O.T. Adenuga. "Zero Defect Manufacturing: A Review." *Procedia CIRP* 63 (2017): 716–721.
- [5] Keyence Corporation. "Vision Sensor – IV Series." Accessed September 4, 2025. <https://www.keyence.eu/>.
- [6] Vasiliu, D., C.G. Vasiliu, and C. Călinoiu. "Dynamics of the electrohydraulic transmissions for automotive applications." *UPB Scientific Bulletin, Series D: Mechanical Engineering* 81, no. 3 (2019): 235–248.
- [7] Groover, M.P. *Automation, Production Systems, and Computer-Integrated Manufacturing*, 4th ed., Pearson, 2015.
- [8] Boothroyd, G., P. Dewhurst, and W. Knight. *Product Design for Manufacture and Assembly*, 3rd ed., CRC Press, 2010.
- [9] Siciliano, B., and O. Khatib (eds.). *Springer Handbook of Robotics*. Springer, 2016.
- [10] Crăciun, Șt.I., I. Ardelean, and V. Csibi. "Considerations regarding of mechatronics systems for positioning in non-destructive testing." *UPB Scientific Bulletin, Series D: Mechanical Engineering* 73, no. 2 (2011): 181-188.
- [11] Dumitrescu, O., and I.-F. Popa. "Design and optimization of a centrifugal pump as part of mechanically pumped fluid loop cooling system for spacecraft." *UPB Scientific Bulletin, Series D: Mechanical Engineering* 83, no. 3 (2021): 277-290.

## The Evolution of Energy Consumption in Electric Mobility in Bucharest in 2024: Between Efficiency and the Potential of Renewable Sources

PhD. Stud. Eng. **Anca-Florentina POPESCU**<sup>1</sup>, PhD. Stud. Eng. **Alexandra BĂDICEANU**<sup>1,\*</sup>,  
Prof. Dr. Habil. Chem. **Ecaterina MATEI**<sup>1</sup>, PhD. Stud. Eng. **Georgiana-Miana ANDRICIUC**<sup>1</sup>,  
Prof. Dr. Habil. Eng. **Andra-Mihaela PREDESCU**<sup>1</sup>

<sup>1</sup> National University of Science and Technology Politehnica of Bucharest, Faculty of Biotechnical Systems Engineering, Romania

\* alexandra.hodoroaba@yahoo.com

**Abstract:** Globalisation has led to serious air pollution challenges, with significant consequences for the environment, human health, and climate, prompting a continuous worldwide search for emission reduction solutions. The transition to sustainable public transport represents one of the major priorities for European cities in the context of the current climate emergency and decarbonization targets. In Bucharest, the electrification of urban public transport has experienced progressive expansion, particularly through the introduction of electric buses in 2024. This article analyses the monthly electricity consumption of the electric vehicle fleet in 2024, focusing on the consumption trends of electric buses and the opportunities for renewable energy supply in an urban context, but also on the evolution of GHG emissions and carbon footprints for electric buses after upgrading.

**Keywords:** Renewable energy, public transport, electric bus fleet, carbon footprint, GHG emissions

### 1. Introduction

Air pollution, particularly carbon dioxide (CO<sub>2</sub>) emissions, constitutes a major environmental problem, with anthropogenic activities accounting for most emissions. The most significant sources of primary and secondary pollutants include industrial processes, the transport sector, and energy production [1].

These pollutants, with toxic effects on human health, account for up to 8.2% of total global greenhouse gas emissions [2] and contribute to the increase in global CO<sub>2</sub> concentrations, amplifying the climate change process.

Air pollution is associated with approximately 6.7 million premature deaths each year [3], and while the global average temperature has risen by about 0.85°C due to pollution [4], Europe's warming trend over the last three decades exceeded the global average, averaging 0.48°C, compared to the total global increase [5].

Greenhouse gas emissions from diesel use have been estimated to account for 26% of global black carbon emissions [6]. That is why specific measures are needed to mitigate these emissions by adopting the most advanced pollution control technologies and withdrawing high-emission diesel vehicles in service. As a result, the implementation of vehicle emission standards, fleets electrification, and quality requirements for alternative fuels in the European Union helped cut air pollution emissions from road transport [7,8].

Electrifying vehicle fleets offers high potential for reducing short-lived climate pollutants (SLCPs), particularly black carbon. According to Jacobson's estimates, replacing vehicles in the United States with electric, plug-in hybrid, or hydrogen-powered models from renewable energy sources (wind, solar, hydroelectric, etc.) could eliminate approximately 160 Gg/year of black carbon generated from fossil fuel combustion — equivalent to about 24% of national black carbon emissions (or 1.5% of global emissions) — and could reduce CO<sub>2</sub> emissions by about 26% nationally [9].

The targets set at European Union level for 2030 provide for a 55% net reduction in greenhouse gas emissions, and the target for 2050 is to become climate neutral [10].

In 2021, Romania was ranked 48th worldwide in greenhouse gas (GHG) emissions, with its contribution representing approximately 0.22% of the global total [11]. It is estimated that the transport sector is responsible for approximately 4.2 million premature deaths worldwide because



of outdoor air pollution [12]. Among the various pollutants it generates, carbon dioxide (CO<sub>2</sub>) is the primary product of the complete combustion of carbon-based fuels and a major contributor to anthropogenic greenhouse gas emissions.

The transport sector is a major source of anthropogenic greenhouse gas (GHG) emissions, accounting for approximately 29% of total global emissions. These emissions consist mainly of carbon dioxide (CO<sub>2</sub>), generated primarily by the combustion of fossil fuels in internal combustion engines, and are therefore a major contributor to climate change [13].

The Bucharest Public Transport Company (STB S.A.) operates an integrated network covering 1,335 km<sup>2</sup>, of which 240 km<sup>2</sup> is within the urban area, serving approximately 1.071 million passengers daily. Its fleet comprises 1,640 buses operating on 122 routes, 265 trolleybuses on 13 routes, and 527 trams on 22 routes [14, 15]. This study presents a broad look at how improving Bucharest's urban transport system impacts the city, with more cars on the road causing traffic jams and air pollution. The analysis looks at the potential of renewing the fleet and upgrading transport infrastructure as ways to make public transport more attractive. Furthermore, the survey underlines the need of implementing urgent and specific measures and adopting sustainable environmental policy to mitigate the harmful effects of urban air pollution [16]. STB-S.A.'s fleet has been modernized by 43% over the last four years with electric buses, EURO 6 buses, new trams, and new trolleybuses, and in 2024, 58 out of 100 ZTE GRANTON electric buses entered service.

## 2. Materials and methods

Using data collected from the Technical and Operations Departments of STB - S.A., we have analysed the monthly electricity consumption of the electric vehicle fleet and associated maintenance units of STB S.A. in 2024, focusing on the evolution of electric bus consumption and opportunities for renewable energy supply in an urban context. The introduction of electric buses has provided an overview of the energy consumption of urban mobility systems and the potential for integrating renewable energy sources into the power supply infrastructure. In 2024, the bus fleet of public transport operator in Bucharest is presented in Figure 1.

The ZTE Granton bus specifications indicate that the total battery capacity is 383.23 kWh, providing a range of 314.3 km, according to the SORT 1—SORT UITP Project report [17]. Producers recommend maintaining the battery state of charge above 75-80%.

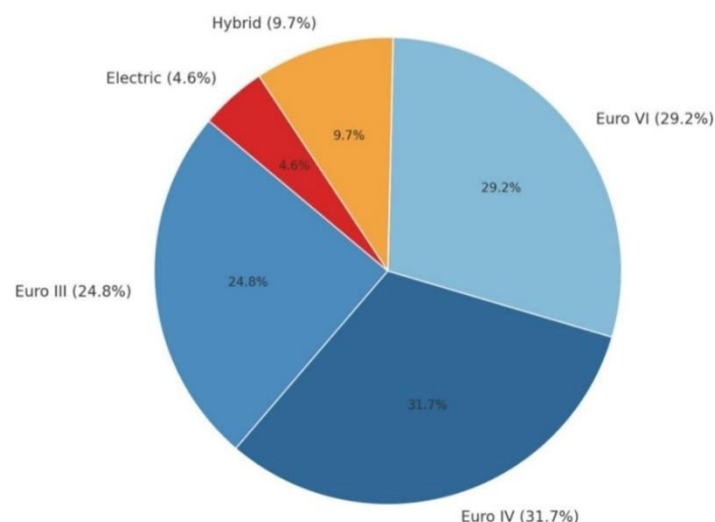


Fig. 1. STB-S.A. bus fleet percentage in December 2024 [14]

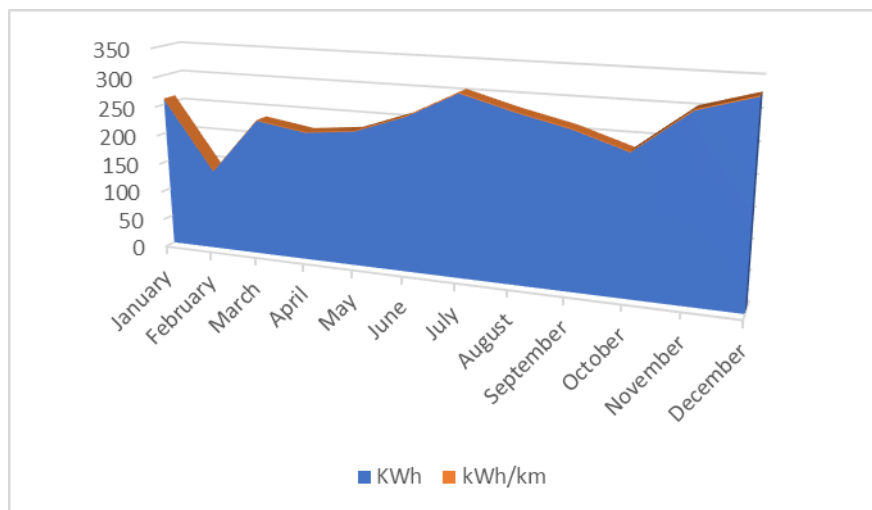
### 2.1 Electricity consumption for the bus fleet of the public transport operator in Bucharest

The evolution of energy consumption and specific energy for electric buses in 2024 is presented in Table 1 and Figure 2, based on the collected data.

**Table 1:** Energy consumption and specific energy for bus fleet of public transport operator in 2024

Month	KWh	kWh/km
January	258.574	1.478
February	138.198	0.79
March	233.771	1.336
April	220.219	1.258
May	228.976	1.308
June	259.361	1.482
July	302.992	1.731
August	279.418	1.597
September	259.352	1.482
October	231.209	1.321
November	300.614	1.718
December	326.608	1.866

The highest consumption (both total and specific) is recorded in the cold months (**December, January, November**) and in the middle of summer (July–August) due to increased energy consumption for heating systems for passenger comfort and to maintain the battery at optimal temperatures (in winter) and because of high consumption from using air conditioning in the summer.

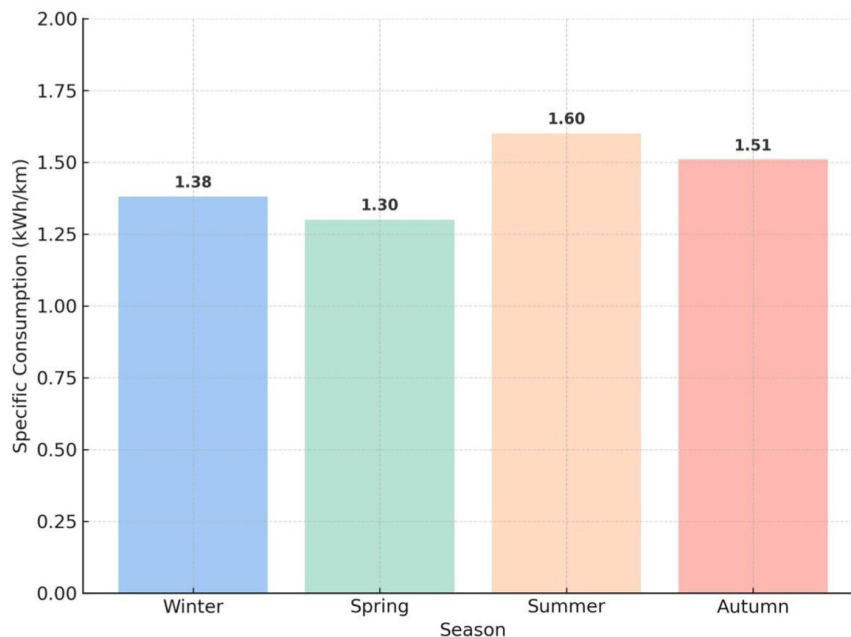
**Fig. 2.** STB-S.A. bus fleet energy consumption and specific energy in 2024

Seasonal averages for specific consumption of electric buses in 2024 are presented in Table 2.

**Table 2:** Seasonal averages for specific consumption of electric buses in 2024

Season	Month	Specific energy consumption [kWh/km]
Winter	December-February	1.38
Spring	March-May	1.30
Summer	June-August	1.60
Autumn	September November	1.51

Figure 3 highlights the impact of seasonal weather conditions on the energy performance of electric buses. They are more efficient in periods with moderate temperatures and less efficient in winter and summer, which require additional battery power for air conditioning and heating.



**Fig. 3.** Seasonal specific energy evolution of the public transport operator in Bucharest 2024

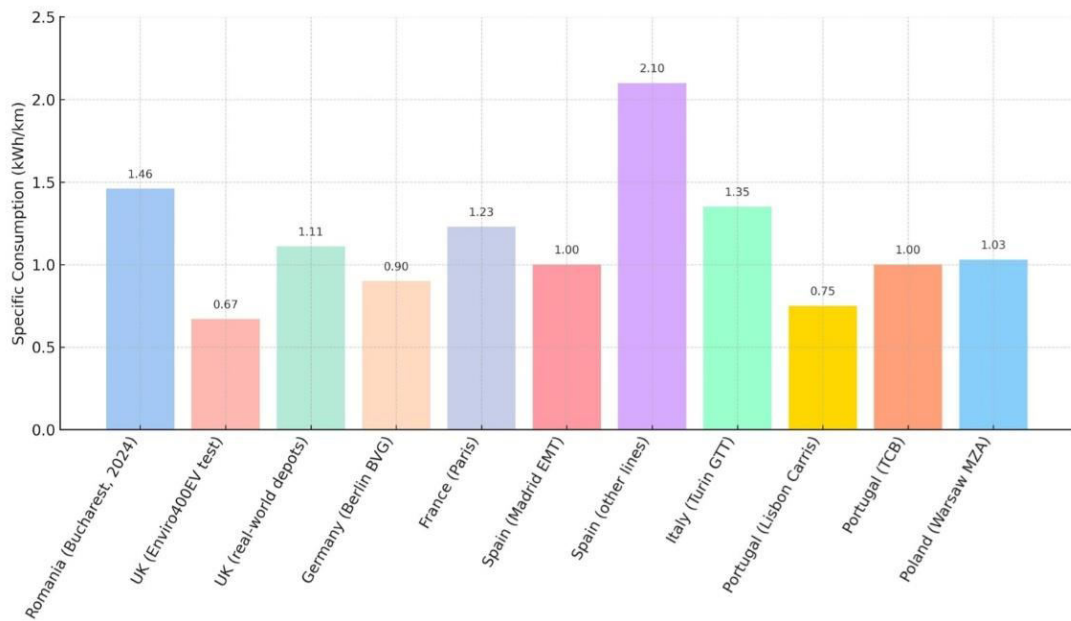
The consumption of electric buses in Bucharest varies between 1.30 and 1.60 kWh/km depending on the season. The climate and the use of HVAC (heating/cooling) systems are the main factors causing the variation.

A comparison of specific energy consumption for transport fleets in some different European countries is presented in Table 3 and Figure 4.

**Table 3:** Specific energy consumption comparison in European cities [14, 18-28]

Country	Specific Consumption (kWh/km)
Romania (Bucharest, 2024)	1.46
UK (Enviro400EV test)	0.67
UK (real-world depots)	1.11
Germany (Berlin BVG)	0.90
France (Paris)	1.23
Spain (Madrid EMT)	1.00
Spain (other lines)	2.10
Italy (Turin GTT)	1.35
Portugal (Lisbon Carris)	0.75
Portugal (TCB)	1.00
Poland (Warsaw MZA)	1.03

A comparative analysis of specific energy consumption in European countries reveals notable regional differences. In Bucharest (1.46 kWh/km), consumption is above the European average (1.2–1.3 kWh/km), mainly due to traffic congestion, climatic conditions, and the use of heating, ventilation, and air conditioning systems.



**Fig. 4.** Comparison of specific energy consumption of fleet bus in different European cities [14, 18-28]

The United Kingdom reports values of up to 0.67 kWh/km in standardized tests, although actual figures are closer to 1.1 kWh/km. Germany (0.9 kWh/km) and France (1.23 kWh/km) demonstrate efficient operation, supported by advanced infrastructure and a temperate climate. Southern European cities such as Madrid (1.0-2.1 kWh/km) and Turin (1.35 kWh/km) show greater seasonal variability, largely influenced by high cooling demand during the summer. Portugal has some of the best results (0.5-0.75 kWh/km in Lisbon), while Poland (about 1.03 kWh/km on average) experiences significant seasonal fluctuations, with winter peaks of up to 3 kWh/km. Overall, Romania is more in line with the higher consumption trends in Southern and Eastern Europe, emphasizing the importance of optimizing the vehicle fleet and infrastructure, energy-efficient vehicle technologies, and improving operational practices.

## 2.2 Status of charging stations for electric buses in Bucharest

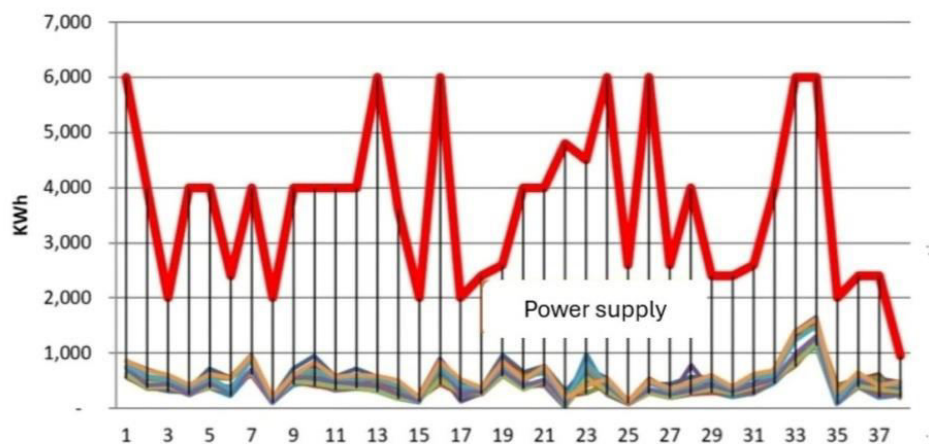
Twenty slow charging stations have been installed within the URAC to serve 20 electric buses from the existing transformer stations on the low voltage network. The charging stations have a power of 90 kW, a supply voltage of 400 V AC—alternating current—and a maximum current consumption of 165 A, all provided by the electric bus provider [14]. The maximum power that can be absorbed for charging electric buses is 2000 kW, in accordance with the existing Technical Connection Certificate. The electrical power supply of URAC, who provides manufacturing and repair services for the STB-S.A. tram fleet, is provided by the national distribution network and operates at a voltage of 10 kV.



**Fig. 5.** Power supply for electric vehicles from the tram traction network

These charging stations at URAC are a temporary solution, as three depots are currently being upgraded to provide charging facilities for electric buses: Berceni, Bujoreni, and Bucurestii Noi, with a total installed power of 4950 kW and a total power of 90 kW.

As part of the European project, it has been found that, following the modernization of the drive systems installed on electric vehicles, energy consumption has decreased, and it has been calculated that the average hourly consumption and maximum hourly consumption for the 38 existing electrical substations. Using this energy resource for charging electric vehicle batteries is associated with additional energy losses, which can reach approximately 40% of the total energy used. That's why an energy balance should be made to see if this solution is feasible given the transport infrastructure that's about to be upgraded.



**Fig. 6.** Maximum hourly consumption and installed power (KWh) / (KVA)

In order to utilize this energy resource, additional energy loss may occur during the charging of electric vehicle batteries, which may represent up to approximately 40% of the total energy used; based on the specifics of the existing transport infrastructure and the location of the stations, an energy balance should be done to see if this solution is feasible for the transport infrastructure that's going to be upgraded.

The upgraded infrastructure for environmentally friendly transport operates in accordance with European standards in vigour - European Directive 2009/33/EC promoting clean and sustainable transport, which started in 2024.

### 2.3 Emissions estimation and the carbon footprint for the bus fleets of the public transport operator in Bucharest

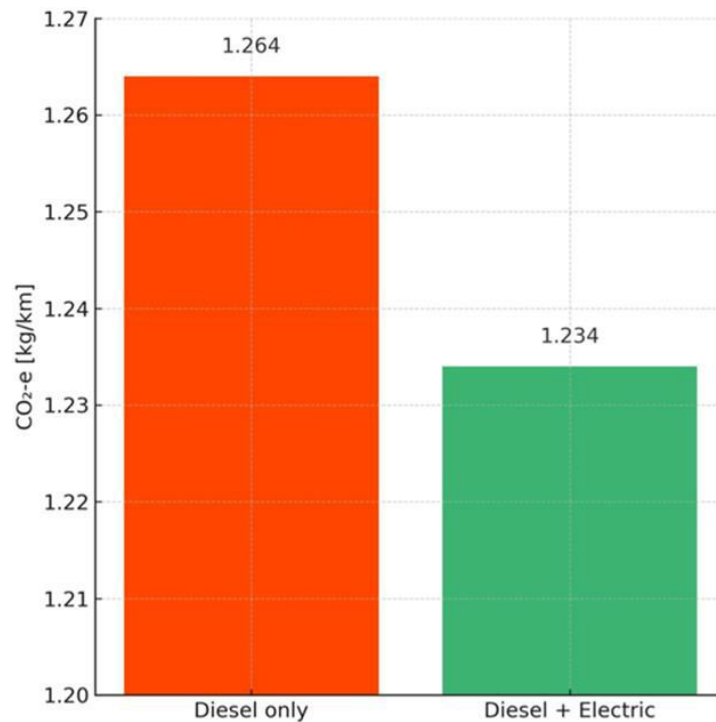
The bus fleet emissions were estimated using Joint Assistance to Support Projects in European Regions (JASPERS) method [15], applied for estimating the greenhouse gas (GHG) emissions in the transport sector [17, 29-33], drawing upon cumulative records of the annual mileage of the bus fleet operating in the Bucharest public transport network. According to the JASPERS Cost-Benefit Analysis (CBA) Guidance, the standardized emission factor for electricity generation in Romania is 0.517 kg CO<sub>2</sub> per kWh, which was applied in this study to estimate associated greenhouse gas emissions [31].

The introduction of electric buses in 2024 reduced emissions by 12 kilotons of CO<sub>2</sub>e compared to 2023, representing a 13% decrease in these types of emissions compared to the previous year. In 2024, electric buses accounted for approximately 3.47% of the total distance travelled by the entire bus fleet.

A relevant comparison can be made between 2023 and 2024. Although the reduction per kilometer may seem moderate, over the typical long distances of urban transport systems, it substantially reduces total greenhouse gas emissions.

With the introduction of electric buses in 2024, specific emissions per kilometer were 1.234 kg/km, a reduction of 2.68% compared to the previous year, which is illustrated in Figure 7.





**Fig. 7.** Specific CO<sub>2</sub>e emissions per km in 2024

The estimated greenhouse gases and carbon footprint obtained during the analyzed period (2021-2024) after the introduction of electric buses in 2024, are presented in Table 4.

**Table 4:** Estimated GHG emissions for bus fleet of public transport operator in 2021-2024

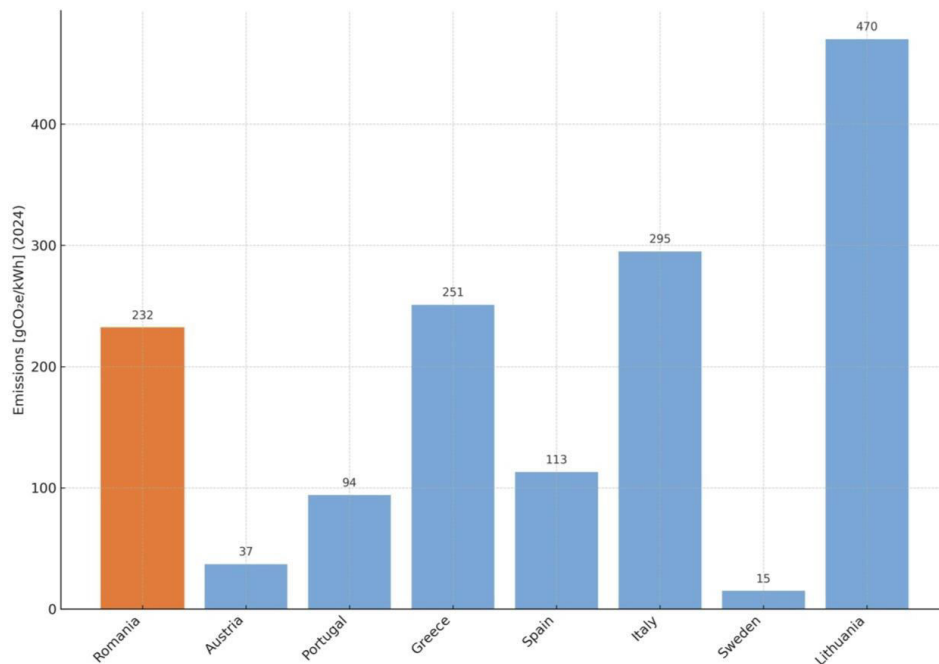
Year	CO <sub>2</sub> [kg]	N <sub>2</sub> O [kg]	CH <sub>4</sub> [kg]	CO <sub>2e</sub> [kg]
2021	86,118,608.29	4532.55	4532.55	87,573,559.51
2022	81,739,580.79	4302.08	4302.08	83,120,549.50
2023	83,963,198.9	4419.11	4419.11	85,381,735.05
2024	72,176,673.81	3798.77	3798.77	74,485,933.81

For Bucharest case (Romania), indirect greenhouse gas emissions were calculated using the national average emission factor for electricity for 2024, quantified at 232 g CO<sub>2</sub>e per kWh (i.e., 0.232 kg CO<sub>2</sub>e/kWh) [34]. Table 5 and Figure 8 present a comparison between CO<sub>2</sub>e/kWh values in Romania and those reported for other European countries.

**Table 5:** CO<sub>2</sub>e/kWh for Romania compared with other states of European Union [34]

Country	Current Emissions [gCO <sub>2e</sub> /kWh] in 2024
Romania	232
Austria	37
Portugal	94
Greece	251
Spain	113
Italy	295
Sweden	15
Lithuania	470

The table highlights the significant differences between countries in terms of carbon intensity of electricity production. Romania performs in the middle of the ranking — well ahead of countries with a coal/gas-based energy mix, but far behind countries with green or nuclear energy.



**Fig. 8.** CO<sub>2e</sub>/kWh comparison between Romania and European countries

### 3. Discussion

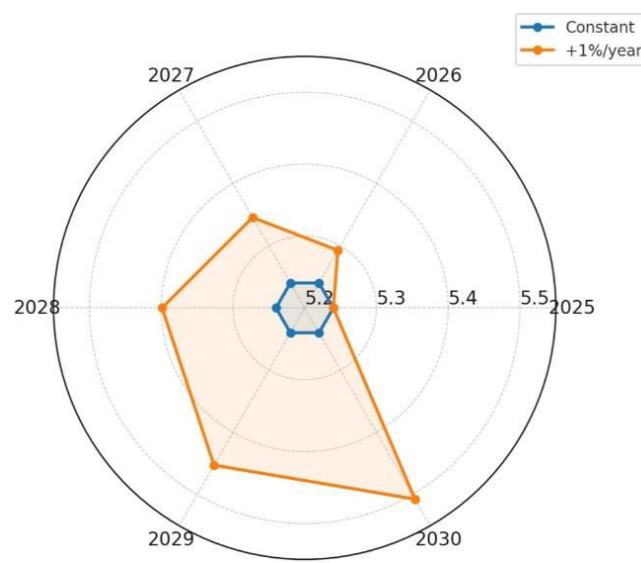
Projections suggest that by 2030, electric buses will represent over 30% of the national fleet, consistent with Romania's obligations under the European Green Deal and the “Fit for 55” package, which foster the shift towards sustainable, low-emission mobility [16].

If the number of electric buses doubles (from 58 to 100), then total energy consumption also doubles (assuming approximately constant mileage per bus) is presented in table 6 and Figure 9. We've considered two scenarios: a static scenario (no increase), a dynamic scenario (with small increase, 1% per year). Monthly electricity consumption data for 2024 indicated an average of 1.46 kWh/km, which was used as the reference factor for estimating annual fleet demand and projecting scenarios for 2025–2030.

**Table 6:** The evolution of electricity consumption of the electric bus fleet in two scenarios

Year	Constant	1%/YEAR
2025	5.24	5.24
2026	5.24	5.29
2027	5.24	5.34
2028	5.24	5.39
2029	5.24	5.44
2030	5.24	5.5

The sensitivity scenario was applied to take account of potential variations in energy demand by introducing an annual growth rate of 1%. According to this assumption, the annual electricity consumption of 5.24 GWh in 2025 increases to approximately 5.50 GWh by 2030.

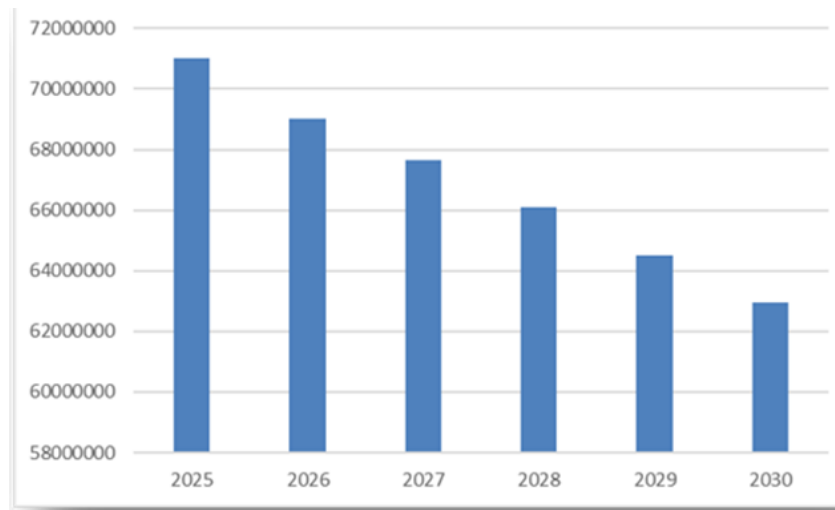


**Fig. 9.** Comparison of the static scenario (no changes) and the dynamic scenario (1% annual growth) of electricity consumption based on data from 2024

Blue line (constant) = 5.24 GWh/year, constant over the period 2025-2030.

Orange line (+1 %/year) = increases from 5.24 GWh in 2025 to 5.50 GWh in 2030.

For the period 2025–2030, we have modeled a scenario that predicted the replacement of 50 diesel buses with electric buses each year, contributing to the gradual transition to a low-emission fleet. By 2030, almost 80% of the Bucharest operator's bus fleet would be modernized, with an estimated reduction of over 11 kilotons of CO<sub>2</sub>e compared to 2024 levels, as shown in Figure 10.



**Fig. 10.** Estimated GHG and carbon footprint scenario with 50 electric buses replacement in public transport operator between 2025-2030

The decreasing greenhouse gas emissions tendency at both local and European level corresponds to the initiatives of most Romanian municipalities, which are developing Sustainable Energy Action Plans (SEAPs) [35] or Climate and Sustainable Energy Action Plans (CSEAPs) [36] to build coherent and tangible inventories and decisions for reducing urban emissions.

Cutting down on local air pollution by getting rid of PM, NO<sub>x</sub>, and VOC emissions will directly contribute to long-term health benefits, like respiratory and cardiovascular diseases and other health issues directly linked to air pollution. This is in coherence with Romania's pledges as part of the European Green Deal and the "Fit for 55" framework, that promote the transition to transport based on low emissions [37] by achieving the 2030 target of additional procurement of 250 non-polluting buses, as stipulated in the P.M.U.D. [38].

The transport sector significantly affects air quality due to internal combustion engine vehicles, which emit pollutants such as PM, NO<sub>x</sub>, CO, and VOCs, contributing to urban environmental quality decline and detrimental health effects. That is why the electric buses represent a concrete solution for cutting greenhouse gas emissions and reducing air pollution.

#### 4. Conclusions

The introduction of 58 electric buses into Bucharest's public transport fleet generated a quantifiable decarbonization impact, saving 13% of carbon dioxide equivalent emissions in comparison with 2023.

Moreover, the specific carbon footprint of electric bus operations decreased by approximately 2.68%, representing a total reduction of approximately 11 kilotons of CO<sub>2</sub>e, partly attributable to the decline of diesel-only buses.

The specific annual average electricity consumption for Granton buses is approximately 1.46 kWh/km in 2024, which represents the reference factor for the future consumption forecasts and for fleet energy performance assessment.

The data provides a solid basis for sustainability reports and strategies to expand the electric fleet, especially as charging stations for electric buses are being completed at the Bujoreni, Berceni, and Bucurestii Noi depots. This will allow the deployment of the remaining electric buses purchased in 2023.

Sustainable and resilient future recommendations for public transportation:

- Gradual phase-out of Euro III-V vehicles, supported by binding requirements or stimulus packages for their removal from service.
- The completion of the modernization of the charging infrastructure for electric buses to allow the new electric buses to start operating.
- The expansion of electromobility (replacing trams, introducing new, environmentally friendly electric buses and trolleybuses)
- Developing more ambitious environmental policies that consider the circular economy and EU regulations
- Reducing operating costs by granting subsidies for energy used in electric traction and preferential energy tariffs for public transport operators.

Future prospects:

- Expanding GHG emissions calculations using the JASPERS method for all electrified public transport in Bucharest
- Quantifying electricity consumption for electric bus charging stations to estimate the carbon footprint for these terminals
- The estimation of black carbon (BC) emissions, which also include PM<sub>2.5</sub>, and short-lived climate pollutants (SLCPs), such as CH<sub>4</sub>, using adequate calculation methods
- Scenario screening for the alternative options, such as hydrogen, as an energy source for buses, which represent a promising solution for conventional electrification, especially on extended routes or in heavy-duty conditions, where electric charging infrastructure deployment is challenging.

Upgrading the public transport fleet in Bucharest will increase the attractiveness and efficiency of the mobility, bring socio-economic gains while generate significant benefits for the city's environment.

#### Abbreviations

The following abbreviations are used in this manuscript:

GHG Greenhouse Gases

CO<sub>2</sub> Carbon dioxide

CO<sub>2</sub>e Carbon dioxide equivalent

N<sub>2</sub>O Nitrous oxide

CH<sub>4</sub> Methane

NO<sub>x</sub> Nitrogen oxides

PM Particulate matter

VOC Volatile Organic Compounds

BC Black Carbon  
 SLCP Short-lived climate pollutant emissions  
 STB S.A. Bucharest Public Transport Company  
 URAC Repair Work and Central Factory  
 UITP The International Association of Public Transport  
 UE European Union  
 JASPERS Joint Assistance to Support Projects in European Regions  
 Web TAG Web-based Transport Analysis Guidance  
 PMUD Sustainable Urban Mobility Plan  
 HVAC Heating, Ventilation, and Air Conditioning

## References

- [1] European Environment Agency (EEA). “Air pollution sources”, 2022. Accessed July 28, 2022. <https://www.eea.europa.eu/themes/air/air-pollution-sources-1>.
- [2] Eguluz-Gracia, I., A.G. Mathioudakis, S. Bartel, S.J. Vijverberg, E. Fuertes, P. Comberiat, Y.S. Cai, P.V. Tomazic, Z. Diamant, J. Vestbo, C. Galan, and B. Hoffmann. “The need for clean air: the way air pollution and climate change affect allergic rhinitis and asthma.” *Allergy* 75, no. 9 (2020): 2170–2184. <https://doi.org/10.1111/all.14177>.
- [3] International Energy Agency. “Energy and Air Pollution. World Energy Outlook Special Report”, 2016. Accessed July 28, 2022. <https://www.iea.org/reports/energy-and-air-pollution>.
- [4] Bein, T., C. Karagiannidis, and M. Quintel. “Climate change, global warming, and intensive care.” *Intensive Care Medicine* 46 (2020): 485–487. <https://doi.org/10.1007/s00134-019-05888-4>.
- [5] NOAA National Centers for Environmental Information. “Monthly Global Climate Report for Annual 2020”, January 2021. Accessed July 28, 2022. <https://www.ncei.noaa.gov/access/monitoring/monthly-report/global/202013>.
- [6] Klimont, Z., K. Kupiainen, C. Heyes, P. Purohit, J. Cofala, P. Rafaj, J. Borken-Kleefeld, and W. Schöpp. “Global anthropogenic emissions of particulate matter including black carbon.” *Atmospheric Chemistry and Physics* 17, no. 13 (2017): 8681–8723. <https://doi.org/10.5194/acp-17-8681-2017>.
- [7] AirParif. “Air-Climate-Energy Inventory. Île-de-France Report — Year 2021 / Inventaire Air-Climat-Énergie. Bilan Île-de-France — Année 2021”, March 2024. Accessed September 2, 2025. [https://www.airparif.fr/sites/default/files/document\\_publication/bilan\\_emissions\\_IDF\\_2021.pdf](https://www.airparif.fr/sites/default/files/document_publication/bilan_emissions_IDF_2021.pdf).
- [8] European Environment Agency. “Emissions of air pollutants from transport in Europe”, October 28, 2024. Accessed September 2, 2025. <https://www.eea.europa.eu/en/analysis/indicators/emissions-of-air-pollutants-from>.
- [9] Jacobson, M.Z. *Short-lived global warming agents and strategies to reduce them*. Institute for Governance & Sustainable Development, 2008. <https://igsd.org/docs/BC%20Summary%206July08.pdf>.
- [10] European Parliament. “Greenhouse gas emissions by country and sector (infographic)”, December 2, 2024. Accessed September 2, 2025. <https://www.europarl.europa.eu/topics/en/article/20180301STO98928/greenhouse-gas-emissions-by-country-and-sector-infographic>.
- [11] Boyle, R. “Greenhouse Gas Emissions in Romania.” *Emission Index*, July 16, 2024. Accessed September 3, 2025. <https://www.emission-index.com/countries/romania>.
- [12] World Health Organization. “Ambient (Outdoor) Air Pollution”, October 24, 2024. Accessed September 3, 2025. [https://www.who.int/news-room/fact-sheets/detail/ambient-\(outdoor\)-air-quality-and-health](https://www.who.int/news-room/fact-sheets/detail/ambient-(outdoor)-air-quality-and-health).
- [13] United States Environmental Protection Agency (EPA). “Inventory of U.S. Greenhouse Gas Emissions and Sinks: 1990–2021”, 2023. Accessed September 3, 2025. <https://www.epa.gov/ghgemissions/inventory-us-greenhouse-gas-emissions-and-sinks-1990-2021>.
- [14] Bucharest Transport Company - STB Inc. / Societatea de Transport Bucuresti STB S.A. “Statistics / Statistici.” Accessed September 3, 2025. <http://stbsa.ro/statistici>.
- [15] Badiceanu, A., A.F. Popescu, A.I. Balint, and E. Matei. “Impact of PM10 emissions from transport sector on air quality in the Bucharest-Ilfov area.” *UPB Scientific Bulletin, Series B: Chemistry and Materials Science* 87 (2025): 227–236.
- [16] Popescu, A.-F., E. Matei, A. Bădiceanu, A. I. Balint, M. Râpă, G. Coman, and C. Predescu. “An optimistic vision for public transport in Bucharest City after the bus fleet upgrades.” *Environments* 12, no. 7 (2025): 242. <https://doi.org/10.3390/environments12070242>.
- [17] International Association of Public Transport (UITP). “SORT 1–Urban cycle energy consumption and range values.” In *SORT & E-SORT–Standardised on Road Test Cycles for Buses* [Report]; Brussels, Belgium, 2021.



- [18] Alexander Dennis Ltd. “Next-generation Alexander Dennis Enviro400EV is driving value through efficiency with benchmark 0.67 kWh/km energy consumption. Alexander Dennis”, February 26, 2024. Accessed August 18, 2025. <https://www.alexander-dennis.com/next-generation-alexander-dennis-enviro400ev-is-driving-value-through-efficiency-with-benchmark-0-67kwh-km-energy-consumption>.
- [19] Zenobē. “Driving the adoption of zero-emission buses in the UK: Energy efficiency and fleet data”, 2023. *Zenobē Energy*. Accessed August 18, 2025. <https://www.zenobe.com>.
- [20] European Commission. “Ebusco 2.2 electric bus performance in Berlin”, 2022. *EU Commission Transport Innovation Portal*. Accessed August 18, 2025. from <https://ec.europa.eu/transport>.
- [21] Basma, H., M. E. J. Stettler, and E. Gaitanidou. “Real-world energy consumption and CO<sub>2</sub> emissions of electric buses in Paris.” *Sustainability* 13, no. 21 (2021): 12011. <https://doi.org/10.3390/su132112011>.
- [22] Madrid Municipal Transport Company / Empresa Municipal de Transportes (EMT) de Madrid. “Operational performance of inductive-charged electric buses in Madrid”, 2020. Accessed August 18, 2025. <https://www.emtmadrid.es>.
- [23] López, A., and J. García. “Impact of HVAC on electric bus energy consumption in Southern Europe.” *Energy Reports* 7 (2021): 5889–5899. <https://doi.org/10.1016/j.egyr.2021.09.123>.
- [24] Dalla Chiara, B., G. Pede, F. Deflorio, and M. Zanini. “Electrifying buses for public transport: Boundaries with a performance analysis based on method and experience.” *Sustainability* 15, no. 19 (2023): 14082. <https://doi.org/10.3390/su151914082>.
- [25] Instituto Superior Técnico. “Performance of electric buses in Lisbon: Case study of Carris.” IST – University of Lisbon, 2021. Accessed August 18, 2025. <https://tecnico.ulisboa.pt>.
- [26] Barreiro Public Transport / Transportes Colectivos do Barreiro (TCB). “Energy efficiency report of the electric bus fleet”, 2022. Accessed August 18, 2025. <https://www.tcb.pt>.
- [27] Municipal Bus Companies / Miejskie Zakłady Autobusowe (MZA). Warsaw Transport Authority. “Electric bus operations in Warsaw: Efficiency and seasonal performance”, 2021. Accessed August 18, 2025. <https://www.mza.waw.pl>.
- [28] Solaris Bus & Coach. “Technical performance of Solaris electric buses in Central Europe”, 2021. Accessed August 18, 2025. <https://www.solarisbus.com>.
- [29] Kourti I., N. Di Volo, A. Gonzalez Sanchez, and L. Popova. “Guidance Note. Support for the Development of a National Climate Proofing Guidance for Spain.” Joint Assistance to Support Projects in European Regions (JASPERS), October 15, 2024. Accessed August 18, 2025. [https://agaur.gencat.cat/web/.content/09\\_Transferencia/Singulars/Documents/2\\_Climate\\_proofing\\_Version\\_Jaspers.pdf](https://agaur.gencat.cat/web/.content/09_Transferencia/Singulars/Documents/2_Climate_proofing_Version_Jaspers.pdf).
- [30] International Energy Agency. “CO<sub>2</sub> Emissions from Fuel Combustion: Highlights (2017 Edition)”, 2017. Accessed February 28, 2025. <https://euagenda.eu/upload/publications/untitled-110953-ea.pdf>.
- [31] Eurostat. “National passenger road transport performance by type of vehicles registered in the reporting country”. Accessed August 18, 2025. [https://ec.europa.eu/eurostat/databrowser/view/ROAD\\_PA\\_MOV/default/table?lang=en%20](https://ec.europa.eu/eurostat/databrowser/view/ROAD_PA_MOV/default/table?lang=en%20).
- [32] Joint Assistance to Support Projects in European Regions (JASPERS). European Investment Bank. “JASPERS Transport–Cost-Benefit Analysis Guide: Annex A–Emission Factors”, Luxembourg, 2021. <https://jaspers.eib.org>.
- [33] Department for Transport - United Kingdom Government. “Transport Analysis Guidance (WebTAG)”, Version 1.4; 10 April 2025. <https://www.gov.uk/guidance/transport-analysis-guidance-webtag>.
- [34] Nowtricity. “Real Time Electricity Production Emissions by Country – Current emissions in Romania.” Accessed August 18, 2025. <https://nowtricity.com>.
- [35] Bertoldi, P., D. Bornas Cayuela, S. Monni, and R. Piers De Raveschoot. “Guidebook “How to Develop a Sustainable Energy Action Plan (SEAP)””. Publications Office of the European Union: Luxembourg, 2010. Accessed August 18, 2025. <https://publications.jrc.ec.europa.eu/repository/handle/JRC57789>.
- [36] Davide, M., J. Bastos, P. Bezerra, G. Hernandez Moral, V. Palermo, et al. *How to develop a Sustainable Energy and Climate Action Plan (SECAP)*. Covenant of Mayors Guidebook - Main document. JRC142148. Luxembourg, Publications Office of the European Union, 2025.
- [37] Panton, A.J. “Making Romania Fit and Resilient for the Net Zero Transition.” *IMF Selected Issues Paper*, no. 063. International Monetary Fund: Washington, DC, USA, 2023.
- [38] Bucharest City Hall / Primăria Municipiului București. “Sustainable Development Strategy of the Municipality of Bucharest 2018–2030 / Strategia de dezvoltare durabilă a Municipiului București 2018–2030”, 2018. Accessed August 18, 2025. [https://www.pmb.ro/documents/strategia\\_de\\_dezvoltare\\_2018\\_2030.pdf](https://www.pmb.ro/documents/strategia_de_dezvoltare_2018_2030.pdf).

The paper is part of **The 2nd International Conference on Advanced Autonomous Systems ICAAS 2025**, which will be organized under the auspices of the National University of Science and Technology POLITEHNICA Bucharest, during November 13-14, 2025.

## Pedagogical Valences of Computer-Assisted Instruction in the Professional Training of Soil Remediation Specialists

MA stud. **Ioana-Elisabeta CIORUȚA**<sup>1,2</sup>, PhD Eng. IT exp. **Bogdan V. CIORUȚA**<sup>1,3,4,\*</sup>,  
Assoc. Prof. PhD Eng. habil. **Mirela-Ana COMAN**<sup>5,6</sup>, Eng. IT exp. **Alexandru L. POP**<sup>1,3</sup>

<sup>1</sup> Technical University of Cluj-Napoca - North University Centre of Baia Mare, Faculty of Letters, Department of Specialty with Psychopedagogical Profile, 76 Victoriei Str., 430083, Baia Mare, Romania

<sup>2</sup> "Little Prince" Extended Program Kindergarten, 8B Cuza Vodă Str., 430034, Baia Mare, Romania

<sup>3</sup> Technical University of Cluj-Napoca - North University Centre of Baia Mare, Office of Informatics, 62A Victor Babeș Str., 430083, Baia Mare, Romania

<sup>4</sup> Technical University of Cluj-Napoca - North University Centre of Baia Mare, Faculty of Science, 76 Victoriei Str., 430072, Baia Mare, România

<sup>5</sup> Technical University of Cluj-Napoca - North University Centre of Baia Mare, Faculty of Engineering - Department of Mineral Resources, Materials and Environmental Engineering, 62A Victor Babeș Str., 430083, Baia Mare, Romania

<sup>6</sup> University of Agricultural Sciences and Veterinary Medicine from Cluj-Napoca, 3-5 Calea Mănăștur, 4000372, Cluj-Napoca, Romania

\* bogdan.cioruta@staff.utcluj.ro

**Abstract:** *The accelerated degradation of soil resources represents one of the most pressing global challenges of the 21st century, requiring a rapid and well-founded response from society. In this context, the professional training of specialists capable of efficiently and innovatively addressing complex problems related to soil pollution becomes a strategic priority. As such, the present research aims to analyze and argue the implications and valences of Computer-Assisted Instruction (CAI) as a modern and indispensable pedagogical solution in the training of these specialists. The motivation for this scientific approach stems from the need to adapt educational methods to the rapid evolution of remediation technologies and the increasing complexity of pollution scenarios. By integrating CAI, the radical transformation of the learning process aims to shift from a passive model (based on the transmission of information) to an active, interactive one tailored to individual needs. Digital technologies (computer simulations, virtual reality, and e-learning platforms) offer the opportunity to reproduce pollution scenarios in controlled environments, to practice remedial interventions without risks, and to assimilate cutting-edge knowledge. At the same time, CAI is not only a content delivery tool, but a skills development platform essential to prepare a new generation of specialists capable of acting effectively in the face of ecological emergencies. This article demonstrates that the digitalization of the educational process in the field is a requirement for efficiency and sustainability, contributing decisively to the protection of the environment and natural resources.*

**Keywords:** *Digitalization, vocational training, assisted training, soil protection, decontamination technologies.*

### 1. Introduction

Soil degradation is not only an ecological problem (via agricultural development and ecological sustainability), but also a socio-economic and public health one [1-3]. Its effective approach requires a specialized workforce, capable of using the latest technologies and remediation methodologies [4-6]. In this context, in human interaction with the environment [7], the purpose of this study is to argue for the essential role of Computer-Assisted Instruction (CAI) as a modern and efficient tool in the professional training of soil remediation specialists, but also as an integrated part of Environmental Information Systems (EISs) and Environmental Informatics (EI) [8,9]. The intended purpose is not only to describe a teaching method, but to demonstrate that CAI can build a superior educational framework, directly responding to the needs of the ecological emergencies. Classical training programs are often based on static materials and on content that can quickly become outdated, given the rapid pace of innovations in the field of bioremediation,

phytoextraction, or stabilization techniques. They have difficulties in realistically simulating the complexity of a polluted site, with types of contaminants, geological layers, and potential risks. In light of the above, Table 1 illustrates the evolution of methods and tools used in the training of soil remediation specialists, reflecting technological progress and paradigm shifts in environmental education over several decades. The latter can be grouped into three distinct stages, reflecting the evolution of the relevance and complexity of soil remediation specialist training.

**Table 1:** A perspective on the dynamics of professional training of specialists in soil decontamination, by reporting to the reference interval 1950-2030

Stage	Decade	Technologies and training tools available to specialists	Observations
Stage 1 <i>Fundamental training</i>	1950-1960	Textbooks, classical university courses, lessons in the amphitheater	Training based on theoretical knowledge. Emphasis on chemistry, geology, and basic principles of hydrology. Absence of a discipline dedicated to soil decontamination.
	1960-1970	Lessons, small-scale practical demonstrations & first written case studies	The emergence of the first courses focused on pollution. The beginning of the application of knowledge in case studies, but limited to descriptions and theoretical analyses.
	1970-1980	The use of early computers for calculation and mathematical modeling	Computers are used to run simple pollutant dispersion models. The training tools remain theoretical and mathematical, accessible only in specialized research centers.
Stage 2. <i>Training through transition to technology</i>	1980-1990	Specialized software programs (primitive GIS), access to rudimentary databases	The first software dedicated to mapping and spatial analysis (GIS) appears. Students begin to work with digital maps, but the interface is complex and limited.
	1990-2000	Educational CD-ROMs, environmental databases, and Internet access	The spread of personal computers and the Internet has revolutionized access to information. CD-ROM courses offer interactive multimedia content. Learning becomes more accessible.
	2000-2010	E-learning platforms (Moodle, Blackboard), online courses, webinars	The emergence of the first large-scale e-learning platforms. Vocational training becomes more flexible. Online communities of practice are developed, and knowledge exchange is facilitated.
Stage 3. <i>Digitalized &amp; integrated training</i>	2010-2020	3D Simulations, Virtual Reality (VR), Mobile Applications, Big Data	An explosion of immersive technologies. Learners can "explore" polluted sites in VR. Using Big Data from IoT sensors for real-time analysis. Mobile micro-learning is becoming popular.
	2020-2030	Adaptive learning with AI, blockchain for certification, Augmented Reality (AR)	AI personalizes the learning process for each learner. Blockchain ensures the integrity of digital diplomas. Training becomes interconnected, personalized, and transparent.

Each stage marks a qualitative leap, from a purely theoretical approach to a fully integrated, technology-assisted one, as follows:

- **Stage 1 - Fundamental Training (1950-1980)** - this period was marked by a theoretical and rudimentary approach. Training was focused on basic disciplines, such as chemistry, geology, and hydrology, without a dedicated specialization in soil remediation. Training tools were classic, based on textbooks and lectures in the amphitheater. The direct relevance of the training was limited because the available technology was insufficient to model complex processes in the field.

- Stage 2 - **Training through the transition to technology (1980-2010)** - this stage represented a transition from theory to practice, facilitated by the emergence and spread of personal computers and the Internet. Training became more accessible and interactive. The first GIS programs and databases allowed specialists to start working with real data and visualize environmental problems in a spatial context. The emergence of e-learning platforms and online courses democratized access to information, allowing for more flexible learning. However, interaction remained predominantly on the screen, with simulations and practical applications still limited.
- Stage 3 - **Digitalized and Integrated Training (2010-2030)** - the current and future period is defined by a fully integrated and personalized approach, in which technology is no longer a simple tool, but an intrinsic part of the learning process. Technologies such as virtual reality (VR) and augmented reality (AR) allow for immersive simulations and assisted interventions in the field, while artificial intelligence (AI) personalizes the learning trajectory for each specialist. The use of blockchain for certifications ensures transparent and trusted validation of skills. The relevance of the training is maximum, as it prepares specialists not only with knowledge, but also with practical skills and adaptability.

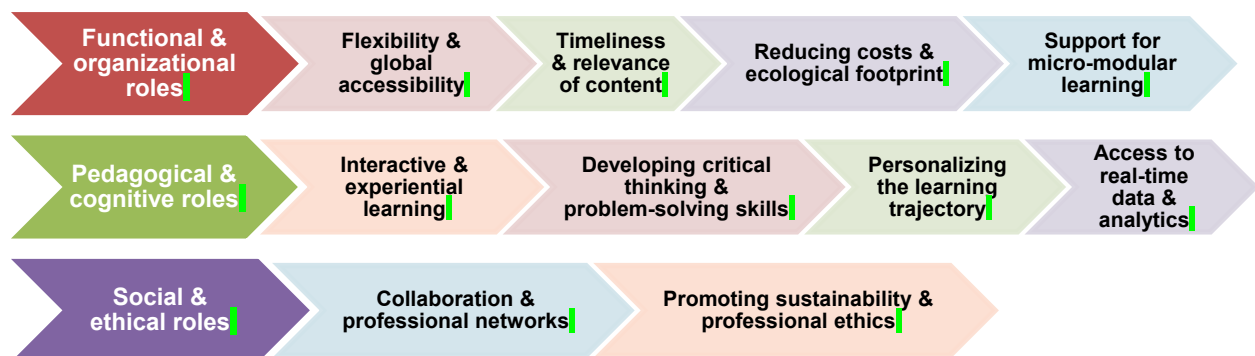
CAI overcomes these barriers by using advanced technologies, such as:

- **Virtual simulations** - allow learners to virtually visit and intervene on a contaminated site, from the initial risk assessment to the planning and implementation of a remediation plan.
- **Interactive e-learning platforms** - provide access to an updated database of case studies, best practices, and current legislation, ensuring a continuous and relevant learning process.
- **Augmented Reality (AR)** - can be used in the field to overlay geological data or contamination maps on the real image of the soil, helping specialists visualize the complexity of the situation.

By integrating these tools, active and personalized learning is facilitated, transforming the learner from a simple receiver of information into an active participant in solving problems. Ultimately, the use of CAI not only modernizes the educational process but also directly contributes to the formation of a new generation of specialists, better prepared, more agile, and more capable of contributing to global environmental protection efforts.

## 2. Literature Review - a Synthesis of Research on CAI in the Training of Specialists with Responsibilities in Soil Decontamination

Recent scientific literature highlights a growing convergence between digital technologies and environmental education, if we consider the mobile applications dedicated to soil protection [10,11]. Most of the considered reference publications demonstrate that the effective use of CAI radically transforms the process of knowledge acquisition and skills development among specialists [12], especially in relation to the integrated development of an environmental virtual field laboratory [13-16], as shown in Fig. 1.



**Fig. 1.** Categories of benefits associated with the integration of CAI in the professional training of soil remediation specialists



The elements presented in Fig. 1, according to the structure that we have built on three categories that reflect the fundamental roles of CAI in professional training, demonstrate to us that the studies considered do not just theorize, but provide concrete evidence of the major benefits of CAI, which go beyond the simple transmission of information. In this regard, we can mention and highlight the following aspects, respectively:

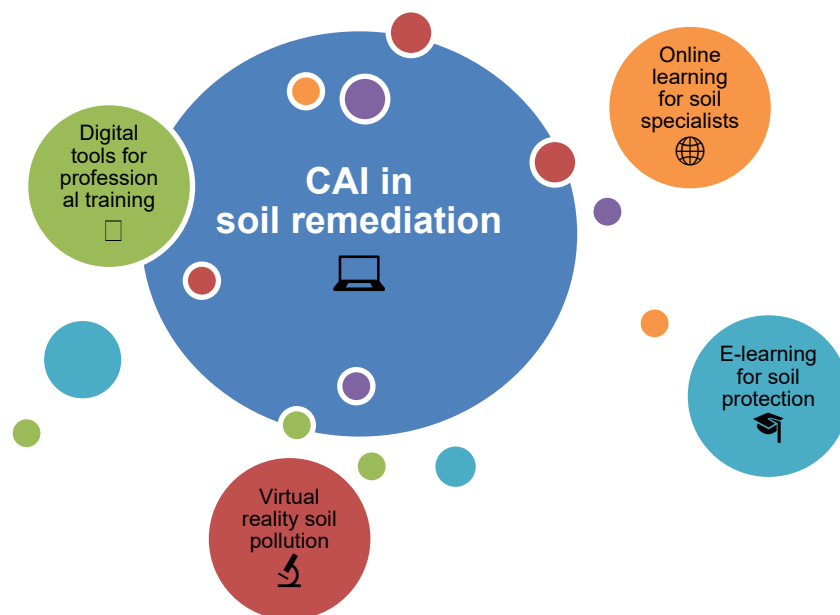
- **Flexibility and global accessibility** - research shows that e-learning formats eliminate geographical and temporal barriers, allowing specialists and students to access high-quality courses remotely; this aspect is crucial for a field with dispersed expertise, facilitating the exchange of good practices globally and access to specialization courses offered by top universities, regardless of the geographical location of the learner.
- **Interactive and experiential learning** - studies on serious games and digital simulations in education emphasize that they significantly increase the information retention rate and the ability to apply knowledge; Unlike a theoretical course, a soil remediation simulation allows students to test different technologies (e.g., *bioremediation*, *phytoextraction*, *stabilization*) and observe in real time the effects of their decisions, more easily understanding the complexity of degradation processes and chemical reactions.
- **Timeliness and relevance of content** - one of the biggest advantages (often discussed in the specialized literature) is the ability of e-learning platforms to be updated quickly. Thus, in a field where legislative regulations and technologies are constantly evolving, this speed of update is essential. Learners have immediate access to the latest research, case studies, and methodologies, ensuring that their training is always in line with the latest standards in the field.
- **Reduction of costs and ecological footprint** - many of the articles in the field emphasize that, in addition to the pedagogical benefits, CAI also contributes to a substantial reduction in training costs (e.g., *costs related to transportation, accommodation, printed materials*), making specialized education more accessible. This aspect is relevant for the field of soil remediation, where the optimization of financial resources is a fundamental principle.
- **Developing critical thinking and problem-solving skills** - CAI platforms, through the use of interactive case studies and problem-based scenarios, encourage learners (future specialists) to analyze complex situations, evaluate multiple remedial options, and adequately justify the decisions made. This approach, supported by research in the field of digital pedagogy, is vital for training specialists who not only know the theories but also know how to apply them in unpredictable situations.
- **Collaboration and professional networks** - the literature indicates an increase in productivity and innovation among online communities of practice. Discussion forums, webinars, and virtual group projects allow specialists to collaborate from different locations, exchange experiences, and build a strong professional network, which is essential for addressing environmental problems (including those associated with soil resource pollution) that do not respect geographical boundaries.
- **Adaptation (appropriate personalization) of the learning trajectory** - modern CAI systems, often based on artificial intelligence algorithms, can monitor the progress of each learner and adapt the didactic content according to the pace and learning style. This ensures a deepening of difficult concepts and an acceleration of learning in familiar areas, thus optimizing training time and guaranteeing better assimilation of knowledge.
- **Support for micro-modular learning** - an emerging trend in professional training, documented by recent studies, is the shift to micro-learning, which involves breaking down complex information into short, easy-to-digest modules. CAI perfectly facilitates this approach, allowing learners to go through specific segments about a particular technology or contaminant when they need it, directly on their mobile. This flexibility is crucial for specialists in the field.
- **Unconditional access to databases and real-time analysis** - CAI platforms can be integrated with geospatial databases and environmental monitoring systems, giving learners access to real-time information on soil conditions, pollution maps, and the progress of remediation projects. This access to big data enables evidence-based learning and a deeper understanding of the impact of decontamination decisions.



- **Promoting sustainability and professional ethics** - through interactive scenarios and case studies focused on long-term impact, CAI can configure, shape, and reinforce a culture of responsibility and professional ethics among future specialists. Simulations can illustrate not only the technical success of a remediation project, but also the social, economic, and ecological consequences of the decisions made, preparing professionals aware of their role in society.

### 3. Materials and Methods

The methodological approach of this study is based on a systematic review of the specialized literature. The main research material consisted of scientific articles, case studies, research reports, and normative documents, all extracted from internationally recognized academic databases. To ensure the quality and relevance of the information, specific and relevant search terms for high-quality publications were used. These were strategically combined to obtain precise results. Among the search terms used (see Fig. 2) are: *e-learning for environmental education*, *computer-assisted instruction in soil remediation* [17-19], *digital tools for professional training in environmental science*, *virtual reality in soil pollution*, *online learning for environmental specialists*, *blended learning in environmental engineering*, *gamification for environmental training*, *micro-learning in professional development* [20-22], *blockchain for professional certification*, *AI in adaptive learning for environmental sustainability*, etc.



**Fig. 2.** Search terms used to index relevant publications associated with the integration of CAI in the professional training of soil remediation specialists

The search process was carried out on academic reference platforms, such as Web of Science, Google Scholar, and on the websites of prestigious organizations, such as the Environmental Protection Agency (EPA) and the European Environment Agency (EEA). The method involved the following stages, namely: identification of relevant literature - an extensive search was carried out using the above terms, with filtering by year (last 5-10 years), to ensure the timeliness of the information, data synthesis - the selected articles were critically analyzed to identify the role, impact and valences of CAI in the context of training specialists in soil remediation, correlation of concepts - a direct correlation was established between the benefits of CAI (e.g., *flexibility*, *interactivity*) and the specific needs of the soil remediation field (e.g., *simulation of complex scenarios*, *access to real-time data*). Based on the synthesized data, a set of concrete proposals and recommendations for good practice was developed, aimed at maximizing the efficiency of vocational training.

#### 4. Results on the Synergy between Technology and Human Expertise in Soil Remediation

The analysis of the role, impact, and purpose of CAI in the professional training of soil remediation specialists reveals a complex pedagogical architecture, which, according to our results, summarized in Table 2, demonstrates that CAI is a catalyst in the development of essential skills that contribute to the formation of a specialist better equipped to face the challenges in the field.

**Table 2:** A perspective on CAI, as an efficient and innovative pedagogical architecture, in relation to the professional training of soil remediation specialists

Stage & assoc. level	The role of CAI in training	Impact on future specialists	Pedagogical purpose (finality)
Stage 1. <b>Substantiation &amp; assimilation</b> (introductory level)	<i>E-learning platforms with online courses</i> (🎓)	<i>Access to updated content, tailored to needs</i> The platforms not only offer courses, but also integrate self-assessment modules, expert discussion forums, and global case study databases, ensuring that future specialists are up to date with the latest regulations.	Ensuring a high level of theoretical knowledge and continuous learning
	<i>Digitalized tests and assessments</i> (✅)	<i>Self-assessment of progress and identification of learning gaps</i> Digitalized assessment systems provide fast and personalized feedback, allowing a future specialist to be evaluated based on performance in simulation scenarios.	Personalize your learning journey and get quick feedback
Stage 2. <b>Practice &amp; experimentation</b> (intermediate level)	<i>Databases and interactive GIS</i> (🗺️)	<i>Ability to analyze and visualize complex data</i> CAI platforms can integrate data on soil types, specific contaminants, and pollution history, which allows for a more informed intervention plan.	Developing data analysis and strategic planning skills
	<i>Simulations and VR</i> (🎮)	<i>Improving decision-making in complex and dynamic pollution scenarios</i> Students (future specialists) can navigate through the 3D structure of the soil, visualize the spread of pollutants, and simulate the impact of various intervention methods, which contributes to refining professional judgment.	Developing practical skills without the risks and costs of real operations
	<i>Interactive case studies and gamification</i> (🎲)	<i>Motivating and increasing engagement in learning</i> Students solve complex case studies as if they were on a mission, applying knowledge in a fun and stimulating way, which strengthens not only knowledge but also team spirit.	Increasing the efficiency of the learning process through active involvement and intrinsic motivation
Stage 3. <b>Connection &amp; continuous development</b> (advanced level)	<i>Online collaboration through forums and webinars</i> (👥)	<i>Connecting with experts in the field</i> Interactive webinars and forums transform learners into active members of a community, thus creating a synergy that stimulates innovation and collective solving of complex problems.	Creating a community that leads to the exchange of experiences and the solving of common problems
	<i>Micro-learning on mobile devices</i> (📱)	<i>Adaptive, continuous, and rapid learning</i> Specialists can access short learning modules directly on their mobile devices to quickly familiarize themselves with a new sampling technique or work protocol.	Ensuring real-time skills and professional adaptability to field needs

The use of CAI tools aims to create more agile, informed, and adaptable specialists, able to use technology not only as a tool, but also as a way of thinking and solving problems. Ultimately, the impact extends beyond the individual, contributing to a more effective and sustainable approach to pollution problems at the societal level.

## 5. Perspectives and Proposals - a Strategic Vision for the Future of Soil Remediation Specialist Training










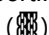
For CAI to become an essential component and not just a complement to traditional soil remediation training, it is crucial to outline a clear vision and formulate concrete proposals based on current technological and pedagogical trends. Beyond the simple use of e-learning platforms, a deeper integration of technology is needed to create a complete educational ecosystem.

To maximize the impact of CAI in the training of soil remediation specialists, we believe it is crucial to formulate concrete proposals, each supported by a solid pedagogical justification. In these circumstances, Table 3 presents a synthesis of the strategic vision, associating each proposal with the educational reasoning that underlies it.

The proposals in Table 3 are ordered chronologically and pedagogically, starting from an introductory and fundamental level (familiarization with the basic notions), towards an advanced level (practical application and innovation). This order reflects a logical training path, from theory to practice and from the individual to the community, which is based on:

- **recognized digital certifications** - to motivate students and provide them with a concrete goal, it is essential to establish a clear system of recognition of skills at the beginning; this way, the learner knows from the very beginning that their efforts will be validated.
- **development of integrated educational platforms** - an immediate next step is to create the learning environment, in the form of a unified platform that serves as the foundation, on which all other stages will be built.
- **integration of AI and adaptive learning** - as learners start using the previously developed platform, the AI can start analyzing their progress; as such, personalization of learning becomes effective only after there is a sufficient volume of data.
- **creation of virtual remediation laboratories** - once learners have assimilated the theoretical concepts, it is time to apply them. Virtual laboratories provide a safe environment to experiment, understand, and learn the principles of how remediation methods work.
- **IoT integration in simulations** - integrating real-time data through IoT sensors makes exercises more realistic and allows learners to learn to manage dynamic information.
- **AR for field interventions** - represents a transition from the virtual to the physical environment. AR assists the specialist directly in the field, combining digital data with reality, a crucial stage before taking on full responsibilities.
- **mirror decontamination projects** - at this level, the learner applies all the knowledge in a real project, while benefiting from the support and data of an existing project. It is an advanced stage of practical learning, which closely imitates professional work.
- **virtual mentoring systems** - as they become more advanced, learners need guidance from experts. Virtual mentoring systems become a valuable tool to deepen knowledge and navigate the complexities of the job market.
- **modular courses based on crisis scenarios** - represent the culmination of training, preparing specialists for emergencies; previously acquired skills are tested under pressure, in a controlled environment.
- **use of blockchain for certification of skills** - once training is completed, diplomas and certifications must be secure and verifiable. The use of blockchain, at the end of the educational path, ensures the integrity and professional value of all efforts made.

**Table 3:** A perspective on CAI, as a significant strategic vision, in relation to the professional training of specialists in soil decontamination

Stage & assoc. level	Proposal (strategic vision)	Pedagogical justification (CAI involvement)	Pedagogical purpose (finality)
<b>Stage 1.</b> <b>Substantiation &amp; assimilation</b> (introductory level)	<i>Recognized digital certifications</i> 	<i>Increasing credibility and motivation</i> Official recognition of skills acquired online transforms e-learning from a simple optional activity into a valid professional path.	Increasing the professional value of specialists & facilitating their employment on the labor market
	<i>Development of integrated educational platforms</i> 	<i>Holistic &amp; contextual training</i> A unified platform allows learners to connect theoretical information with practical applications, creating a learning environment that reflects reality.	Training specialists with an integrated vision of decontamination processes
	<i>Integrating AI &amp; adaptive learning</i> 	<i>Personalizing learning</i> AI allows the content and pace of study to be adjusted according to the individual needs of each learner, maximizing the efficiency of the process.	Optimizing training time & ensuring deep assimilation of knowledge
<b>Stage 2.</b> <b>Application &amp; experimentation</b> (intermediate level)	<i>Creating virtual decontamination laboratories</i> 	<i>Learning by doing</i> Virtual labs provide a safe environment to experiment, test hypotheses, and observe the consequences of actions.	Developing critical thinking & practical skills without risks or material costs
	<i>Integrating IoT into simulations</i> 	<i>Data-driven learning</i> Connecting simulations to real data, transmitted via IoT, transforms the case study into a dynamic experience.	Developing data analysis skills & the ability to make informed decisions
	<i>AR for field interventions</i> 	<i>Real-time cognitive assistance</i> AR provides visual and informational support directly on the ground, overlaying virtual data over the real environment.	Optimizing decision-making in the field & reducing professional errors
<b>Stage 3.</b> <b>Practice, collaboration &amp; specialization</b> (advanced level)	<i>Decontamination projects in the mirror</i> 	<i>Connecting theory with practice</i> Participation in projects that reflect real field work bridges the gap between knowledge and application in authentic situations.	Training specialists with practical experience relevant to the challenges in the field
	<i>Virtual mentoring systems</i> 	<i>Collaborative &amp; guided learning</i> Virtual mentoring allows junior specialists to benefit from the experience of seniors in a flexible format.	Facilitating the transfer of tacit knowledge & building solid professional networks.
	<i>Modular courses based on various crisis scenarios</i> 	<i>Developing emergency response skills</i> Crisis simulations force learners to quickly apply knowledge, make decisions under pressure, and manage resources.	Training specialists to deal with unpredictable & dangerous situations, with rapid reaction.
<b>Stage 4.</b> <b>Consolidation &amp; validation</b> (post-training level)	<i>Using blockchain for skills certification</i> 	<i>Ensuring transparency &amp; trust</i> An immutable, verifiable, blockchain-based certification gives a high level of reliability to degrees earned online.	Strengthening employers' trust in digital training & combating fraud.

Consequently, we can say that the future of professional training for soil remediation specialists is digital. Therefore, the previous proposals do not only aim at modernizing the tools, but at a fundamental transformation of the way specialists are trained, transforming them into agile, innovative, and well-connected professionals to the global community.











## 6. Conclusions and Good Practice Recommendations

The best practice recommendations for integrating CAI into the training of soil remediation specialists, explained in Table 4, can be ordered in a logical and pedagogical sequence, from strategic planning to implementation and continuous evaluation. This process can be structured in three distinct stages, which build on each other, respectively:

- **Stage 1 - Strategic planning and substantiation** - is critical and precedes the launch of any digital training program. Without a solid foundation, subsequent efforts risk being ineffective or unrecognized.
  - **creating a legislative and regulatory framework** - the first step is to obtain legitimacy, without the official recognition of digital diplomas and certifications, training efforts would have no value on the labor market. This legal framework ensures that professionals are validated and that employers have confidence in their skills.
  - **partnerships with industry** - to guarantee relevance, collaboration with companies in the field is essential. Thus, the programs align with real market requirements and ensure access to case studies and practical data.
  - **investment in digital infrastructure and OER** - a CAI program cannot function without a robust technological base. Investments in e-learning platforms and open databases are essential to support large-scale training and to democratize access to education.
  - **creation of training of trainers programs** - even with the best tools, success depends on the quality of teaching. Preparing educators to effectively use new technologies ensures quality content delivery and maximizes the potential of CAI tools.
  - **standardization of formats and interfaces** - to avoid technological barriers, platforms and materials must be standardized and compatible. This makes the learning process accessible and uniform for all learners.
- **Stage 2 - Implementation and Execution** - focuses on applying modern pedagogical principles in the actual conduct of training, transforming theory into practice.
  - **blended learning** - the learning process must combine the flexibility of online courses with practical sessions in the laboratory or in the field. This balanced approach ensures a complete transfer of skills from theory to practice.
  - **gamification of the learning process** - to maintain commitment and increase motivation, gamification elements must be integrated from the beginning. This turns the study into a more enjoyable and efficient experience, stimulating the active involvement of learners.
  - **continuous and project-based assessment** - throughout the training, a constant assessment, focused on practical projects, ensures that specialists not only accumulate knowledge, but can also effectively apply it in solving complex problems in the field.
- **Stage 3 - Monitoring, evaluation, and continuous development** - after implementation, the focus shifts to maintaining the program relevance and encouraging long-term learning.
  - **continuous monitoring and evaluation of CAI programs** - once the program is underway, it is essential to collect feedback and analyze performance to identify strengths and make necessary adjustments.
  - **promoting a culture of lifelong learning** - most importantly, CAI must cultivate a mindset of continuous learning among specialists. Digital platforms are also the ideal tool to support this approach in the long term, ensuring that specialists always remain relevant and competitive in the labor market.



**Table 4:** A perspective on good practice recommendations associated with the integration of CAI in the continuous and long-term professional training of soil remediation specialists

Stage & assoc. level	Good practice recommendation	Pedagogical justification (CAI involvement)	Pedagogical purpose (finality)
Stage 1. <b>Strategic planning &amp; substantiation</b> (introductory level)	<i>Creating a coherent legislative and regulatory framework</i> 	Official validation of digital training provides credibility and professional security. This legitimate framework ensures that online training efforts are recognized by employers and authorities.	Increasing trust in digital training and recognition on the labor market of skills obtained online
	<i>Partnerships with industry</i> 	Collaboration with companies in the field ensures the relevance of educational content and its alignment with the real demands of the labor market.	Aligning vocational training with the concrete needs of the labor market
	<i>Creating training of trainers programs</i> 	Training educators to effectively use new technologies ensures the quality delivery of digital content. A good trainer can maximize the potential of CAI tools.	Increasing the quality of teaching and the efficiency of training programs
	<i>Investments in digital infrastr. &amp; OER</i> 	Investments in platforms and open resources contribute to the democratization of education and stimulate innovation. Access to a common knowledge base improves the quality of training.	Ensuring a solid technological base and the necessary resources to support CAI at scale
	<i>Standardization of formats and interfaces</i> 	National and international standardization of content and interfaces eliminates technological barriers and ensures a uniform learning experience.	Democratizing access to training and optimizing the user experience
Stage 2. <b>Implementation &amp; execution</b> (intermediate level)	<i>Blended learning</i> 	Combining online courses with practical sessions (laboratory/field) provides a balanced approach that connects theory with practice.	Ensuring complete skills and professional adaptability in the field
	<i>Gamification of the learning process</i> 	Integrating game elements increases student motivation and engagement, transforming the learning process into a memorable and more engaging experience.	Increasing information retention rate and training efficiency
	<i>Continuous and project-based evaluation</i> 	A continuous assessment system, based on virtual projects, allows for real-time progress monitoring and provides personalized feedback, emphasizing the application of knowledge in solving real dynamic problems.	Training specialists with demonstrated practical skills, not just theoretical knowledge
Stage 3. <b>Monitoring, evaluation &amp; continuous development</b> (advanced level)	<i>Continuous monitoring and evaluation of programs</i> 	Collecting feedback and analyzing performance data allows programs to be adjusted according to the needs of learners and the evolution of the field.	Continuous improvement of the quality of CAI programs, based on concrete evidence
	<i>Promoting lifelong learning</i> 	CAI is the ideal tool to facilitate continuous learning, providing flexible and constant access to new information.	Ensuring that specialists remain relevant and competitive in a constantly evolving field

The integration of CAI into the training of soil remediation specialists is no longer a simple option, but a fundamental necessity imposed by the complexity of environmental problems and the rapid pace of technological innovation. The analysis highlighted that CAI transforms the educational process from a static and passive one, based on the unidirectional transmission of information, into a dynamic, interactive, and adaptive one.

CAI acts as a catalyst for the modernization of environmental education, enabling the transition from a didactic model focused on memorization to a pedagogical one focused on the development of skills. By using simulations, interactive databases, and virtual (immersive) case studies, CAI drastically reduces the gap between theoretical knowledge and its practical application; this is, moreover, an essential condition for the training of a new generation of professionals capable of efficiently and sustainably addressing complex pollution problems, in a way that would not be possible through traditional training methods.

CAI does not replace human expertise, but rather we can consider it as amplifying it. Digital platforms, based on AI/GenAI, allow for a personalization of the learning path, adapting to the specific needs of each learner (future specialist). This approach ensures that specialists are not only informed but also agile, innovative, and well-prepared to use technology as an essential tool in solving environmental problems. The real impact of CAI extends beyond the individual, contributing to a more effective and sustainable approach to pollution problems at the societal level.

## References

- [1] Wang, J.Z., J.N. Zhen, W.F. Hu, S.C. Chen, I. Lizaga, M. Zeraatpisheh, and X.D. Yang. "Remote sensing of soil degradation: Progress and perspective." *International Soil and Water Conservation Research* 11, no. 3 (2023): 429-454. DOI10.1016/j.iswcr.2023.03.002.
- [2] Jiang, C., H.W. Guo, Y.P. Wei, Z.Y. Yang, X.C. Wang, M.L. Wen, L. Yang, L.L. Zhao, H.Y. Zhang, and P. Zhou. "Ecological restoration is not sufficient for reconciling the trade-off between soil retention and water yield: A contrasting study from a catchment governance perspective." *Science of the Total Environment* 754 (2021): 142139. DOI10.1016/j.scitotenv.2020.142139.
- [3] Ferreira, C.S.S., S. Seifollahi-Aghmiuni, G. Destouni, N. Ghajarnia, and Z. Kalantari. "Soil degradation in the European Mediterranean region: Processes, status and consequences." *Science of the Total Environment* 805 (2022): 150106. DOI10.1016/j.scitotenv.2021.150106.
- [4] Lee, H., K. Sam, F. Coulon, S. De Gisi, M. Notarnicola, and C. Labianca. "Recent developments and prospects of sustainable remediation treatments for major contaminants in soil: A review." *Science of the Total Environment* 912 (2024): 168769. DOI10.1016/j.scitotenv.2023.168769.
- [5] Aparicio, J.D., E.E. Raimondo, J.M. Saez, S.B. Costa-Gutierrez, A. Alvarez, C.S. Benimeli, and M.A. Polti. "The current approach to soil remediation: A review of physicochemical and biological technologies, and the potential of their strategic combination." *Journal of Environmental Chemical Engineering* 10, no. 2 (2022): 46-57. DOI10.1016/j.jece.2022.107141.
- [6] Gu, F., J.P. Zhang, Z.Q. Shen, Y. Li, R.T. Ji, W. Li, L.J. Zhang, J.G. Han, J.M. Xue, and H. Cheng. "A review for recent advances on soil washing remediation technologies." *Bulletin of Environmental Contamination and Toxicology* 109, no. 4 (2022): 651-658. DOI10.1007/s00128-022-03584-6.
- [7] Coman M., and B. Cioruța. *From Human-Environment Interaction to Environmental Informatics / De la interacțiunea om-mediu la informatica mediului*. Cluj-Napoca, AcademicPres Publishing House, 2021.
- [8] Cioruța, B.V., and M.A. Coman. *Protecția solurilor și informatica mediului*. Cluj-Napoca, AcademicPres Publishing House, ISBN 630309177-8 CD, 2025.
- [9] Cioruța, B.V., and I.E. Cioruța. *Soil Protection and Environmental Informatics*. Cluj-Napoca, AcademicPres Publishing House, ISBN 630309179-2 CD, 2025.
- [10] Cioruța, B.V., I.E. Cioruța, M.A. Coman, and A.L. Pop. "Pedagogical Valences of the MIT App Inventor® Platform in Creating Applications for Soil Monitoring and Protection." *Hidraulica Magazine*, no. 4 (2023): 43-49.
- [11] Cioruța, B.V., I.E. Cioruța, M. Sălișcan, A.L. Pop, and M.A. Coman. "My Soil Protection App" - A Mobile-Based Dedicated Environmental Information System - from a User Testing and Validation Perspective." *Hidraulica Magazine*, no. 1 (2025): 83-91.
- [12] Cioruța, B. V., I.E. Cioruța, and A.L. Pop. "From computer-assisted instruction to the challenges of STE(A)M education / De la instruirea asistată de calculator la provocările educației STE(A)M." In Maier, M. *The use of new technologies in academic instruction - Milestones in the initial and continuing training of teachers / Utilizarea noilor tehnologii în instruirea academică - Repere în formarea inițială și continuă a cadrelor didactice*. GlobeEdit Publishing House, ISBN 978-620-6-79562-9 (2023): 152-173. [www.morebooks.shop/shop-ui/shop/product/978-620-6-79562-9](http://www.morebooks.shop/shop-ui/shop/product/978-620-6-79562-9).

- [13] Ramasundaram, V., S. Grunwald, A. Mangeot, N.B. Comerford, and C.M. Bliss. "Development of an environmental virtual field laboratory." *Computers & Education* 45, no. 1 (2005): 21-34. DOI10.1016/j.compedu.2004.03.002.
- [14] Çaliskan, O. "Virtual field trips in education of earth and environmental sciences." *Procedia - Social and Behavioral Sciences* 15 (2011): 3239-3243. DOI10.1016/j.sbspro.2011.04.278.
- [15] Krivka, Z., O. Jiráček, and Z. Vasíček. "Integrated Development Environment for Virtual Laboratory." Paper presented at the 5th International Technology, Education and Development Conference, Valencia, Spain, March 7-9, 2011.
- [16] Kaliszan, D., F. Koczorowski, C. Mazurek, N. Meyer, M. Procyk, T. Rajtar, D. Stokłosa, and M. Stroinski. "Virtual Laboratory of Interactive Teaching - a Live Laboratory for Environmental Science Education." Paper presented at the 4th International Conference of Education, Research and Innovation (ICERI), Madrid, Spain, November 14-16, 2011.
- [17] Hinckley, E.L.S., and S. Fendorf. "Field science in the age of online learning: Dynamic instruction of techniques to assess soil physical properties." *Frontiers in Education* 7 (2022): 959776. DOI10.3389/feduc.2022.959776.
- [18] Wadoux, A.M.J.C., and A.B. McBratney. "Digital soil science and beyond." *Soil Science Society of America Journal* 85, no. 5 (2021): 1313-1331. DOI10.1002/saj2.20296.
- [19] Reyes-Sanchez, L.B. "Teaching soil science: strategies and guarantees for the future." *Spanish Journal of Soil Science* 2, no. 1 (2012): 87-99.
- [20] Balseiro-Romero, M., and P.C. Baveye. "Book Review: Soil Pollution: A Hidden Reality." *Frontiers in Environmental Science* 6 (2018): 130. DOI10.3389/fenvs.2018.00130.
- [21] Baker, D., T. Selzner, J.H. Göbbert, H. Scharr, M. Riedel, E.T. Hvannberg, A. Schnepf, and D. Zielasko. "Hands-On Plant Root System Reconstruction in Virtual Reality." Paper presented at the 30th ACM Symposium on Virtual Reality Software and Technology VRST '24, Trier, Germany, October 9 - 11, 2024.
- [22] Tsai, H.H., X.Y. Hou, C.T. Chang, C.Y. Tsai, P.T. Yu, J.S. Roan, and K.C. Chiou. "Interactive Contents with 360-degree Panorama Virtual Reality for Soil and Water Conservation Outdoor Classroom." Paper presented at the 2020 International Symposium on Educational Technology (ISET), Bangkok, Thailand, August 24-27, 2020.

## Numerical Investigation of Energy Dissipation Efficiency in Stepped Spillway Designs under Flow Conditions

Associate professor Fănel Dorel ȘCHEAUA<sup>1,\*</sup>

<sup>1</sup> Dunarea de Jos University of Galati, MECMET Research Center

\* fanel.scheaua@ugal.ro

**Abstract:** Stepped spillways are widely applied in dam engineering due to their ability to dissipate water flow energy and mitigate cavitation risk. However, the efficiency of energy dissipation depends strongly on step geometry, slope and flow conditions. This study presents a comprehensive numerical analysis of novel stepped spillway configurations, including rectangular, trapezoidal and curved step profiles, under a range of discharges corresponding to skimming and transition flow regimes. Three-dimensional Computational Fluid Dynamics (CFD) simulations were carried out using the Volume of Fluid (VOF) method and a Reynolds-Averaged Navier–Stokes (RANS) turbulence model to resolve free surface flow, velocity and pressure distribution. The results obtained are showing good agreement in velocity profiles and energy dissipation rates. Parametric analysis revealed that stepped spillways excel in localized energy dissipation, particularly for steep slopes and moderate flows, while labyrinth spillways excel in maximizing discharge capacity while maintaining lower flow velocities, making them efficient for high-flow, low-footprint designs. Overall, the proposed geometrical constructive versions provide higher energy dissipation efficiency compared with conventional designs. These findings highlight the potential of optimized step geometries to improve hydraulic performance and ensure the safety of spillway structures under extreme hydrological conditions.

**Keywords:** Water flow, spillway constructive versions, stepped, labyrinth, numerical analysis

### 1. Introduction

Energy dissipation in spillway design is crucial for downstream safety and structural integrity. Stepped spillways characterized by their unique geometrical configuration are widely recognized for enhancing energy dissipation, fostering aeration, and mitigating cavitation risk, ultimately reducing stilling-basin dimensions and construction cost.

Research shows that stepped chutes dissipate more energy as smooth chutes under similar conditions, for instance, energy dissipation ranged between 43% and 46% in stepped chutes versus about 20% in smooth types. Further experimental data suggest that downward-inclined steps can significantly reduce dissipation (by around 21%), while upward-inclined steps improve it by up to 6%.

Regarding the impact of step geometry several studies underscore how step geometry profoundly influences hydraulic performance.

Pooled configurations often outperform flat ones in fostering aeration and enhancing energy dissipation, offering better pressure profiles and higher turbulent kinetic energy.

The novel geometries on trapezoidal and circular (or labyrinth-shaped) stepped spillway types show superior dissipation compared to traditional flat steps. For example, trapezoidal steps proved especially effective in the skimming flow regime.

Circular-stepped designs achieved up to 50% higher energy dissipation, particularly with smaller radii and increased step depth.

Meanwhile, circular labyrinth configurations (e.g. two- to four-cycle designs) enhanced dissipation by 28 %, with three-cycle patterns yielding the highest efficiency and further introducing curved risers an improved energy dissipation by around 3% at low flow rates is observed, with negligible effect under higher discharges.

While extensive numerical and experimental work validates the potential of stepped spillways, a meaningful gap remains, related to the combined effects of innovative geometric modifications on energy dissipation, cavitation risk and aeration under varied flow regimes, which are still under-

explored. Furthermore, the relative performance of novel configurations through rigorous numerical simulation, supported by field or lab validation, remains limited [1-5].

This study addresses these gaps by conducting numerical analysis via CFD method, employing VOF and a validated turbulence closure, to assess stepped spillways with hybrid geometries of labyrinth constructive version. The analysis will examine key performance metrics such as energy dissipation, pressure distribution, cavitation index across water flow regime. The goal is to determine whether the novel hybrid geometry substantially improves hydraulic performance compared to traditional configurations, offering actionable guidance for resilient spillway engineering [3-9].

## 2. The 3D virtual model and methodology

The study employs a computational approach to evaluate the total energy value described by the following equation:

$$E = \frac{v^2}{2} + \frac{p}{\rho} + gz \quad (1)$$

where  $v$  is the local water velocity magnitude,  $p$  is the static pressure,  $\rho$  is water density,  $g$  gravity and  $z$  is the point elevation. The equation is used to compute inlet/outlet energy heads and sectional average values.

The specific head ( $H$ ) value per unit weight can be calculated as:

$$H = \frac{\alpha v^2}{2g} + \frac{p}{\rho g} + z \quad (2)$$

With  $\alpha$  as the kinetic-energy correction coefficient which is obtained from the equation:

$$\alpha = \int A \frac{u^3}{v_m^3 A} dA \quad (3)$$

The head loss or energy dissipation per unit weight, for a control volume between section 1 represented by water inlet and section 2 considered as water outlet:

$$\Delta H = H_1 - H_2 \quad (4)$$

The total dissipated power or rate of energy loss in this case is described by the following relation:

$$P_d = \rho \cdot g \cdot Q \cdot \Delta H \quad (5)$$

where  $Q$  is volumetric flow rate as discharge ( $\text{m}^3/\text{s}$ ).

For this water flow regime it is of importance to consider the cavitation index, as a safety metric, in order to check flow cavitation risk at local minimum values of pressure:

$$\sigma = \frac{2(p - p_v)}{\rho v^2} \quad (6)$$

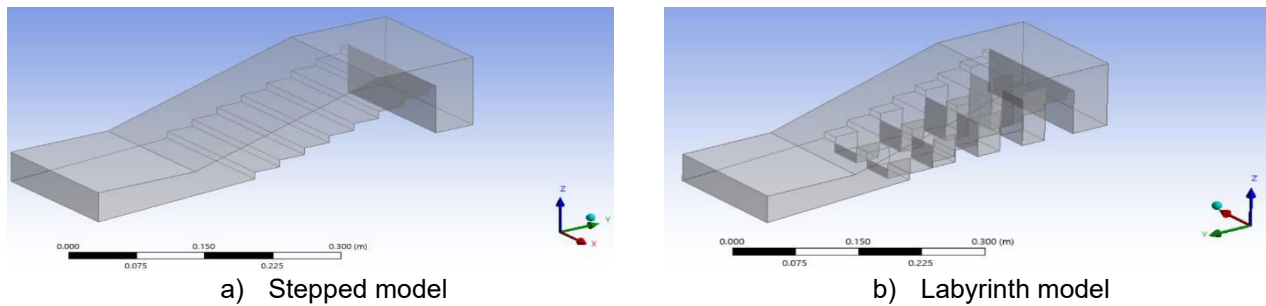
where  $p_v$  is the vapour pressure. Low  $\sigma$  indicates a higher cavitations risk.

Based on two constructive versions of spillway made to be introduced into the numerical flow analysis with ANSYS CFX, the construction possibilities and the solution of problems related to the controlled direction and capture of water flows are shown. The models are related to stepped and labyrinth versions (figure 1) in order to counteract the water flow potential energy and further proportional conversion into kinetic energy.

For a smooth spillway constructive version the potential energy of the upstream water head is mostly converted into kinetic energy at the outlet region with high-velocity jet. This often requires a stilling basin to dissipate energy safely.

A stepped spillway interrupts the water free fall, forcing part of the potential energy to be dissipated through re-circulation zones in step cavities, which are capable to form local turbulence. Shear stresses between steps and re-circulation zones provide impact in turbulence production and further the steps reduce the downstream kinetic energy peak.





**Fig. 1.** The 3D model of stepped water spillway constructive versions

Energy dissipation within the structure reduces the needs for a massive stilling basin downstream and ensuring a safer discharge conditions with less erosion.

Hydraulic safety conditions with smoother pressure gradients comparative to a smooth version.

A flat step version is simple to build, good for low to moderate discharges, while the labyrinth version is expected to provide improved fluid flow entrainment, smoother water flow transition regimes, reducing the negative pressures, mitigate cavitations and increase dissipation efficiency. Both constructive versions show a compact design, economical compared to large stilling basins.

### 3. Numerical analysis for water flow on construction models

The flow analysis is made with ANSYS CFX software, considering the two model versions, in order to establish the flow regimes for each constructive solution based on special parameters involved.

The flow simulation is aimed to reproduce the hydraulic behaviour of the stepped spillway under controlled conditions, with specific expectations related to flow hydraulics representation where it can be captured the velocity field along the constructive versions geometry, showing acceleration zones from the crest to the base, identify recirculation zones inside step cavities where vortices form and quantify the maximum velocities and flow attachment on step crests.

The main details for analysis are presented in table 1, while the mesh and special domain configuration on constructive models are showed in figure 2.

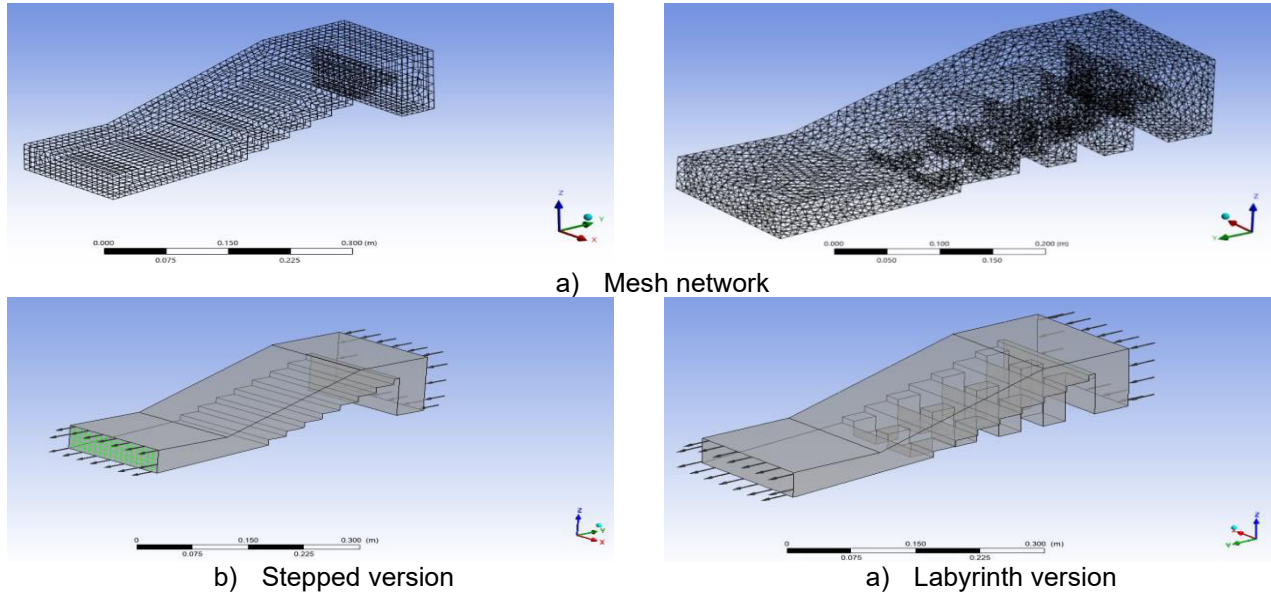
**Table 1:** The details of numerical flow analysis

Parameter	Value
Solver	ANSYS CFX 2025 R2
Flow regime	Incompressible, isothermal
Fluid	Water ( $\rho=1000 \text{ kg/m}^3$ , $\mu=0.001 \text{ Pa}\cdot\text{s}$ )
Inlet boundary	Velocity = 1.0 m/s
Outlet boundary	Pressure = 0 Pa (gauge)
Walls	No-slip
Top boundary	Opening (atmospheric)
Gravity	$9.81 \text{ m/s}^2$ ( $-Z$ )
Turbulence model	SST $k-\omega$
Free surface model	VOF
Time step	0.001–0.005 s
Convergence criteria	RMS residuals $< 1 \times 10^{-4}$
Mesh size	0.005–0.01 m avg.

For pressure distribution will be visual the total and static pressure fields to assess regions of high and negative pressure, evaluate the potential cavitation-prone zones in the step cavities and compare the pressure gradients between different geometries (stepped and labyrinth).

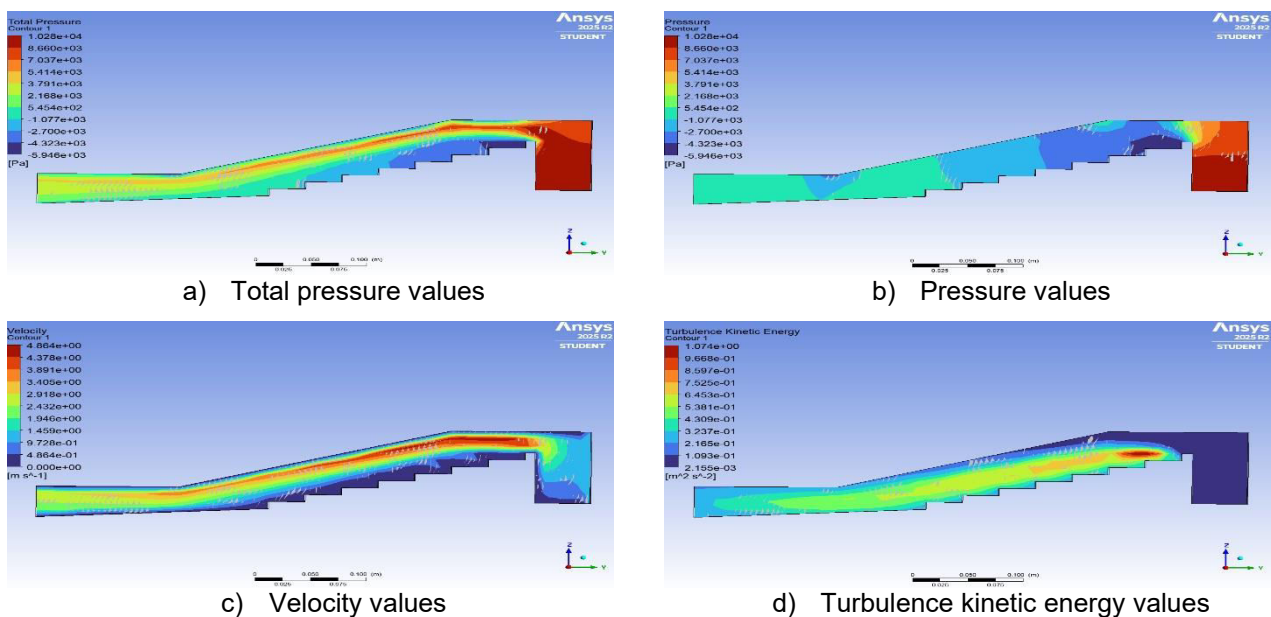
Regarding the energy dissipation efficiency it is possible to estimate the head loss between inlet and outlet using pressure–velocity data, determine the proportion of potential energy converted into turbulence and dissipated and compare dissipation efficiency across step geometries. The obtained results make possible a design evaluation of the models and verify whether the stepped geometry and labyrinth model effectively reduces downstream kinetic energy, which will provide insights into optimal geometry for maximizing energy dissipation while minimizing cavitation risk.

The expectation from the ANSYS CFX simulations is a clear understanding of how potential energy is partially dissipated via turbulence and step geometry interaction, thus validating the role of stepped spillways as efficient flow energy dissipators.



**Fig. 2.** Mesh network and domain flow analysis details

The obtained results for the two cases corresponding to the constructive versions analyzed are presented in figures 3 and 4.



**Fig. 3.** Results for stepped spillway model version

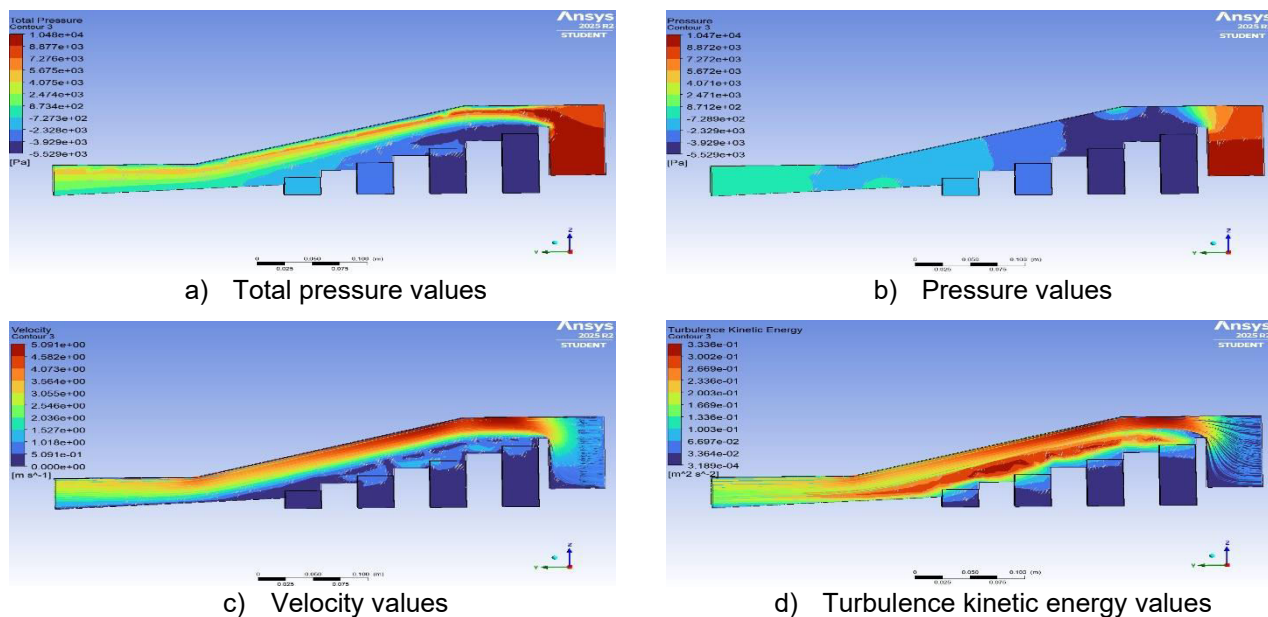


Fig. 4. Results for labyrinth stepped spillway model version

The obtained results show the velocity values contour in a range of 1–4.8 m/s, while this velocity rise corresponds to a pressure drop described by Bernoulli principle, while the spillway model converts potential energy into kinetic energy, which is then partly dissipated at steps.

For step cavities as recirculation zones, the velocity contour show values in range of 0–0.5 m/s, indicating near-stagnant recirculation vortices inside step cavities.

The fluid recirculation enhances turbulence and energy dissipation but increases cavitations risk. Energy dissipation efficiency for high velocities and alternating pressure fluctuations ensure step-induced turbulent kinetic energy production.

Compared to a smooth spillway, the stepped profile reduces downstream jet momentum, lowering scour potential.

The pressure distribution results show values ranged from about –6000 Pa to +10,280 Pa with high total pressure concentrated at the upstream inlet region, where water impinges and accelerates over the crest.

Lower pressures values appear in the circulation cavities behind the steps which is typical for water flow on stepped spillways.

The flow structure indicate that energy loss is enhanced along the model geometry as water passes step by step to the outlet region, where pressure decreases as the flow accelerates downstream.

The alternating zones along the free surface and negative values in the step cavities indicate zones of flow separation and reattachment.

Energy dissipation is provided when negative or low pressure values behind steps are registered where turbulent eddies form, as main mechanism of energy loss within stepped spillways.

Regarding the hydraulic safety aspect the most negative pressures (–6000 Pa) are relatively close to vapor pressure (depending on water temperature), while these zones meet the cavitations conditions.

#### 4. Conclusions

The numerical simulations carried out in ANSYS CFX demonstrated that both stepped and labyrinth spillway geometries are effective in dissipating flow energy within the chute. The stepped model dissipates energy primarily through localized recirculation in step cavities, producing predictable pressure fluctuations and strong but confined shear layers. In contrast, the labyrinth geometry generated larger recirculation zones and stronger turbulence, which enhanced overall energy dissipation but also broadened the regions of negative pressure, increasing cavitations risk.

Velocity fields confirmed that the labyrinth configuration reduced the mean downstream jet momentum more effectively, while the stepped model maintained higher outlet velocities but with greater aeration at each cavity. Pressure contours indicated that both step variants can reduce localized suction, making the stepped chute a safer choice in terms of cavitations.

In summary, the labyrinth design achieved higher energy dissipation efficiency, but the stepped spillway provided more stable hydraulic performance and lower structural risk.

The choice between the two constructive versions should be guided by site conditions and design priorities, balancing maximum dissipation with cavitations safety.

### Acknowledgments

The research within this paper was conducted within Fluid Mechanics Laboratory, Engineering Sciences and Management Department, Engineering and Agronomy Faculty of Braila, "Dunarea de Jos" University of Galati and with the support of Machine Mechanics and Technological Equipments - MECMET Research Center, "Dunarea de Jos" University of Galati, Engineering and Agronomy Faculty of Braila and received no external funding.

### References

- [1] Jahad, Udai A., Ali Chabuk, Riyadh Al-Ameri, Hasan Sh. Majdi, Ali Majdi, Nadhir Al-Ansari, and Salwan Ali Abed. "Flow characteristics and energy dissipation over stepped spillway with various step geometries: case study (steps with curve end sill)." *Applied Water Science* 14 (2024): 60.
- [2] Farooq, U., S. Li, and J. Yang. "Numerical Analysis of Flow Characteristics and Energy Dissipation on Flat and Pooled Stepped Spillways." *Water* 16, no. 18 (2024): 2600.
- [3] İkinçioğulları, E. "Energy dissipation performance of the trapezoidal stepped spillway." *Journal of Engineering Research* 11, no. 2A (2021): 131-142.
- [4] İkinçioğulları, E. "Stepped spillway design for energy dissipation." *Water Supply* 23, no. 2 (2023): 749–763.
- [5] Gubashi, K. R., S. Mulahasan, Z. A. Hacheem, and A. Q. Rdhaiwi. "Effect of the stepped spillway geometry on the flow energy dissipation." *Civil Engineering Journal* 10, no. 1 (2024): 145–158.
- [6] Saleh, Shawnm Mudhafar, Sarkawt Hamarrahim Muhammad, and Abdulla Abdulwahid Abo. "Effect of pooled and flat stepped spillway on energy dissipation using computational fluid dynamics." *Tikrit Journal of Engineering Sciences* 29, no. 2 (2022): 75-79.
- [7] Bekheet, A. A., N. M. Aboul Atta, N. Y. Saad, and D. A. El-Molla. "Energy dissipation in stepped spillways: a comprehensive review of the recent research." *Innovative Infrastructure Solutions* 10 (2025): 253.
- [8] Matos, Jorge, Carolina Kuhn Novakoski, Rute Ferla, Marcelo Giulian Marques, Mauricio Dai Prá, Alba Valéria Brandão Canellas, and Eder Daniel Teixeira. "Extreme Pressures and Risk of Cavitation in Steeply Sloping Stepped Spillways of Large Dams." *Water* 14, no. 3 (2022): 306.
- [9] Saleh, S. M., and S. M. Husain. "Numerical Study to Evaluate the Performance of Non-uniform Stepped Spillway Using ANSYS-CFX." *Polytechnic Journal* 10, no. 2 (2020): 1-9.

## Pneumatically Driven Generator for Use with Small-Scale Compressed Air Energy Storage System

PhD Eng. Radu-Iulian RĂDOI<sup>1,\*</sup>, MSc. Eng. Bogdan-Alexandru TUDOR-ROTILĂ<sup>1</sup>,  
PhD Student Eng. Robert BLEJAN<sup>1</sup>, MSc. Eng. Ștefan-Mihai ȘEFU<sup>1</sup>

<sup>1</sup> National Institute of Research & Development for Optoelectronics/INOE 2000, Subsidiary Hydraulics and Pneumatics Research Institute/IHP, Romania

\* radoi.ihp@fluidas.ro

**Abstract:** To cover the peak load in the energy systems, energy storage facilities are needed during periods when energy production is in excess. During sunny days, photovoltaic energy production can reach a level that exceeds the demand in the power grid. During these periods, battery storage systems, pumped storage hydroelectric plants or compressed air energy storage (CAES) can be used. CAES systems use compressors to store compressed air and air turbines coupled with generators to produce electricity. They can be large-scale with storage in caverns or former mines and small-scale (SS-CAES) with storage in air tanks. An SS-CAES uses a piston or screw compressor, and as an expander it can use an air turbine or a pneumatic motor coupled to an electric generator. The article presents the realization of a control system for an SS-CAES and of an electricity generation unit with a pneumatic motor and permanent magnet generator usable for SS-CAES in rural or isolated areas.

**Keywords:** Pneumatic drive, energy storage, control, SS-CAES

### 1. Introduction

To support the transition toward a sustainable energy sector, energy storage systems are becoming indispensable, as they enable the efficient use of renewable sources with variable output, such as solar and wind energy.

The basic principle consists of compressing air into pressurized tanks when there is an energy surplus (usually from renewable sources such as solar or wind), and later, this compressed air is released and used to generate electricity during periods of high demand.

Unlike traditional CAES systems, which require large-scale infrastructures (geological cavities or underground reservoirs), SS-CAES is designed for smaller-scale applications, using commercial pressure tanks and modular components. Thus, these systems are suitable for:

- microgrids and isolated communities,
- integration of intermittent renewable sources.

The main advantages of SS-CAES include modularity, high reliability, durability, and lower environmental impact compared to electrochemical storage solutions. S-CAES also faces challenges related to energy efficiency (thermal losses during compression and expansion) and lower energy density compared to batteries.

Research and development in the field of SS-CAES aim to optimize components and processes to improve system performance and support its applicability in microgrids, isolated communities, and hybrid power generation systems.

Ghadi et al. [1] propose the use of SCAES units as aggregators in distribution networks for participation in day-ahead energy markets. A dual-agent model (aggregator + distribution operator) optimizes costs, losses, emissions, etc.

Congedo et al. [2] conduct a feasibility study on micro-CAES systems combined with thermal storage for a single-family home with 3 kW PV. They perform multi-objective optimization, performance analysis, and comparison with batteries. Result: low efficiency for CAES in this context, but exploitable advantages (lifetime, thermal recovery).

Rabi et al. [3] provide an updated overview of CAES variants (diabatic, adiabatic, isothermal), advantages and disadvantages at different scales; they discuss technical challenges, costs, applications integrated with renewable energy systems, and the inclusion of smaller/distributed storage concepts.



Luo et al. [4] give an overview of energy storage technologies and highlight that SS-CAES is particularly suitable for integration into microgrids and for balancing renewable generation. Budt et al. [5] detail the operating principles of CAES, classify systems into adiabatic, diabatic, and isothermal, and highlight the potential for reducing energy losses in small-scale applications. Raju & Khaitan [6] present a simulation model of compressed air storage in caverns, which can be scaled and applied for SS-CAES sizing at local or community levels. Gupta & Saini [7] review the performance and challenges of SS-CAES, concluding that innovations in materials and thermal management are key to improving small-scale efficiency. Mohammadi & Mehrpooya [8] analyze hybrid systems (e.g., CAES + solar/biomass plants), revealing that SS-CAES is attractive for decentralized and residential applications. IRENA [9] reports costs and market projections, showing that SS-CAES has the potential for cost reduction by 2030, especially if standardized above-ground tanks are used. Alami [10] presents a case study on integrating SS-CAES with photovoltaic panels, demonstrating that a hybrid system can ensure supply continuity in the absence of sunlight, at affordable costs. Zakeri & Syri [11] compare life-cycle costs of different storage technologies and show that SS-CAES becomes competitive in long-term applications, where the number of cycles is high.

## 2. Thermodynamic equations for air storage and utilization

### Ideal Gas Law

The fundamental relation is:

$$p \cdot V = n \cdot R \cdot T \quad (1)$$

where:

- $p$  = pressure (Pa),
- $V$  = volume (m<sup>3</sup>),
- $n$  = number of moles of gas (mole),
- $R$  = universal gas constant (8.314 J/(mole · K)),
- $T$  = absolute temperature (K).

This relationship is used to relate the pressure, volume and temperature of air in pneumatic tanks.

### Compression and expansion processes

Depending on the heat transfer, the isothermal model and the adiabatic model are distinguished:

#### • Isothermal compression/expansion (T = const.)

$$p \cdot V = \text{const.} \quad (2)$$

Energy stored in compressed air in an isothermal process:

$$E_{\text{isot}} = n \cdot R \cdot T \cdot \ln\left(\frac{p_2}{p_1}\right) \quad (3)$$

where  $p_1$  și  $p_2$  are the initial and final pressures.

This model has a high theoretical efficiency and requires intense heat exchange with the environment.

#### • Adiabatic compression/expansion (no heat exchange with the outside)

$$p \cdot V^\gamma = \text{const.} \quad (4)$$

where  $\gamma = \frac{c_p}{c_v}$  is the ratio of specific heats ( $\approx 1.4$  for air)

Energy stored in an adiabatic process

$$E_{\text{adiab}} = \frac{p_2 \cdot V_2 - p_1 \cdot V_1}{\gamma - 1} \quad (5)$$

This model describes the real situation of rapid compression, where the temperature increases significantly, requiring cooling systems to avoid energy losses.

### Efficiency and losses

The overall efficiency of the conventional CAES cycle varies between 40...60%, but by implementing the advanced adiabatic system (AA-CAES), where the heat of compression is stored and reused, values of 70% or even more can be achieved.

The efficiency of a compression and expansion system is influenced by:

- Heat losses through tank walls
- Internal friction in compressors and actuators
- Leakage losses through valves and connections

### Calculating the energy stored in a tank

For a tank of constant volume  $V$ , charged from pressure  $p_1$  to pressure  $p_2$ , the additional energy stored is approximated by:

$$E = \frac{(p_2 - p_1) \cdot V}{\gamma - 1} \quad (6)$$

This simplified formula is frequently used for sizing pneumatic accumulators and quickly assessing storage capacity.

## 3. Test stand for a small scale compressed air energy storage system

The system was developed for laboratory experiments and can use the maximum compressed air pressure of 10 bar, the tank being a standard one for compressors of maximum 10 bar. The system characteristics are found in table 1. For increased storage capacities, tanks and compressors of 35÷40 bar or higher can be used. High pressures involve the management of the heat generated when compressing the air and the low temperature from the expansion of the air through the turbine or pneumatic motor.

**Table 1:** Technical characteristics of the system

Compressor	Pneumatic motor	Generator	Air tank	Control system
<ul style="list-style-type: none"> <li>• Power: 2200 W</li> <li>• Flow: 392 l/min</li> <li>• Max. pressure: 8 bar</li> </ul>	<ul style="list-style-type: none"> <li>• Max. power: 1.25 kW</li> <li>• Speed: 300÷3000 rev/min</li> <li>• Air consumption: 3÷30 l/s</li> <li>• Torque: max. 10 Nm</li> </ul>	<ul style="list-style-type: none"> <li>• Type: permanent magnets</li> <li>• Power: 1000 W</li> <li>• Speed: 750 rev/min</li> <li>• Voltage: 24 V</li> </ul>	<ul style="list-style-type: none"> <li>• Volume: 350 l</li> <li>• Max. pressure: 11 bar</li> <li>• Pressure transducer: 25 bar</li> </ul>	<ul style="list-style-type: none"> <li>• PLC based</li> <li>• Electric energy meter</li> <li>• PC application for control and data acquisition</li> </ul>

### 3.1 Pneumatic diagram of the system

The pneumatic diagram of the system in figure 1 contains the compressor for charging the air storage tank with its pressure switch and safety valve. A pressure regulator is connected from the compressor tank followed by a directional valve for directing the air to the storage tank. In order to avoid air losses, a check valve was installed after the directional valve DV1. The air then reaches the storage tank through an isolation valve. A directional valve DV2 is connected to the tank pipe followed by a group with a filter, pressure regulator and lubricator, because the pneumatic motor has a working pressure of 6.5 bar and requires lubrication. The proportional flow regulator was installed to correct the speed of the pneumatic motor depending on load fluctuations, through the control unit made with a programmable logic controller (PLC). The diagram also includes temperature and pressure sensors, and a torque and rotary speed transducer is installed between the pneumatic motor and the generator (energy conversion device). To monitor electrical energy consumption, an EM energy meter is used that measures the power delivered to load resistors.

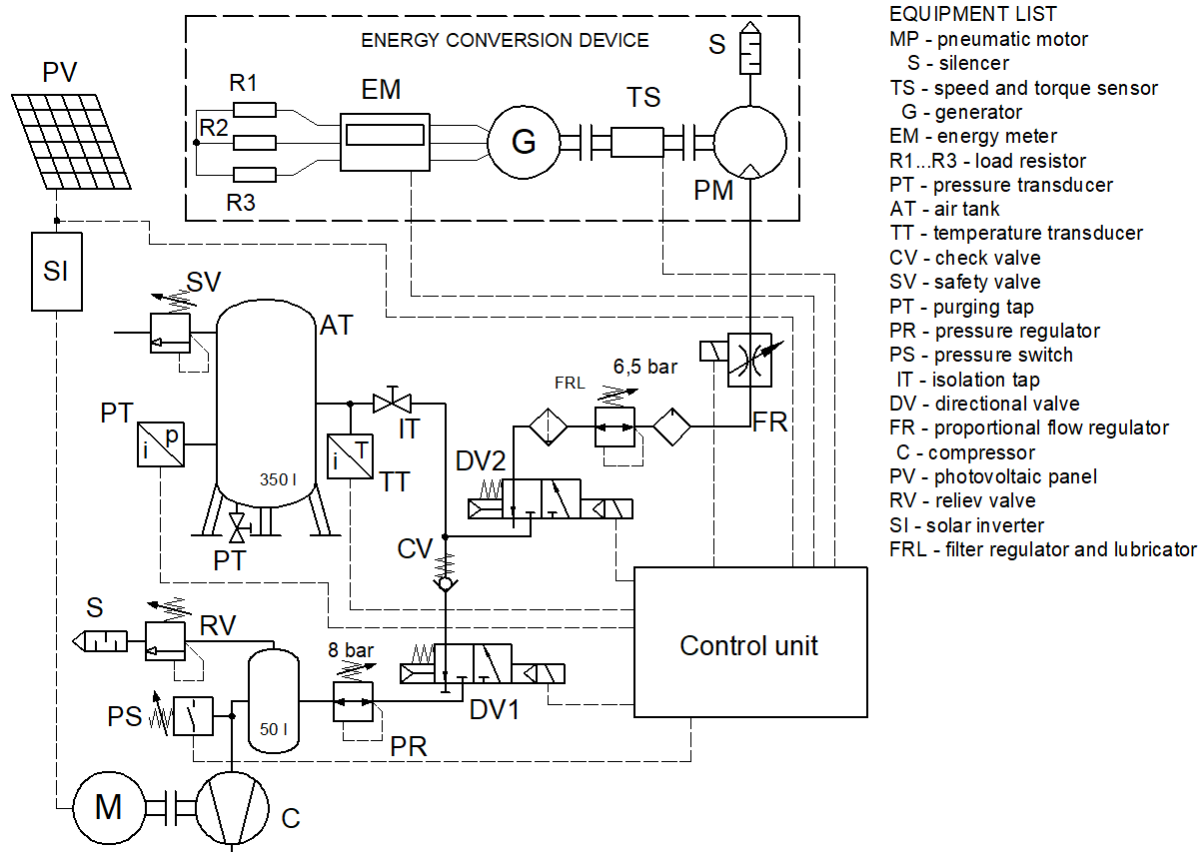


Fig. 1. Scheme of an SS-CAES system for research purposes

### 3.2 The control and data acquisition system

The control and data acquisition system is installed in an electrical cabinet (figure 2) containing: automatic circuit breaker, 24 Vdc power supply, PLC type TM221CE24T from Schneider Electric, module with 4 analog inputs (0...10V, 4...20mA) for transducers, 4 intermediate relays for commands and a three-phase energy meter, type A9MEM3155, for monitoring electrical energy. The controller has implemented a software for data acquisition regarding system parameters and for managing compressed air storage and consumption. The following elements are connected to the controller inputs: pressure transducer, temperature transducer, torque and rotation speed transducer and the signal regarding the voltage of the solar panels. The pressure switch is connected to a digital input, and the solenoids of the pneumatic directional valves and the contactor for powering the compressor electric motor are connected to the digital outputs.

The system control algorithm takes into account the pressure in the storage tank and the voltage present at the photovoltaic panels. If the voltage is within parameters, i.e. there is sufficient solar radiation, the compressor is started to charge the storage tank. If the solar radiation drops below a certain level or if the maximum pressure has been reached, the compressor stops. When the compressor starts, DV1 is also switched to direct the air to the tank.

To use the stored compressed air, DV2 is switched on and the pneumatic motor is started, which drives the generator. The generator speed can be corrected to maintain the delivered voltage by adjusting the control signal of the flow regulator within a range of values. If the pressure in the storage tank drops below the nominal working pressure of the pneumatic motor of 6.5 bar and the generator load is too high, the generator is disconnected and the system enters the compressed air recharge mode.

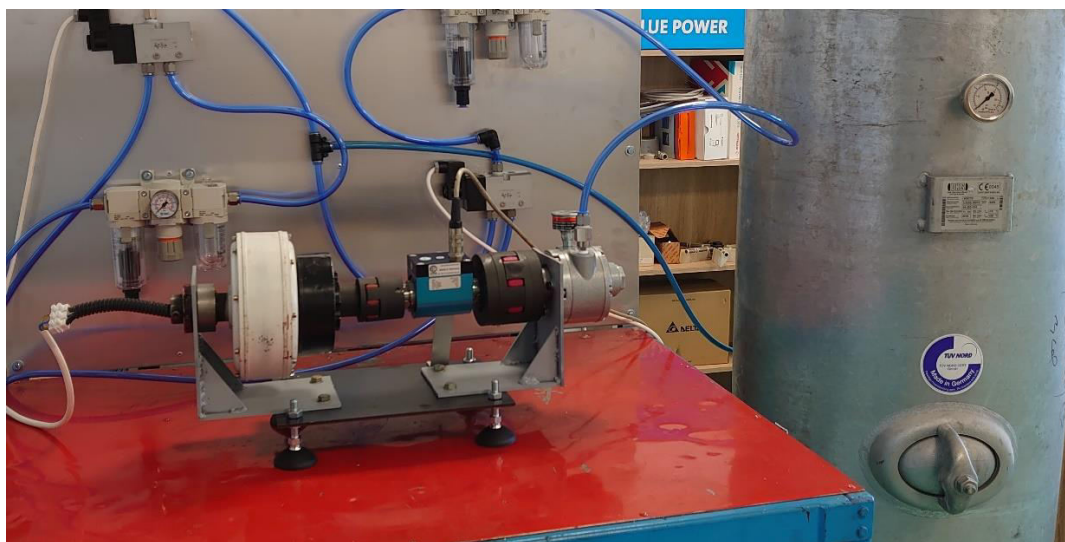


**Fig. 2.** Assembled control and data acquisition system

The system can communicate via Modbus TCP/IP protocol with a PC application that allows viewing of operating parameters.

### 3.3 Energy conversion device

The device can convert compressed air energy into electrical current and contains a permanent magnet generator, a torque and speed transducer, a pneumatic vane motor type AM4-NRV-22B from Gast and 2 rotary couplings. The physical implementation of the energy conversion device can be seen in the figure 3.



**Fig. 3.** Physical realization of the compressed air electricity generation device

## 4. Conclusions

The generator driven by a pneumatic motor allows the implementation of SS-CAES for isolated areas.

The stand designed to test the generator driven by a pneumatic motor allows testing of different control strategies for SS-CAES for use by beneficiaries in isolated areas.

Standard air tanks and modular components can be used to create SS-CAES.

SS-CAES allow integration with intermittent renewable energy sources and have a longer lifespan compared to battery storage for long-term applications.

### Acknowledgments

This work was carried out through the Core Program within the National Research Development and Innovation Plan 2022-2027, carried out with the support of MCID, project no. PN 23 05.

### References

- [1] Ghadi, Mojtaba Jabbari, Ali Azizivahed, Dillip Kumar Mishra, Li Li, Jiangfeng Zhang, Miadreza Shafiekhah, and João P.S. Catalão. "Application of small-scale CAESs (SCAESSs) in the daily operation of an active distribution system." *Energy* 231 (2021): 120961.
- [2] Congedo, Paolo Maria, Cristina Baglivo, Simone Panico, Domenico Mazzeo, and Nicoletta Matera. "Optimization of Micro-CAES and TES Systems for Trigeneration." *Energies* 15, no. 17 (2022): 6232.
- [3] Rabi, Ayah Marwan, Jovana Radulovic, and James M. Buick. "Comprehensive Review of Compressed Air Energy Storage (CAES) Technologies." *Thermo* 3, no. 1 (2023): 104-126.
- [4] Luo, X., J. Wang, M. Dooner, and J. Clarke. "Overview of current development in electrical energy storage technologies and the application potential in power system operation." *Applied Energy* 137 (2015): 511–536.
- [5] Budt, M., D. Wolf, R. Span, and J. Yan. "A review on compressed air energy storage: Basic principles, past milestones and recent developments." *Applied Energy* 170 (2016): 250–268.
- [6] Raju, M., and S. K. Khaitan. "Modeling and simulation of compressed air storage in caverns: A case study of the Huntorf plant." *Applied Energy* 89, no. 1 (2012): 474–481.
- [7] Laijun, Chen, Tianwen Zheng, Shengwei Mei, Xiaodai Xue, Binhui Liu, and Qiang Lu. "Review and prospect of compressed air energy storage system." *Journal of Modern Power Systems and Clean Energy* 4 (2016): 529–541.
- [8] Guo, Huan, Haoyuan Kang, Yujie Xu, Mingzhi Zhao, Yilin Zhu, Hualiang Zhang, and Haisheng Chen. "Review of Coupling Methods of Compressed Air Energy Storage Systems and Renewable Energy Resources." *Energies* 16, no. 12 (2023): 4667.
- [9] International Renewable Energy Agency (IRENA). *Electricity storage and renewables: Costs and markets to 2030*. Abu Dhabi, 2017.
- [10] Castellani, Beatrice, Elena Morini, Benedetto Nastasi, Andrea Nicolini, and Federico Rossi. "Small-Scale Compressed Air Energy Storage Application for Renewable Energy Integration in a Listed Building." *Energies* 11, no. 7 (2018): 1921.
- [11] Zakeri, B., and S. Syri. "Electrical energy storage systems: A comparative life cycle cost analysis." *Renewable and Sustainable Energy Reviews* 42 (2015): 569–596.



## Pedagogical Implications of Computer-Assisted Instruction in Reconfiguring Contents for General and Applied Ecology

PhD Eng. IT exp. **Bogdan V. CIORUȚA**<sup>1-3,\*</sup>, MA stud. **Ioana-Elisabeta CIORUȚA**<sup>2,4</sup>,  
Assoc. Prof. PhD Eng. habil. **Mirela-Ana COMAN**<sup>5,6</sup>, Eng. IT exp. **Alexandru L. POP**<sup>1,2</sup>

<sup>1</sup> Technical University of Cluj-Napoca - North University Centre of Baia Mare, Office of Informatics, 62A Victor Babeș Str., 430083, Baia Mare, Romania

<sup>2</sup> Technical University of Cluj-Napoca - North University Centre of Baia Mare, Faculty of Letters, Department of Specialty with Psychopedagogical Profile, 76 Victoriei Str., 430083, Baia Mare, Romania

<sup>3</sup> Technical University of Cluj-Napoca - North University Centre of Baia Mare, Faculty of Science, 76 Victoriei Str., 430072, Baia Mare, România

<sup>4</sup> "Little Prince" Extended Program Kindergarten, 8B Cuza Vodă Str., 430034, Baia Mare, Romania

<sup>5</sup> Technical University of Cluj-Napoca - North University Centre of Baia Mare, Faculty of Engineering - Department of Mineral Resources, Materials and Environmental Engineering, 62A Victor Babeș Str., 430083, Baia Mare, Romania

<sup>6</sup> University of Agricultural Sciences and Veterinary Medicine from Cluj-Napoca, 3-5 Calea Mănăştur, 4000372, Cluj-Napoca, Romania

\* bogdan.cioruta@staff.utcluj.ro

**Abstract:** *The present research explores the pedagogical implications of Computer-Assisted Instruction (CAI) in reconfiguring educational content for General and Applied Ecology (EGA). The article demonstrates that CAI fundamentally transforms the learning process, moving it from a theoretical, passive approach to a practical and interactive one, essential for future specialists in the field. Through dynamic simulations and massive data analysis, students become active participants, able to explore complex ecological phenomena, such as population dynamics, climate change, and biogeochemical cycles, in a controlled virtual environment. The working methodology, focused on in-depth consultation of the specialized literature as the main method, emphasizes the importance of the theoretical foundation of any practical endeavor. The results reveal that CAI not only consolidates knowledge but also develops a series of essential skills for the modern ecology specialist, including critical thinking, data management, problem solving, and teamwork. Another central component is the ability to integrate information from various fields - biology, geography, and sociology - promoting a holistic and interdisciplinary vision of environmental issues. In conclusion, the CAI is not just an auxiliary tool, but a catalyst for a new educational paradigm that forms adaptable professionals with critical thinking and solid technical expertise, prepared to face the complex and dynamic challenges of the contemporary world.*

**Keywords:** *Applied ecology, computer-aided instruction, environmental protection, digitalization.*

### 1. Introduction

The present research examines the pedagogical implications of Computer-Assisted Instruction (CAI) and its significant role in reconfiguring and modernizing educational content for the study of General and Applied Ecology (GAE). This methodological approach - striving for the predictive understanding of complex systems [1] - revolutionizes teaching and learning, overcoming the limits of traditional methods. By integrating CAI, ecology is transformed from a predominantly theoretical discipline into an extremely practical and interactive one, that can support biodiversity conservation and food production [2]. Under the above conditions, students are no longer mere recipients of information but become active participants in the instructional and educational process [3-5]. They can simulate complex phenomena, from population dynamics to the global carbon cycle, analyze massive data sets, and visualize the long-term consequences of environmental decisions. This ability to “experiment” in a virtual environment strengthens the understanding of abstract concepts (such as climate change) [6], and connects theory to ecological reality, providing a relevant context for future specialists to better understand the ecological behavior [7].

The transition from a passive to an active teaching model is perhaps the most significant contribution of CAI and GenAI to ecology [8,9]. Traditional courses, focused on memorizing definitions and classifications, fail to capture the complexity and interdependence of ecological systems. Through CAI, fundamental concepts, such as interspecific competition or ecological succession, come to life in dynamic simulations. A student no longer just reads about the logistic growth model, but can directly manipulate variables (e.g. *environmental carrying capacity*, *reproductive rate*) to observe how they directly influence the evolution of a population. This direct interaction stimulates critical thinking and causal reasoning, essential for making informed predictions and developing viable solutions to environmental problems.

Equally, CAI facilitates an interdisciplinary approach to ecology. Computational models allow the integration of data from various fields - biology, chemistry, geography, and sociology - to provide a holistic view of ecological systems. For example, a species distribution model can include not only climatic and biological variables, but also sociological data on land use by local communities [10], thus highlighting the link between ecology and social factors. Thus, educational contents are reconfigured to prepare specialists capable of approaching environmental problems not only from an ecological perspective, but also from an economic, social, and ethical point of view.

In essence, CAI is not just an auxiliary tool but a catalyst for a new educational paradigm, which forms adaptable professionals with critical thinking, prepared to face the complex and dynamic challenges of the contemporary world. In addition to the cognitive benefits, CAI plays a crucial role in developing technical skills directly applicable in the job market. Data management and technology become core skills, not optional. Students learn to use specialized GIS mapping software to create conservation maps, apply statistical algorithms to analyze large pollution monitoring data sets, and develop simulation models to predict the effectiveness of a forest management plan [11]. These skills transform future ecologists from passive observers into ecosystem engineers, capable of generating data-driven solutions and collaborating effectively in multidisciplinary teams. The CAI thus reflects professional reality, preparing students for a field where technology is a central element of research and practice.

## 2. Working methodology - consultation and interpretation of specialized literature

The working methodology is based on an analytical and synthetic approach, with an emphasis on the systematic consultation of the specialized literature. This fundamental stage provides the theoretical foundation necessary to evaluate the effectiveness of CAI in the pedagogical context of ecology. The research began with a thorough review of scientific articles (theoretical foundation), reports, and case studies published in databases such as Web of Science®, Scopus®, ResearchGate®, and Google Scholar®.

The search targeted keywords such as *Instructional Computing in Ecology*, *Ecological Modeling Education*, *GIS in Environmental Education*, and *Pedagogical Innovations in Applied Ecology*, which allowed the identification of the existing conceptual framework and research gaps.

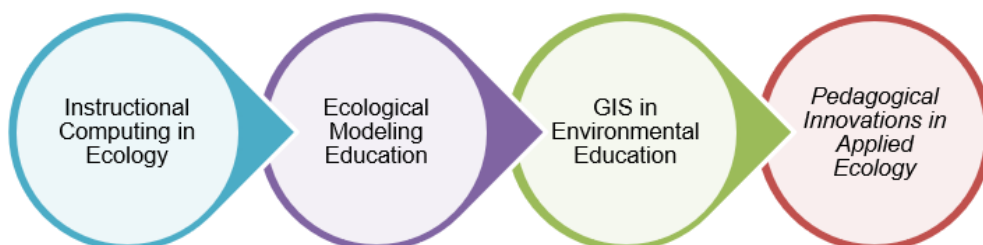


Fig. 1. Examples of keywords used in consulting and analyzing specialized literature

The information collected was synthesized to highlight how CAI reconfigures curricular content. A comparative analysis was conducted between traditional and CAI-based pedagogical methods, focusing on five key competencies identified as essential for the modern ecology specialist: critical thinking, modeling and simulation, data management, problem solving, and collaboration. In addition, a correlation matrix was created between the competencies facilitated by CAI and the specific modules of general and applied ecology.








### 3. Results and Discussions regarding the Pedagogical Implications of CAI in Ecology

Computer-assisted instruction (CAI) is proving to be an essential pedagogical tool for training ecologists, providing concrete results and contributing to the development of a wide range of skills. In addition to understanding theoretical concepts, students acquire practical modeling and simulation skills, allowing them to virtually experiment with complex ecological systems and visualize the consequences of human actions.

- **Ecosystem dynamics and structure** show us how life develops and interacts within an ecosystem, from the individual level to that of the entire community, by referring to:
  - **interspecific relationships** - basic interactions (predation, competition) define how species coexist;
  - **population dynamics** - these interactions directly influence the numerical growth or decline of populations;
  - **ecological succession** - populations and their interactions determine how an ecological community evolves and matures over time;
  - **ecological evolution** - in the long term, these interactions and environmental changes lead to the adaptation and evolution of species;
  - **biodiversity** - the result of these processes of evolution, interaction, and succession is reflected in the richness of species and the genetic variety associated with them;
  - **aquatic ecosystems**, respectively **coastal ecosystems** - are only a small part of specific examples of environments in which all the processes mentioned above take place, one after the other.
- **Ecological flows and cycles** describe the movement of energy and matter, fundamental to the functioning of any ecosystem, by directly relating to:
  - **primary production** - the beginning of any energy flow, where plants (producers) convert solar energy into biomass;
  - **energy flow** - the energy stored in biomass is transferred along food chains;
  - **biogeochemical cycles** - in parallel with the energy flow, matter (elements such as carbon, nitrogen) continuously circulates between organisms and the environment;
  - **hydrological cycles** - the water cycle is essential and interconnected with the other cycles, transporting nutrients;
  - **biomagnification** - occurs as a result of the energy flow and matter cycles, where pollutants accumulate along the food chain.
- **Anthropogenic impact and pollution** describe how human intervention affects natural processes, from cause to effect, by relating to:
  - **atmospheric pollution** - industrial emissions are the primary source of pollutants;
  - **greenhouse effect** - occurs as a direct consequence of atmospheric pollution, through the accumulation of greenhouse gases;
  - **climate change** - the increase in the greenhouse effect leads to long-term changes in the global climate;
  - **pesticide effects** and **the impact of mining** - are only a small part of the concrete examples of activities that lead to specific pollution and degradation;
  - **antibiotic resistance** - is reflected as a consequence of the use of chemical substances in the environment, affecting biological processes;
  - **waste management** - comes as a response to the problem of pollution, representing efforts to minimize the impact.
- **Landscape ecology and resource management** refer to planning and interactions on a larger scale, often related to land use, by referring to:
  - **landscape ecology** - the analysis of the structure and composition of the landscape is invariably the starting point;
  - **habitat fragmentation** - a consequence of human development that alters the structure of the landscape;

- **forest resource management** and **the impact of tourism** - also just a small part of the examples of specific management activities that influence the landscape;
- **ecosystem services** - the functioning of the landscape provides benefits (services) to society, and their management is crucial.
- **Urban ecology and stress response** focuses on the interaction between the urban and natural environment, but also on the capacity of organisms to adapt, by referring to:
  - the relationship between **urbanization and ecosystems** - the initial process that inevitably alters the natural environment;
  - **urban ecology** - a branch of ecology that studies ecosystems in cities, as a reaction to urbanization;
  - **urban sprawl** - a specific problem of the urban environment that naturally and inevitably arises from urbanization;
  - **stress response of organisms** - a fundamental biological response to altered environmental conditions (e.g., *pollution, drought, desertification*);
  - **host-parasite relationship** and **the impact of invasive species** - are only some of the ecological relationships that can be intensified or modified in the context of urban stress;
  - **ecological monitoring** - a method to measure and evaluate all these processes, being a final step in understanding and managing them.

**Table 1:** Pedagogical implications of CAI in relation to the dynamics and structure of ecosystems

Indicatorul considerat	Implications in General Ecology	Implications in Applied Ecology	Pedagogical purpose
<b>Interspecific relationships</b> (  )	Models competition, predation, and symbiosis relationships	Control agricultural pests by simulating their interactions	<b>Understanding complex interactions</b> It helps students visualize and understand the hidden dynamics behind ecological relationships.
<b>Population dynamics</b> (  )	Simulates complex growth and interaction models	Plan for the management of threatened species	<b>Developing predictive thinking</b> It builds the ability to forecast changes in populations and plan interventions.
<b>Ecological succession</b> (  )	Simulates the development stages of ecosystems	Restore degraded habitats by designing regeneration scenarios	<b>Strengthening the concept of ecosystem evolution</b> It allows accelerated observation of slow regeneration processes.
<b>Ecological evolution</b> (  )	Models evolutionary processes at the population and species level	Predicts the evolution of pathogens and harmful species	<b>Illustrating evolutionary mechanisms</b> It provides a platform to see natural selection and adaptation in action.
<b>Biodiversity</b> (  )	Analyze species distribution and richness	Identify priority conservation areas	<b>Understanding the importance of biodiversity</b> It helps visually identify the links between biodiversity and ecosystem stability.
<b>Aquatic ecosystems</b> (  )	Simulates water quality and marine life	Monitors and prevents water pollution	<b>Study of specific ecosystems</b> It allows detailed exploration of difficult-to-access environments (the ocean floor).
<b>Coastal ecosystems</b> (  )	Simulate their role in coastal protection	Design restoration projects	<b>Applying knowledge in concrete case studies</b> Connect theory to real-world conservation issues.

**Table 2:** Pedagogical implications of CAI in relation to ecological flows and cycles

The indicator considered	Implications in General Ecology	Implications in Applied Ecology	Pedagogical purpose
<b>Primary production</b> (🌱)	Simulates ecosystem productivity	Optimizes fertilization and irrigation in agriculture	<b>Understanding the energetic basis of life</b> Visually explain how energy enters ecological systems.
<b>Energy flow</b> (⚡)	Visualize food chains and webs	Optimize agricultural production by modeling energy efficiency	<b>Strengthening the concept of energy transfer</b> It shows how energy is lost at each trophic level, explaining the structure of the ecosystem.
<b>Biogeochemical cycles</b> (🔄)	Models the circulation of elements (C, N, P)	Assess the impact of pollution on nutrient cycles	<b>Integrating the notions of chemistry and ecology</b> It helps to visualize the circuit of matter on a global and local scale.
<b>Hydrological cycles</b> (💧)	Models water distribution and quality	Manages drinking water resources	<b>Awareness of the importance of water</b> It trains students in managing a critical resource for survival.
<b>Biomagnification</b> (🔍)	Models the accumulation of pollutants in the food chain	Develops hazardous waste management plans	<b>Demonstration of toxic effects over time</b> It illustrates how pollutants accumulate in food chains with a serious impact.

**Table 3:** Pedagogical implications of CAI in relation to anthropogenic impact and pollution

The indicator considered	Implications in General Ecology	Implications in Applied Ecology	Pedagogical purpose
<b>Air pollution</b> (🏭)	Model the dispersion of pollutants	Plan the location to minimize impact	<b>Visualizing the invisible impact</b> It helps to understand how pollutants disperse in the environment.
<b>The greenhouse effect</b> (💡)	Simulates the impact of greenhouse gases on the climate	Develops strategies to reduce emissions	<b>Climate change awareness</b> It demonstrates the direct link between human actions and global warming.
<b>Climate change</b> (☁)	Model climate evolution scenarios	Adapt agricultural strategies to new conditions	<b>Forming adaptive solutions</b> Prepares students to develop strategies for adapting to change.
<b>Effects of pesticides</b> (💀)	Simulates the effects of pesticide residues on organisms	Optimizes pesticide use in agriculture	<b>Understanding chemical risks</b> It shows how chemicals can affect food chains and human health.
<b>The impact of mining</b> (⛏)	Simulates soil and water pollution	Develops plans for the greening of abandoned mining sites	<b>Developing remedial solutions</b> It allows planning and simulation of industrial area restoration processes.
<b>Antibiotic resistance</b> (💊)	Simulates the evolution of resistant bacteria in the environment	Preventing the spread of resistance in water treatment systems	<b>Connecting ecology with public health</b> It shows how ecological processes can directly influence human health.
<b>Waste management</b> (🗑)	Model waste decomposition in landfills	Design efficient composting and recycling systems	<b>Promoting the circular economy</b> Helps to understand recycling processes and their environmental impact.



Table 4: Pedagogical implications of CAI in relation to landscape ecology and resource management

The indicator considered	Implications in General Ecology	Implications in Applied Ecology	Pedagogical purpose
<b>Landscape ecology</b> (🏡)	Analyze the structure and function of the landscape	Plan land use at the regional level	<b>Developing large-scale thinking</b> It helps to understand how landscape elements interact.
<b>Habitat fragmentation</b> (💔)	Analyze the impact of landscape barriers on species	Design ecological corridors to connect habitats	<b>Understanding connectivity</b> It demonstrates the impact of isolation on species and the importance of ecological corridors.
<b>Forest resource management</b> (🌲)	Model tree growth and harvesting	Optimizes cuts for sustainable exploitation	<b>Assimilation of the concept of sustainability</b> It forms the ability to manage natural resources in the long term.
<b>Ecosystem services</b> (📦)	Evaluate the benefits of ecosystems to society	Calculate the economic value of environmental services	<b>Valuing nature</b> It shows students that nature offers quantifiable benefits, not just aesthetic ones.
<b>The impact of tourism</b> (👤)	Modeling tourist pressure on protected areas	Develop sustainable ecotourism strategies	<b>Understanding human pressure</b> It highlights how recreational activities can affect the environment and the need for ecological planning.

Table 5: Pedagogical implications of CAI in relation to urban ecology and stress response

The indicator considered	Implications in General Ecology	Implications in Applied Ecology	Pedagogical purpose
<b>Urbanization and ecosystems</b> (🏙️)	Simulates the impact of urban expansion on the environment	Design green cities and sustainable urban spaces	<b>Understanding coexistence</b> It shows how the natural and built environments can coexist and influence each other.
<b>Urban ecology</b> (🌿)	Simulates the role of green spaces in air purification	Plan parks and green roofs in cities	<b>Developing eco-infrastr. solutions</b> It trains practical skills to integrate nature into the urban environment.
<b>Urban agglomeration</b> (👥)	Analyze the urban heat island effect	Design cooling strategies through urban vegetation	<b>Awareness of city problems</b> It offers solutions to environmental problems generated by urban density.
<b>The body's response to stress</b> (🧘)	Models plant response to drought or salinity	Develop strategies for agriculture in arid environments	<b>Study of biological adaptability</b> It helps to understand the mechanisms by which organisms adapt to extreme environmental conditions.
<b>Host-parasite relationship</b> (🐛)	Model the dynamics of parasite populations	Controls diseases in natural and agricultural ecosystems	<b>Understanding biological control</b> It shows how natural processes can be used to manage problems in agriculture.
<b>Impact of invasive species</b> (🐉)	Simulates the spread and impact of non-native species	Develop control plans for invasive species	<b>Preventing biological risks</b> It builds the ability to identify and control threats to local biodiversity.
<b>Ecological monitoring</b> (📊)	Analyze data to detect changes	Early warning systems for pollution	<b>Training in monitoring skills</b> Prepares students to use technology in data management.

The last column in the above tables explains the educational purpose of each implication of CAI, showing how the use of these tools contributes to the formation of theoretical skills and (re)adaptation of practical skills among students, as future specialists in the field.

Moreover, from a pedagogical point of view, in order to highlight the connection between IAC and general and applied ecology, we can also consider the types of skills and competences developed by students. Some of these are reproduced in Table 6, in a natural (chrono)logical chain, which reflects a progressive learning path, where each level builds on the previous one, namely:

- **Critical Thinking & Analysis** - this is the foundational level; before students can use digital tools or plan projects, they need to understand the basic concepts. IAC provides models so that students can analyze and interpret cause-and-effect relationships.
- **Modeling & Simulation** - once the student understands the theoretical principles, they can move on to applying them in virtual models. This level transforms abstract knowledge into controlled experiments. Simulations are used to test hypotheses and understand how ecological systems work without the need for costly practical effort.
- **Mapping & Visualization** - once the student understands the processes, they need to place them in a spatial context. Mapping and visualizing geographic data is crucial for seeing how ecological phenomena are distributed on a map and how they change over time. It is a transition from understanding processes at a local scale to visualizing them at a global scale.
- **Data Management & Technology** - this level focuses on concrete tools. IAC is not just about visualizing, but also about working with large data sets. The ability to collect, organize, and use specialized software becomes vital to process information obtained from simulations or from the field.
- **Communication & Presentation** - once the data has been analyzed and interpreted, the results must be communicated effectively. This competency refers to transforming complex information into clear (info)graphics and reports, accessible to the general public or decision-makers.
- **Collaboration & Teamwork** - environmental projects are rarely carried out by a single person. IAC facilitates collaboration through virtual platforms. This level of competency develops as students learn to work together, share tasks, and combine individual results into a common project.
- **Problem Solving & Decision Making** - using analysis, simulation, data, and collaboration, students learn to approach complex environmental problems and formulate concrete solutions. It is the level where theory is transformed into action, making informed decisions to solve an environmental problem.
- **Project Planning & Management** - involves organizing and implementing a solution; a student competent in this area can structure a project from A to Z, allocate resources and monitor progress, applying environmental knowledge in a realistic setting.
- **Ethics & Social Responsibility** - this level is the highest, integrating all the others; it is the point where the student understands not only how to solve a problem, but also why and for whom. IAC offers complex scenarios to discuss the ethical implications of environmental decisions, developing a sense of professional responsibility.

All the skills mentioned complement each other and culminate in problem-solving and decision-making, where students apply critical thinking and technical knowledge to develop viable solutions to real environmental challenges, all of which contribute to a complete and relevant education for the job market. Furthermore, CAI provides an ideal framework to overcome traditional disciplinary boundaries, promoting a holistic and interdisciplinary view of environmental issues. Using simulations and shared databases, students learn to integrate knowledge from ecology, computer science, chemistry, sociology, and even economics. For example, a specialist can use a CAI model to analyze not only the ecological impact of a project, but also its economic and social consequences. This approach allows future specialists to communicate effectively with experts from various fields, from engineers and urban planners to policymakers.

Therefore, CAI not only improves technical knowledge but also contributes to the training of professionals capable of navigating the complexity of global problems and developing integrated solutions adapted to reality.

Table 6: Skills developed among students as a result of IAC's foray into ecology

Level of competence	Relevance* (%)	Skills developed (General Ecology)	Practical Applications (Applied Ecology)
<b>Critical thinking &amp; analysis</b> (🧠)	15%	Analysis of ecological data (e.g., growth curves) Identification of causes and effects within ecosystems	Assessing the impact of an industrial project on an ecosystem Analysis of water and air quality monitoring data
<b>Modeling &amp; simulation</b> (💻)	15%	Understanding complex processes (e.g., <i>ecological succession</i> ) Experimenting with multiple variables in a virtual environment	Simulating the spread of an invasive species Modeling reforestation scenarios
<b>Mapping &amp; visualization</b> (🗺️)	10%	Interpreting ecological maps and spatial data Large-scale visualization of global ecological phenomena Understanding the spatial distribution of species and habitats	Creating flood risk maps based on vegetation Planning migration corridors for animals Identifying areas with potential for eco-energy development
<b>Data management &amp; technology</b> (💻)	15%	Collecting, storing, and organizing large data sets Using specialized software Familiarizing with remote sensing and monitoring technologies	Implementing automated environmental monitoring systems Analysis of genetic data for biodiversity conservation Automating environmental impact reports
<b>Communication &amp; presentation</b> (🗣️)	5%	Creating clear visual representations of ecological data Developing reports and presentations based on simulations Explaining complex concepts to non-specialist audiences	Creating infographics about local biodiversity Presenting the results of an environmental impact study Developing interactive educational materials for schools
<b>Collaboration &amp; teamwork</b> (🤝)	15%	Using online platforms to work on joint projects Dividing tasks and integrating individual contributions	Collaboration with experts from various fields for environmental projects Development of a common, widely accessible species database
<b>Problem solving &amp; decision making</b> (💡)	10%	Systematic approach to complex environmental problems Collaborating in virtual teams to solve practical cases	Developing a management plan for a national park Making informed decisions about resource use
<b>Project planning &amp; management</b> (📅)	5%	Structuring an ecological study in stages (analysis, reporting) Allocation of resources for a virtual project	Managing a degraded habitat restoration project Planning an invasive species inventory campaign
<b>Ethics &amp; social responsibility</b> (👤)	10%	Recognizing the ethical implications of ecological research Assessing the risks and benefits of environmental decisions	Ethical analysis of a natural resource exploitation project Assessing the social impact of pollution on communities

\* relevance for the future ecology specialist

#### 4. Perspectives and Proposals in relation to the Integration of IAC in Ecology

Despite the obvious benefits, the implementation of CAI in environmental education faces challenges related to access to technology and teacher training. To maximize the potential of this approach, the following development directions are proposed:

- **creating integrated educational platforms** - developing customized software suites that combine simulations, data analysis, and GIS tools in a single platform would facilitate the learning process and reduce technological barriers.
- **continuous training of teaching staff** - refresher courses for teachers are essential to familiarize them with new pedagogical tools and methodologies, ensuring an effective integration of IAC into the curriculum.
- **promoting pedagogical research** - it is necessary to carry out rigorous impact studies to assess the extent to which CAI improves learning outcomes in the long term, providing concrete data to justify investments in technology.
- **developing case studies based on real data** - using current data sets from environmental agencies or active research would increase the relevance and realism of student projects.

CAI represents an indispensable component for the future of ecological education, providing a bridge between theoretical knowledge and practical application. By proactively adopting this approach, educational institutions can train a new generation of specialists, capable of responding effectively and innovatively to the complexity of the ecological challenges of the 21st century.

#### 5. Conclusions and Good Practice Recommendations

Based on the analysis of the specialized literature and pedagogical results, it can be concluded that Computer-Assisted Instruction (CAI) is essential for the modernization of ecology education. This approach transforms the learning process, shifting the emphasis from a passive assimilation of information to an active and interactive participation. Through simulations, data analysis, and visualizations, CAI provides a solid bridge between theoretical knowledge in general ecology and practical applications of applied ecology. The formation of skills such as critical thinking, modeling, data management, and collaboration is fundamental to preparing a new generation of specialists capable of successfully addressing complex environmental challenges. To maximize the benefits of CAI in ecological education, the following good practice recommendations are proposed:

- **holistic curricular integration** - CAI should not be treated as a separate module, but as an integrated tool in all ecology disciplines, from basic courses to advanced research projects. Educational institutions should reassess and restructure curricula to coherently incorporate digital tools.
- **universal access to specialized tools** - ensuring students have access to specialized software, either through university licenses or through the use of open-source tools, is crucial. This will bridge the technology gap and allow all students to develop relevant skills.
- **development of personalized teaching materials** - teachers are encouraged to create case studies and exercises based on real ecological data, specific to their region or country. This motivates students by connecting theory to local problems.
- **continuous teacher training** - organizations and universities should offer regular training sessions for teachers, focused on the latest CAI techniques and platforms. A well-trained teaching workforce is key to a successful implementation of this methodology.
- **promoting interdisciplinary projects** - encouraging students to participate in projects that involve collaboration with specialists from other fields will simulate the real work environment and emphasize the importance of a holistic approach in solving environmental dynamic problems.

Finally, adopting this pedagogical approach represents not only an improvement in teaching methods but also a strategic investment in the training of competent professionals capable of responding with innovation and responsibility to the complexity of the ecological challenges of the future.

**References**

- [1] Han, B.A., K.R. Varshney, S. LaDeau, A. Subramaniam, K.C. Weathers, and J. Zwart. "A synergistic future for AI and ecology." *roceedings of the National Academy of Sciences (PNAS)* 120, no. 38 (2023): 34-46. DOI10.1073/pnas.2220283120.
- [2] Rader, R., M.A. Nuñez, T. Siqueira, Y. Zou, C. Macinnis-Ng, L. Marini, P. Batáry, R. Gordon, L. Groves, and J. Barlow. "Beyond yield and toward sustainability: Using applied ecology to support biodiversity conservation and food production." *Journal of Applied Ecology* 61, no. 6 (2024): 1142-1146. DOI10.1111/1365-2664.14653.
- [3] Opre, D., C. Serban, A. Vescan, and R. Iucu. "Supporting students' active learning with a computer based tool." *Active Leraning in Higher Education* 25, no. 1 (2022): 135-150. DOI10.1177/14697874221100465.
- [4] Young, C., B. Mitchell-Yellin, and G.K. Randall. "Engaging classroom observation: A brief measure of active learning in the college classroom." *Active Leraning in Higher Education* 26, no. 1 (2025): 46-97. DOI10.1177/14697874241229421.
- [5] Buchner, J., Z. Altinay, M. Chang, R. Kuo, and A. Tili. "Embodying nature in virtual reality generates different presence levels and learning outcomes." Paper presented at the 24th IEEE International Conference on Advanced Learning Technologies (ICALT 2024), Nicosia, North Cyprus, June 28, 2024.
- [6] Deringer, S.A., and A. Hanley. "Virtual Reality of Nature Can Be as Effective as Actual Nature in Promoting Ecological Behavior." *Ecopsychology* 13, no. 3 (2021): 219-226. DOI10.1089/eco.2020.0044.
- [7] Rafiq, K., S. Beery, M.S. Palmer, Z. Harchaoui, and B. Abrahms. "Generative AI as a tool to accelerate the field of ecology." *Nature Ecology & Evolution* 9, no. 3 (2025): 378-385. DOI10.1038/s41559-024-02623-1.
- [8] Aguado-Terrón, J.M., and M.D. Grandío-Pérez. "Toward a Media Ecology of GenAI: Creative Work in the Era of Automation." *Palabra Clave* 27, no. 1 (2024): 23-46. DOI10.5294/pacla.2024.27.1.8.
- [9] Bono, E.L. "Global Compact on Education and the challenges of Artificial Intelligence and Integral Ecology in Education." *Revista Pistis & Praxis-Teologia e Pastoral* 16, no. 2 (2024): 208-220. DOI10.7213/2175-1838.16.002.DS01.
- [10] Coman, M. *Ecological Management / Management ecologic*. Cluj-Napoca, Risoprint Publishing House, 2009.
- [11] Coman, M. *Ecosystem Investigation Techniques / Tehnici de investigare a ecosistemelor*. Cluj-Napoca, Risoprint Publishing House, 2011.

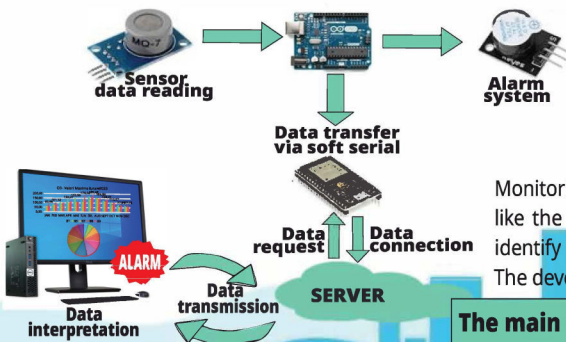


# Smart Air Quality Monitoring Autonomous Systems and AI

Authors: Alexandra BĂDICEANU, Anca-Florentina POPESCU\*,  
Georgiana-Miana ANDRICIUC, Ecaterina MATEI, Andra-Mihaela PREDESCU  
\*ancaflorentinapopescu@gmail.com

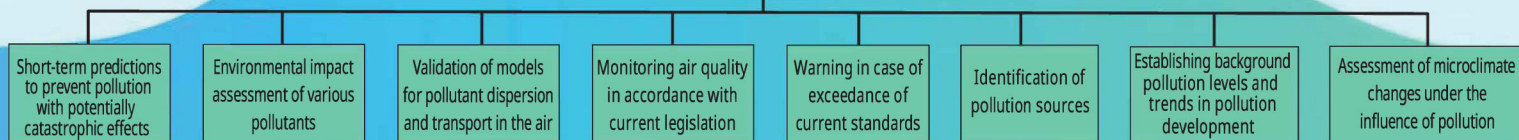
## 1. Introduction

Air quality is crucial for health, ecosystems, and climate. Pollution is a global problem that requires effective monitoring. Autonomous systems and AI enable real-time data collection and analysis, supporting quick actions and better decisions for protecting the environment and public health. This study emphasizes their role in managing resources and reducing pollution impacts.



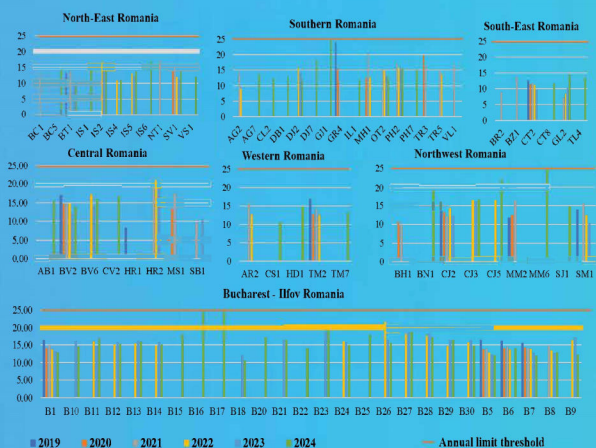
Monitoring air quality involves conducting observation and quantitative and qualitative measurements of indicators like the concentrations of different air components. This system generates important data that helps to quickly identify polluted areas and supports strategic and tactical decisions aimed at reducing and preventing pollution. The development of an air quality monitoring system follows several stages, which will be detailed below.

### The main objectives of the Air Quality Monitoring System



## 3. Results and Discussion

PM<sub>2.5</sub> particulate matter - Annual average values in Romania, 2019-2024



The annual average concentrations of PM<sub>2.5</sub> particulate matter in the air from 2019-2024. By analyzing the plot values, we notice that the annual daily average PM<sub>2.5</sub> concentration for the county with sufficient data available for the period 2019-2024 has exceeded the annual limit of 25 µg/m<sup>3</sup> only twice. Both exceedances have occurred in 2019, respectively at the monitoring station MM6, located in Sighetu Marmatiei, which registered a measured value of 30.60 µg/m<sup>3</sup>, and at the monitoring station B17, situated in Bucharest, sector 3, which registered a monitored value of 25.24 µg/m<sup>3</sup>. The data in the figure also indicates a slightly declining trend in the PM<sub>2.5</sub> concentrations, which might point towards a potential improvement in air quality. However, the significant annual variability highlights the influence of different meteorological conditions, industrial activities and the implemented pollution control efficiency.

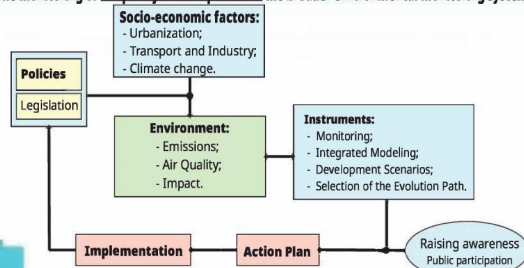
## 4. Conclusions

The global trend in primary particulate matter emissions at national level during 2019-2024 has been upward. This assessment suggests that despite efforts to reduce pollution, primary particulate matter emissions have been increasing substantially, which raises serious concerns about the impact on public health and air quality. It is imperative to investigate the sources of this growth and to implement efficient measures to effectively reverse this development. Romania has an extensive national air quality monitoring network essential for protecting public health, vegetation, and ecosystems. The system includes various stations equipped with advanced technologies for continuous measurement of pollutants and meteorological factors. Intelligent monitoring stations are crucial for early detection of air quality issues, enabling prompt corrective measures. They provide accurate, real-time data, leading to more effective environmental management and protection of public health and ecosystems. These systems support evidence-based environmental policies and continuous monitoring to prevent serious pollution incidents.

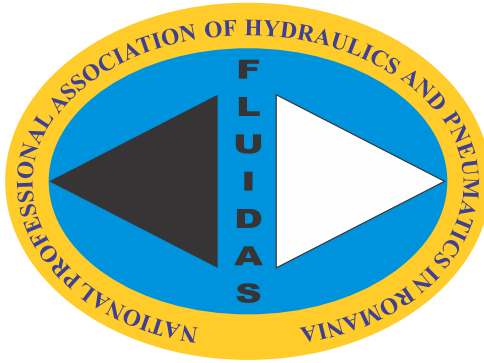
## 2. Methodology

This report relies on data from Romania's National Air Quality Monitoring Network (RNMCA), which currently has 152 stations continuously monitoring air quality parameters across the country.

The monitoring of air quality is a component of the broader environmental monitoring system.



# FLUIDAS



**NATIONAL PROFESSIONAL ASSOCIATION OF  
HYDRAULICS AND PNEUMATICS IN ROMANIA**



**fluidas@fluidas.ro**